The Role of Two Putative Ca^{2+} Transporters in the *Chlamydomonas reinhardtii* CO$_2$-Concentrating Mechanism

Tsz Kam Kwok
Doctor of Philosophy

University of York
Biology
September 2022

Abstract

There is an urgent need to double global crop production by 2050 to meet the demands of population growth, diet changes and biofuel production. A promising solution is to increase crop yields by enhancing plant photosynthesis. One approach is to engineer a CO_2-concentrating mechanism (CCM) into C3 crops to increase photosynthetic carbon fixation efficiency. The CCM of the green alga *Chlamydomonas reinhardtii* is a good candidate as it shares close phylogeny and similar photosynthetic traits with higher plants. The CCM is only induced under low CO_2 conditions, but it is unknown how the alga senses CO_2 changes to regulate this process. To dissect the CO_2-sensing pathway in the CCM, this study set out to identify candidate CO_2 sensors in *Chlamydomonas* by adopting a target reverse genetic screen. A list of candidate genes were identified as homologues of characterised CO_2-sensors in other species and their *Chlamydomonas* mutants were screened in an autotrophic growth assay. The mutants of two genes, *CGLD1* and *CPLD63*, were found to have a disturbed CCM and photosynthesis respectively, and failed to correctly transcriptionally regulate known CCM genes like the HCO_3^- transporter *LCIA*. Bioinformatics study showed that they belong to the UPF0016 family and contain two highly conserved motifs that are important for Ca^{2+} transport in their yeast homologue Gdt1p. Fluorescence protein tagging also revealed that CGLD1 localises to the thylakoid membrane while CPLD63 concentrates at the chloroplast envelope. Meanwhile, growth assays in different Ca^{2+} concentrations showed that CGLD1 is important for the limiting-CO_2 growth of *Chlamydomonas* in low Ca^{2+}. As Ca^{2+} elevation in the algal pyrenoid is important for the CCM, data in this study indicates that CGLD1 and CPLD63 are putative Ca^{2+} transporters with potential roles in regulating the *Chlamydomonas* CCM via a Ca^{2+}-induced retrograde signal from the chloroplast to the nucleus.

Table of content

4

List of Tables

List of Figures

Acknowledgements

I would like to express my greatest gratitude towards my primary supervisor, Prof Luke Mackinder, for being extremely supportive and understanding with me. I would never have been able to complete my project without your guidance and patience. Thank you very much for everything during my while PhD programme.

I would also like to thank my co-supervisor, Dr Gareth Evans, for also being very supportive and understanding with me, and often provided great advice for difficulties I have encountered in my project. I am really grateful to have had you and Luke to be my supervisors.

Formally, I would like to thank the Pierre Morsomme lab for sending me their BICAT expression plasmid for my Ca^{2+} influx assay. Also, I would like to thank former Mackinder members Dr Gary Yates and Tom Emrich-Mills for developing the recombineering method and tagging plasmids used for cloning *Chlamydomonas* gene used in this study. Finally, I would like to thank the staff in the Technology Facility (TF) of our department for training me on various machines and providing analysis and technical support. I would like to thank Dr Sally James and Dr Lesley Gilbert for teaching me how to plan and use thermocyclers needed for my qPCR experiment. I would like to thank Dr Karen Hogg, Jo Marrison, Dr Graeme Park and Grant Calder for teaching me how to use the Confocal microscope and always helping me to solve the various little problems I encounter while using the machine. Finally, I would like to thank Dr Andrew Leech for providing me support in using the different plate readers in the TF.

I would also like to thank every member of the Mackinder lab for providing great professional and emotional support to me in this difficult journey of accomplishing a PhD. I especially want to thank Dr Charlotte Walker and Dr Philipp Girr for helping me a lot with my experiments, teaching me different laboratory and research analysis skills, and counselling me when I was experiencing breakdown. I would also like to thank Dr Abi Perrin for always supporting me and being a really great lab bench neighbour. And I must give my thanks to my fellow PhD student colleague James Barrett for helping me with the gas system needed for my growth assays, and also to my fellow Hong Kong buddy Justin Lau in the lab for always helping me with any experimental problems and also for providing great emotional support. Finally, I would like to thank the rest of the lab

members, Dr Mihris Naduthodi, Dr Onyou Nam, Matt Dowson, Sabina Musial and Caroline McKenzie, as well as former members, Dr Gary Yates again, Dr Guoyan Zhao, and Dr Irina Grouneva, for all the support to me during my times in the lab.

I am also very grateful for the research community both at the University of York and across the UK such as the Algae-UK for providing great research support and networking opportunities for all of us young starting researchers. The different social events for sharing insights on science really open my eyes and inspire me on my own research idea. I am thankful to be a part of this wonderful community.

I would also like to thank my great friends Amy Stonadge and Jessie Downing for always being there for me and helping me with any problems I face. My PhD life would not be as exciting and colourful without you two here. I would also like to thank my best friend Rebecca Barker, who I have known since my first time in UK studying my Bachelor back in Durham, and her family for always looking after me. Becky, you have been a most supportive and wonderful friend to me. I wish you good luck with your PhD thesis too.

Finally, I would not forget to thank the two greatest persons in the world: my dearest parents. You not only provide me financial support needed for the PhD, but also still taking good care of me in every way even after I have grown up to be an adult for a long time now. My caring mother, I give my greatest thanks to you, for always being there for me, checking in on me to make sure I am alright during many stressful and difficult times, and never giving up on me when I have many times want to do so. Your loving words and insightful life advice always comfort me and help me a lot. My witty father, thank you for always inspiring me with your intelligent views on life, and sharing your interests with me, and supporting me through hard times. Your beautiful photographs often put a smile on me and your occasional message on life wisdom always inspire me. I will not forget the hard work you both have done for so many years to nurture me and ensure me the best standard of life. It is the hope to go back to you guys with a proudly earned PhD certificate that have kept me going. I thank you both deeply.

Author's Declaration

I declare that this thesis is a presentation of original work and I am the sole author. This work has not previously been presented for an award at this, or any other, University. All sources are acknowledged as References.

Tsz Kam Kwok

1   Introduction

1.1   Tackling global food security challenges

The world faces increasing demands for food production resulting from rapid population growth, changed diet habit and competition from biofuel production (Ray et al., 2013; Fischer, Byerlee and Edmeades, 2014). It has been estimated that staple crop production must increase by at least 60% between 2010 and 2050 to obtain global food security (Ray et al., 2013; Fischer, Byerlee and Edmeades, 2014). Although global production rates of major crops including wheat, rice, maize and soybean are experiencing a steady increase over the years, it is not enough to achieve this goal (Ray et al., 2013; Fischer, Byerlee and Edmeades, 2014). On the other hand, cropland and irrigation water resources are becoming limited while climate change could create challenges for higher crop production (Fischer, Byerlee and Edmeades, 2014; Long, Marshall-Colon and Zhu, 2015; Bailey-Serres et al., 2019). There is a need for new strategies that allow faster crop yield enhancement with efficient usage of agricultural resources. Conventional breeding methods alone are not adequate to reach this goal anymore. With recent advances in technology, the use of genetic engineering techniques to increase crop yields has become a popular alternative (Long, Marshall-Colon and Zhu, 2015; Bailey-Serres et al., 2019; Ahmar et al., 2020).

One genetic engineering approach looks into enhancing the efficiency of photosynthesis in crops to obtain higher genetic yield potential (Bailey-Serres et al., 2019; Long et al., 2006; Long, Marshall-Colon and Zhu, 2015). Photosynthesis is an important biological process that converts light energy and inorganic carbon (Ci) into chemical energy and organic carbon, which are essential for the growth of almost all living organisms on Earth. The efficiency of this process in many modern crops has yet to reach its maximum, leaving room for improvement to achieve higher crop yields (Long et al., 2006; Long, Marshall-Colon and Zhu, 2015). A limiting step of photosynthesis that has been targeted for improvement by many approaches is the fixation of carbon dioxide (CO_2) to ribulose-1,5-bisphosphate (RuBP) in the Calvin-Benson-Bassham (CBB) cycle by the enzyme ribulose-1,5-bisphosphate carboxylase/oxygenase (Rubisco) to create downstream carbohydrates (Benson and Calvin, 1950). Apart from CO_2 fixation, Rubisco also acts as an oxygenase that fixes oxygen (O_2) to RuBP, generating the compound phosphoglycolate (Figure 1.1). This compound then has to be metabolised using the

energy-consuming photorespiration pathway to regenerate RuBP in the photosynthetic cells (Spalding, 1989). Whether Rubisco will exhibit carboxylation or oxygenation catalytic function depends on the CO_2/O_2 concentration ratio around it. Under current atmospheric CO_2/O_2 ratios Rubisco's oxygenation reaction can limit carbon fixation efficiency in many photosynthetic organisms including C3 crop plants. As a result, improvement of carbon fixation efficiency of Rubisco is a potential strategy for increasing photosynthesis in crops. One approach is to engineer a biophysical CO_2-concentrating mechanism (CCM) into C3 crop plants.
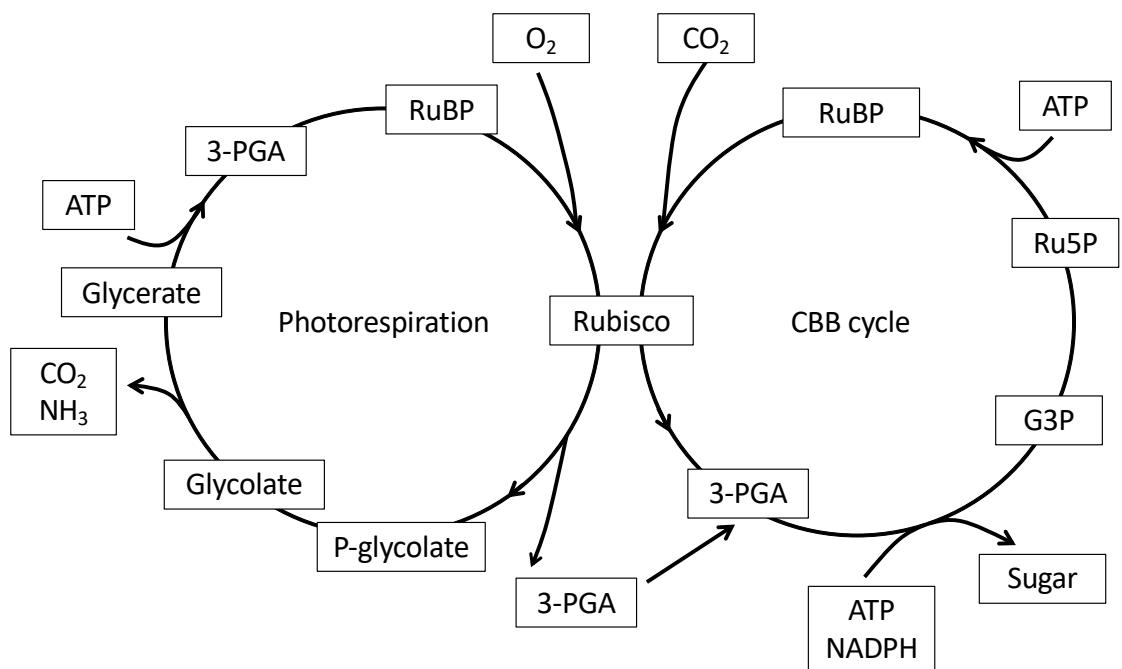
Figure 1.1 A simplified model of photorespiration and CBB cycle.
Rubisco can fix CO_2 to RuBP in the CBB cycle to generate 3-PGA. It can also fix O_2 to RuBP to generate P-glycolate and 3-PGA. P-glycolate then enters the photorespiration pathway to regenerate RuBP, which consume ATP and causes the loss of carbon as CO_2. Abbreviations: ATP = Adenosine Triphosphate, CBB = Calvin-Benson-Bassham, RuBP = ribulose-1,5-bisphosphate, 3-PGA = 3-phosphoglycerate, G3P = triose phosphate, Ru5P = ribulose-5-phosphate, P-glycolate = phosphoglycolate

1.2 The *Chlamydomonas reinhardtii* CCM is a good candidate for engineering into C3 crop plants

Some photosynthetic organisms, such as cyanobacteria, green algae, diatoms, C4 and Crassulacean acid metabolism (CAM) plants, have developed CCMs to increase the concentration of CO_2 around Rubisco. This enhances their growth and allows them to maintain high carbon fixation efficiency when CO_2 levels become limiting in their natural habitats. There are different CCMs existing in nature, including the biochemical CCMs - C4 photosynthesis and CAM - seen in higher plants like maize and pineapple, and the biophysical CCMs found in cyanobacteria and green algae (Wang, Stessman and Spalding,

2015; Yang et al., 2015; Long et al., 2016; Schuler, Mantegazza and Weber, 2016; Rae et al., 2017; Liu et al., 2018; Mackinder, 2018). Due to a CCMs ability to increase photosynthetic efficiency, engineering a CCM into C3 crop plants has become a promising approach for improving their photosynthesis to achieve greater yields. In fact, it has been shown by mathematical simulation that the crop yield of a C3 crop can be enhanced by 36% to 60% through introducing a cyanobacterial CCM (McGrath and Long, 2014).

Considerable research has been conducted to study the different CCMs and test the possibility of engineering one successfully in a higher plant (Wang, Stessman and Spalding, 2015; Yang et al., 2015; Long et al., 2016; Schuler, Mantegazza and Weber, 2016; Rae et al., 2017; Liu et al., 2018; Mackinder, 2018). One extensively studied CCM system belongs to the green alga, *Chlamydomonas reinhardtii* (*Chlamydomonas* from herein). This alga is a well-established model organism for the study of eukaryotic photosynthesis and the algal CCM (Harris, 2001; Wang, Stessman and Spalding, 2015; Mackinder, 2018), and is also used in the industry to produce commercial bioproducts (Khan, Shin and Kim, 2018). Its genome is well-annotated and a large library of mutants is available for the study of its genes (Merchant et al., 2007; Blaby et al., 2014; Li et al., 2016, 2019a). Recent studies have also helped develop a vast number of molecular tools and techniques to clone and edit *Chlamydomonas* genes (Crozet et al., 2018; Emrich-Mills et al., 2021; Fischer and Rochaix, 2001; Baier et al., 2020). Furthermore, *Chlamydomonas* is phylogenetically closer to higher plants when compared to cyanobacteria and diatoms, and the two share similar photosynthetic traits (Spalding, 1989; Merchant et al., 2007; Rochaix, 2011). All these make its CCM a good candidate for introducing into C3 crops. Understanding the *Chlamydomonas* CCM can provide insights into how they acclimate to a changing environment, a genetic toolbox to engineer algae with higher biomass yields for commercial applications, and guidance on engineering an algal CCM into C3 crop plants.

1.3 Current views on the *Chlamydomonas* CCM

1.3.1 Important elements of a biophysical CCM

From the beginning of this century, many advances have been made to identify the important algal CCM components and their molecular and biochemical traits (Wang, Stessman and Spalding, 2015; Rae et al., 2017; Mackinder, 2018). Both algae and

cyanobacteria operate biophysical CCMs (Rae et al., 2017). This type of CCM has four essential components: active Ci transport (energy-consuming), existence of carbonic anhydrases (CAs) to catalyse conversion between CO_2 and bicarbonate ions (HCO_3^-), a compartment that sequesters Rubisco (carboxysome in cyanobacteria and pyrenoid in the alga), and a barrier or recapture system to avoid diffusion of CO_2 away from Rubisco (Figure 1.2). On top of them, regulatory components are present to ensure tight control of the CCM. Recent advances have helped in identifying these components and to characterise their functions in the *Chlamydomonas* CCM. The following will give a summary on the current view on the *Chlamydomonas* CCM model (Figure 1.3).
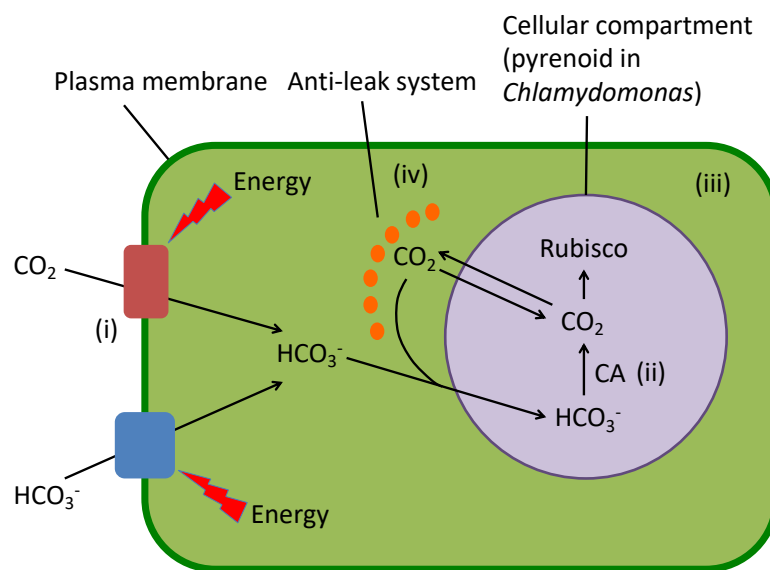
Figure 1.2 Simplified biophysical CCM model in cyanobacteria and algae.
The algal CCM is fundamentally similar to the cyanobacterial CCM, sharing four essential components: (i) active Ci transport (energy-consuming), (ii) existence of carbonic anhydrases (CAs) to catalyse conversion between CO_2 and bicarbonate ions (HCO_3^-), (iii) a compartment that sequester the Rubisco, and (iv) a barrier or recapture system to avoid diffusion of CO_2 away from Rubisco.

1.3.2 The *Chlamydomonas* CCM has three CO_2 acclimation states

During the study of the *Chlamydomonas* CCM, it has been found that the alga has three CO_2 acclimation states: high CO_2 (HCO_2, 0.5-5%), low CO_2 (LCO_2, 0.03-0.4%) and very low CO_2 ($VLCO_2$, <0.02%) (Vance and Spalding, 2005; Wang, Stessman and Spalding, 2015; Mackinder, 2018). The CCM is induced under LCO_2 and $VLCO_2$ (collectively referred to as limiting CO_2), and it has been shown that the CCM has different physiological traits during algal acclimation to these two states (Wang and Spalding, 2014). In addition, the pH of the environment also contributes to the change in the CO_2 concentration. For example, an aeration of LCO_2 combined with pH 7.0 for 24 hours results in a calculated CO_2 concentration of 2.9 µM, which falls into the threshold of $VLCO_2$ (<7 µM; 7-70 µM for LCO_2; >70 µM for HCO_2) instead of LCO_2 (Yamano et al., 2022). Because of this, care must

be taken when investigating the properties of the proteins involved in the CCM by ensuring tight control of CO_2 concentration during cultivation and experiment. For simplicity and consistency, unless otherwise stated the study will refer to the three acclimation states according to the % of CO_2 aired to the medium.
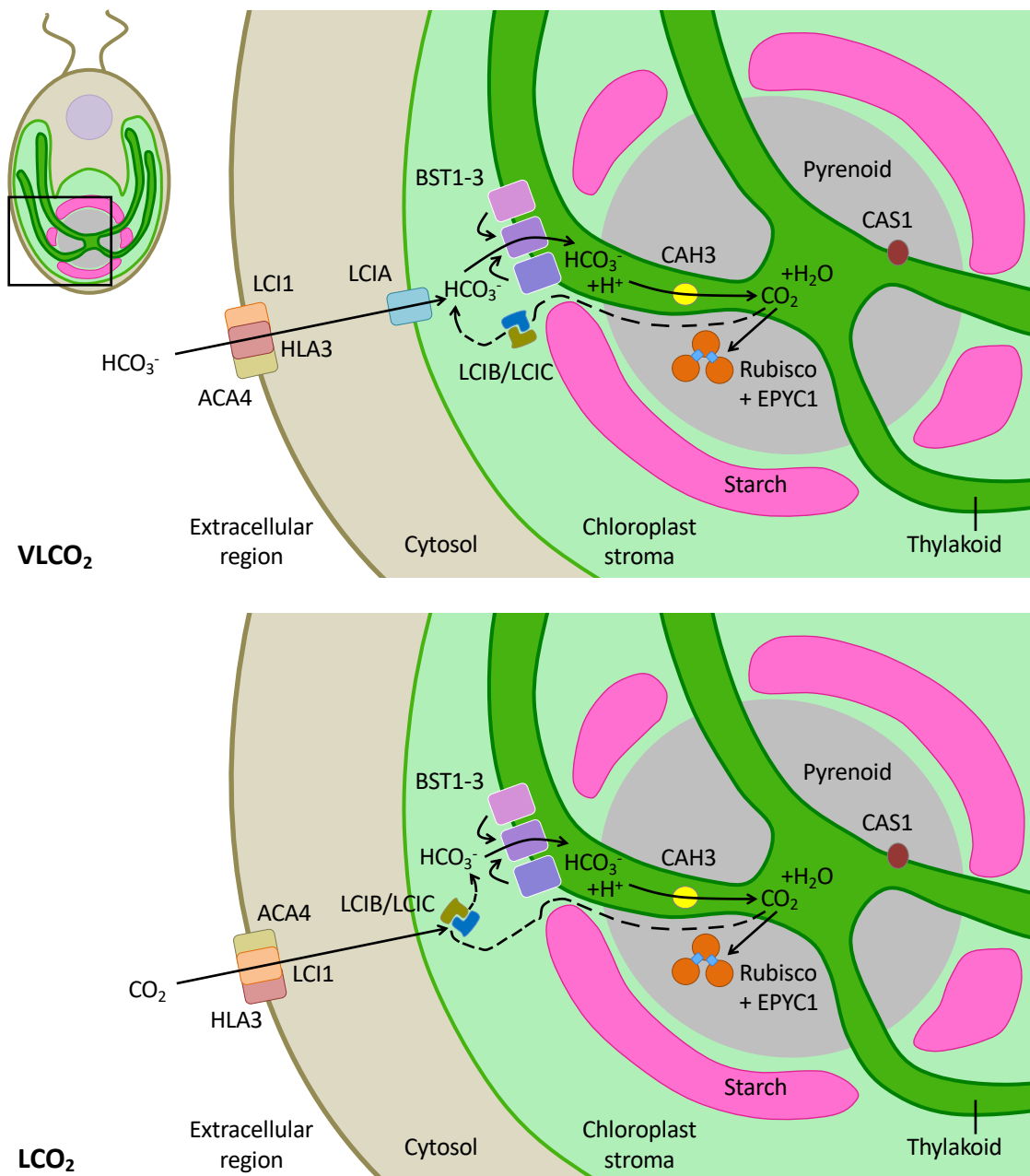
Figure 1.3 The proposed *Chlamydomonas* CCM.
There are two acclimation states for this CCM: at VLCO$_2$ (<7µM) when it depends on an active HCO_3^- transport system to the chloroplast stroma by HLA3 and LCIA; and at LCO$_2$ (7-70µM) when it depends on a LCIB-associated CO_2 uptake system by LCI1 to contribute to chloroplast stromal HCO_3^- pool. HLA3, ACA4 and LCI1 are proposed to form a complex in the plasma membrane and act together to transport Ci across the membrane. LCIA is localised to the chloroplast envelope and transports HCO_3^- ions into the chloroplast stroma. BST1-3 are found at the thylakoid membrane and suggested to transport HCO_3^- ions into the thylakoid lumen. CAH3 is a CA located in the thylakoid lumen; it relocates to the thylakoid tubules in the pyrenoid during CCM activation and catalyses the conversion of HCO_3^- back to CO_2, which diffuses out of the tubules into the pyrenoid matrix. In the matrix, EPYC1 links Rubisco proteins together to aggregate them, allowing the concentration of CO_2 around most Rubisco proteins. LCIB and LCIC are distributed throughout the stroma; they form a complex and accumulate to around the pyrenoid during CCM activation at VLCO$_2$. They are CAs proposed to facilitate the unidirectional conversion of CO_2 that is either leaked from the pyrenoid or

transported from the cytosol to HCO_3^- to prevent CO_2 diffusion out of the stroma. CAS1 is a Ca^{2+}-binding protein found at the thylakoid membrane and acts as transcriptional regulator of HLA3 and LCIA

1.3.3 *Chlamydomonas* CCM- active Ci transport to Rubisco

With the help of transcriptomics, mutants and localisation studies, components crucial for the active transport of Ci to Rubisco in the *Chlamydomonas* CCM have been identified as HLA3, LCI1, ACA4, LCIA, LCIB and BST1-3 (Wang and Spalding, 2014; Wang, Stessman and Spalding, 2015; Mackinder, 2018; Mukherjee et al., 2019; Yamano et al., 2022).

The proposed *Chlamydomonas* CCM model (Figure 1.3) consists of two acclimation states: $VLCO_2$ and LCO_2. In $VLCO_2$, an active HCO_3^- transport system dependent on HLA3 and LCIA contribute to Ci accumulation in the CCM. HLA3 (High Light Activated 3) is an ATP-binding cassette transporter (Gao et al., 2015) that is proposed to form a complex with LCI1 (Low CO_2 Inducible gene 1) at the plasma membrane (Ohnishi et al., 2010; Mackinder et al., 2017). Studies looking into the Ci accumulation in *Chlamydomonas* mutants of the two proteins have suggested that HLA3 is a HCO_3^- transporter (Gao et al., 2015), while a recent studies on the crystal structure of LCI1 and its Ci species preferences in the green alga reveals that it is a CO_2 transporter (Ohnishi et al., 2010; Kono et al., 2020). Together they are involved in the active transport of Ci from the extracellular region to the cytosol in the two different limiting CO_2 acclimation states. In addition to these transporters, unpublished data identified and proposed that an H^+ (proton) ATPase called ACA4 also form a complex with them and drives their Ci transportation through the creation of an electrochemical gradient in the plasma membrane by proton pumping. Next, HCO_3^- ions are transported across the chloroplast envelope by the formate-nitrate transporter LCIA (Low CO_2 Inducible protein A (Miura et al., 2004; Wang and Spalding, 2014; Yamano et al., 2015). LCIA and HLA3 are found to be needed for acclimation at $VLCO_2$ and showed a strong synergistic relationship with each other that the overexpression of them together increased Ci affinity in *Chlamydomonas* cells while the single overexpression of either of them could not (Yamano et al., 2015). Also, a mutant study shows that expression of LCIA is needed to maintain HLA3 stability in the algal CCM, further establishing the close relationship between the two.

When in LCO_2 condition, Ci influx into the chloroplast is less dependent on HLA3 and LCIA transport but switches to a CO_2 uptake system dependent on LCI1 and β-CA LCIB (Low CO_2 Inducible protein B). As mentioned above LCI1 is proposed to be a CO_2 transporter. This is supported by the discovery of its crystal structure and the findings that its function

in the *Chlamydomonas* CCM is dependent on CO_2 not HCO_3^- in wild type, *lcia* and *lcib* mutants (Kono et al., 2020). Meanwhile, LCIB forms a complex with its homologous protein LCIC (Low CO_2 Inducible protein C), and they co-localise in the chloroplast stroma (Wang and Spalding, 2006, 2014; Yamano et al., 2010, 2022; Jin et al., 2016). LCIB was found to be irreplaceable in algal acclimation at LCO$_2$ as *lcib* mutants are unable to grow at LCO$_2$ but can survive at HCO$_2$ and VLCO$_2$ states (Wang and Spalding, 2006, 2014). At VLCO$_2$, LCIB is shown to complement for the action of LCIA when the latter is mutated but is not needed when both HLA3 and LCIA are available and functional in the CCM (Duanmu, Wang and Spalding, 2009; Gao et al., 2015; Wang and Spalding, 2014), whereas LCI1 does not complement the HCO_3^- uptake role of LCIA in both limiting CO_2 conditions (Yamano et al., 2015; Kono et al., 2020). In addition, the function of LCIB in the CCM is found to be dependent on CO_2 and appeared to be complementary with the function of LCI1 in above air-level CO_2 (Kono et al., 2020). On the other hand, LCIB is found to change its position from throughout the stroma to concentrating around the pyrenoid when transiting from HCO$_2$ to limiting CO_2 (Yamano et al., 2010). More detailed studies revealed that LCIB stays dispersed in the stroma when the medium CO_2 concentration is within HCO$_2$ (>70 µM) and LCO$_2$ (7-70 µM) ranges but aggregates to a ring-like structure around the pyrenoid in VLCO$_2$ (<7 µM) range (Toyokawa, Yamano and Fukuzawa, 2020; Yamano et al., 2022), and this relocalisation requires the accumulation of LCIC. Because of all these traits, LCI1 and LCIB/LCIC are proposed to play important roles in CO_2 uptake of the CCM in LCO$_2$, with LCI1 acting as an active CO_2 transporter at the plasma membrane and the CAs catalysing the directional hydration of CO_2 to HCO_3^- in the stroma (Kono et al., 2020). In VLCO$_2$, the active transport of Ci across the plasma membrane becomes more dependent on HLA3 instead of LCI1, while LCIB/LCIC concentrates around the pyrenoid and mainly contributes to the recapture of CO_2 diffused away from the Rubisco in the pyrenoid either through its CA function or forming a barrier (Wang and Spalding, 2006, 2014; Duanmu, Wang and Spalding, 2009; Wang, Stessman and Spalding, 2015; Mackinder, 2018; Toyokawa, Yamano and Fukuzawa, 2020; Yamano et al., 2022).

Finally, the HCO_3^- ions in the stroma are transported into the thylakoid lumen, possibly through the recently identified bestrophin-like proteins- BST1, BST2 and BST3 (known as BST1-3 collectively) (Mukherjee et al., 2019). These proteins are located on the thylakoid membrane with a concentration at the pyrenoid periphery, their expression is

upregulated in LCO_2 and BST1 and BST3 are found to interact with LCIB/LCIC (Mackinder et al., 2017). Mutants with reduced expression of all three proteins, but not those with a single defective BST3, show a lethal growth phenotype at LCO_2 conditions and lower Ci affinity and uptake compared to the wild type (Mukherjee et al., 2019). These all highly suggest that BST1-3 proteins work redundantly in transporting HCO_3^- from the stroma into the thylakoid lumen.

1.3.4 *Chlamydomonas* CCM- conversation of HCO_3^- to CO_2 by CAH3

Once in the thylakoid lumen, HCO_3^- ions are converted into CO_2 by an α-type CA called CAH3 (Karlsson et al., 1998). The CO_2 molecules then diffuse out into the pyrenoid matrix concentrating around the aggregated Rubisco. CAH3 is found to be important for proton removal of photosystem II (PSII) by catalysing formation of HCO_3^- (Karlsson et al., 1998; Villarejo et al., 2002; Shutova et al., 2008; Benlloch et al., 2015), but is also suggested to play a role in converting HCO_3^- to CO_2 for Rubisco in the pyrenoid during CCM induction (Mitra et al., 2004; Markelova et al., 2009; Moroney et al., 2011; Blanco-Rivero et al., 2012; Sinetova et al., 2012). Studies have found that *CAH3* mutants cannot acclimate to LCO_2 condition and have an over-accumulation of internal Ci compared to the wild type (Spalding, Spreitzer and Ogren, 1983; Moroney, Tolbert and Sears, 1986; Funke, Kovar and Weeks, 1997; Karlsson et al., 1998; Markelova et al., 2009). Furthermore, in limiting CO_2 CAH3 is phosphorylated and relocalises to concentrate more in the thylakoid tubules crossing the pyrenoid, where PSII is absent (Gunning and Schwartz, 1999; Blanco-Rivero et al., 2012), while in HCO_2 it is evenly distributed across the thylakoid stroma, where PSII is present (Gunning and Schwartz, 1999; Blanco-Rivero et al., 2012). This supports its dual functional roles in proton removal of PSII and the CCM, and suggests that post-translational modification is involved in the regulating the CCM function of CAH3.

1.3.5 *Chlamydomonas* CCM- Rubisco packaging in the pyrenoid

One important element for the CCM to be fully functional is the aggregation of Rubisco in the pyrenoid (Figure 1.3). The pyrenoid is a liquid-like compartment containing tightly packed Rubisco (Freeman Rosenzweig et al., 2017). It is traversed by thylakoid membranes, which forms the pyrenoid tubules (Engel et al., 2015), and surrounded by a starch sheath that is made up of multiple starch plates (Sager and Palade, 1957). Correct pyrenoid assembly is necessary to establish a functional CCM (Caspari et al., 2017; Mitchell et al., 2017). Several key cellular components of this process have been

identified, including: algal Rubisco small and large subunits (SSU and LSU); the EPYC1 linker protein; the *CIA6* gene; and the protein SAGA1 (Rawat et al., 1996; Genkov et al., 2010; Ma et al., 2011; Meyer et al., 2012; Mackinder et al., 2016; Atkinson et al., 2017; Itakura et al., 2019).

Chlamydomonas mutants lacking the whole Rubisco protein (due to mutation in Rubisco LSU *rbcL* gene) are shown to have no pyrenoid at all (Rawat et al., 1996), while mutants containing hybrid Rubisco with non-native Rubisco SSU fail to form a pyrenoid (Genkov et al., 2010). With further investigation, it is found that the SSU is specifically needed for the targeting of Rubisco to the pyrenoid, and two α-helices exposed on the surface of the algal SSU are required for aggregation of the protein in the pyrenoid (Genkov et al., 2010; Meyer et al., 2012). On the other hand, the successful aggregation of Rubisco in the pyrenoid also requires a repeat protein, EPYC1 (Essential Pyrenoid Component 1). The protein is found to interact with the SSU of Rubisco physically in *Chlamydomonas* and is proposed to help the packaging of Rubisco proteins into the pyrenoid by directly linking them together (Mackinder et al., 2016; Atkinson et al., 2019). This is supported by further studies showing that EPYC1 and hybrid *Arabidopsis thaliana* (*Arabidopsis* from herein) Rubisco with native LSU and *Chlamydomonas* SSU could phase separate into liquid droplets *in vitro* (Atkinson et al., 2019), as well as into a single compartment *in vivo* when expressed in *Arabidopsis* chloroplasts (Atkinson et al., 2020). In addition, a peptide tiling array and single-particle cryo-electron microscopy conducted on EYPC1 peptides and purified *Chlamydomonas* Rubisco have revealed that EPYC1 has five Rubisco-binding regions while one Rubisco holoenzyme has eight binding sites on each SSU for EPYC1 (He et al., 2020). Combined with data gathered from *in situ* cryo-electron tomography of the pyrenoid matrix, a model is proposed where EPYC1 and Rubisco form a network through multivalent and specific low-affinity bonds that create the liquid-like nature of the pyrenoid matrix (He et al., 2020).

Another gene, *CIA6*, is also found to be needed for the correct formation of the pyrenoid, as the mutant of the gene, *cia6*, contain irregularly-shaped pyrenoids and a dysfunctional CCM with reduced expression of CCM genes *LCIB*, *CAH4* and *CCP1* (Ma et al., 2011). Nevertheless, it is not clear how *CIA6* functions in the CCM or pyrenoid formation. A more recently discovered protein, SAGA1 (StArch Granules Abnormal 1), is found to be needed for the correct formation of the pyrenoid and starch sheath (Itakura et al., 2019).

The mutation of *SAGA1* is found to cause a disturbed CCM as well as the formation of aberrant starch sheaths and multiple pyrenoids within a single *Chlamydomonas* cell. Most of these pyrenoids did not contain any visible pyrenoid tubules. In addition, SAGA1 is found to interacts with the LSU and SSU of Rubisco physically. Therefore, it is proposed that SAGA1 facilitates the correct formation of the starch sheath that is needed for the establishment of only one pyrenoid that contains the thylakoid-pyrenoid tubules in a *Chlamydomonas* cell.

The discovery of these components has helped us understand more about the correct formation of the pyrenoid and provided more guidance on what components should be engineered into C3 crop plants for a functional CCM. However, our knowledge is still not complete as there are still unknown components needed for pyrenoid formation not yet identified (e.g. what is needed for the correct position of pyrenoid in the chloroplast and the arrangement of thylakoid tubules into the organelles). This will require further study.

1.3.6 *Chlamydomonas* CCM- CO_2 anti-leak system

A final crucial biophysical element of the *Chlamydomonas* CCM is an anti-leak system for the CO_2 in the pyrenoid. Without it, the higher concentration of CO_2 in the pyrenoid compared to the outside can lead to its diffusion out into the chloroplast stroma and eventually out of the cell. To this date, three components have been proposed to be part of this anti-leak system: the LCIB/LCIC complex, BST1-3 and the starch sheath (Wang and Spalding, 2014; Wang, Stessman and Spalding, 2015; Mackinder, 2018; Ramazanov et al., 1994; Toyokawa, Yamano and Fukuzawa, 2020).

As mentioned in section 1.3.3, because of its CA structure, its function in complementing the action of LCIA, and its relocalisation to around the pyrenoid in VLCO$_2$, LCIB together with LCIC as a complex is suggested to play a role in the CO_2 anti-leak system. Meanwhile, BST1-3 are found concentrated at the periphery of the pyrenoid and interact with LCIB/LCIC. They are therefore suggested to also participate in the recapture of CO_2 diffused from the pyrenoid by cooperating with LCIB/LCIC: the CA complex first converts the CO_2 back to HCO_3^-, which is then transported back into the thylakoid lumen by BST1-3 (Mukherjee et al., 2019). On the other hand, the starch sheath surrounding the pyrenoid is also proposed to play a part in the CO_2 anti-leak system. Studies have shown that starch sheath forms rapidly when the CCM is induced in limiting CO_2 conditions (Kuchitsu, Tsuzuki and Miyachi, 1988; Ramazanov et al., 1994). By studying a starchless

mutant strain of the gene *ISA1* (*Isoamylase1*), it was found that the starch sheath is essential for the correct localisation of LCIB/LCIC as well as the functioning of the CCM in VLCO$_2$ (Toyokawa, Yamano and Fukuzawa, 2020). In addition, a recent preprint by Fei et al., 2021 showed in their chloroplast-scale reaction-diffusion model that a physical barrier like thylakoid stacks or a starch sheath is required for an effective CCM by limiting CO$_2$ leakage out of the pyrenoid matrix. All of these support the proposition that the starch sheath helps reduce CO$_2$ diffusion out of the pyrenoid by acting as a physical barrier around the organelle and facilitating the correct relocalisation of LCIB/LCIC in VLCO$_2$ either through direct or indirect interaction, or by maintaining a high concentration of Ci around the pyrenoid.

1.3.7 *Chlamydomonas* CCM- regulation

The versatile regulation of the algal CCM is important for quick acclimation towards the fluctuating CO$_2$ levels in the natural habitat of *Chlamydomonas*. It is also necessary to implement such regulation when engineering the CCM in C3 crop plants to allow tight control of the on/off state of the mechanism. However, the regulatory mechanism involved in the algal CCM are not yet well established. Up to this date, CIA5 (also called CCM1), LCR1 and CAS (or CAS1) have been identified as regulatory elements associated with the *Chlamydomonas* CCM.

CIA5 is regarded as a master regulator of the algal CCM that affects the expression of many CCM-related genes, including *HLA3*, *LCIA*, *LCIB and BST1-3*, as well as CO$_2$-responsive genes (Fukuzawa et al., 2001; Xiang, Zhang and Weeks, 2001; Brueggeman et al., 2012; Fang et al., 2012). It is located to the nucleus (Wang et al., 2005) and was first identified to be important for Ci accumulation when its mutant (*cia5*) was shown to require high CO$_2$ for growth (Moroney et al., 1989). This high-CO$_2$-requiring phenotype was also shown in another *cia5* mutant (C16) in a later study (Fukuzawa et al., 2001). In addition, many CCM-related genes were found to be inhibited in limiting CO$_2$ in the *cia5* mutant (Fang et al., 2012). These all indicate that CIA5 is required for a functional CCM. Structurally, the regulator contains two N-terminal zinc-binding regions and an 130-aa acidic C-terminal activation domain important for its regulation of CO$_2$-responsive gene expression (Fukuzawa et al., 2001; Xiang, Zhang and Weeks, 2001; Chen et al., 2017). In fact, the presence of an altered CIA5 construct containing only these domains is shown to be sufficient enough to complement a *cia5* mutant (Chen et al., 2017). The

identification of these domains provides some insights into the molecular mechanism behind the function of CIA5 in the CCM. The zinc-binding regions might be important for sensing CO_2 change for activation of the CCM by CIA5, as the necessity of zinc binding for protein function is also found in CA, which is important for sensing CO_2 (Moroney et al., 2011). Meanwhile, the C-terminal activation domain shows autoactivation in yeast and is able to activate gene expression when replacing the transcription activator-like element (TALE) activation domain in a designed TALE (dTALE) system (Chen et al., 2017). Furthermore, when a truncated *CIA5* gene fragment lacking 161 nt of the 3' coding region is introduced in *cia5* mutants in a complementation experiment, four CO_2-responsive genes were found to be expressed constitutively in both high and low CO_2 conditions (Xiang, Zhang and Weeks, 2001). These all suggest that the C-terminal domain of CIA5 is important for the robust regulation of CO_2-responsive pathways and might also be important for CO_2 sensing in *Chlamydomonas*. Whether CIA5 can interact with CO_2 directly or requires an upstream CO_2 sensor for its function in the CCM is not known.

Downstream of CIA5/CCM1, the Myb-type transcription factor LCR1 (Low-CO_2 stress Response 1) is found to regulate the expression of genes responsive to limiting CO_2 like *LCI1*, *LCI6* and *CAH1* (Yoshioka et al., 2004). The Myb transcription factors make up one of the largest protein families in plants and share highly conserved Myb DNA-binding domain repeats at the N-terminal (Ambawat et al., 2013; Roy, 2016; Wang, Niu and Zheng, 2021). They regulate a diverse range of biological processes in plants, ranging from the control of anther and pollen development to abiotic and biotic stress responses. LCR1 is also found to contain the DNA-binding Myb domain at the N-terminal and protein sequence alignments show that this domain is more similar to the R3 domain of multiple-type plant Myb proteins (multiple DNA-binding domains) compared to single-type ones (single DNA-binding domain) (Yoshioka et al., 2004; Ambawat et al., 2013; Roy, 2016; Wang, Niu and Zheng, 2021). Gel mobility shift assays also reveal that this Myb domain of LCR1 binds to the promoter of *CAH1*. In addition, the expression of *LCR1* is induced by LCO_2 levels and regulated by CIA5 (Yoshioka et al., 2004). It is therefore suggested to enhance and maintain the constant levels of CAH1 proteins in LCO_2 conditions (Yoshioka et al., 2004). However, this model has yet to be verified and other potential targets of LCR1 still remain unknown. Further research involving protein-protein interactions study techniques would be needed for deeper understanding of the regulatory role of LCR1 in the CCM.

Recently, the Ca^{2+}-binding protein CAS1 has been identified as crucial for the CCM and has been shown to upregulate the expression of *HLA3* and *LCIA* (Wang et al., 2016c). CAS1 is found distributed across the thylakoid membrane in HCO_2 and relocates to the pyrenoid tubules under limiting CO_2 conditions (Wang et al., 2016c; Yamano, Toyokawa and Fukuzawa, 2018). A mutant without CAS1 is found to have lower photosynthetic Ci affinity and is unable to upregulate *HLA3* and *LCIA* expression at LCO_2 (Wang et al., 2016c). Meanwhile, it is shown that Ca^{2+} concentration increases in the pyrenoid at LCO_2-light conditions and this process is also needed for the accumulation of the two HCO_3^- transporters under LCO_2 conditions. As CAS1 has been found to bind Ca^{2+} with low affinity but in high capacity (Trippens, Reißenweber and Kreimer, 2017), it could possibly be activated by the elevated Ca^{2+} in the pyrenoid to send a retrograde signal (meaning towards the nucleus) to positively regulate the expression of *HLA3* and *LCIA*, linking Ca^{2+} signalling directly to the CO_2-related response of some CCM genes.

The algal CCM is also regulated by light and the circadian clock. Studies have shown that the CCM is downregulated in the dark but induced in the light, and multiple CCM-related genes show circadian rhythm in their expression (Marcus et al., 1986; Mitchell, Meyer and Griffiths, 2014; Tirumani et al., 2014; Strenkert et al., 2019). For example, *LCIB* and *CAH3* expression are upregulated at the dark period just before the light phase begins (Mitchell, Meyer and Griffiths, 2014). The LCIB/LCIC complex and CAS1 also shows different localisations in dark and light in limiting CO_2 concentrations: they are distributed across the chloroplast stroma in dark but concentrated around the pyrenoid (LCIB) or inside the pyrenoid (CAS1) in light (Yamano et al., 2014; Wang et al., 2016c; Yamano, Toyokawa and Fukuzawa, 2018).

Finally, CO_2 and Ca^{2+} also serve as key regulators of the CCM. CO_2 concentration greatly affects the induction of the CCM. Limiting CO_2 conditions induce or upregulate the expression of many CCM-related genes such as *HLA3*, *LCI1* and *LCIA* (Brueggeman et al., 2012; Fang et al., 2012). In addition, as mentioned before, core CCM proteins LCIB/LCIC, CAH3 and CAS1 all show different localisations in HCO_2 vs limiting CO_2 conditions (Yamano et al., 2010; Blanco-Rivero et al., 2012; Wang and Spalding, 2014; Wang et al., 2016c; Yamano, Toyokawa and Fukuzawa, 2018). These all show that CO_2 concentration is a key regulator of the *Chlamydomonas* CCM on/off state. Meanwhile, the study on CAS1 reveals the importance of Ca^{2+} elevation in the pyrenoid for the accumulation of

the HCO_3^- transporters HLA3 and LCIA (Wang et al., 2016c), indicating the importance of Ca^{2+} signalling in the regulation of the CCM.

1.3.8 *Chlamydomonas* CCM- the unknown in CO_2 sensing and Ca^{2+} signalling

The past studies on the *Chlamydomonas* CCM have provided more guidance on what components should be engineered into C3 crop plants for a functional CCM. However, there are still unknown parts of it, including the mechanisms behind how the cell senses CO_2 levels and components involved in the Ca^{2+}-mediated regulation of the CCM. As the regulatory pathway involving Ca^{2+} signalling is most likely controlled by an upstream CO_2-sensing mechanism, understanding both parts would help illustrate the whole picture on the CO_2-related regulatory system of the CCM. This would allow the engineering of such a system to ensure a tight control of the algal CCM in an industrial setting or when introduced into a C3 crop plant. The next section will now focus on exploring the currently characterised CO_2-sensing mechanisms in different organisms, the possible components involved in CO_2 sensing in *Chlamydomonas* and those that link the Ca^{2+}-signalling pathway to the CO_2-dependant regulation of the CCM, with an aim of providing more background for the current project.

1.4 Dissecting the CO_2 sensing pathway in the *Chlamydomonas* CCM

CO_2 sensing is essential for the regulation of many important biological processes in the different life forms on earth. Studies have been carried out to identify what directly senses CO_2 and dissect the CO_2 sensing pathways in different organisms (Cummins et al., 2014). Many of the CO_2-sensing systems discovered share similar components and features, and these could be used as guidance on characterising the vastly unknown CO_2-sensing mechanism in *Chlamydomonas*.

1.4.1 CO_2 sensing mechanisms in different organisms

A common way of sensing CO_2 throughout different biological systems is the cooperative use of a CA to maintain CO_2/HCO_3^- equilibrium and a HCO_3^- or pH sensor for detection (Tresguerres, Buck and Levin, 2010; Buck and Levin, 2011; Cummins et al., 2014). There are also components that sense CO_2 directly (Cummins et al., 2014). These mechanisms have been extensively investigated in both photosynthetic and non-photosynthetic organisms.

The optimal living environment for bacteria is often the body of a multicellular organism, which usually contains CO_2 concentrations higher than air levels due to respiration. As a result, the ability to sense the changes in the surrounding CO_2 levels is important for bacteria to determine when to enhance their virulence for successful colonisation and infection of the host. For example, elevated CO_2 upregulates the expression of the AtxA regulon, which is required for induction of capsule and toxin gene expression, in the pathogen *Bacillus cereus* (Bongiorni et al., 2008; Passalacqua et al., 2009). In many bacteria, Ci species are sensed through Class III adenylyl cyclases (ACs). For instance, the ACs CyaB and Rv1319c of bacteria *Stigmatella aurantiaca* and *Mycobacterium tuberculosis* respectively are stimulated by HCO_3^- (Cann et al., 2003), while it has been shown that the ACs Slr1991 and CyaB1 of cyanobacteria *Synechocystis* PCC 6803 and *Anabaena* PCC 7120 are responsive to CO_2 directly (Hammer, Hodgson and Cann, 2006). It has also been shown that CA is needed for CO_2-dependent virulence induction. In the two biotypes of cholera-causing *Vibrio cholera*, classical and E1 Tor, the addition of CA inhibitor ethoxyaolamide causes a reduction in HCO_3^--responsive virulence activity induced by the ToxT protein, indicating the importance of CA catalysis of CO_2/HCO_3^- conversion (Abuaita and Withey, 2009). In another human pathogen, *Pseudomonas aeruginosa* PAO1, the psCA1 is shown to be important for survival in air CO_2 concentrations and might play a role in virulence (Lotlikar et al., 2013).

Fungi often experience large changes in environmental factors throughout their life cycles. These include the fluctuations in CO_2 environment. An efficient CO_2-sensing mechanism is vital for them to adapt to different habitats quickly. Once again, the coupling of CA and AC is a common system used for it. In the human pathogen *Cryptococcus neoformans*, the CA CAN2 is found to be required for growth in ambient air (natural environment) but not in elevated CO_2 (in a host) (Bahn et al., 2005), whereas the activation of its AC Cac1 by HCO_3^- is essential for capsule synthesis in both air and high CO_2 levels (Mogensen et al., 2006). These indicate that when CO_2 concentrations is limiting, conversion of CO_2 to HCO_3^- by CAN2 is required to stimulate Cac1 for capsule synthesis, while in high CO_2 levels, the spontaneous conversion between CO_2 to HCO_3^- is enough for activation of Cac1. A similar mechanism is also used in pathogenic *Candida albicans*, in which the AC Cyr1 (also called Cdc35) is stimulated by HCO_3^- to induce filamentation in high CO_2, while in low CO_2, equilibrium of CO_2 and HCO_3^- maintained by the CA NCE103 is required as well for such a process (Klengel et al., 2005; Hall et al.,

2010). The filamentation induced by Cyr1 also requires regulation by the GTPase Ras1 and the tricarboxylic acid (TCA) cycle through enhancement of Cyr1 activity, in which the latter could be activated by CO_2/HCO_3^- directly (Fang and Wang, 2006; Tao et al., 2017). On the other hand, recent studies have shown there is also a CO_2-sensing pathway independent of AC in *C. albicans* and other yeasts like *Saccharomyces cerevisiae* (Du et al., 2012; Pohlers et al., 2017). In this pathway, the AGC (homologous to protein kinases A, G and C) family protein kinase Sch9 plays a repressor role in inhibiting the expression of NCE103 in high CO_2 conditions by phosphorylation-induced inhibition of the transcription factor Cst6/Rca1 of the CA. Sch9 itself is activated by the upstream kinases Pkh1 and Pkh2, homologues of the mammalian 3-phosphoinositide-dependent protein kinase. These kinases are therefore proposed to sense the rise in CO_2 to activate Sch9 to create downstream signalling cascade to repress *NCE103* expression. As Pkh1/2 activity is influenced by phytosphingosine and phosphatidylinositol, it is considered that lipid signalling also plays a role in the CO_2-mediated regulation of NCE103.

In plants, the stomata act as a main entrance for CO_2 into the leaf for subsequent fixation in the CBB cycle. At the same time, they also facilitate water loss through transpiration. To ensure adequate CO_2 entry with minimised water loss, the opening size of the stomata must be tightly regulated. This is done by the guard cells surrounding them and is mediated by a number of environmental factors including plant hormone abscisic acid (ABA) and CO_2 (Engineer et al., 2016). High CO_2 concentrations will trigger stomatal closure, whereas low CO_2 concentrations stimulate the opening of the stomata. The current model for the mechanism behind CO_2-induced stomatal closure suggests that carbonic anhydrases CA1 and CA4, and the MATE (Multidrug And Toxic compound Etrusion) transporter-like protein RHC1 are needed for CO_2 sensing in the process (Engineer et al., 2016). CA1 and CA4 are β-CAs located at guard cell chloroplasts and the plasma membrane respectively (Hu et al., 2015). Double mutants of the two CAs show impaired CO_2-related stomatal changes, which can be restored by introducing either CA1 or CA4 into them (Hu et al., 2010). RHC1 (Resistant to High Carbon dioxide 1) is found at the plasma membrane of guard cell and is shown to interact with CA4 directly (Tian et al., 2015). RHC1 is also essential for downstream HCO_3^- activation of S-type anion channels, which induces stomatal closure directly. The activation of S-type anion channels is also affected by ABA-induced signalling pathway and increased sensitivity of Ca^{2+} signals, though these are independent of RHC1 regulation and other CO_2-sensing

mechanisms are most likely involved (Engineer et al., 2016). In addition, expression of RHC1 alone in *Xenopus laevis* oocytes is enough to create anion channel currents in the cells (Wang et al., 2016b), although this is not dependent on HCO_3^-. These studies therefore propose that the activation of RHC1 by HCO_3^- generated from surrounding and intracellular CO_2 through catalytic action of CA1 and CA4 is the upstream CO_2-sensing mechanism in guard cells for mediating CO_2-related stomatal closure.

In animal systems, CO_2 sensing is very important for regulation of different physiological processes. Once again, the coupling of a CA and a HCO_3^- or pH sensor is a mechanism widely used for it. Carbonic anhydrase II (CAII) is needed for the sensing of CO_2 in mammalian systems like the olfactory sensory neurons and cone cells in mice (Sun et al., 2009; Duda et al., 2015; Duda, Pertzev and Sharma, 2018). In sour taste receptor cells, carbonic anhydrase IV is present instead to convert CO_2 to HCO_3^- and H^+, of which the H^+ is then sensed by ion channel PKD2L1 to initiate downstream CO_2-related response (creating a taste of carbonation) (Chandrashekar et al., 2009). On the other hand, the HCO_3^--sensitive cAMP and cGMP pathways are also used for CO_2 sensing in many animal systems. Soluble adenylyl cyclase (sAC) is an important HCO_3^- sensor in different biological processes, such as sperm capacitation and motility for fertilisation (Chen et al., 2000; Esposito et al., 2004; Hess et al., 2005; Xie et al., 2006), as well as mitochondrial response to CO_2 generated by Krebs Cycle (Acin-Perez et al., 2009a, 2009b). It has also been shown that mammalian AC can be activated directly by CO_2 (Townsend et al., 2009), suggesting that some systems might not require a CA for detecting CO_2 change. Guanylyl cyclase (GC), or guanylate cyclase, is also used in different animals for sensing CO_2. Examples include guanylyl cyclase-D (GC-D) of mice olfactory sensory neurons and ROS-GC1 of cone cells (Sun et al., 2009; Duda et al., 2015; Duda, Pertzev and Sharma, 2018). In the nematode *Caenorhabditis elegans*, the receptor-type guanylate cyclase GCY-9 in the BAG neurons is responsible for sensing CO_2 to initiate avoidance behaviour towards CO_2 (Hallem et al., 2011). One thing of note is that in some of the animal CO_2 or HCO_3^- sensing pathways synergises with Ca^{2+} signalling pathways in inducing cAMP or cGMP production, as seen in sperm cells and cones (Jaiswal and Conti, 2003; Duda, Pertzev and Sharma, 2018).

CO_2 sensing is also essential in aquatic organisms due to the rapid fluctuations between CO_2 and HCO_3^- concentrations in the water. Again, the coupled action of a CA and sAC is

found to be essential for this as found in different aquatic animals like sharks and boney fishes (Tresguerres et al., 2014). A recent study also shows that the CgsAC of pacific oyster *Crassostrea gigas* is found to be needed for sensing ocean acidification caused by elevated CO_2 levels (Wang et al., 2016d). In the diatom *Phaeodactylum tricornutum*, it is found that cAMP accumulation is required for sensing increased CO_2 in regulation of CO_2 acquisition (Harada et al., 2006). A GUS expression assay showed that the core regulatory region of PtCA1, a β-CA regulated by air CO_2 and light and considered to be an important CCM component in the pyrenoid, is inhibited by enrichment of cAMP. Further investigation suggests that cAMP inhibits *PtCA1* expression via the putative cAMP-response element CRE1 in HCO_2 condition. However, the AC responsible for this regulatory pathway has not been identified yet. A more recent study identified the more precise regions of the CO_2-cAMP-Responsive Element1 (CCRE1), CCRE2 and CCRE3 in PtCA1 and found that the transcription factor PtbZIP11, which contains a basic zipper (bZIP) region homologous to that of human ATF6 (Activating Transcription Factor6), bound specifically to them (Ohno et al., 2012). As PtbZIP11 is constitutively expressed in both high and air CO_2, the study suggests that it is activated by cAMP in HCO_2 by post-translational regulation to bind to CCREs and repress *PtCA1* expression.

1.4.2   Possible CO_2-sensing components in *Chlamydomonas*

As seen in many CO_2-sensing systems, the coupling of a CA and AC or GC is a common way of sensing CO_2. There are at least 15 genes translating the many CA isoforms in *Chlamydomonas* and some of them are very likely to participate in CO_2-sensing pathways (Moroney et al., 2011; Aspatwar, Haapanen and Parkkila, 2018). Meanwhile, *Chlamydomonas* has 51 members of class III ACs and GCs family, which is also the largest gene family in the alga (Merchant et al., 2007). All these suggest that *Chlamydomonas* could utilise CA and AC/GC to sense CO_2 changes, similar to bacterial, fungal and animal systems. Here, a few CO_2-sensing candidate components in the alga are listed out.

As discussed in section 1.3.7, CIA5 could sense CO_2 directly or through an CO_2 sensor upstream. On the other hand, two of the proteins found to interact with HLA3 in an interactome study by Mackinder et al., 2017 could also be potential CO_2 sensing candidates. One is an EF-hand-containing protein kinase that is dependent on Ca^{2+}/calmodulin named CDPK13 (Calcium-Dependent Protein Kinase 13, Cre13.g571700). As the Ca^{2+}-binding CAS is found to be responsible for CO_2-related gene expression

change of *HLA3*, this kinase could be involved in post-translational modification of HLA3 in response to different CO_2 levels and potentially sense CO_2 directly. The other protein is the adenylyl/guanylyl cyclase CYG63 (Cre05.g236650). Since it interacts with a core CCM protein, it is highly possible that it is involved in sensing HCO_3^-, the downstream signal of CO_2, in the CCM.

The flagella of *Chlamydomonas* could potentially play a role in CO_2 sensing as well. Flagella are important for the motility of the alga in response to environmental cue, such as light (Silflow and Lefebvre, 2001). Chemotaxis of *Chlamydomonas* towards HCO_3^- has been shown by a recent study (Choi et al., 2016). As the CA CAH6 is found to localise in the algal flagella (Mackinder et al., 2017), it is possible that the flagella senses CO_2/HCO_3^- through CAH6 and other proteins (HCO_3^- or pH sensors) in it. Interestingly, the chemotactic response towards HCO_3^- is lost when *CIA5* is mutated in the alga (Choi et al., 2016), once again suggesting the important role of CIA5 in mediating CO_2-sensitive responses.

1.4.3 Ca^{2+} pathway and CO_2 sensing in the *Chlamydomonas* CCM

As mentioned before, the second messenger Ca^{2+} is also an important regulator of the *Chlamydomonas* CCM. However, the mechanism behind the regulation of the CCM by the Ca^{2+} signalling pathway remains unclear. Ca^{2+} is found to be important for the initiation of the algal CCM, possibly through CAS1-upregulation of HLA3 and LCIA (Wang et al., 2016c). As this regulation is induced under LCO_2 conditions, there must be upstream CO_2-sensing components that regulate this Ca^{2+} transduction pathway. Thus, dissecting the Ca^{2+}-signalling pathway involved in the CCM could help identify these components. So far, only CAS1, TRP2, and CDPK13 have been identified that could participate in Ca^{2+}-related regulation of the CCM.

Section 1.3.7 explained how CAS1 can link Ca^{2+} signalling and CCM regulation together through Ca^{2+}-activated retrograde signalling to the nucleus. However, little is known about what upstream components regulate the elevation of Ca^{2+} in the pyrenoid needed for the CCM function of CAS1. Identifying them would not only help clarify the mechanism behind Ca^{2+}-dependent accumulation of HLA3 and LCIA, but also help discover the possible CO_2 sensor in the *Chlamydomonas* CCM.

Recently, a putative Ca^{2+} channel, TRP2 (Transient Receptor Potential), was found to be needed for acclimation to limiting CO_2 in *Chlamydomonas* cells (Christensen et al., 2020). CIA5 is needed for the expression of TRP2 and the expression is further upregulated in LCO_2. Mutation of TRP2 led to a downregulation of CAS1. In addition, it is predicted to locate to the chloroplast and contain the *transient receptor ion channel II* domain, which has been shown to allow passing of Ca^{2+} ions (Vannier et al., 1999; Christensen et al., 2020). Therefore, it is proposed that TRP2 is a Ca^{2+} channel that plays a role in the regulation of the CCM. However, experimental evidence showing the channel property of TRP2 for Ca^{2+} is not established yet. Further study is needed to further characterise the function of TRP2 in the Ca^{2+}-signalling pathway in the CCM.

In the meantime, as described in section 1.4.2, CDPK13 is a putative Ca^{2+}/calmodulin-dependent protein kinase that is found to interact with HLA3 (Mackinder et al., 2017). Although CDPK13 might sense CO_2 directly, it might also be activated by Ca^{2+}/calmodulin mediated by upstream CO_2-sensing mechanism to post-translationally regulate HLA3 at the plasma membrane. Therefore, linking Ca^{2+} signalling to the initiation of the CCM.

Since many Ca^{2+} signalling components identified in biological systems and the interplay between Ca^{2+} and CO_2 signalling has been established in terrestrial plants such as the regulation of stomatal closure *Arabidopsis* (Hubbard et al., 2012; Engineer et al., 2016), looking into these well-studied Ca^{2+} transduction system in other organisms could help identify candidate genes involved in the Ca^{2+} signalling pathway active in the *Chlamydomonas* CCM.

1.5   The current project

The successful dissection of the CO_2-sensing and Ca^{2+}-signalling pathways in *Chlamydomonas* would help establish a tight regulatory system of the CCM when engineering into a C3 crop plant. This laid the foundation for the principal aim of the project: to identify the pathways involved in CO_2-sensing and Ca^{2+}-signalling for a better understanding of CCM induction in *Chlamydomonas reinhardtii*. The objectives of the project were to: identify proteins that sense Ci or participate in the CO_2-mediated Ca^{2+} transduction pathway in *Chlamydomonas*; locate the main site of function of these proteins; identify their function and downstream targets in *Chlamydomonas*; and construct a complete CO_2-sensing/Ca^{2+}-signalling pathway in the *Chlamydomonas* CCM.

A targeted reverse genetics approach was adopted to identify a set of target genes for characterisation. The experiments and data analysis conducted in the project are grouped into three main experimental chapters, chapters 2-4, and outlined as follows.

Chapter 2 involves the identification of candidate genes with potential roles in CO_2 sensing or Ca^{2+} signalling pathway needed in the *Chlamydomonas* CCM by finding homologues of characterised CO_2 sensors and Ca^{2+} transporters from other species through BLAST. *Chlamydomonas* mutants of these genes were then screened in a growth assay with different CO_2 conditions to identify those with potential CCM function. Using the growth assay screen and further *in silico* analysis including domains and structure prediction, and phylogeny tree analysis, three proteins, CDPK13, CGLD1 (Conserved in the Green Lineage and Diatoms 1, Cre02.g084350) and CPLD63 (Conserved in Plantae and Diatoms 63, Cre16.g660000), were identified as potential components that could link Ca^{2+}-signalling to the CCM.

Chapter 3 focuses on the characterisation of CGLD1 and CPLD63, the homologues of *Arabidopsis* Ca^{2+} transporters BICAT1 and 2 as well as yeast Ca^{2+} transporter Gdtp1, in *Chlamydomonas*. Further comparison between CGLD1 and CPLD63 and their homologues in *Arabidopsis* and yeast were performed through alignments of their protein sequences and predicted 3D structure models to confirm they could potentially transport Ca^{2+}. Growth assay screen of the mutants and their complemented lines were conducted in different Ca^{2+} and Mn^{2+} concentrations to study which ions are associated with the functions of the proteins in the CCM and whether the phenotypes of the mutants were caused by the disruption of the genes. Confocal microscopy was used to check the localisation of the two in *Chlamydomonas* cells. Finally, attempts had been made to visualise Ca^{2+} ions in the pyrenoid of WT and mutants of *CGLD1* and *CPLD63*, as well as expressing CGLD1 and CPLD63 in bacterial system for Ca^{2+} influx assay to check whether they have Ca^{2+} transporting activity.

Chapter 4 investigates the traits of core CCM genes in the *cgld1* and *cpld63* mutants. The expression of selected CCM genes including *HLA3*, *LCIA* and *CAS1* in LCO_2 were studied in WT and mutants using qRT-PCR. Their expression data were then compared to literature data. The relocalisation of LCIB and CAS1 in LCO_2 was also visualised and quantified in these strains. Together, downstream CCM genes potentially regulated by

CGLD1 and CPLD63 were identified, aiding in constructing the hypothesis on the potential roles of these two proteins in the CCM.

2 Mutant screening identifies CDPK13, CGLD1 and CPLD63 as potential regulators of the *Chlamydomonas* CCM

2.1 Abstract

The green alga *Chlamydomonas* lives in diverse habitats where CO_2 concentration can range from enriched to depleted. To cope with the restrain on its photosynthetic activity caused by limiting CO_2 level, *Chlamydomonas* evolved a CCM that enables the concentration of CO_2 around Rubisco through active Ci uptake. CO_2 concentration and Ca^{2+} signals have been found to be important regulators of the algal CCM, but the components involved in CCM-related CO_2 sensing or Ca^{2+} signalling remain greatly uncharacterised. *Chlamydomonas* mutants of three genes- *CDPK13*, *CGLD1* and *CPLD63*- were found to have a disturbed CCM. CDPK13 is a putative Ca^{2+}/calmodulin-dependent protein kinase that has been found previously to interact with the CCM HCO_3^- transporter HLA3 in *Chlamydomonas*. CGLD1 and CPLD63 were found to be part of the UPF0016 protein family, in which some members have been identified as Ca^{2+} transporters in different species. These proteins could link Ca^{2+}-signalling to the *Chlamydomonas* CCM as CDPK13 could be involved in regulating HLA3 post-translationally through Ca^{2+}/calmodulin-dependent phosphorylation, while CGLD1 and CPLD63 could act as putative Ca^{2+} transporters essential for initiating a Ca^{2+} induced retrograde signal from the chloroplast to the nucleus needed for the regulation of the CCM.

2.2 Introduction

Chlamydomonas is a single-celled green alga with two flagella and lives in temperate soil habitats (Sasso et al., 2018). It can grow in the dark when carbon source is available, but can also photosynthesise in light to produce carbon for its growth. When environmental CO_2 becomes limiting (its concentration reaches below 0.5%), the photosynthetic activity in the alga can become constricted as the carboxylation catalytic activity of Rubisco becomes limited by the low CO_2 concentration and also outcompeted by its oxygenase activity due to the higher O_2/CO_2 ratio. To ensure its survival in such situations, *Chlamydomonas* activates its CCM to actively transport Ci, which include CO_2 and HCO_3^-, from the surroundings into the cell to concentrate CO_2 around Rubisco that is aggregated inside a non-membrane-bound organelle in the chloroplast called the pyrenoid (Badger, Kaplan and Berry, 1980; Badger et al., 1998; Meyer et al., 2012; Mackinder et al., 2016). Considerable research has been conducted to identify different components of the *Chlamydomonas* CCM in the hope of engineering a functional CCM into C3 crop plants to enhance photosynthesis for higher crop yield (Wang, Stessman and Spalding, 2015; Rae et al., 2017; Mackinder, 2018). Multiple CCM components that contribute to the active Ci uptake and transport system as well as the aggregation of Rubisco inside the pyrenoid have been identified. However, only a few regulatory components have been found. As mentioned in Chapter 1, these include CIA5, LCR1, and CAS1. And even for these regulators the molecular details of their regulatory mechanism in the CCM are still not fully established. It is necessary to study more on the regulation of the *Chlamydomonas* CCM as it could provide methods to tightly control the on/off state of the CCM either in an industrial setting to boost bioproducts production or when it is successfully engineered into a C3 crop plant.

A key regulator of the *Chlamydomonas* CCM is CO_2 concentration. As CO_2 concentrations can fluctuate between high and limiting in its native environment, *Chlamydomonas* needs to be able to turn on or off its CCM to acclimate. This acclimation response can be seen in the molecular and physiological changes of the alga across different CO_2 levels. As described in Chapter 1, limiting CO_2 conditions induce or upregulate the expression of many CCM-related proteins such as the Ci transporters HLA3, LCI1 and LCIA (Brueggeman et al., 2012; Fang et al., 2012). They can also induce the relocalisation of essential CCM proteins LCIB, CAS1 and CAH3 (Yamano et al., 2010; Blanco-Rivero et al., 2012; Wang and Spalding, 2014; Wang et al., 2016c). In addition, the CCM proteins

exhibit different levels of significance in the operation of the mechanism at different CO_2 acclimation states: an HCO_3^- uptake system dependent on HLA3, LCIA and LCIB at $VLCO_2$ (Wang and Spalding, 2014; Yamano et al., 2015), and a CO_2 uptake system reliant on LCI1 and LCIB in LCO_2 (Duanmu, Wang and Spalding, 2009; Gao et al., 2015; Wang and Spalding, 2014; Kono et al., 2020). Collectively, these suggest the presence of a versatile regulatory mechanism that can sense the change in environmental CO_2 levels and rapidly respond to it by turning the CCM on or off. Nevertheless, there is currently little known about how *Chlamydomonas* senses CO_2. One possible approach would be to look at the different CO_2 sensors already found in other biological systems and characterise their homologues in *Chlamydomonas*.

CO_2 sensing is essential for the regulation of many important biological processes in the different forms of life on earth. Again as mentioned in Chapter 1, different studies have contributed to the identification of what directly senses CO_2 and dissecting the CO_2 sensing pathways in different organisms (Cummins et al., 2014). Many of the CO_2-sensing systems discovered share similar components and features. For example, the cooperative use of a carbonic anhydrase (CA) to maintain CO_2/HCO_3^- equilibrium and a HCO_3^- or pH sensor for detection to sense CO_2 can be found in different organisms (Tresguerres, Buck and Levin, 2010; Buck and Levin, 2011; Cummins et al., 2014). Many actual examples of these components and features have been described in previous chapter. They could be used as guidance on characterising the vastly unknown CO_2-sensing mechanism in *Chlamydomonas*.

Another important regulator of the *Chlamydomonas* CCM is the second messenger Ca^{2+}. The mechanism linking the regulation of the CCM and Ca^{2+} signalling is poorly understood. As explained before Ca^{2+} is first found to be important for the initiation of the algal CCM in a study by Wang et al., (2016c). Using a Ca^{2+}-sensitive fluorescent dye to visualise the ion in *Chlamydomonas* cell, they discovered that Ca^{2+} accumulates in the pyrenoid when transferred from HCO_2 to LCO_2 in light. They also showed that when extracellular Ca^{2+} is depleted, the upregulated expression of HLA3 and LCIA required for the CCM is hindered. These both suggest that Ca^{2+} signal transduction plays a significant role in regulating the algal CCM. Again, as mentioned in Chapter 1, three components have been identified that might participate in Ca^{2+}-related regulation of the CCM: the Ca^{2+}-binding CAS1 that is also needed for HLA3 and LCIA accumulation in LCO_2; the putative Ca^{2+} channel TRP2

that is needed for the algal limiting CO_2 acclimation and the expression of CAS1 in LCO_2; and CDPK13, the putative Ca^{2+}/calmodulin-dependent protein kinase found to interact with HLA3 at the plasma membrane and hypothesised to be a post-translational regulator of the transporter. However, there are still many unknowns about the full pathway linking Ca^{2+} signalling to CO_2-sensing, such as what components regulate the Ca^{2+} elevation in the pyrenoid during the CCM, or experimental evidence that confirm the roles of TRP2 and CDPK13 in Ca^{2+} signal transduction.

Since the mechanism that utilises Ca^{2+} as a second messenger to control the CCM is likely regulated by an upstream CO_2 sensor, dissecting the CCM-related Ca^{2+} signalling pathway could possibly help find members of the CO_2-sensing pathway. As the link between Ca^{2+} and CO_2 signalling has been established in other organisms before (Hubbard et al., 2012; Engineer et al., 2016), looking into the discovered components involved in Ca^{2+} signals transduction in these organisms could help identify candidate genes involved in the Ca^{2+} signalling pathway needed in the *Chlamydomonas* CCM.

This study aims to identify components involved in the CCM-related CO_2 sensing and Ca^{2+} signalling pathways in *Chlamydomonas*. A list of candidate genes was first established by a search of for *Chlamydomonas* homologues of already discovered CO_2 sensing and Ca^{2+} signalling related genes in other biological systems. *Chlamydomonas* mutants of these homologues were obtained and tested in a growth assay to discover the strains with a disturbed CCM and hence the genes that might be important in the functioning of the CCM. This helped narrow down the list of candidate genes for further characterisation in Chapters 3 and 4.

2.3 Materials and Methods

2.3.1 Algal strains and culture conditions

Chlamydomonas strain CC-4533 was used as the wild type (WT). This strain was also used as the background strain for generating the mutants in the *Chlamydomonas* Library Project (CLiP) database (https://www.chlamylibrary.org/) (Li et al., 2016). The WT was maintained on the shelf under constant light of ~5-10 µmol photons m^{-2} s^{-1} on Tris-acetate-phosphate (TAP) medium agar plate with revised Hutner's trace elements (Kropat et al., 2011) without antibiotics while the CLiP mutants were maintained on the same medium with 20 µg ml^{-1} paromomycin at 21°C in a temperature-controlled room. When transferred to liquid culture for experiments, 2 µg ml^{-1} paromomycin was used.

2.3.2 Identification of candidate genes and their mutants

Important CO_2-sensing and Ca^{2+}-signalling components from other organisms were identified from the literatures (Table 2.1). A BLAST alignment was done between the protein sequences of these components and the *Chlamydomonas* reference peptide sequence to find homologous genes (NCBI Resource Coordinators, 2016). These genes, together with CDPK13 (CDPK13) and CYG63 (Cre05.g236650) formed a list of CO_2-sensing candidate genes. The available mutants of these genes were identified in the CLiP database, which also contains information on the site of insertion and the confidence of the insertion (Li et al., 2016).

2.3.3 Spot test of mutants

The CLiP mutants of candidate genes were first cultured heterotrophically in liquid TAP medium with 2 µg ml^{-1} paromomycin. *Chlamydomonas* WT strain was also cultured at the same time in liquid TAP medium. For light-dark cycle spot tests, cultures were first synchronised in a 12:12 light:dark cycle at ~130 µmol photons m^{-2} s^{-1} light intensity until their density reached ~2-6 x 10^6 cells ml^{-1}. In order to make sure they were synchronised, their cell density was monitored daily until it was certain that cell division occurred just after light-dark transition, which is a trait of 12:12 light:dark cycle synchronization (Cross and Umen, 2015; Zones et al., 2015). For constant light spot tests, cultures were incubated under constant light of ~50 µmol photons m^{-2} s^{-1}. Before the spot test, 10^6 cells for each strain were first centrifuged (1500 x g, 10 min, room temperature). The supernatant was discarded and the cell pellet was re-suspended in 200 µl of Tris-phosphate (TP) minimal medium. The cells were spun down again (1500 x g, 5 min, room

temperature) to wash out residual TAP medium. The supernatant was discarded and the cell pellet was re-suspended in 1 ml TP medium. The cells were then diluted by 1:10, 1:100 and 1:1000 so that a series of dilutions of cells (1000, 100, 10) could be used in the spot test. 10 µl of each dilution was pipetted twice separately (to create duplicates) onto a TP agar plate with set pH per mutant for one experimental condition. The plate was then incubated at different CO_2 conditions for a total of 7 to 8 days under either the 12:12 light:dark cycle for the synchronised cells, or constant light for the non-synchronised cells. The light intensity was changed from low light to high light gradually to allow the cells to slowly adapt to the high light intensity: 50 µmol photons m^{-2} s^{-1} intensity for the first 24 h, 150 µmol photons m^{-2} s^{-1} intensity for the next 24 h, and 400 µmol photons m^{-2} s^{-1} intensity for the following days. Each strain was tested at three different pH- 7.4, 7.8 or 8.0- in either HCO_2 (3%), LCO_2 (0.04%) or $VLCO_2$ (0.01%). WT cells were spotted on each plate as a positive control and for comparison to the growth of the mutants. As a positive control for growth, all strains were also spotted on a TAP agar plate and cultured under either 12:12 light:dark cycle or constant 50 µmol photons m^{-2} s^{-1} light at air levels of CO_2 for as long as the spot test was carried out. After narrowing down the number of candidate genes to study from the initial tests, the corresponding mutants were screened again with the addition of mutant *epyc1* as a negative control. All plates were imaged with an Epson Perfection V370 Photo scanner after the experiment.

2.3.4 Structural and functional prediction of candidate genes

The candidate genes of mutants showing interesting phenotypes in the initial spot tests were selected for further analysis. Their protein sequences were extracted from the Phytozome database (https://phytozome.jgi.doe.gov/pz/portal.html) and submitted to Pfam (http://pfam.xfam.org) for domain prediction. The different bioinformatics analysis listed on Phytozome database for these proteins were also studied to check their predicted structures and functions.

After further spot tests, the list of candidate genes was narrowed down to CDPK13, CGLD1 and CPLD63. The protein sequence of CDPK13 was submitted to Phyre2 (Kelley et al., 2015) for 3D structure prediction. The 3D structure models predicted in Phyre2 were visualised and edited using PyMol (https://pymol.org/2/). On the other hand, the protein sequences of CGLD1 and CPLD63 were submitted to TMHMM v.2.0

(http://www.cbs.dtu.dk/services/TMHMM/) for transmembrane region prediction. The sequences of all three proteins were submitted to PredAlgo (Tardif et al., 2012) and Target2.0 (Armenteros et al., 2019) to predict their localisation in *Chlamydomonas*.

2.3.5 Mutant gDNA extraction and insertion site verification

The mutants from the CLiP database are generated by the random insertion of a DNA cassette- the CIB1 cassette- in the *Chlamydomonas* genome (Li et al., 2016, 2018). To ensure that the ordered CLiP mutants were the correct mutants, the insertion sites of the CIB1 cassette in their target genes were checked by genome-cassette junction PCR (Polymerase Chain Reaction) of their genomic DNA (gDNA) using the method described by Li et al., 2018. The primers used (Appendix A, Table A.1) were either the referenced ones listed on the CLiP website or were designed using the software Geneious (download site https://www.geneious.com) (Kearse et al., 2012). To extract gDNA, single colony of the mutant was picked from the maintained TAP agar plate and first resuspended in 50 µl 10 mM EDTA and then vortexed for 30 s. The sample was then incubated in a thermocycler at 100°C for 10 min, cooled down to 4°C for at least 1 min then centrifuged at 1000 x g for 1 min. 40 µl of the supernatant, which contained the gDNA, was taken out from the centrifuged sample. The gDNA was then used for mutant verification or stored at -20°C if the verification was not done straight away. The PCR was carried out in 25 µl reaction volume containing the following reagents: 12.5 µl OneTaq Hot Start Quick-Load 2X Master Mix with GC Buffer (NEB, #M0489S), 1.25 µl OneTaq High GC Enhancer (NEB, #B9026A), 1.25 µl each of forward and reverse primers, 1 µl gDNA, and 9 µl MilliQ water. DNA was PCR amplified as follows: 94°C initial denaturation for 5 min, 38-40 cycles of 30 s 95°C denaturation, 45 s 57°C annealing and 1 min and 30 s 72°C extension, then 72°C final extension for 10 min and 4°C hold. The PCR products were all checked on 1% agarose gel (ethidium bromide was used for staining). The amplified genome-cassette fragments were sent to ATCC for sequencing to determine the site and orientation of CIB1 insertion.

2.3.6 Phylogenetic trees construction

Members of *Chlamydomonas* CDPKs (including CDPK13), and selected human, yeast and *Arabidopsis* protein kinase representatives from each family as catalogued by Manning et al., 2002, and Lehti-Shiu and Shiu, 2012, and other characterised kinases from *Chlamydomonas* and *Arabidopsis* were first identified from the literature (Shiu and

Bleecker, 2001; Berman et al., 2003; Depège, Bellafiore and Rochaix, 2003; Wilson and Lefebvre, 2004; Pollock et al., 2005; Mori et al., 2006; Gokhale, Wirschell and Sale, 2009; Pesaresi et al., 2009; Lemeille et al., 2010; Lehti-Shiu and Shiu, 2012; Hamel, Sheen and Séguin, 2014; Li et al., 2019b). The kinase domain sequences from the human and yeast members were obtained from http://kinase.com/web/current/ and those from *Chlamydomonas* and *Arabidopsis* were obtained from the supplementary data of Lehti-Shiu and Shiu, (2012) or Pfam (http://pfam.xfam.org). Multiple sequence alignment was performed using the ClustalW algorithm on the MEGA X software (Kumar et al., 2018). For CGLD1 and CPLD63, protein sequences were blasted against available NCBI database to obtained homologues from other species (NCBI Resource Coordinators, 2016). Multiple sequence alignments of CGLD1 and CPLD63 with their respective homologues were performed using the ClustalW algorithm on Geneious 11.1.5 (https://www.geneious.com) (Kearse et al., 2012). A phylogenetic tree was constructed from each alignment using the MEGA 11 software with a maximum likelihood method and 1000 bootstrap replicates (Tamura, Stecher and Kumar, 2021). The visualisation of the trees were edited using the online software iTOL (Letunic and Bork, 2019)

2.4 Results

2.4.1 Identifying CO_2-sensing and Ca^{2+} signalling-related candidate genes

An initial list of CO_2-sensing components from different organisms was constructed from a literature search (Table 2.1). Homologues in *Chlamydomonas* were identified via BLAST and are summarised in Table 2.1. In addition, extra genes were added to the list because of their potential roles in sensing Ci or in the Ca^{2+} signaling pathway involved in the regulation of the algal CCM. These genes includes: *CDPK13* and *CYG63*, a Ca^{2+}/calmodulin-dependent kinase and an adenylyl/guanylyl cyclase found to interact with HLA3 in the study by Mackinder *et al.*, 2017; *CGLD1* and *CPLD63*, homologues of the *Arabidopsis* Ca^{2+} transporters *Bivalent Cation Transporter 1* (*BICAT1*) and *BICAT2* (Frank et al., 2019); and *CIA5* and *LCR1*, the master regulator and one of the downstream regulators of many CCM genes.

Table 2.1 CO_2 sensors in different biological systems and their homologues in *Chlamydomonas*

Biological system	Group	CO_2 sensor(s)	Reference(s)	*Chlamydomonas* homologous
Mycobacterium tuberculosis	bacteria	Rv1319c (AC)	(Cann et al., 2003)	Cre12.g547351
Stigmatella aurantiaca	bacteria	CyaB	(Cann et al., 2003)	Cre09.g412600 (CYG52)
Anabaena PCC 7120	cyanobacteria	CyaB1	(Cann et al., 2003)	Cre13.g605100 (PDE20), Cre14.g612200 (CYG16)
Synechocystis PCC 6803	cyanobacteria	Slr1991 (AC)	(Hammer, Hodgson and Cann, 2006)	N/A
Cryptococcus neoformans	fungi	CAN2 (CA), Cac1 (AC)	(Bahn et al., 2005; Mogensen et al., 2006)	Cre13.g607350 (CAH7), Cre09.g405750 (CAH8), Cre16.g676800
Candida albicans	fungi	NCE103 (CA), Cyr1 (AC)	(Klengel et al., 2005; Hall et al., 2010)	Cre02.g092150

Plant guard cell	plant	CA1 and CA4 (CAs), RHC1 (MATE transporter-like protein)	(Hu et al., 2010, 2015; Tian et al., 2015; Engineer et al., 2016)	Cre09.g415700 (CAH3), Cre13.g580750
Sperm cell	animal	Mammalian sAC	(Chen et al., 2000; Jaiswal and Conti, 2003; Esposito et al., 2004; Hess et al., 2005; Xie et al., 2006)	N/A
Mice olfactory sensory neurons	animal	CAII (CA), guanylyl cyclase-D (GC-D)	(Sun et al., 2009)	Cre07.g348650 (CYG65), Cre09.g387200 (CYG28), Cre09.g387350 (CYG30)
Cone cells	animal	CAII (CA), ROS-GC1 (GC)	(Duda et al., 2015; Duda, Pertzev and Sharma, 2018)	Same as previous one
Caenorhabditis elegans BAG neurons	animal	GCY-9 (receptor-type GC)	(Hallem et al., 2011)	Cre07.g348650 (CYG65)
Sour taste receptor cells	animal	Carbonic anhydrase IV, ion channel PKD2L1	(Chandrashekar et al., 2009)	Cre17.g715300 (PKD2)
Crassostrea gigas	animal	CgsAC	(Wang et al., 2016d)	Cre01.g053450 (CYA1)

2.4.2 Initial spot tests of CLiP mutants of candidate genes

To find out whether the candidate genes played a role in the *Chlamydomonas* CCM or not, an initial spot test of available CLiP mutants of these genes was conducted first. The genes and the corresponding mutants tested are summarised in Table 2.2. At least one mutant was obtained for all the candidate genes with the following priorities: insertion site in CDS (coding sequence) or intron and with mapping confidence ≥73%, except for *CAH3* due to growth failure of the received mutant.

The initial spot test was carried out in different batches due to limited space but the settings were kept as close as possible. The conditions were also a bit different between the assay of *cdpk13* and *cyg63* mutants and the assay of the other mutants: the former

test was conducted under continuous light and pH 7.4, 7.8, 8 and 8.4 while the latter was conducted under a 12:12 light:dark cycle and pH 7.4, 7.8 and 8. The change in light setting was explored as it has been shown that the CCM response in synchronised cells can be different to asynchronous cells: the two groups have different transcriptional patterns of CCM genes (Mitchell, Meyer and Griffiths, 2014). The pH settings were adjusted as WT cells did not grow well in pH 8.4 in limiting CO_2 conditions. The mutant *cdpk13-2* was also was also screened again in one of these tests as it was found to exhibit a CCM phenotype (Appendix A, Figure A.1) - in which it can grow as well as WT in HCO_2 but cannot do so in LCO_2 or/and $VLCO_2$ - from the initial screen of *cdpk13* and *cyg63* mutants.

When looking at the results of the spot test, it is important to compare the strains on the same plate to reduce the influence of technical difference between different plates. Therefore, the growth phenotypes of the mutants at each condition were compared to that of the WT on the same plate. The initial screen showed that a total of 12 mutants exhibited variations of CCM phenotypes (Figure 2.1 and Table 2.2), whereas the rest had the same phenotype as WT (Appendix A, Figure A.2-Figure A.5). When compared to the WT on the same plate, *cah7* had a slightly reduced growth only in $VLCO_2$ condition at all pH levels, while strain cLM164 displayed a more reduced growth in both limiting CO_2 conditions at all pH levels. Strain cLM166 and *cyg52-1* showed little to no growth in limiting CO_2 conditions at all pH levels except in LCO_2 and at pH 7.8, where cLM166 actually had similar growth as WT and *cyg52-1* had a slightly reduced growth only. On the other hand, *cyg16-1* and *cyg16-2* showed very little growth when compared to the WT in both limiting CO_2 conditions at pH 7.4 and 8.0. The data for their growth at pH 7.8 in limiting CO_2 condition were discarded since the wildtype did not grow on the same plate. Mutant *cya1* showed some curious phenotypes: it had difficulties growing in limiting CO_2 conditions at pH 7.4, while it did not grow well in both HCO_2 and LCO_2 conditions at pH 8.0. Again, data for the remaining CO_2 and pH conditions were discarded as the wildtype did not grow on the same plate. Meanwhile, *cia5-1* showed a CCM phenotype in the limiting CO_2 conditions that was subtle at pH 7.4 but became more severe as pH increased to 7.8 and 8.0. Mutant *cgld1* displayed a different phenotype, in which it grew as well as the WT in most conditions but had a subtle CCM phenotype at pH 7.8 in LCO_2 and at pH 8.0 in both limiting CO_2 conditions. The two *cpld63* mutants appeared to have a paler green colour and slightly reduced growth compared to the WT in HCO_2. This is the same case in limiting CO_2 with the reduced growth becoming more

severe at the two higher pH levels. It is noted that *cpld63-2* showed a much more reduced growth compared to *cpld63-1* in these conditions (it could not grow at all at pH 8.0 in limiting CO_2). These mutants helped narrow down the list of candidate genes that might play a role in the *Chlamydomonas* CCM. Finally, *cdpk13-2* showed a different phenotype from its initial spot test screen: instead of a severe CCM phenotype, it only showed a slightly paler green colour compared to the WT in limiting CO_2 at all pH levels. This is either caused by a technical error (like contamination from strains without CCM phenotype) or the change of continuous light condition to a 12:12 light:dark cycle.

The results helped narrow down the CCM regulator candidate genes to 10 members: *CAH7*, Cre16.g676800, Cre02.g092150, *CYG52*, *CYG16*, *CYA1*, *CIA5*, *CGLD1*, *CPLD63* and *CDPK13*.

Table 2.2 CO_2-sensing and Ca^{2+} signalling related candidate genes in *Chlamydomonas* and their CLiP mutants

Gene ID	Gene name	Mutant CLiP ID	Mutant name
Cre13.g607350	*CAH7*	LMJ.RY0402.196371	*cah7*
Cre09.g405750	*CAH8*	LMJ.RY0402.182607	*cah8*
Cre16.g676800	N/A	LMJ.RY0402.187045	cLM164
		LMJ.RY0402.183271	cLM165
Cre02.g092150	N/A	LMJ.RY0402.162033	cLM166
Cre09.g412600	*CYG52*	LMJ.RY0402.200699	*cyg52-1*
		LMJ.RY0402.150881	*cyg52-2*
Cre12.g547351	N/A	LMJ.RY0402.196894	cLM169
		LMJ.RY0402.209593	cLM170
Cre13.g605100	*PDE20*	LMJ.RY0402.147142	*pde20-1*
		LMJ.RY0402.152074	*pde20-2*
Cre14.g612200	*CYG16*	LMJ.RY0402.145196	*cyg16-1*
		LMJ.RY0402.202728	*cyg16-2*
Cre13.g580750	N/A	LMJ.RY0402.128253	cLM175
		LMJ.RY0402.108626	cLM176
Cre01.g053450	*CYA1*	LMJ.RY0402.181750	*cya1*
Cre07.g348650	*CYG65*	LMJ.RY0402.205369	*cyg65-1*
		LMJ.RY0402.119504	*cyg65-2*
Cre09.g387200	*CYG28*	LMJ.RY0402.061732	*cyg28-1*
		LMJ.RY0402.242774	*cyg28-2*

Cre09.g387350	*CYG30*	LMJ.RY0402.219652	*cyg30-1*
		LMJ.RY0402.065119	*cyg30-2*
Cre17.g715300	*PKD2*	LMJ.RY0402.204581	*pkd2-1*
		LMJ.RY0402.061021	*pkd2-2*
Cre02.g096300	*CIA5* or *CCM1*	LMJ.RY0402.099043	*cia5-1*
		LMJ.RY0402.038607	*cia5-2*
Cre09.g399552	*LCR1*	LMJ.RY0402.243803	*lcr1-1*
		LMJ.RY0402.115899	*lcr1-2*
Cre12.g485050	*CAH6*	LMJ.RY0402.174362	*cah6-1*
		LMJ.RY0402.255051	*cah6-2*
Cre02.g084350	*CGLD1*	LMJ.RY0402.107036	*cgld1*
Cre16.g660000	*CPLD63*	LMJ.RY0402.085009	*cpld63-1*
		LMJ.RY0402.198191	*cpld63-2*
Cre13.g571700	*CDPK13*	LMJ.RY0402.109542	*cdpk13-1*
		LMJ.RY0402.235547	*cdpk13-2*
Cre05.g236650	*CYG63*	LMJ.RY0402.127108	*cyg63-1*
		LMJ.RY0402.164724	*cyg63-2*
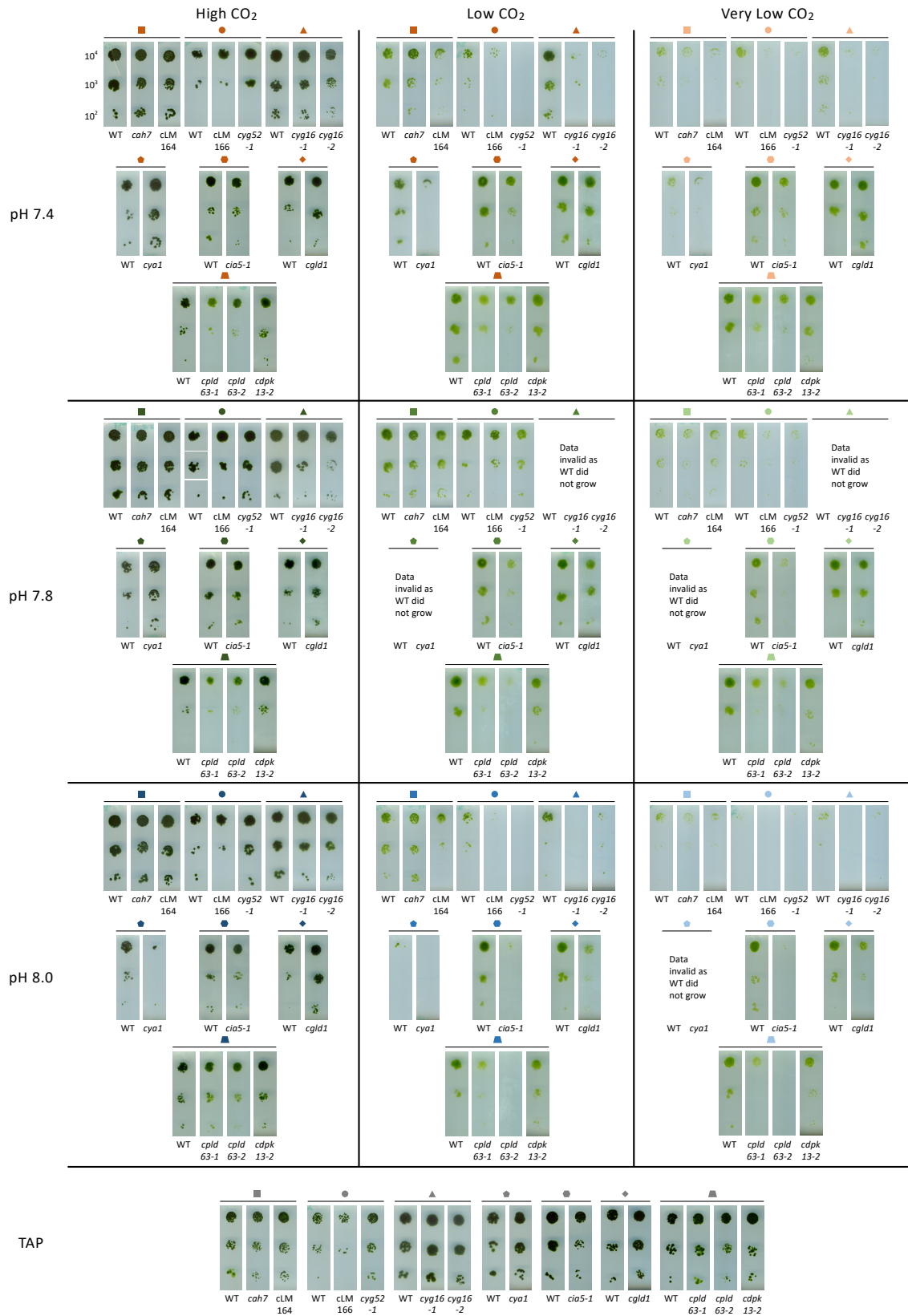
Figure 2.1 Spot test results of the CLiP mutants that showed a different phenotype compared to the WT.
All strains were first synchronised to the 12:12 light:dark cycle and then incubated in groups on individual plates also under the same light-dark cycle. Strains on the same plate are grouped together and given a unique shape (represents the group of strains) and colour (represents the same pH and CO_2 conditions) combination here. Each sample was grown with a series of dilution as indicated by small number on the top left: 10^4, 10^3, and 10^2 cells in total. The plates were scanned after the WT showed adequate growth in all conditions. The growth of the mutant strains was compared to the WT strain on the same plate. However, the WT on some plates did not grow well and therefore, the data of those plates were considered invalid.

2.4.3 Initial bioinformatic analysis of the new list of candidate genes selected according to the preliminary spot test results

A bioinformatic analysis by different programs was conducted to predict the functional domains and transit peptides of the 10 candidate genes found interesting in the initial spot test and the results are summarised in Table 2.3. Most of them contain AC and GC catalytic domains. This is reasonable as they were found by a BLAST search using CO_2 sensors from other organisms and these are mostly ACs or GCs. These genes are likely to encode putative ACs or GCs and sense Ci directly. Whether they are linked directly to CCM regulation requires further experimental study.

Table 2.3 Bioinformatics analysis of the candidate genes of interest from the initial spot tests

Gene ID	Gene Name	Homologous gene (species)	Phytozome/literature Details	Pfam domains	TargetP/ Predalgo
Cre13.g607350	CAH7	Can2 (CA; Cryptococcus neoformans); NCE103 (CA; Candida albicans); BCA1 and BCA4 (CAs; Arabidopsis thaliana)	399aa in length; β-type carbonic anhydrase (CA); constitutively-expressed; no localisation data yet (Ynalvez et al., 2008)	Carbonic anhydrase (96-250aa)	Chloroplast/ Chloroplast
Cre16.g676800	N/A	Cac1 (AC; Cryptococcus neoformans)	1297aa in length; predicted to have adenylyl/guanylyl cyclase catalytic domain	Bacterial extracellular solute-binding protein domain (153-256aa); Adenylate and Guanylate cyclase catalytic domain (964-1171aa)	Secretory/ Secretory Pathway
Cre02.g092150	N/A	Cdc35 or Cyr1 (AC; Candida albicans)	442aa in length; contains leucine-rich repeats and predicted to be Ras suppressor protein	Leucine-rich repeat (72-129aa; 165-223aa; 350-407aa)	Other/ Other
Cre09.g412600	CYG52	CyaB (AC; Stigmatella aurantiaca)	3280aa in length; predicted to have adenylyl/guanylyl cyclase catalytic and response regulator receiver domain	Response regulator receiver domain (901-1016aa); Adenylate and Guanylate cyclase catalytic domain (1056-1245aa)	Other/ Other
Cre14.g612200	CYG16	CyaB1 (AC; Anabaena PCC 7120)	3315aa in length; predicted to have adenylate/guanylate cyclase catalytic	Adenylate and Guanylate cyclase catalytic domain (622-803aa)	Other/ Other

			domain and GAF domain (Interpro)		
Cre01.g053450	*CYA1*	*ADCY10* (AC; *Homo sapiens*); *CgsAC* or Adenylate cyclase type 10 (AC; *Crassostrea gigas*)	2854aa in length; predicted to have adenylate/guanylate cyclase catalytic domain and to be a hybrid signal transduction histidine kinase G protein (PANTHER); P-loop containing nucleoside triphosphate hydrolase and Antifreeze protein Type I domain (Interpro)	Adenylate and Guanylate cyclase catalytic domain (493-598aa)	Other/ Other
Cre02.g096300	*CIA5* or *CCM1*	N/A	Alternative splicing at exon 3 and 4 creates two transcripts: CCM1A (699aa) and CCM1B (698aa, also called CIA5); master regulator of low CO2-inducible genes needed for CCM; contains Zinc finger C2H2-type/integrase DNA-binding domain (Interpro)	Insignificant matches: Aberrant zinc-finger (15-57aa); IBR domain, a half RING-finger domain (26-84aa); Zinc-finger of a C2H2-type (73-83aa)	Other/ Other
Cre13.g571700	*CDPK13*	*CPK2* and *CPK12/CDPK9* (*Arabidopsis thaliana*)	504aa in length; Ca^{2+}/Calmodulin-dependent protein kinase; found to interact with HLA3 (Mackinder et al., 2017)	Protein kinase domain (66-324aa); two EF-hand domain pairs (369-433aa; 442-503aa)	Other/ Mitochondrion
Cre02.g084350	*CGLD1*	*BICAT1* (*Arabidopsis thaliana*)	246aa in length; uncharacterized protein family UPF0016 (with integral membrane proteins of unknown functions); GDT-1 like protein (calcium transporter); Chloroplastic	Uncharacterized protein family UPF0016 (41-123aa; 163-237aa)	Secretory/ Secretory Pathway
Cre16.g660000	*CPLD63*	*BICAT2* (*Arabidopsis thaliana*)	333aa in length; uncharacterized protein family UPF0016 (with integral membrane proteins of unknown functions); GDT-1 like protein (calcium transporter) (PANTHER); Chloroplastic	Uncharacterized protein family UPF0016 (124-203aa; 251-325aa)	Mitochondrion/ Chloroplast

Meanwhile, there are two candidates that do not encode putative ACs or GCs but could still be potential regulators of the CCM. CAH7 is a β-CA found to be constitutively expressed (Ynalvez et al., 2008) and is homologous to CAs that participate in CO_2 sensing in fungi and *Arabidopsis*. As it is predicted to localise to the chloroplast, it could act as an internal CO_2 sensor in regulating the CCM. On the other hand, Cre02.g092150, a protein showing top BLAST hit score with the *C. albicans* AC, Cdc35, is interestingly predicted to be a Ras suppressor protein and contains no AC or GC domains. Ras proteins belong to a group of small GTPases that cycle between an ON state (GTP-bound) and OFF state (GDP-bound) for signal transduction (Bourne, Sanders and McCormick, 1990; Simanshu, Nissley and McCormick, 2017). They often bind to a conserved Ras association (RA) domain of downstream targets to activate them. In fact, *C. albican* Ras1, which is a Ras protein, has been found to interact with the RA domain of Cdc35 (304-393aa; residues K338 and L349 on the domain are important for this interaction), and this is essential to elevate cellular cAMP levels for CO_2-induced hyphal generation (Fang and Wang, 2006). A suppressor might be present to inhibit Ras1 to stop hyphal generation when not in a suitable condition. There might be similar mechanism used for CO_2-sensing in the *Chlamydomonas* CCM, in which Cre02.g092150 could act as the suppressor of a Ras protein to prevent downstream HCO_2-induced cAMP signalling cascade so that the CCM can be induced.

CIA5 has already been found to be a master regulator of the algal CCM but it is unknown if it can sense Ci directly or if it is activated by an upstream CO_2 sensor. *CDPK13* encodes a putative Ca^{2+}/calmodulin-dependent protein kinase and as described before it could possibly link Ca^{2+} signalling and the CCM through phosphorylation of HLA3 after being activated by Ca^{2+}/calmodulin. CGLD1 and CPLD63 could also potentially be involved in Ca^{2+} regulation of the CCM in the chloroplast. They both contain two UPF0016 (Uncharacterised Protein Family 0016) family domains and are predicted to be GDT-1 (Gcr1 dependent translation factor 1) like proteins. In addition, they are homologues to BICAT1 and BICAT2 respectively in *Arabidopsis*. BICAT1, also called CCHA1 (Chloroplast-localised Ca^{2+}/H^+ Antiporter 1) or PAM71 (Photosynthesis-Affected Mutant 71) is suggested to mediate Ca^{2+} uptake into the thylakoid lumen while BICAT2 (also called CMT1, Chloroplast Manganese Transporter 1) is implied to mediate Ca^{2+} transport across the chloroplast envelop in *Arabidopsis* (Frank et al., 2019). This suggests that CPLD63 could possibly function as the Ca^{2+} transporter needed for Ca^{2+} uptake to the chloroplast

stroma while CGLD1 could be essential for Ca^{2+} transport across the thylakoid membrane. These two might play a role in facilitating the transport of Ca^{2+} into the pyrenoid needed for the upregulation of HLA3 and LCIA to initiate the CCM (Wang et al., 2016c).

2.4.4   Further spot tests of CLiP mutants of candidate genes found interesting from the preliminary spot tests

To validate the initial spot test results and examine if the mutant phenotypes were influenced by light regime, two batches of spot tests were conducted again for the mutants with interesting phenotypes under two different light conditions: one under 12:12 light:dark cycle (a replication of the initial spot test in section 2.4.2) and the other under continuous light (Table 2.4). One thing to note is that strain *cpld63-1* was not included in this study due to its subtle CCM phenotype but *cpld63-2* was included as it showed a more distinct phenotype difference to WT in the initial screen.

Table 2.4 Growth phenotypes of mutants compared to the WT on the same plate in the three spot tests

Mutant strain	Spot test	HCO2			LCO2			VLCO2			TAP
		pH 7.4	pH 7.8	pH 8.0	pH 7.4	pH 7.8	pH 8.0	pH 7.4	pH 7.8	pH 8.0	
cah7	Initial (L/D)	0	0	0	0	0	0	2	2	2	0
	2nd (L/D)	0	0	0	0	0	0	0	0	0	0
	3rd (L)	0	0	0	1	1	N/A	1	0	N/A	0
cLM164	Initial (L/D)	0	0	0	3	2	2	3	2	2	0
	2nd (L/D)	0	0	0	1	1	3	1	1	3	0
	3rd (L)	0	0	0	0	3	N/A	0	4	N/A	0
cLM166	Initial (L/D)	0	0	0	3	0	4	4	4	4	0
	2nd (L/D)	3	3	3	3	3	4	3	3	4	2
	3rd (L)	0	0	0	4	4	N/A	4	4	N/A	0
cyg52-1	Initial (L/D)	0	0	0	4	1	4	4	4	4	0
	2nd (L/D)	0	0	0	0	0	0	0	0	0	0
	3rd (L)	0	0	0	0	2	N/A	0	4	N/A	0
cyg16-1	Initial (L/D)	0	0	0	4	N/A	4	4	N/A	4	0
	2nd (L/D)	0	0	0	1	1	1	1	1	1	0
	3rd (L)	0	0	0	0	0	0	0	0	0	0
cyg16-2	Initial (L/D)	0	0	0	4	N/A	4	4	N/A	4	0
	2nd (L/D)	3	3	3	3	3	4	3	3	4	0

	3rd (L)	0	0	0	1	2	2	1	2	2	0
cya1	Initial (L/D)	0	0	4	4	N/A	4	4	N/A	N/A	0
	2nd (L/D)	0	0	0	3	3	3	3	3	3	0
	3rd (L)	2	0	0	2	3	2	2	3	2	3
cia5-1	Initial (L/D)	0	0	0	1	2	4	1	3	4	0
	2nd (L/D)	0	0	0	3	4	4	3	4	4	0
	3rd (L)	0	0	0	2	4	4	3	4	4	0
cgld1	Initial (L/D)	0	0	0	0	1	2	0	0	2	0
	2nd (L/D)	0	0	0	0	4	4	0	4	4	0
	3rd (L)	0	0	0	1	2	4	2	3	4	0
cpld63-1	Initial (L/D)	2	2	1	2	2	2	2	2	2	0
	2nd (L/D)	N/A	N/A	N/A	N/A	N/A	N/A	N/A	N/A	N/A	N/A
	3rd (L)	N/A	N/A	N/A	N/A	N/A	N/A	N/A	N/A	N/A	N/A
cpld63-2	Initial (L/D)	2	2	1	2	3	4	2	3	4	0
	2nd (L/D)	3	3	3	4	4	4	4	4	4	0
	3rd (L)	4	4	4	4	4	4	4	4	4	1
cdpk13-2	Initial (L/D)	0	0	0	1	1	1	1	1	1	0
	2nd (L/D)	0	0	3	1	1	3	1	1	4	0
	3rd (L)	0	0	0	3	3	0	3	3	0	0

L/D = light-dark cycle, L = continuous light; 0 = WT growth, 1 = very subtle, 2 = subtle, 3 = severe, 4 = very severe/ no growth, N/A = no/ invalid data

The results of the replication spot test (Figure 2.2) revealed that some of the mutant strains showed different phenotypes compared to the initial spot test (Table 2.4). Mutant *cah7* did not show any disturbed CCM phenotype this time, which could be argued to be similar to the result last time as the CCM phenotype was almost unnoticeable and only showed at VLCO$_2$ condition then. Strain cLM164 exhibited a very subtle CCM phenotype in both limiting CO$_2$ conditions at pH 7.4 and 7.8, and a more severe one at pH 8.0. This phenotype at the two lower pH was subtler than last time. Strain cLM166 showed less growth in all testing conditions and even in the TAP control plate so it was uncertain whether the phenotypes were a result of disturbed CCM or not, unlike last time in which it showed a clear CCM defect. Mutant *cyg52-1* did not exhibit any reduced growth in all conditions, which was vastly different from the observation last time where it had little to no growth in limiting CO$_2$ conditions at all pH levels except in LCO$_2$ at pH 7.8. On the other hand, the *cyg16* mutants also showed different phenotypes compared to last time.

Here, *cyg16-1* showed a very subtle CCM phenotype at all pH levels whereas *cyg16-2* had reduced growth in all CO_2 and pH conditions. However, they both showed severe CCM phenotypes in the previous test. Mutant *cya1* showed a typical CCM phenotype this time in both limiting CO_2 conditions and did not display disturbed growth at HCO_2 at pH 8.0 like last time. Mutants *cia5-1*, *cgld1* and *cpld63-2* showed similar phenotypes to the first spot test except they were more severe here. The former exhibited a stronger CCM phenotype at both pH 7.8 and 8.0 in all limiting CO_2 conditions, while the latter showed reduced growth in all CO_2 conditions but had normal growth in TAP. For mutant *cdpk13*, it showed a subtle CCM phenotype like the previous spot test except at pH 8.0 where it had a severe growth reduction in all CO_2 conditions.

Figure 2.2 Spot test results of mutants with interesting phenotypes from initial screen under light-dark cycle.
All strains were first synchronised to the 12:12 light:dark cycle and then incubated in groups on individual plates also under the same light-dark cycle. Strains on the same plate is given a unique shape (represents the group of strains) and colour (represents the same pH and CO_2 conditions) combination here. Each sample was grown with a series of dilution as indicated by small number on the top left: 10^4, 10^3, and 10^2 cells in total. The plates were scanned after the WT showed adequate growth in all conditions. The growth of the mutant strains was compared to the WT strain on the same plate.

The spot test conducted under continuous light (Figure 2.3) showed that the reduced growth phenotypes in some mutants were more severe compared to the initial and replicated light-dark cycle spot tests (Table 2.4). For strains *cah7*, cLM164, cLM166 and *cyg52-1*, the WT on the same plate did not grow well in limiting CO_2 at pH 8.0. Therefore, the data obtained at these conditions was considered invalid and will required a repeated experiment to look into again. Mutant *cah7* showed very subtle CCM phenotype at pH 7.4 and 7.8, except that it grew similarly to WT at pH 7.8 in $VLCO_2$. Strain cLM164 did not show a CCM phenotype at pH 7.4 this time, but actually had a more severe CCM phenotype at pH 7.8 in the limiting CO_2 conditions compared to the light-dark cycle tests. Strain cLM166 grew well in HCO_2 conditions and had a much more serious CCM phenotype in limiting CO_2 at pH 7.4 and 7.8 compared to the previous assays. Strain *cyg52-1* this time showed WT phenotype in all CO_2 at pH 7.4 just like it did in the replicated light-dark cycle test, but had a more severe CCM phenotype in the limiting CO_2 conditions at pH 7.8 compared to previous tests. On the other hand, *cyg16-1* actually showed WT phenotype in all conditions while *cyg16-2* had subtler CCM phenotype this time compared to the previous tests. It is noted that *cyg16-2* also did not grow well in HCO_2 at pH 7.4. This could either be due to pipetting errors or a real biological phenotype, which is hard to conclude due to the inconsistency between the results of the initial and replicated spot tests. Mutant *cya1* again showed a CCM phenotype at all pH levels this time. However, it also could not grow as well as WT in HCO_2 at pH 7.4 and on TAP. A replicated spot test in continuous light would be needed to check whether this is a true growth phenotype or just a technical error. Strain *cia5-1* once again showed CCM phenotypes similar to the previous tests except that it was more severe in $VLCO_2$ compared to LCO_2 this time. The *cgld1* and *cpld63* mutants showed similar phenotypes as in the light-dark cycle tests except that *cgld1* also had a very subtle CCM phenotype at pH 7.4 while *cpld63-2* did not grow at all in HCO_2 conditions and also had a slightly reduced growth on the TAP plate this time. Mutant *cdpk13-2* this time showed a more severe CCM phenotype at pH 7.4 and 7.8, like it did in its initial continuous light spot test. However, it grew similarly to WT at pH 8.0 in all CO_2 conditions, which was different from the light-dark cycle tests.
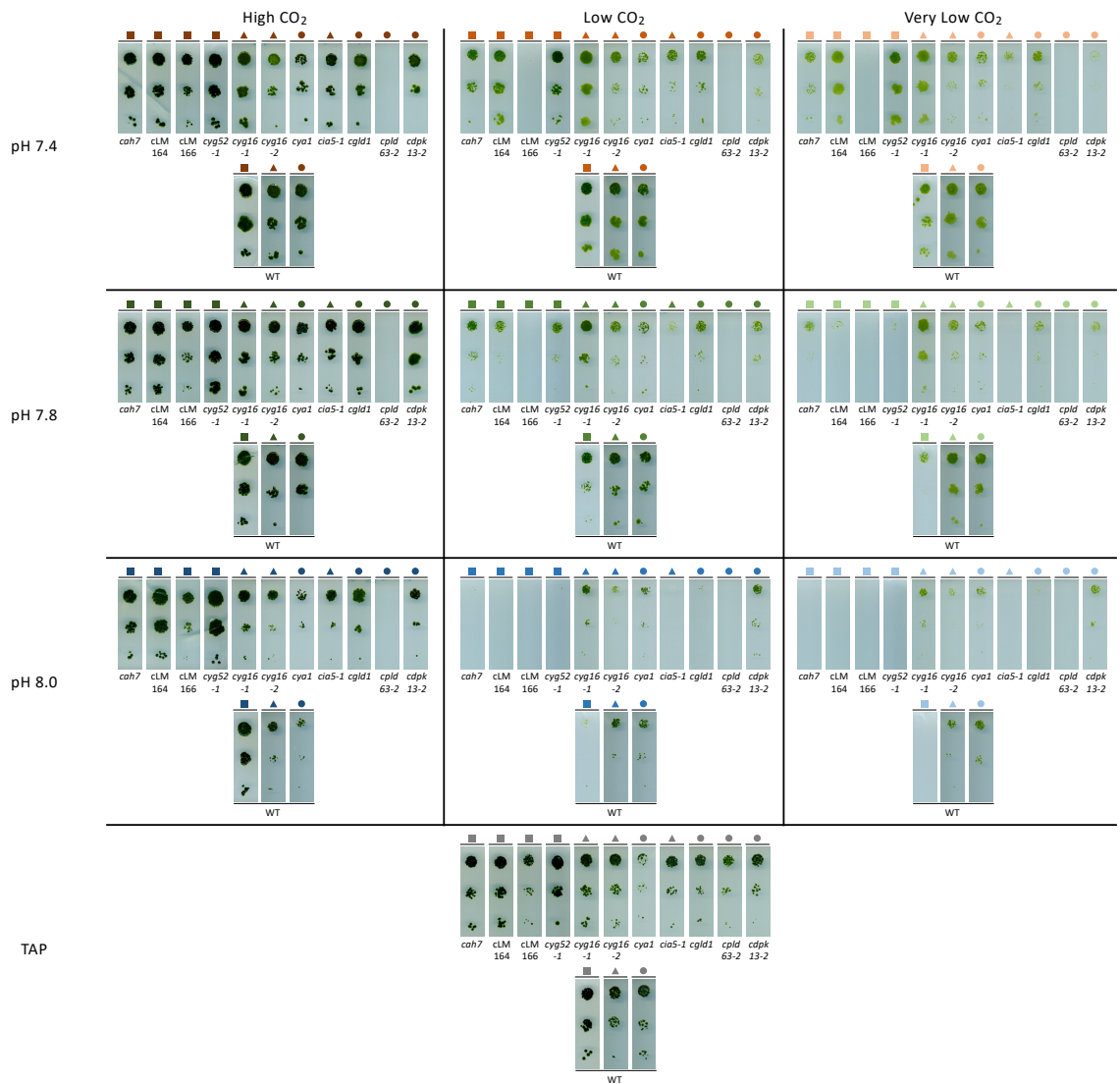
Figure 2.3 Spot test results of mutants with interesting phenotypes from initial screen under continuous light.
All strains were first grown in continuous light and then incubated in groups on individual plates under continuous light as well. Strains on the same plate is given a unique shape (represents the group of strains) and colour (represents the same pH and CO_2 conditions) combination here. Each sample was grown with a series of dilution as indicated by small number on the top left: 10^4, 10^3, and 10^2 cells in total. The plates were scanned after the WT showed adequate growth in all conditions. The growth of the mutant strains was compared to the WT strain on the same plate.

Because of the variation in the results between the initial and replicated light-dark cycle tests for mutants cLM164, cLM166, *cyg52-1* and the *cyg16* mutants, it might not be possible to analyse the difference seen between the light-dark cycle and continuous light tests accurately. For strain *cah7*, its CCM phenotype was too weak to determine whether it was a true phenotype or not. Strains *cya1* and *cia5-1* showed more consistent phenotypes across all spot tests and could be used in the future to study the roles of CYA1 and CIA5 in CO_2-sensing needed for CCM regulation. The mutants of *CDPK13*, *CGLD1* and *CPLD63* also showed similar and clear CCM phenotypes in at least two of the spot tests. Due to limitation of time and that these three genes were predicted to have roles related to Ca^{2+}-signalling, only they were chosen for future study.

2.4.5 Confirmation of CIB1 cassette insertion site in mutants of CDPK13, CGLD1 and CPLD63

In order to verify that *CDPK13*, *CGLD1* and *CPLD63* were disrupted in their respective CLiP mutants, a PCR and sequencing check for the presence of the CIB1 cassette in the gDNA of each mutant was performed. The gDNA of WT and mutant was first amplified with a pair of genomic primers of the disrupted gene that flanks the upstream and downstream of the insertion site of CIB1 cassette indicated on the CLiP database for each mutant. This pair of primers can be seen as P1 and P2 in the schematic in Figure 2.4a. The PCR program has a short incubation time during the annealing step so that fragments larger than 2000 bp are unlikely to be amplified. Since the CIB1 cassette is 2223 bp long while the predicted DNA fragment amplified by each pair of the P1/P2 primers is always shorter than 2000 bp, the PCR will give the predicted product in WT but not in the mutant if the CIB1 cassette is inserted. If the predicted product is amplified in the mutant, then the CIB1 cassette is absence and the target gene is not disrupted. After the presence of CIB1 cassette is verified, a different pair of primers- shown as P3 and P4 in Figure 2.4a- would be combined with either P1 or P2 to amplify the DNA spanning across the genome-cassette region in the target gene. The product was then sent for sequencing to confirm that the cassette was inserted in the way listed in the CLiP database.

The PCR results revealed that all mutants contain the CIB1 cassette in the mutated gene (Figure 2.4b). A fragment of the correct size was amplified as a single bright band in each WT lane and was not seen in the respective mutant lane (Figure 2.4b). This verified that *cdpk13-1* and *cdpk13-2*, *cgld1*, *cpld63-1* and *cpld63-2* are mutants for CDPK13, CGLD1 and CPLD63 respectively. The regions crossing the genome-cassette junction on both ends of the cassette on the disrupted gene were then amplified in each mutant and the products were sent for sequencing. For *cdpk13-1*, the junctions had already been sequenced previously and the results were analysed again. The results confirmed the insertion sites and orientation of the CIB1 cassette in the target genes in the mutants received are the same as the information give on the CLiP database: 3'UTR and sense in *cdpk13-1*; 5'UTR and antisense at 5' end and sense at 3' end (two cassettes are possibly inserted) in *cdpk13-2*; intron and antisense in *cgld1*; CDS and sense in both CPLD63 mutants.

All mutants except *cpld63-2* only have the respective target genes disrupted with CIB1 insertion. Therefore, any non-WT phenotypes in the spot tests are likely the results of the mutation in the target gene. For *cpld63-2*, another gene is also shown to have CIB1 insertion in the CLiP database. This gene is Cre09.g396700 (ACK1), an acetate kinase that was found in the chloroplast and involves in the assimilation of acetate to acetyl-CoA (Park et al., 2015; Yang et al., 2014). The kinase works together with PAT2 to facilitate acetate production under dark anoxic conditions (fermentation metabolism). However, it is also found that acetate can still be produced without the PAT2/ACK pathway (Yang et al., 2014). Furthermore, the CIB1 cassette was found to be inserted in the 3'UTR of *ACK1* in *cpld63-2*. Therefore, the likelihood of its transcription being disrupted and the likelihood that the CCM would be disturbed because of its mutation are very low, suggesting that the phenotype seen in the spot test should be the direct result of *CPLD63* being disrupted.
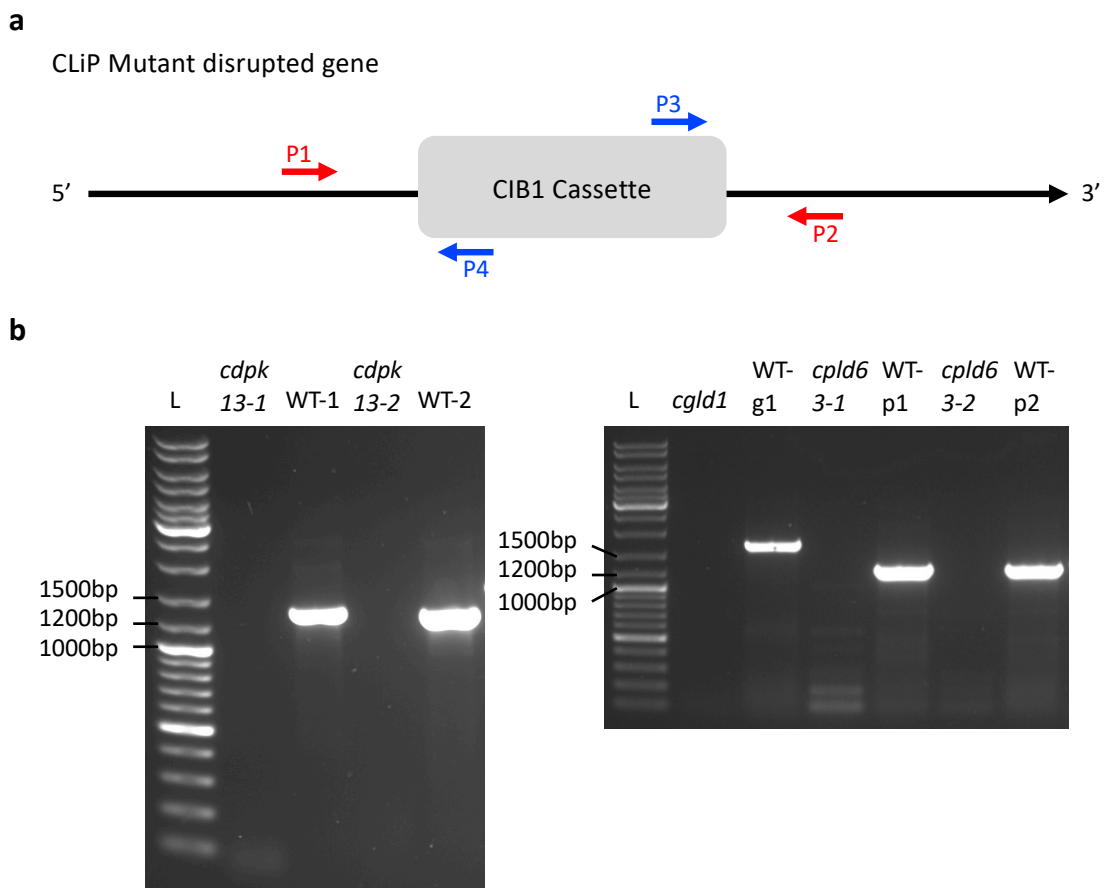
Figure 2.4 Schematic and agarose gel photos of PCR check of CLiP mutants of CDPK13, CGLD1 and CPLD63.
(a) A schematic representation of a disrupted gene in a CLiP mutant. The mutant was generated through insertional mutagenesis using the CIB1 cassette. There are four primers shown: P1 and P2 represents the genomic primers for the disrupted genes, which are used to check whether the CIB1 cassette is inserted or not; P3 and P4 represents the cassette primers, which are paired with either P1 and P2 depending on the orientation of the cassette inserted to be used for amplification and sequencing of the genome cassette junctions. (b) 1% agarose gel photos showing the PCR products amplified from the CLiP mutants and WT gDNA using the respective P1/2 primers for each mutant. The

57

following pairs were amplified using the same pair of primers: *cdpk13-1* and WT-1, *cdpk13-2* and WT-2, *cgld1* and WT-g1, *cpld63-1* and WT-p1, *cpld63-2* and WT-p2.

2.4.6 Bioinformatic prediction of the functional role of CDPK13 in the *Chlamydomonas* CCM

CDPK13 was predicted to contain a protein kinase domain and two EF-hand domains (each EF-hand domain containing two EF-hand motifs) by Pfam (Figure 2.5a). This is consistent with the findings in the literature (Hamel, Sheen and Séguin, 2014; Li et al., 2019b). Phyre2 analysis predicted a 3D structure with template models c3q5iA (protein kinase structure of pbanka_031420) and c3lijA (protein kinase structure of calcium/calmodulin dependent protein kinase cpcdpk3) as the top models aligned to the protein sequence of CDPK13. The important glycine residues of the typical GXGXXG motif in the ATP-binding pocket as well as the EF-hand domains were marked on both models and the predicted 3D structure of CDPK13 (Figure 2.5b). When the model of CDPK13 was aligned to either of the template models, these features all positioned similarly on the models. This suggested that CDPK13 could in theory bind to ATP to carry out phosphorylation.
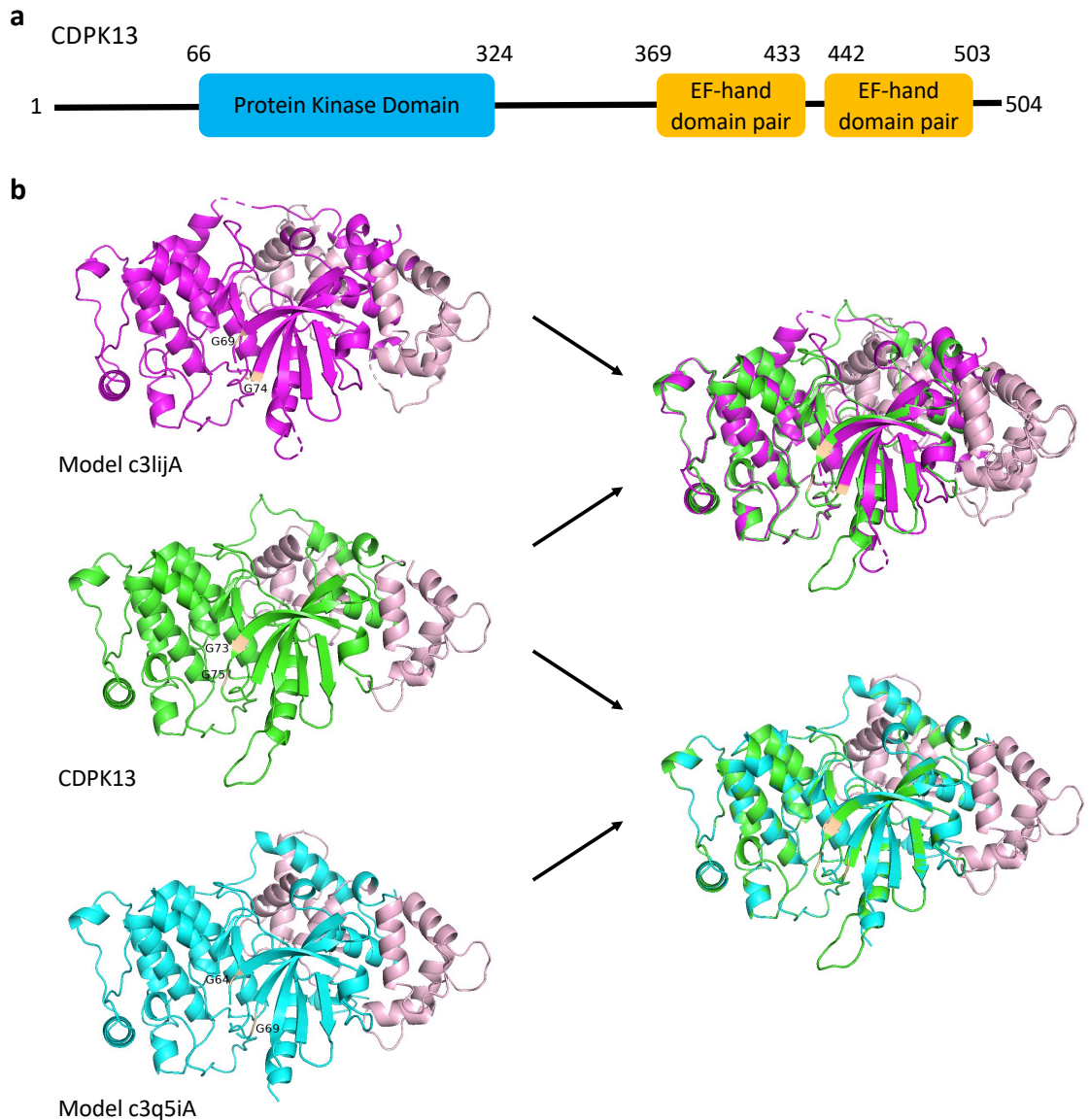
Figure 2.5 Predictions of CDPK13 domain and 3D structure by Pfam and Phyre2 respectively.
(a) A graphic presentation of the domains of CDPK13 predicted by Pfam. The protein is predicted to have a protein kinase domain and two EF-hand domain pair (four EF motifs together) at the C terminus. (b) 3D structures of the top two models aligned to CDPK13 sequence and the predicted 3D structure of CDPK13. Model c3q5iA represents a protein kinase structure of solved from pbanka_031420, while model c3lijA is derived from the crystal structure of the calcium/calmodulin dependent protein kinase cpcdpk3. The important glycine residues of the typical GXGXXG motif in the ATP-binding pocket are coloured in yellow whereas the EF-hand domains are coloured in pink on all structures.

To further confirm whether CDPK13 would function as a CDPK in *Chlamydomonas*, a phylogenetic tree was constructed between its predicted kinase domain and kinase domains of Ca^{2+}/calmodulin-dependent protein kinases and other kinases in *Chlamydomonas* and other model species (Figure 2.6). Most of the kinases were correctly grouped together according to their functions annotated and characterised in the literature (Shiu and Bleecker, 2001; Manning et al., 2002; Berman et al., 2003; Depège, Bellafiore and Rochaix, 2003; Wilson and Lefebvre, 2004; Pollock et al., 2005; Mori et al., 2006; Gokhale, Wirschell and Sale, 2009; Pesaresi et al., 2009; Lemeille et al., 2010; Lehti-Shiu and Shiu, 2012; Hamel, Sheen and Séguin, 2014; Li et al., 2019b). This grouping was

also not dependent on the evolutionary distances between the species. For example, CrSAC3 and AtKIN11 did not clustered together with the *Chlamydomonas* and *Arabidopsis* CDPKs or with each other. This showed that the kinases were clustered mainly according to functional similarity in the tree, indicating that its accuracy is adequate in predict the function of uncharacterised kinases like CDPK13. The tree showed that CDPK13 and most of the other *Chlamydomonas* CDPKs clustered together except Cre10.g418900, which has been predicted to have a tyrosine kinase domain, instead of a serine/threonine specific kinase domain as predicted in all the other CDPKs. This cluster was also shown to be phylogenetically close to human CAMKs (Ca^{2+}/calmodulin-dependent protein kinases) in the tree (Manning et al., 2002). Other CAMKs (but not in the CDPK subfamily) from *Arabidopsis*, yeast and *Chlamydomonas* also grouped together with the human CAMKs. Together, they formed the large family of CAMKs in the tree. The presence of CDPK13 in the CAMK family is consistent with the hypothesis that it functions as a Ca^{2+}/calmodulin-dependent protein kinase in the *Chlamydomonas* CCM.
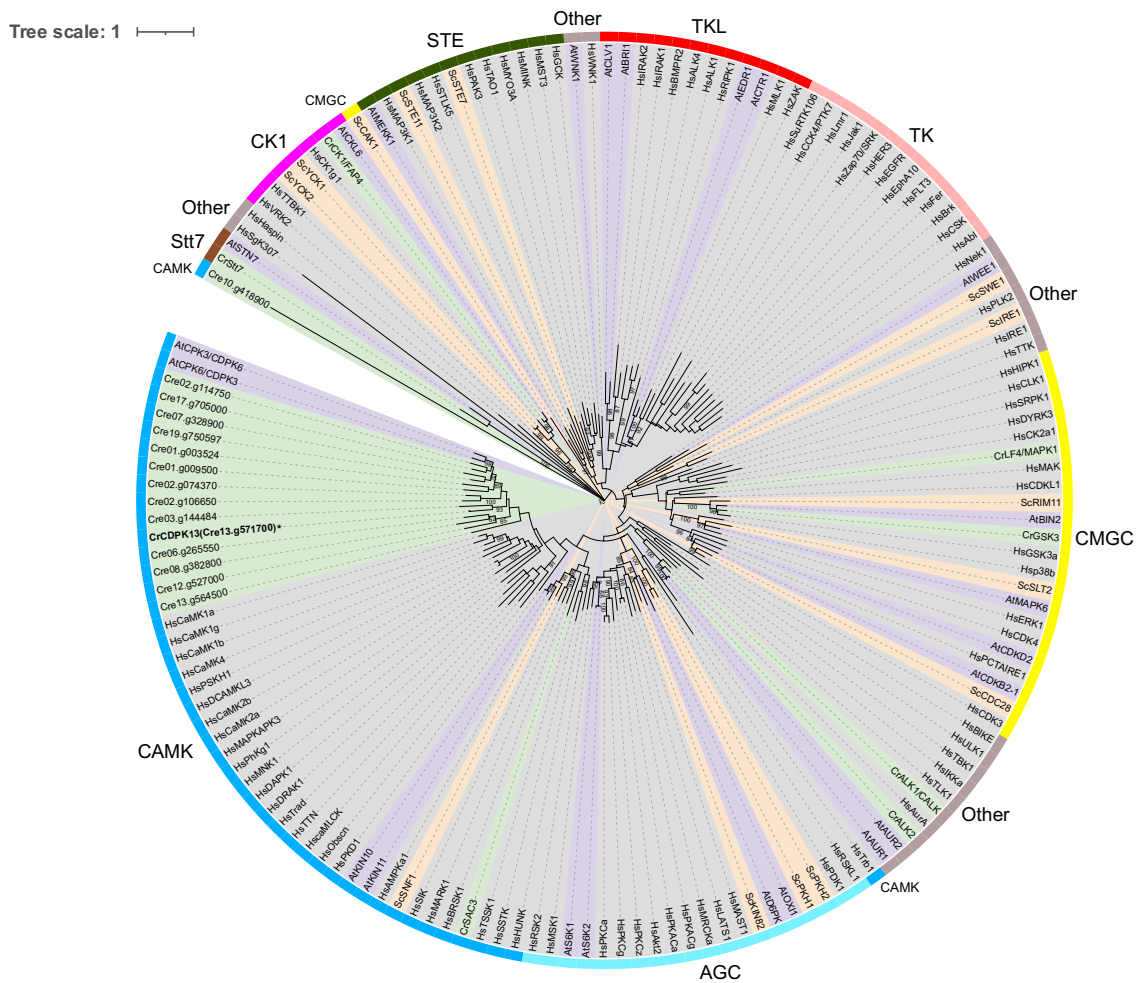
Figure 2.6 Phylogenetic tree of protein kinase domains of *Chlamydomonas* CDPKs and characterised kinases from human, yeast, *Arabidopsis* and *Chlamydomonas*.

The kinases names are coloured according to the species and initials of the species are added to the start of those without the gene ID shown: green and Cr= *Chlamydomonas reinhardtii*; purple and At= *Arabidopsis thaliana*; orange and Sc= yeast (*Saccharomyces cerevisiae*); grey and Hs= human (*Homo sapiens*). The kinases are annotated to the main kinase families as shown by the coloured arcs on the outer ring. The annotations are based on literature data except for Stt7 in *Chlamydomonas* and its *Arabidopsis* homologue STN7, which is shown as a family of its own and not annotated to any of the main families. The label of CDPK13 is bolded and marked with a bolded asterisk at its tree branch. Bootstrap values with 80% or over are shown below the respective branches. Kinases of each family group together mostly except for HsIRAK1, HsIRAK2, AtCLV1 and AtBRI1, which have separated into a single branch from the TLK and TK, different from the tree generated by Manning *et al.*, 2002. Kinase family names: AGC= Collection of PKA, PKG and PKC families; CAMK= Ca^{2+}/calmodulin-dependent protein kinase; CK1= Casein kinase 1; CMGC= Collection of CDK, MAPK, GSK3 and CLK families; STE= yeast Sterile 7, Sterile 11 and Sterile 20 kinases homologues; Stt7 = Stt7 homologues; TK= Tyrosine kinase; TKL= Tyrosine kinase-like; Other= other typical kinase subfamilies.

2.4.7 Bioinformatic prediction of the functional role of CGLD1 and CPLD63 in the *Chlamydomonas* CCM

CGLD1 and CPLD63 are predicted to have two domains belonging to the UPF0016 family by Pfam (Figure 2.7a). The family consists of a group of uncharacterised membrane proteins that often contain two similar regions with three transmembrane domains each (Demaegd et al., 2014; Colinet et al., 2017). Each region often contains a copy of the consensus motif, E-ɸ-G-D-[KR]-[TS] (where ɸ represents any hydrophobic residue), and this motif is present in each UPF0016 domain of CGLD1 and CPLD63. The TMHMM analysis of the two proteins also showed 4 transmembrane helices in CGLD1 and 7 transmembrane helices in CPLD63 approximately at the regions predicted to be UPF0016 domains by Pfam (Figure 2.7b). The numbers of predicted transmembrane helices of both proteins are different from the typical numbers observed in the two-domain members of UPF0016 but this could be due to the technical differences between prediction programs. Nonetheless, CGLD1 and CPLD63 appear to be transmembrane proteins and members of the UPF0016 family.
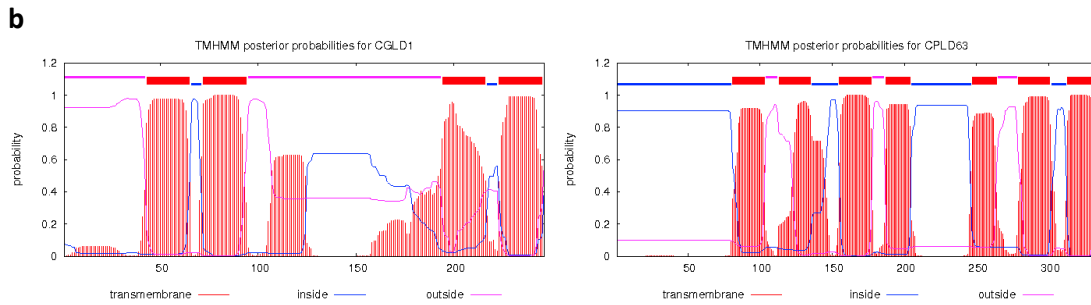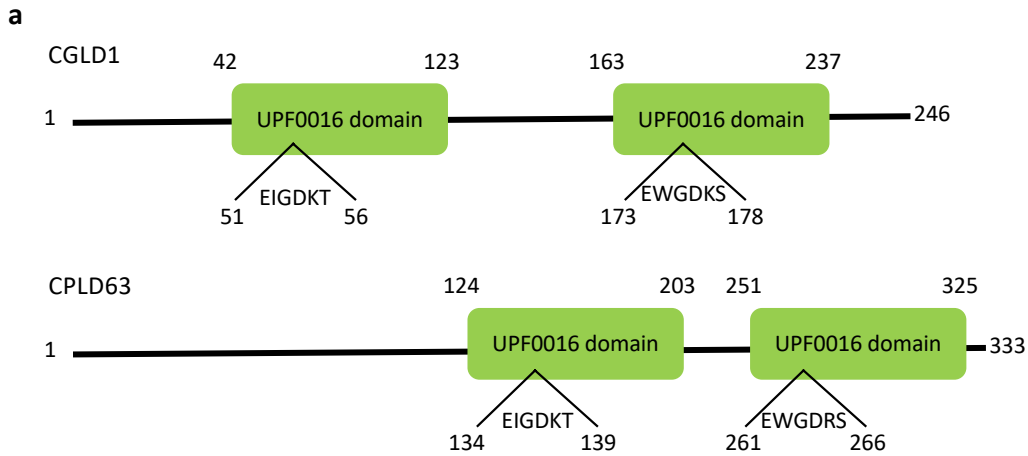
Figure 2.7 Prediction of CGLD1 and CPLD63 domains and transmembrane regions.
(a) Pfam predication of the UPF0016 domains in CGLD1 and CPLD63 are present here. The consensus sequence of each UPF0016 domain is shown as well. The numbers indicate residue numbers. (b) TMHMM prediction of transmembrane regions in CGLD1 and CPLD63.

The phylogenies of CGLD1 and CPLD63 with homologues obtained from BLAST results showed that, apart from the BICATs, they are mainly homologous to PAM71, GDT1 and GDT1-like proteins (Figure 2.8) in closely related species, plants, yeast and human. Among the homologues, the BICATs in *Arabidopsis*, TMEM165 (transmembrane protein 165) in human (*Homo sapiens*) and Gdt1p in yeast (*S. cerevisiae*) have all been found to be important for Ca^{2+} transport (Demaegd et al., 2013; Colinet et al., 2017; Frank et al., 2019). These suggest that CGLD1 and CPLD63 could potentially be Ca^{2+} transporters. Interestingly, CGLD1 is also homologous to Pch2p in yeast, which is a protein important for meiotic checkpoint (San-Segundo and Shirleen Roeder, 1999; Herruzo et al., 2021). It is highly unlikely that CGLD1 contains this function, as most of its homologues are GDT1-like proteins. Meanwhile, another *Chlamydomonas* gene, Cre16.g660050, was shown to be homologous to *CPLD63*. This suggested that *CPLD63* might have experienced a duplication event in the evolutionary history of the green algae and this protein might contain have similar function to *CPLD63*. Cre16.g660050 encodes a putative protein that also contain the conserved motifs of the protein family UPF0016 as predicted by Pfam. Whether it has a role in the *Chlamydomonas* CCM is unknown.

A limitation of the two phylogenetic trees is the large number of branches with low bootstrap values. This could result in different branching when the tree is redrawn. This might be caused by the largely variable regions that are outside of the conserved UPF0016 motifs between the homologues, such as the sequence at the N-terminal that often contains targeting peptides. An alignment of only the regions containing the UPF0016 domains of the homologues should be carried out to improve the tree.
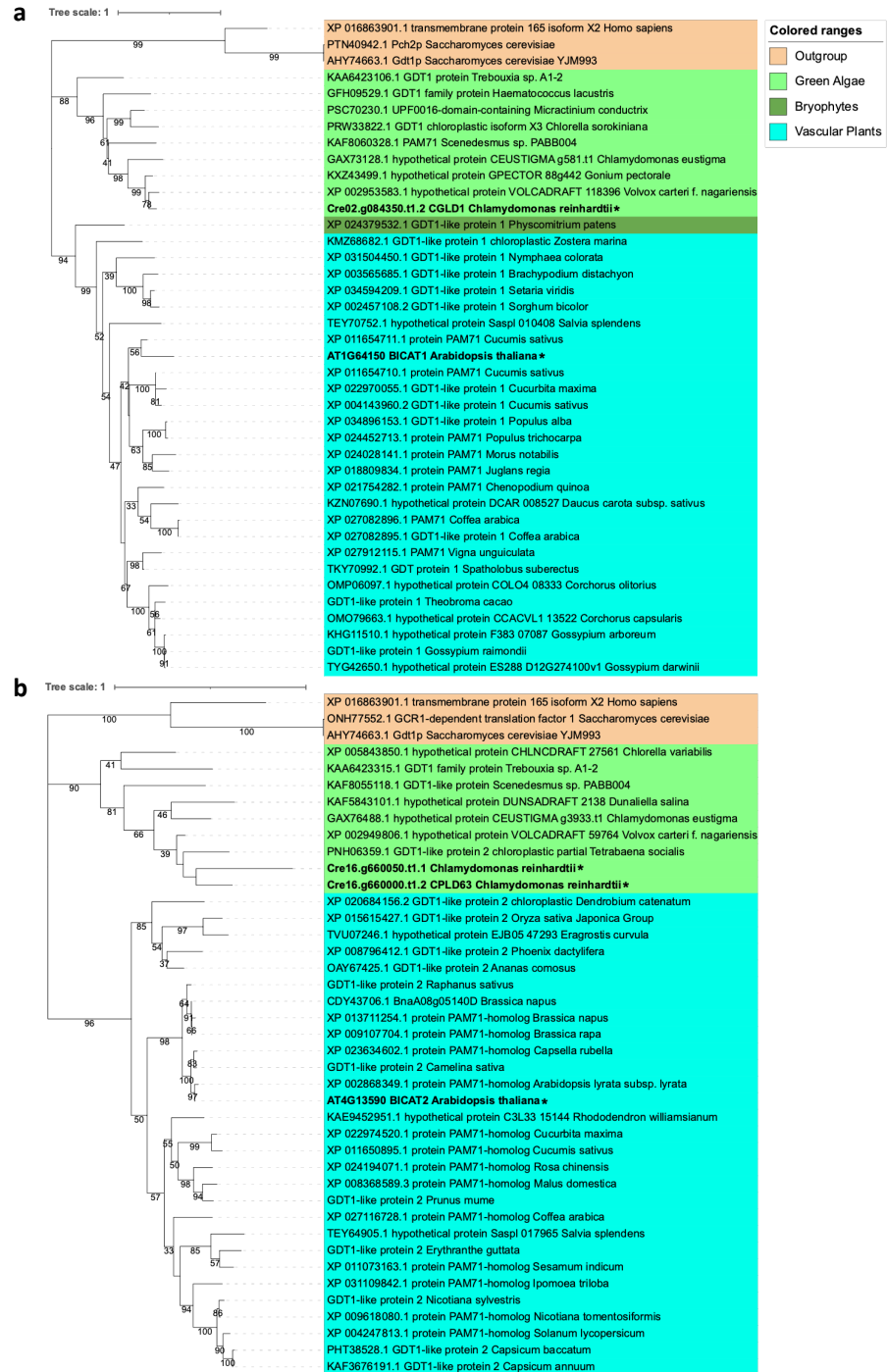
Figure 2.8 Phylogenies of CGLD1 and CPLD63.
(a) Phylogenetic tree drawn using alignments between CGLD1 and its homologues in closely related species and in human and yeast. (b) Phylogenetic tree drawn using alignment between CPLD63 and its homologues in closely related species and in human and yeast. Different colours are used to represent the phylum that the genes belong to. The labels of the homologues in *Chlamydomonas* and *Arabidopsis* are bolded and marked with a bolded asterisk.

63

2.5 Discussion

This study helped prioritise new genes that could possibly play a role in CO_2-sensing or the Ca^{2+} signalling pathway needed for the regulation of the *Chlamydomonas* CCM. The light-dark cycle spot tests revealed a list of CO_2-sensing candidate genes that could be important for the induction of the *Chlamydomonas* CCM despite the inconsistency in the results between replicated tests. CAH7 is a β-type CA predicted to have transmembrane domain near the C terminus and closely related to CAH8, another CA that has been shown to localise to the periplasmic space in *Chlamydomonas* through immunolocalisation studies (Ynalvez et al., 2008). CAH7 could localise to this area as well and participate in the CO_2 sensing pathway like the CAs identified in other organisms did in their CO_2 sensing system (Table 2.1). Its mutant showed an almost unnoticeable CCM phenotype in the tests, indicating that if it does play a role in the CCM, its function could have been compensated by another redundant gene (CAH8 could be a possibility) in the mutant.

Several other candidate genes identified encode putative ACs/GCs and are less characterised. They include Cre16.g676800, Cre02.g092150, *CYG52*, *CYG16* and *CYA1*. Since ACs/GCs can sense HCO_3^- directly and some have been shown to respond to CO_2 directly in other organisms (Townsend et al., 2009), these genes could be the CO_2 sensors in regulation of the *Chlamydomonas* CCM. However, the mutant of *CYA1* was the only one showing relatively similar phenotypes across the initial and replicated spot test. The varied phenotypes in the mutants of the other four genes made it difficult to deduce whether they really play a part in the *Chlamydomonas* CCM. When looking at the data in a recent study (Fauser et al., 2022), the growth of the mutants of these genes in liquid culture did not differ a lot between air CO_2 or HCO_2 conditions (often <2-fold increase or decrease). On the occasion when one mutant had a >4-fold decrease in the growth in air CO_2 (*CYG16* and *CYA1*), the same decrease was not seen in replicated tests or ins other mutants of the same gene (Fauser et al., 2022). This indicated that they likely do not have a defected CCM, contradicting the result from the spot test in this study. Nevertheless, the tests in the literature were conducted under low light (~50-100 μmol photons m^{-2} s^{-1}) while this study used high light (~400 μmol photons m^{-2} s^{-1}), which could have worsened any subtle decrease in the growth of the mutants in LCO_2 conditions. These genes could still play a role in the CCM. To draw a more solid conclusion for their roles in the CCM, further spot tests under different light intensities should be carried out in the

future with care to ensure technical errors are minimised. On the other hand, growth assay that allows quantification of the phenotypes (e.g. doubling rate of the strains in liquid culture under different conditions) could be a better method to study these mutants as it eliminates the need to compare the phenotypes by human eyes like in the spot test, which could create errors if the differences are subtle.

On the other hand, mutants of *CIA5*, *CGLD1* and *CPLD63* showed similar growth phenotypes that were distinctive from the WT throughout the initial and replicated spot tests, allowing a more accurate interpretation of their results. Mutant *cia5-1* showed a CCM phenotype in all spot tests. This agreed with the fact that CIA5 is a master regulator of core CCM genes and its mutation would cause a disturbed CCM. Mutant *cgld1* only showed a CCM phenotype at higher pH, suggesting that it could be an important CCM component when HCO_3^- becomes an even more dominant species of Ci compared to CO_2 in the surroundings (see Figure 2.9 for the abundance of Ci species at different pH). Mutant *cpld63-2* showed reduced growth compared to the WT in all CO_2 and pH levels but grew as well as the WT on the TAP control plate (contain carbon source in the media) in the light-dark cycle spot tests. This suggested that its photosynthesis was disrupted and CPLD63 might be functionally important for photosynthesis in general.
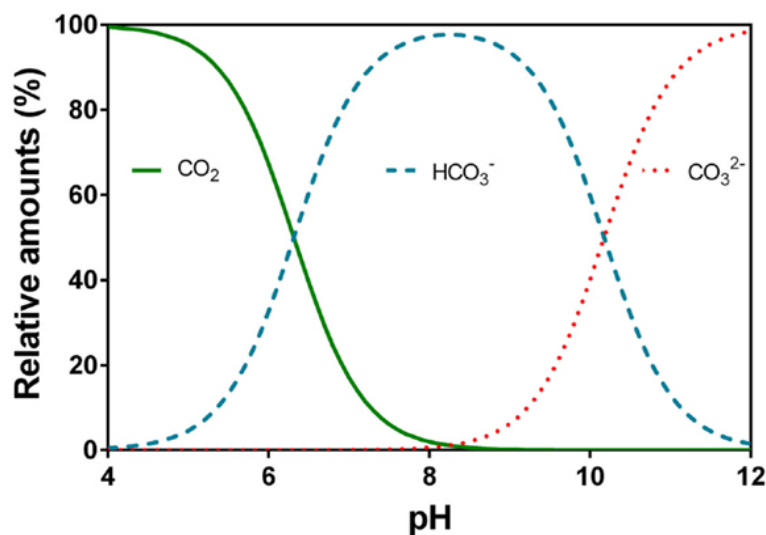
Figure 2.9 Speciation of carbon dioxide (CO_2), bicarbonate (HCO_3^-), and carbonate (CO_3^{2-}) in water as a function of pH
The figure was extracted from the paper by Pedersen et al., 2013, in which they calculated the data at 20°C and electrical conductivity of 250 μS cm^{-1} using CurTiPot developed by Gutz, 2012. Here, pK_1 = 6.532 and pK_2 = 10.329 (Schwarzenbach and Meier, 1958).

The remaining candidate gene found is *CDPK13*. Its mutant *cdpk13-2* showed a strong CCM phenotype in its first spot test conducted under constant light. However, this phenotype became very subtle in both spot tests when a light-dark cycle was implemented. This could possibly be due to the change in lighting conditions. Within the

two light-dark cycle tests, *cdpk13-2* shared similar phenotypes at pH 7.4 and 7.8- slightly reduced growth compared to WT in limiting CO_2- but not at pH 8.0 as it could not grow well in all CO_2 condition in the second test while it only had a subtle CCM phenotype in the first one. This could either be due to pipetting error in the second test. Nevertheless, the subtle CCM phenotype at the lower pH levels still suggested that CDPK13 might have a functional role in the CCM.

When the spot tests were carried out again in the continuous light, the phenotypes of the mutants either stayed the same or became more serious. It must be noted that the mutants of Cre16.g676800, Cre02.g092150, *CYG52*, *CYG16* were not included here as their results in the initial and replicated spot test showed variations that made it hard to compare with the results in continuous light. The increase in the severity of the reduced growth phenotype was seen in *cpld63-2* and *cdpk13-2*. The CPLD63 mutant exhibited no growth under all autotrophic conditions and showed a slightly reduced growth when in the TAP control plate where carbon source was available when everything was incubated under continuous light. For mutant *cdpk13-2*, its CCM phenotype was more severe at pH 7.4 and 7.8 under continuous light, which was similar to its first continuous light spot test screen. Both mutants actually grew better in the same conditions in the spot test carried out under a 12:12 light:dark cycle. These indicated that prolonged light stress could worsen the non-WT phenotypes seen in both mutants, suggesting that both proteins might have a role in the acclimation to light stress in *Chlamydomonas*. Nevertheless, since the project's focus is on CO_2-sensing and Ca^{2+}-signalling, the effect of light on the mutants was not studied in subsequent experiments. Instead, every *Chlamydomonas* strain experiments was carried out under continuous light using non-synchronised cultures as the phenotypes in the mutants were clearer in the spot test under these conditions.

After further consideration on the spot test results, *CDPK13*, *CGLD1* and *CPLD63* were chosen as the candidate genes for further study. The focus of the project also shifted to Ca^{2+} signalling more as these genes encode putative proteins with Ca^{2+} related function.

CDPK13 could play a role in regulating the *Chlamydomonas* CCM based on the findings in both the literature (Mackinder et al., 2017) and this research. As mentioned before, the kinase has been found as an interactor of the CCM Ci transporter HLA3 by Mackinder et al., 2017. This suggested that it could play a role in the functioning of the

Chlamydomonas CCM. Indeed, this was confirmed from the showing of CCM phenotypes in the spot tests by its mutant in this study. The *in silico* analysis performed so far also provides evidence that it might function as a Ca^{2+}/calmodulin-dependent kinase. A hypothesis of the role of CDPK13 in the *Chlamydomonas* CCM is that it phosphorylates HLA3 and possibly other important CCM proteins to induce the CCM pathway in response to change in Ca^{2+} and/or CO_2 concentration in the environment. It is possible that CDPK13 can sense CO_2 or HCO_3^- directly, but there has not been an example of a CDPK protein with such ability known yet. It is more likely that an upstream regulator that senses Ci directly is present to regulate CDPK13 through the usage of Ca^{2+} as a second messenger. In order to test this hypothesis, it is important to first validate that the disruption of *CDPK13* gene is the cause of the CCM phenotype in *cdpk13-2* by performing a complementation experiment. If the mutant grew well in limiting CO_2 conditions after being complemented with the gene, it could be confirmed that the disturbed CCM phenotype was indeed caused by the mutation of *CDPK13*. On the other hand, adding protein kinase domains from other superfamily in *Chlamydomonas* and other species to the phylogenetic tree could help improve the tree's accuracy in indicating the possible function of CDPK13. In addition, bioinformatic software like the Predikin webserver (Saunders and Kobe, 2008) could be used to predict the consensus motifs in the substrates of CDPK13 and thus aid in finding downstream targets of the kinase. Biological experiments such as *in vitro* kinase assays of purified CDPK13, phosphoproteomics analysis of HLA3 and other CCM proteins in WT and *cdpk13-2*, pull-down experiments, localisation and qRT-PCR of CCM genes in *cdpk13-2* should also be carried out in the future to investigate the biological function, interacting partners and the role of CDPK13 in the *Chlamydomonas* CCM.

As for CGLD1 and CPLD63, the spot test results showed that the former might play a more specific role in regulating the CCM whereas the latter might be more important for photosynthesis in general. Both proteins were predicted to be members of the UPF0016 family. Although the family contains mostly uncharacterised proteins, two members, TMEM165 in human and Gdt1p in yeast, have been found to be involved in Ca^{2+} transport and pH homeostasis (Demaegd et al., 2013, 2014). In fact, they were found to be homologues of CGLD1 and CPLD63 together with many other GDT-like proteins in species that are more closely related to *Chlamydomonas* as shown in their phylogeny trees (Figure 2.8). In addition, CGLD1 and CPLD63 are homologues of *Arabidopsis* BICAT1 and

BICAT2 respectively. The BICATs have recently been found to transport Ca^{2+} across the thylakoid membrane (BICAT1) and the chloroplast envelope (BICAT2) (Frank et al., 2019). CGLD1 and CPLD63 could also function as Ca^{2+} transporter in the same cellular compartments in *Chlamydomonas.* However, this would have to be confirmed with localisation data obtained by microscope imaging or biochemical methods, as the prediction from TargetP and Predalgo showed that CGLD1 is located in the secretory pathway while CPLD63 is located either in the mitochondrion or the chloroplast. If CGLD1 and CPLD63 are indeed confirmed to locate at the thylakoid membrane and the chloroplast envelope respectively as well as perform Ca^{2+} transport activity in *Chlamydomonas*, it could be hypothesised that they work together to facilitate the unidirectional transport of Ca^{2+} from the cytosol into the pyrenoid-thylakoid tubules to elevate the Ca^{2+} concentration in the pyrenoid needed for the upregulation of HLA3 and LCIA expression, possibly through CAS1, when the CCM is initiated. To test this hypothesis, the two proteins were characterised in different experiments afterwards and the results will be discussed in the next two chapters. It is noted that as the spot test results of *cpld63-2* and a previous research paper of CGLD1 (Xing et al., 2017) suggest that they are also important for the photosynthesis process with CGLD1 also being found to involve in Manganese (II) ions (Mn^{2+}) uptake in *Chlamydomonas*, controls were established carefully in the characterisation experiments to study their roles in the algal CCM and transporting Ca^{2+} specifically.

There were several discrepancies seen the results of this study that should be addressed in future researches. The first one happened in the spot tests, in which many mutants showed different phenotypes across two replicated experiments. It is unclear why this was the case. All the conditions were the same except the agar used was changed from typical agar to plant agar when preparing the TP agar, which should have little effect on the growth of the strains. A possible reason could be there was cross contamination between species as the starting cultures had been subcultured continuously in 15 ml falcon tubes for about two months. The spot test under both light-dark cycle and continuous light should be carried out again using fresh cultures and freshly made media for the mutants with inconsistent phenotypes to validate the results of the spot tests on this study. By making sure that all materials are fresh might help prevent cross-contamination between strains and ensure the strains are healthy before the experiment. The second one is the inconsistency seen in the protein kinase family annotation of the

HsTrb1 and ScCAK1 group between this study and the literature when constructing the phylogeny tree for CDPK13. This is likely caused by the different alignment and tree construction methods used: the alignment and tree-building were done with ClustalW and maximum likelihood in this study, while Manning et al., (2002) first built an initial tree using ClustalW and neighbour-joining and then modified the tree using references from other methods such as hmmalign and parsimony trees. Next time multiple statistical models should be combined in usage to construct a more accurate tree.

In conclusion, CDPK13, CGLD1 and CPLD63 could be members of important components involved in linking the Ca^{2+} signalling pathway to the *Chlamydomonas* CCM. Since there is a time limit on the project, and that the *cgld1* and *cpld63* mutants showed more consistent phenotypes in the spot test compared to *cdpk13-2*, the two putative Ca^{2+} transporters became the focus of the characterisation experiment in the following chapters. CDPK13 was put into the list of interesting CCM candidate together with the other interesting proteins found in the beginning of this study for the lab to look into in the future.

3 Characterisation of CGLD1 and CPLD63

3.1 Abstract

Ca^{2+} signalling is important for many biological processes in many organisms. This includes the regulation of the CCM and photosynthesis in *Chlamydomonas*. Two UPF0016 proteins, CGLD1 and CPLD63, were found to be important for these two processes from previous chapter. They are hypothesised to be Ca^{2+} transporters that would help link Ca^{2+} signalling to the CCM. In this study, some evidences of the two proteins being Ca^{2+} transporters were established. CGLD1 was found to localise to the thylakoid membrane while CPLD63 was found enriched at the chloroplast envelope. However, due to failure to visualise Ca^{2+} in the *Chlamydomonas* pyrenoid using a fluorescent Ca^{2+} dye and to express CGLD1 and CPLD63 in *E. coli* cells for Ca^{2+} influx assay, a direct investigation of whether the two proteins have Ca^{2+} transport activity was not possible. Future experiments would be needed to fully understand the function of CGLD1 and CPLD63 in the green alga.

3.2 Introduction

The signal transduction molecule Ca^{2+} has always played an important role in the regulation of many biological processes in response to environmental changes in eukaryotes. In humans, Ca^{2+} signalling affects the function and properties of many proteins to regulate different physiological systems (Clapham, 2007; Uhlén and Fritz, 2010; La Rovere et al., 2016; Toth, Shum and Prakriya, 2016), and its dysfunction is found to cause many human genetic disorders such as various cardiovascular, musculoskeletal and neurodegenerative diseases (Hörtenhuber et al., 2017; Pchitskaya, Popugaeva and Bezprozvanny, 2018). In fungi, maintaining Ca^{2+} homeostasis is important for growth, virulence and stress response in diverse environments (Su et al., 2009; Deka and Tamuli, 2013; De Castro et al., 2014; Kim et al., 2015; Jiang et al., 2018; Zhang et al., 2019; Lange and Peiter, 2020). In plants, Ca^{2+} signal transduction is not only important for growth, development and stress response, it is also important in the regulation of photosynthesis (Demidchik et al., 2018; Kudla et al., 2018; Wang et al., 2019; Navazio et al., 2020; Pirayesh et al., 2021). The same goes for *Chlamydomonas*, where Ca^{2+} signalling plays an important role in different biological processes (Wheeler, 2017) such as flagella function and motility (Wheeler, Joint and Brownlee, 2008; Aiyar et al., 2017; Fort et al., 2021), response to salt and osmotic stress (Pittman et al., 2009; Bickerton et al., 2016), photosynthesis (Petroutsos et al., 2011; Terashima et al., 2012; Trippens, Reißenweber and Kreimer, 2017), and the CCM (Wang et al., 2014, 2016c; Christensen et al., 2020).

The importance of Ca^{2+} in regulating the *Chlamydomonas* CCM was established when it was discovered that depleted extracellular Ca^{2+} disrupted the accumulation of the CCM Ci transporters HLA3 and LCIA in LCO_2 condition (Wang et al., 2016c). Furthermore, it was found that Ca^{2+} in the chloroplast accumulated in the pyrenoid when transferred from HCO_2 to LCO_2 condition in light. It is suggested that the mechanism behind this involves the Ca^{2+}-mediated retrograde signalling by CAS1 from the pyrenoid to the nucleus to up-regulate the transcription of HLA3 and LCIA (Wang et al., 2016c; Pivato and Ballottari, 2021). This is based on the findings that the Ca^{2+}-binding CAS1 was also needed for the accumulation of the two Ci transporters in the CCM and that CAS1 proteins transitioned from being dispersed throughout the thylakoid membrane in HCO_2 to being enriched in the thylakoid-pyrenoid tubules in LCO_2 (Wang et al., 2014, 2016c). In addition, it was found that there was no disturbance to the LCO_2-induced elevation of Ca^{2+} in the pyrenoid in *cas1* mutant (H82) cells. Collectively, this implies that an influx of Ca^{2+} into

the pyrenoid happens upstream of CAS1 upon transition to LCO_2 condition and this activates the retrograde signalling of CAS1 to the nucleus to enhance the expression of HLA3 and LCIA, thus inducing and maintaining the CCM.

Currently, there is little known about the components involved in the active transport of Ca^{2+} into the pyrenoid needed for this mechanism. A recent study showed that TRP2, a putative Ca^{2+} channel, was needed for acclimation to limiting-CO_2 conditions in *Chlamydomonas* and the mutation of *TRP2* in the mutants resulted in a decrease in *CAS1* expression (Christensen et al., 2020). Moreover, TRP2 is predicted to localise to the chloroplast and contain the *transient receptor ion channel II* domain that is required for passage of Ca^{2+} (Vannier et al., 1999; Christensen et al., 2020). The study therefore proposed that TRP2 acted as a Ca^{2+} channel that played a role in the Ca^{2+}-dependent pathway in the *Chlamydomonas* CCM. Nevertheless, the evidence linking TRP2 directly to Ca^{2+} changes in the pyrenoid is still lacking and warrants further studies.

In the meantime, the possibility that other Ca^{2+} channels or transporters are involved in Ca^{2+}-mediated regulation of the CCM could not be dismissed. In fact, the results in Chapter 2 suggest that CGLD1 and CPLD63 could hypothetically function as such Ca^{2+} transporters. The two proteins belong to the UPF0016 family and are homologues of many GDT-like proteins in other organisms (see Chapter 2). The UPF0016 family contains a group of largely uncharacterised transmembrane proteins that share one or two copies of the consensus motif E-ɸ-G-D-[KR]-[TS] (Demaegd et al., 2014; Colinet et al., 2017; Thines, Stribny and Morsomme, 2020). Recent studies on different members of the family in bacteria, human, yeast and plant have helped shed light on their function as cation transporters of either Mn^{2+}, Ca^{2+} and/or H^+ (Reviewed by Thines, Stribny and Morsomme, 2020). A few members found to be linked to Ca^{2+} homeostasis include yeast Gdt1p, human TMEM165, and *Arabidopsis* BICAT1 and BICAT2. Gdt1p is a Ca^{2+}/H^+ antiporter that localises to the Golgi in yeast and co-operates with Ca^{2+}/Mn^{2+} P-type ATPase PMR1 (Plasma Membrane ATPase Related 1) to maintain Ca^{2+} and Mn^{2+} homeostasis in the Golgi lumen (Demaegd et al., 2013, 2014; Colinet et al., 2016, 2017; Dulary et al., 2018; Thines et al., 2018). TMEM165 is a Ca^{2+}/H^+ antiporter found located to the Golgi in human and also important for the Ca^{2+} and Mn^{2+} homeostasis in the Golgi lumen (Demaegd et al., 2013; Reinhardt, Lippolis and Sacco, 2014; Potelle et al., 2016). BICAT1 and BICAT2 are found at the thylakoid membrane and chloroplast envelope

respectively of *Arabidopsis* and shown to be important for the Mn^{2+} transport to the thylakoid lumen and also play a function in Ca^{2+} homeostasis in the chloroplast (Schneider et al., 2016; Wang et al., 2016a; Eisenhut et al., 2018; Zhang et al., 2018; Frank et al., 2019). As homologues to BICAT1 and BICAT2 respectively, there is a possibility that CGLD1 and CPLD63 also act as Ca^{2+} transporters needed for the uptake of Ca^{2+} from the cytosol into the chloroplast stroma and thylakoid lumen and finally the pyrenoid needed for the induction of the CCM.
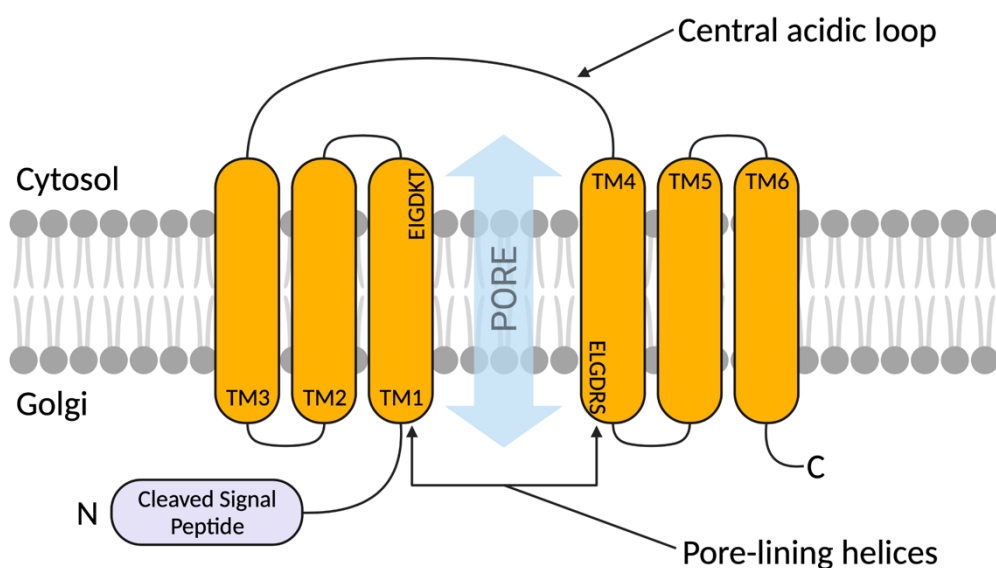
Figure 3.1 Topology predicted for Gdt1p.
This schematic is redrawn from the predicted topology schematics of Gdtp from existing literatures (Demaegd et al., 2014; Colinet et al., 2017). The two UPF0016 consensus motifs are located to the pore-lining helices.

Through bioinformatic analysis, the UPF0016 members are classified into 12 subfamilies (I to XII), with prokaryotic members in the subfamilies I to VI and eukaryotic members in the subfamilies VII to XII (Demaegd et al., 2014). Topology analysis predicts that the eukaryotic members are single proteins that contain two homologous regions with three transmembrane helices each except for the plant subfamily VII, which includes an extra transmembrane span before the first transmembrane region. With further study on the yeast Gdt1p (Colinet et al., 2017), it was identified that the two consensus E-ɸ-G-D-[KR]-[TS] motifs are located on transmembrane 1 (TM1) and transmembrane 4 (TM4), and that these two transmembrane helices are predicted to make up the inner lining of the pore in the transporter (Figure 3.1). It is also found that the acidic and uncharged polar residues of these two consensus motifs (E53, D56, T58, E204, D207 and S209) are essential for the calcium transport activity of Gdt1p and calcium tolerance in yeast, and

are therefore proposed to make up the Ca^{2+}-binding site in Gdt1p. An investigation into whether CGLD1 and CPLD63 contain these important features could help increase the probability that the two *Chlamydomonas* UPF0016 have Ca^{2+} transporting activity.

The two *Chlamydomonas* proteins themselves remain largely uncharacterised in *Chlamydomonas*. They were identified as GreenCut proteins (proteins conserved among green algae and land plants but not found in non-photosynthetic organisms) and only a few studies have been done on CGLD1 (Merchant et al., 2007; Heinnickel and Grossman, 2013; Schneider et al., 2016; Xing et al., 2017). CGLD1 has been found to be important for the maintenance of the structure and function of PSII, as well as tolerance against photo-oxidative stress in *Chlamydomonas* (Schneider et al., 2016; Xing et al., 2017). A supplement of excess Mn^{2+} but not Ca^{2+} was also shown to rescue the impaired PSII activity in two *cgld1* mutants (Schneider et al., 2016; Xing et al., 2017). Therefore, CPLD1 was proposed to be involved in Mn^{2+} homeostasis rather than Ca^{2+}. Nevertheless, the mechanism behind this is still unknown and data directly showing Mn^{2+} transport activity in CGLD1 has yet to be obtained. Meanwhile, a study on *Chlamydomonas* acetate-requiring mutants identified *CPLD63* to be one of the genes disrupted but was not considered as higher-confidence photosynthesis candidate genes after further manual curation of the disrupted genes (Wakao et al., 2021). The exact roles of CGLD1 and CPLD63 in *Chlamydomonas*, let alone their possible link to the algal CCM, still require further investigation.

This study therefore aims to characterise the roles of CGLD1 and CPLD63 in the *Chlamydomonas* CCM and investigate whether they contain Ca^{2+} transport activity. The effects of different Mn^{2+} and Ca^{2+} concentrations on the growth of the mutants tested in the previous chapter were investigated again using spot tests. To check whether *CGLD1* and *CPLD63* were the causative genes for the phenotypes of the mutants, they were complemented in the respective mutants and tested in a spot test again. Furthermore, WT and complemented lines transformed with fluorescently tagged CGLD1 or CPLD63 were imaged with confocal microscope to check the localisation of the two proteins. Finally, protein sequence and predicted 3D structure alignments between the two proteins and their *Arabidopsis* and yeast homologues as well as attempts to visualise Ca^{2+} in the *Chlamydomonas* pyrenoid and to express CGLD1 and CPLD63 in *E. coli* strains for

Ca^{2+} influx assay were carried out in order to check whether they exhibit Ca^{2+} transport activity.

3.3 Materials and Methods

3.3.1 Algal strains and culture conditions

Chlamydomonas strain CC-4533 was used as the WT. The CLiP mutants of CGLD1 and CPLD63 (Li et al., 2016) used here were the same ones tested in Chapter 2. All strains were maintained under low light (~5-10 µmol photons m^{-2} s^{-1}) on TAP medium agar plate with revised Hutner's trace elements (Kropat et al., 2011) at 21°C in a temperature-controlled room. WT strain was maintained on TAP plates without antibiotics; the CLiP mutants and strains transformed with fluorescently-tagged or untagged plasmids were maintained on plates with 20 µg ml^{-1} paromomycin or 25 µg ml^{-1} hygromycin or a combination of them. When transferred to liquid culture for experiment, all antibiotics were used at a ten times dilution of that in the agar medium.

3.3.2 Spot test of *Chlamydomonas* lines

To test whether CGLD1 and CPLD63 are important for the homeostasis of Mn^{2+} or Ca^{2+} in *Chlamydomonas*, mutants of *CGLD1* and *CPLD63* were screened in spot tests at different Mn^{2+} and Ca^{2+} concentrations. The WT and mutant strains *epyc1*, *cgld1*, *cpld63-1*, *cpld63-2* were first prepared and tested via spot tests under continuous light using the same procedures as in Chapter 2 but under different experimental conditions. They were tested either under a set of varying Mn^{2+} concentrations of 0.25, 6 or 60 µM, or under a set of different Ca^{2+} concentrations of 0.068, 0.34011 or 2 mM, with the pH being kept at 7.8. This pH was selected because mutants of both genes showed clear defect in growth compared to WT in previous spot tests. For the set with varying Mn^{2+} concentrations, the strains were washed with TP minimal medium with 0.25 µM Mn^{2+} before spotting, whereas TP medium with 0.068 mM Ca^{2+} was used to wash the other set with different Ca^{2+} concentrations beforehand. A TAP plate with 6 µM Mn^{2+} and 0.34011 mM Ca^{2+} was also included as controls.

Another batch of spot tests was also carried out for the mutants and their complemented lines. The basic procedures were the same for all tests in this batch except the following conditions. Mutant *cgld1* and its complemented lines were tested at two different Ca^{2+} concentrations (0.068 and 0.34011 mM) while the pH was kept the same at 7.8. The results of lines with the most significant phenotype rescue are shown in the results. The mutants of CPLD63 and their respective complemented lines were tested at pH 7.8 and

8.0 while the Ca^{2+} concentration was kept the same at 0.34011 mM. Again, a TAP plate was included for each test as control.

3.3.3 Plasmids cloning and construction

To localise different target genes in *Chlamydomonas* cells and to complement the disrupted gene in the mutant strains, different plasmids were constructed using the recombineering method developed by Emrich-Mills et al., 2021. The backbones of these plasmids were first amplified from the tagging plasmid Hygro_mScarlet-i (with hygromycin resistant and mScarlet-i tag) using different pairs of primers (Appendix B, Table B.1). The target genes were then inserted into the amplified backbones through homologous recombination between the backbone and the bacterial artificial chromosomes (BACs) containing these genes. The following plasmids were constructed: CGLD1 tagged with mScarlet-i (CGLD1_mScarlet-i), CGLD1 without any tags (CGLD1_Hygro), CPLD63 tagged with mScarlet-i (CPLD63_mScarlet-i) and CPLD63 without any tags (CPLD63_Hygro).

To express CGLD1 and CPLD63 in *Escherichia coli*, two expression plasmids were designed and attempts were made to construct them using a technique called Ligation Independent Cloning (LIC). The technique has been optimised for our lab by postdoctoral researcher Philipp Girr and PhD student James Barrett. DNA inserts of *CGLD1* and *CPLD63* were amplified by Phusion DNA Polymerase (Thermofisher, #F-530S) from cDNA obtained previously from LCO$_2$-acclimated *Chlamydomonas* WT strain using primers designed with LIC fusion tags added (Appendix B, Table B.1). They were then purified using the QIAquick PCR Purification Kit (Qiagen, 28104 and 28106). The plasmid pET His6 TEV LIC cloning vector (1B) was obtained from Addgene (a gift from Scott Gradia, plasmid # 29653; http://n2t.net/addgene:29653; RRID: Addgene_29653) and was digested with SspI-HF (New England BioLabs, #R3132L) and purified using the QIAEX II Gel Extraction Kit (Qiagen, #20021) to provide the backbone vector. A LIC reaction was then carried out for the vector and the two inserts respectively. Varied amount of vector and inserts were used in this step depending on how much would be used in the annealing step later. The vector was mixed with 1 µl NEBuffer 2.1 (New England BioLabs, #B7202S), 2 µl 25 mM dGTP (Sigma-Aldrich, #D5038), 1 µl 100 mM DTT (from the reverse transcriptase kit mentioned in section 3.3.5), 0.4 µl T4 DNA polymerase (New England BioLabs, #M0203L) and made to a final volume of 10 µl with molecular grade water. Each insert was also

mixed with the same reagents except that dGTP was swapped to dCTP (Sigma-Aldrich, #D4913). After that, the reaction mixtures were first incubated at 20°C for 40 min and then at 75°C for 20 min. Next, an annealing step was carried out by mixing the vector LIC reaction with either *CGLD1* or *CPLD63* insert LIC reaction in a mass ratio of 1:3 in a total volume of 5-10 μl and incubating the mixture at room temperature for 30 min. The mixture was then transformed into DH5α competent cells. The cells were selected on 50 μg ml^{-1} kanamycin LB agar plates. Plasmid DNA was miniprepped from grown colonies and sent to Eurofins Genomics for sequencing. After many cloning attempts, only the expression plasmid with *CGLD1* insert was successfully constructed. It was named pET-1B-CGLD1.

3.3.4 Transformation of *Chlamydomonas* strains

WT and mutant *Chlamydomonas* strains were transformed with the recombineered plasmids mentioned above using the electroporation method described by Mackinder et al., 2017. Two different restricrion enzymes, I-SceI (New England BioLabs, #R0694L) or EcoRV (Promega, #R635A), were used in the digestion step depending on the plasmids used. The combination of plasmids and strains are: WT with either CGLD1_mScarlet-i or CPLD63_mScarlet-i; *cgld1* with either CGLD1_mScarlet-i or CGLD1_Hygro; *cpld63-1* and *cpld63-2* with either CPLD63_mScarlet-i or CPLD63_Hygro. The transformants were spread on TAP agar plates with the suitable antibiotics and grown under 50 μmol photons m^{-2} s^{-1} until colonies appeared. The following antibiotics combination were used for the plates: 20 μg ml^{-1} paromomycin and 25 μg ml^{-1} hygromycin for transformed mutant strains; 25 μg ml^{-1} hygromycin for transformed WT. For the co-localisation of CGLD1 with PSAF, and CPLD63 with TIC20, positive colonies of WT transformed with CGLD1_mScarlet-i or CPLD63_mScarlet-i were also transformed with plasmids PSAF_Venus and TIC20_Venus (with paromomycin resistant and CrVenus tag) respectively. PSAF_Venus was constructed through recombineering by former lab member Gary Yates while TIC20_Venus was constructed using Gibson assembly by Chris Chen in the study done by Mackinder et al., (2017). To test whether the target genes had been successfully tagged in the strains, their colonies were first scanned using a GE Amersham Molecular Dynamics Typhoon 8610 Bio Molecular Imager (Chlorophyll with Ex 633nm and Em 670/30nm, Venus with Ex 532nm and Em 555/20nm, mScarlet-i with Ex 532nm and Em 610/30nm). The positive colonies were then imaged with a confocal microscope. For strains expressing untagged plasmids, gDNA of grown colonies were

screened in a PCR test using primers (Appendix B, Table B.3) that amplify the target genes in the plasmid. Those with amplification were then screened in a spot test to see if they complemented the phenotype of the mutants or not.

3.3.5 RNA extraction and reverse transcription PCR (RT-PCR)

To verify whether the target genes were expressed in the complemented lines of the mutants, a RT-PCR was conducted on the total RNA extracted from LCO_2-acclimated WT, mutants and the complemented lines using different primers designed for the transcripts of CGLD1 and CPLD63 (Appendix B, Table B.4). The strains were first cultured in TAP medium until log phase cell density reached 2-6 x 10^6 cells ml^{-1}. They were then diluted and transferred to TP medium at pH 7.8 under a light intensity of about 150 µmol photons m^{-2} s^{-1} and bubbled with HCO_2 (3%) until the cell density reached about 2-6 x 10^6 cells ml^{-1} again. After that, they were transferred to LCO_2 (0.04%) bubbling for 5 hours. 2 ml of sample was then taken for each strain and centrifuged at 4000 x g for 4 min at 4°C. The supernatant was discarded and each cell pellet was resuspended with 750 µl TRIzol^{TM} Reagent (Invitrogen, #15596018). Total RNA was extracted from them following the TRIzol^{TM} Reagent RNA isolation protocol provided by the manufacturer. The extracted RNA was then treated with DNase-I, RNase-free (Thermo Fisher Scientific, #EN0521) according to the manufacturer's protocol (1 unit of enzyme per 2.5 µg RNA). After that, cDNA was generated from 500 ng of the DNAse-treated RNA for each sample in a 20 µl reaction mix following the manufacturer's protocol for SuperScript^{TM} IV Reverse Transcriptase (Invitrogen, #18090050). Reagents used for the reverse transcription not present in the transcriptase kit included: Oligo(dT)$_{18}$ Primer (Thermo Fisher Scientific, #SO132), dNTP mix (Thermo Fisher Scientific, #R0192), and RNaseOUT™ Recombinant Ribonuclease Inhibitor (Invitrogen, #10777019). The cDNA was then tested with PCR using the same protocol used for testing the gDNA in Chapter 2 except for the following steps: the annealing temperature was 59°C for CGLD1 primers and 55°C for CPLD63 primers, and the extension temperature was 68°C. The products were checked on a 1% agarose gel.

3.3.6 Confocal microscope imaging of fluorescently-tagged proteins

The selected colonies from the *Chlamydomonas* strains transformed with fluorescently-tagged target genes were imaged using confocal microscopy. They were first grown in TAP liquid medium to adequate cell density and then cultured in TP liquid medium for at

least 24 hours to induce the CCM before imaging. The strains were imaged using a Zeiss LSM 880 with Airyscan on a fully motorised inverted microscope (561nm Ex, 570-615nm Em for mScarlet-i, 514nm Ex, 525-550nm Em for Venus, 633nm Ex, >660nm Em for Chlorophyll). The images were processed using Fiji (ImageJ software, download site https://fiji.sc).

3.3.7   Chlorophyll measurement of *cpld63-1* and its complement lines

To verify whether the complement lines of mutant *cpld63-1* had a rescued phenotype in regards to the mutant's paler colour in spot test, a chlorophyll measurement of autotrophically grown liquid cultures of WT, *cpld63-1* and its complement lines was carried out. The strains were first cultured in TAP medium until cell density reached 2-6 x 10^6 cells ml^{-1}. They were then washed with TP medium first and diluted to 2 x 10^5 cells ml^{-1} in 50 ml TP of pH 7.8 each. They were then incubated in air (about 0.04% CO_2) until cell density reached as close to 2 x 10^6 cells ml^{-1} as possible under light conditions used in the continuous light spot test (see Chapter 2). Afterwards, 3 ml of sample was taken from each strain and pelleted and resuspended in 1 ml 100% methanol. After thoroughly mixing by vortexing and an incubation of 10 min, the sample was centrifuged at full speed for 5 min. The absorbance of the obtained supernatant was measured at 652nm and 665nm (UV/Visible Spectrophotometer 1000 series, Cecil Instruments) and the concentration of chlorophyll (a, b and a+b) was calculated using the equation provided by Porra, Thompson and Kriedemann, 1989.

3.3.8 Ca^{2+} staining in *Chlamydomonas*

To visualise the Ca^{2+} distribution in WT *Chlamydomonas* cells after CCM activation, WT cells acclimated in air (0.04% CO_2) in TP medium under ~150 µmol photons m^{-2} s^{-1} light were then incubated with either 15, 30, or 75 µM CalciumGreen-1, AM (Thermo Fisher Scientific, Invitrogen[TM] #C3011MP) under low light (about 10-15 µmol photons m^{-2} s^{-1}) following the protocol as described by (Wang et al., 2016c). The cells were either washed with Ca^{2+}-free (treated with 1mM EGTA) TP medium or High-Salt Medium (HSM) before incubation. Different duration times of the incubation step with the Ca^{2+} indicator, 30 min or >2.5 hours, were also tested to optimise the procedure. The cells were then imaged using a Zeiss LSM 780 multiphoton inverted microscope using 488nm excitation and 500-550nm emission for CalciumGreen-1, AM, and 633nm excitation and 638-740nm emission for chlorophyll.

3.3.9   CGLD1 and BICAT1 expression in *E. coli*

To express proteins CGLD1 and its *Arabidopsis* homologue BICAT1 in *E. coli* cells, ≤100 ng of pET-1B-CGLD1 and pBAD-BICAT1, the plasmid that was obtained from the Pierre Morsomme lab, were transformed into 25 µl Rosetta 2(DE3)pLysS Competent Cells (Merck, Novagen, #71403-3) individually and the expression of the proteins was performed using the BICAT1 expression protocol by Frank et al., 2019. The pBAD-BICAT1 plasmid was also transformed into BL21 pLysS cells as used by Frank et al., 2019. The transformed cells were grown in LB media with antibiotics (25 µg ml^{-1} chloramphenicol and 50 µg ml^{-1} kanamycin for pET-1B-CGLD1; 25 µg ml^{-1} chloramphenicol and 100 µg ml^{-1} carbenicillin for pBAD-BICAT1) at 37°C overnight and sub-cultured into fresh LB with antibiotics and incubated at 37°C again. For cells with pET-1B-CGLD1, the culture was grown until OD600 reached around 1 and IPTG was added to a final concentration of 0.5 mM to induce expression. For cells with pBAD-CGLD1, one set of cultures was grown until OD600 reached 0.6-0.8 while another set was grown until it reached 0.9-1.0 at which the expression was induced either by 1%, 0.1% or 0.01% L-arabinose. To check the technical accuracy of the procedure involved in processing the cells for running the SDS-PAGE gel and Western blot, expression of a His-tagged BST1 was also induced in Rosetta 2(DE3)pLysS cells previously transformed with an expression plasmid also constructed using the pET His6 TEV LIC cloning vector (1B) as the backbone. The BST1 induction was carried out using 1mM IPTG when the OD600 reached around 1. All cultures were incubated at 25°C after induction. Samples were taken for each culture before and 16 hours after induction except for BST1 the samples were taken before and 4 hours after induction. They were first centrifuged at 8000 x g at room temperature and were resuspended in 50 µl Laemmli SDS sample buffer, reducing (6X) (Alfa Aesar, #J61337), in which their OD600 were normalised to 2, and boiled at 100°C for 10 min to isolate total protein. 15 µl was then taken from each sample to be checked by SDS-PAGE using 10% Mini-Protean TGX precast protein gel (Bio-Rad Laboratories). After running the gel, proteins were transferred from it to an Immobilon-FL PVDF Membrane (Merck, Millipore, #IPFL00010) using a Bio-Rad Trans-blot SD Semi-dry Transfer Cell. The membrane was then blocked in 5% milk TBST- TBS with 0.1% Tween 20- at 4°C overnight. After rinsing with 1x TBST, the membrane was incubated in 3% milk TBST with 6x-His Tag Monoclonal Antibody (HIS.H8) Alexa Fluor 488 (Invitrogen, #MA1-21315-A488) added at a 1:10000 dilution for 1.5 hours in dark at room temperature. This antibody was used as both pET-

1B-CGLD1 and pBAD-BICAT1 contained His tag. Afterwards, the membrane was washed 3 times with 1x TBST for 10 min and then imaged with 488nm laser excitation and the Cy2 emission filters on a GE Amersham Typhoon 5 Scanner.

3.3.10 Bioinformatics analyses

The multiple alignment of the protein sequences of CGLD1, CPLD63 , BICAT1, BICAT2 and Gdt1p was performed using the ClustalW algorithm on the MEGA X software (Kumar et al., 2018). These sequences were also submitted to ColabFold for 3D structure prediction (Mirdita et al., 2022) and the top structure models predicted were visualised, aligned and edited using PyMol (https://pymol.org/2/). Protein molecular weights were calculated using the Protein Molecular Weight module of the Sequence Manipulation Suite (Stothard, 2000).

3.3.11 Statistical analysis

The chlorophyll measurements of WT, *cpld63-1* and its complemented strains were evaluated statistically by performing independent t-tests on the technical replicates using SPSS (IMB Corp, 2020).

3.4 Results

3.4.1 Structural comparison between CGLD1 and CPLD63 with their homologues

To check whether CGLD1 and CPLD63 contain structures needed for transporting Ca^{2+} as seen in some members of the UPF0016 family, their protein sequences and predicted 3D structures were compared to those of their *Arabidopsis* homologues BICAT1 and BICAT2, as well as the yeast Gdt1p. As shown in Figure 3.2 (red boxes), the two UPF0016 consensus motifs E-ф-G-D-[KR]-[TS] in CGLD1 aligned with those in BICAT1 and Gdt1p with a few different residues. This is the same case for the motifs in CPLD63, BICAT2 and Gdt1p. All the acidic and uncharged polar residues within the two motifs aligned perfectly within the two groups of protein (Figure 3.2, blue boxes): E51, D54, T56, E173, D176 and S178 in CGLD1; E170, D173, T175, E297, D300 and S302 in BICAT1; E53, D56, T58, E204, D207 and S209 in Gdt1p; E134, D137, T139, E261, D264 and S266 in CPLD63; and E157, D160, T162, E287, D290 and S292 in BICAT2. As these residues have been found to be important for the Ca^{2+} transport activity of Gdt1p and Ca^{2+} tolerance in the yeast (Colinet et al., 2017), it is likely that they play the same crucial role in CGLD1, CPLD63, BICAT1 and BICAT2. The few different residues in the consensus motifs between the proteins include: I52 and I54 in CGLD1 and Gdt1p but L171 in BICAT1; W174 and W298 in CGLD1 and BICAT1 but L205 in Gdt1p; K177 and K299 in CGLD1 and BICAT1 but R208 in Gdt1p; and W262 and W288 in CPLD63 and BICAT2 but L205 in Gdt1p. However, these changes between the residues are conservative and since the mutations of the residues outside of the acidic and uncharged polar residues of the two consensus motifs to alanine in Gdt1p did not affect the Ca^{2+} tolerance in the yeast, it is likely that such changes would not affect the Ca^{2+} activity of CGLD1 and CPLD63. In fact, BICAT1 and BICAT2 were still found to be important in Ca^{2+} transport in *Arabidopsis* despite the few differences between them and Gdt1p.
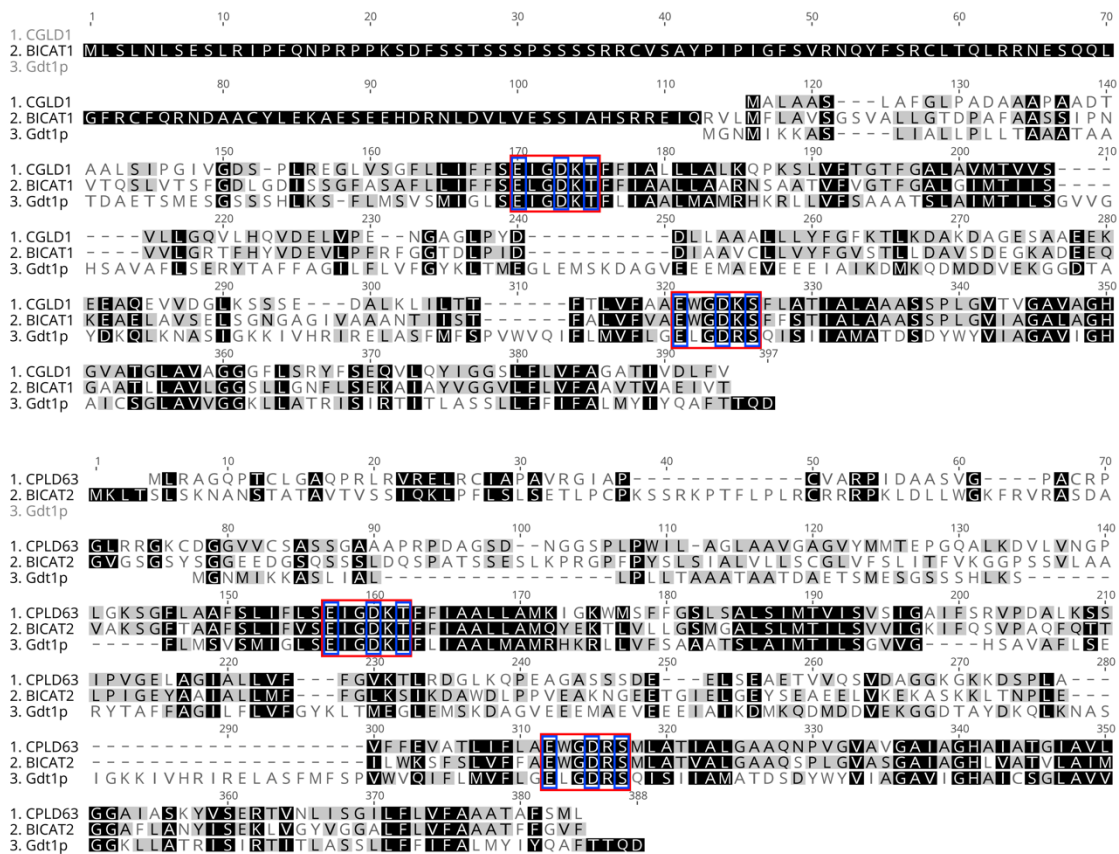
Figure 3.2 Protein sequences alignment of CGLD1 and CPLD63 to their homologues in *Arabidopsis* and yeast.
The consensus motifs, E-φ-G-D-[KR]-[TS], of the UPF0016 family are marked with the red boxes in each alignment. The blue boxes mark the important acidic and uncharged polar residues (E53, D56, T58, E204, D207 and S209) found important for the Ca^{2+} transport role of the yeast Ca^{2+} transporter Gdt1p (Colinet et al., 2017) as well as the corresponding residues in CGLD1 (E51, D54, T56, E173, D176 and S178), CPLD63 (E134, D137, T139, E261, D264 and S266), and the *Arabidopsis* Ca^{2+} transporters BICAT1 (E170, D173, T175, E297, D300 and S302) and BICAT2 (E157, D160, T162, E287, D290 and S292). The alignment was performed using the ClustalW algorithm in MEGA X software (Kumar et al., 2018).

Although the acidic and uncharged polar residues on the two consensus motifs in CGLD1 and CPLD63 align perfectly with those in their respective BICAT homologues and Gdt1p in the protein sequence alignment, it is important to also look at the actual positions of these residues on the 3D structure of proteins to determine whether they would serve the same roles in Ca^{2+} transport. As eukaryotic UPF0016 subfamily members are predicted as monomeric two-domain proteins (Demaegd et al., 2014), all proteins were modelled as monomers in ColabFold. The two consensus motifs are located in transmembrane domain 1 and 4 in Gdt1p and predicted to be two putative helices that form the pore-lining regions of the transporter (Colinet et al., 2017). This fits nicely into the 3D structure model predicted for Gdt1p by ColabFold, in which the acidic and uncharged polar residues on the two consensus motifs (Figure 3.3, marked in yellow on the blue structure) locate to the helices in the centre. The corresponding residues in CGLD1 and CPLD63 also localise to the innermost helices of their predicted 3D models (Figure 3.3, marked in yellow on the green and white structure), as do those in the

models predicted for the BICAT proteins (Figure 3.3, marked in yellow on the magenta and pink structure). When the model of CGLD1 is aligned with the BICAT1 model, their helices containing the consensus motifs line up well in position with the important acidic and uncharged polar residues overlapping each other between the two proteins. This can also be seen in the alignment of the models of CPLD63 and BICAT2. When aligned to the model of Gdt1p, these helices in CGLD1 and CPLD63 still line up with those in the yeast Ca^{2+} transporter but with a looser fit compared to when aligned with the BICAT proteins. Nevertheless, the acidic and uncharged polar residues of the two consensus motifs in CGLD1 and CPLD3 still fit in similar positions relative to those in Gdt1p on the helices. These all indicated that the two UPF0016 consensus motifs important for Ca^{2+} transport function are likely to form the pore-lining regions in CGLD1 and CPLD63 needed for transporting the cation across the membrane. One interesting feature to note from the alignments is that CPLD63, BICAT1, BICAT2 and Gdt1p all have an extra helix near the N terminal while CGLD1 does not possess this extra helix.
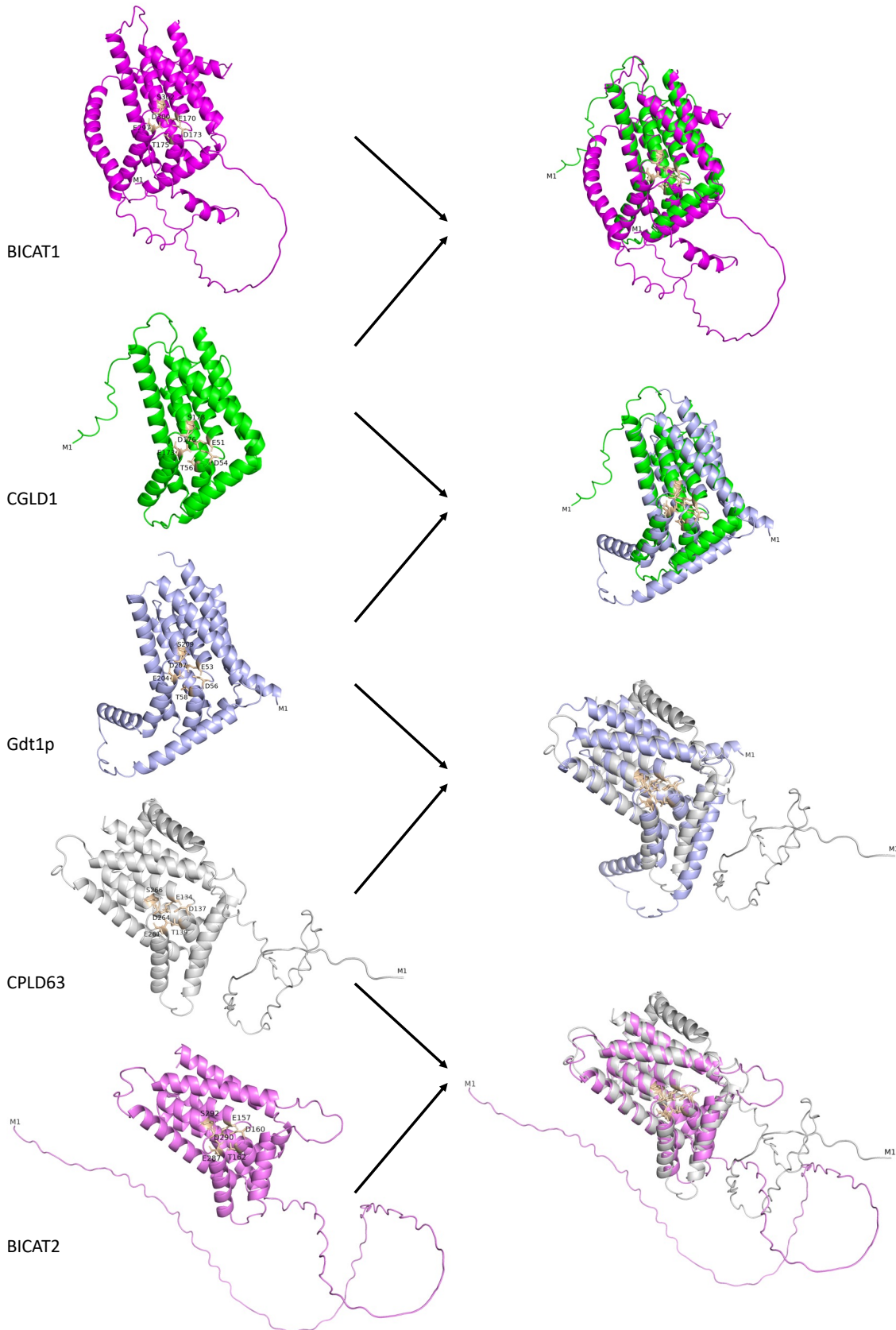
Figure 3.3 Visualisation and alignment of 3D structure models predicted for CGLD1, CPLD63, BICAT1, BICAT2 and Gdt1p. The important acidic and uncharged polar residues (E53, D56, T58, E204, D207 and S209) for Ca^{2+} transport in Gdt1p (Colinet et al., 2017) and the corresponding residues in the others are shown in yellow in each predicted 3D model. ColabFold (Mirdita et al., 2022) was used for the 3D structure prediction and PyMol was used to visualise, align and edit the predicted 3D models.

3.4.2 Spot test results of WT and mutants under different Mn^{2+} and Ca^{2+} concentrations

To check whether CGLD1 and CPLD63 were involved in maintaining Mn^{2+} or Ca^{2+} homeostasis needed in the functioning of the *Chlamydomonas* CCM, spot tests were conducted for their mutants and WT using TP agar with different Mn^{2+} and Ca^{2+} concentrations. Similar to the previous spot test, *cgld1* and *cpld63-2* exhibited a disturbed CCM and photosynthesis phenotype respectively when grown on TP plates at pH 7.8 with the standard Mn^{2+} (6 µM) and Ca^{2+} (0.34011 mM) concentrations used in the lab (Figure 3.4). Mutant *cpld63-2* showed a delayed growth even on the TAP plate, which contains a carbon source but was incubated under about 50 µmol photons m^{-2} s^{-1} light, suggesting that it could be sensitive to light. On the other hand, mutant *cpld63-1* grew relatively well in all conditions but exhibited a paler green colour in general when compared to the WT. This paler colour was more visible in photosynthetic conditions and barely noticeable on TAP. The changing concentrations of Mn^{2+} and Ca^{2+} in the media did not have any apparent effect on the *cpld63* mutants as they all grew similarly in all CO_2 conditions (Figure 3.4). However, the CCM phenotype of *cgld1* appeared to be rescued as the Mn^{2+} concentration increased, shown by its better growth in 6 µM and 60 µM Mn^{2+} at both LCO_2 and $VLCO_2$. On the other hand, when only the concentration of Ca^{2+} was varied, the lower Ca^{2+} concentration at 0.068 mM caused a more severe CCM phenotype in *cgld1*. This was shown by its more disturbed growth compared to the WT on the same plates when compared to the other two Ca^{2+} concentrations. In the meantime, the increase of Ca^{2+} concentrations from 0.34011 mM to 2 mM did not affect its phenotype.
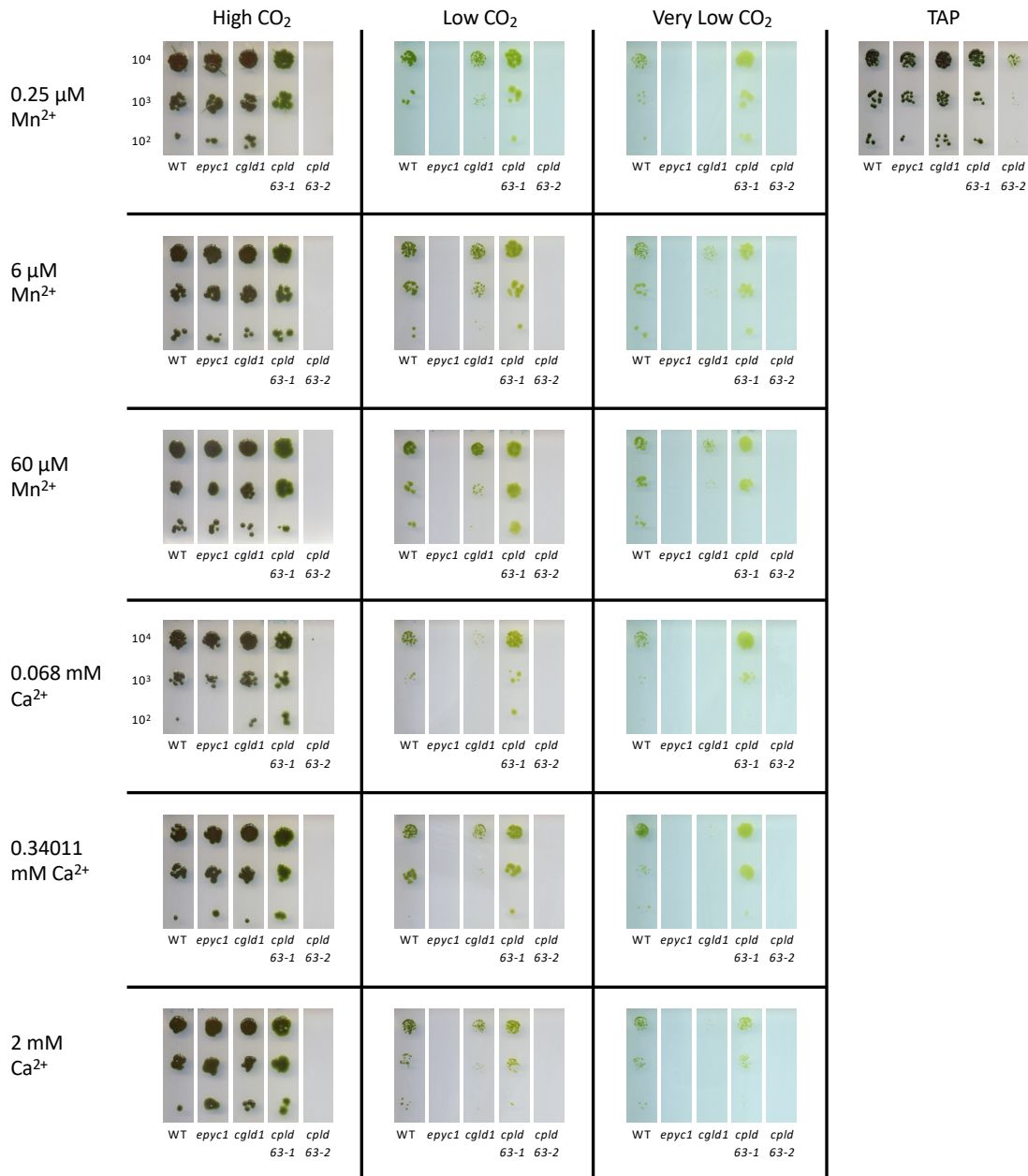
Figure 3.4 Spot test results of WT, *cgld1* and the two *cpld63* mutants in different Mn^{2+} and Ca^{2+} concentrations. The mutant strains were grown in groups on individual plates and their growth was compared to the WT strain on the same plate as them. Each sample was grown with a series of dilution: 10^4 (top), 10^3 (middle), and 10^2 (bottom) cells in total. They were also spotted on a TAP plate that was incubated under 50 µmol photons m^{-2} s^{-1} light as a control.

3.4.3 Growth assays and RT-PCR check of complemented mutant lines

To check whether the phenotypes of the mutants seen in previous spot tests were the results of disruption of the target genes, complemented lines were created and screened in spot tests. For *cgld1*, since the lower Ca^{2+} caused a more severe CCM phenotype, its complemented lines were screened at two different Ca^{2+} concentrations: 0.068 mM and 0.34011 mM to check whether they could also rescue the phenotype when Ca^{2+} was low. The result (Figure 3.5, top big row) showed three untagged complemented lines of *cgld1* (*cgld1*:CGLD1_Hygro) that had the most rescued phenotypes among the lines screened. The *cgld1*:CGLD1_Hygro lines A3, A4 and A5 all showed a rescued CCM phenotype in

LCO$_2$. Their growth was almost similar to WT as seen at the lower Ca^{2+} concentration while *cgld1* had very little growth. At the higher Ca^{2+} level, they appeared to have a very subtly better growth compared to *cgld1*, which was showing a very subtle CCM phenotype. In VLCO$_2$, line A3 showed better growth compared to *cgld1* at both Ca^{2+} concentrations, whereas lines A4 and A5 could only partially rescue the CCM phenotype at the higher Ca^{2+} level. In all cases where the *cgld1*:CGLD1_Hygro lines showed rescued CCM phenotypes compared to *cgld1*, they did not grow as well as the WT. All these showed that the lines had partially complemented the disruption of CGLD1 in the mutant.

On the other hand, the tagged and untagged complemented lines of the two *cpld63* mutants were tested with varying pH instead as the different Mn^{2+} or Ca^{2+} did not affect the mutants' phenotypes. Mutant *cpld63-1*, showed a paler green colour compared to the WT in all CO$_2$ conditions, while its tagged complemented lines (*cpld63-1*:CPLD63_mScarlet-i), B5 and B6, and untagged complemented lines (*cpld63-1*:CPLD63_Hygro), B3 and B4, appeared to have a slightly deeper green compared to it (Figure 3.5, middle big row). However, this difference in colour was not big enough to be reliably conclude by the naked eye solely and required further testing. As for mutant *cpld63-2*, its tagged complemented lines (*cpld63-2*:CPLD63_mScarlet-i), C6 and C7, and untagged complemented lines (*cpld63-2*:CPLD63_Hygro), C4 and C5, had rescued the growth defect of *cpld63-2* in HCO$_2$ condition and on the TAP plate (Figure 3.5, bottom big row). They appeared to have grown better than the WT, but this was likely due to contamination of the WT strains in this batch of experiment (seen clearly as the white spots growing in the WT spots on the TAP plate). Nevertheless, they grew well compared to the mutant. However, these complemented lines still could not grow well in limiting CO$_2$ conditions. These showed that the disruption of CPLD63 most likely caused the disturbed photosynthetic, or the increased light sensitivity, phenotype in *cpld63-2*. As discussed in Chapter 2, the insertion of CIB1 cassette into ACK1 in *cpld63-2* is unlikely to have caused its phenotypes in the spot tests, the presence of CCM phenotype in the *cpld63-2* complemented lines suggested that a third gene that is important for the *Chlamydomonas* CCM was disrupted in the mutant.
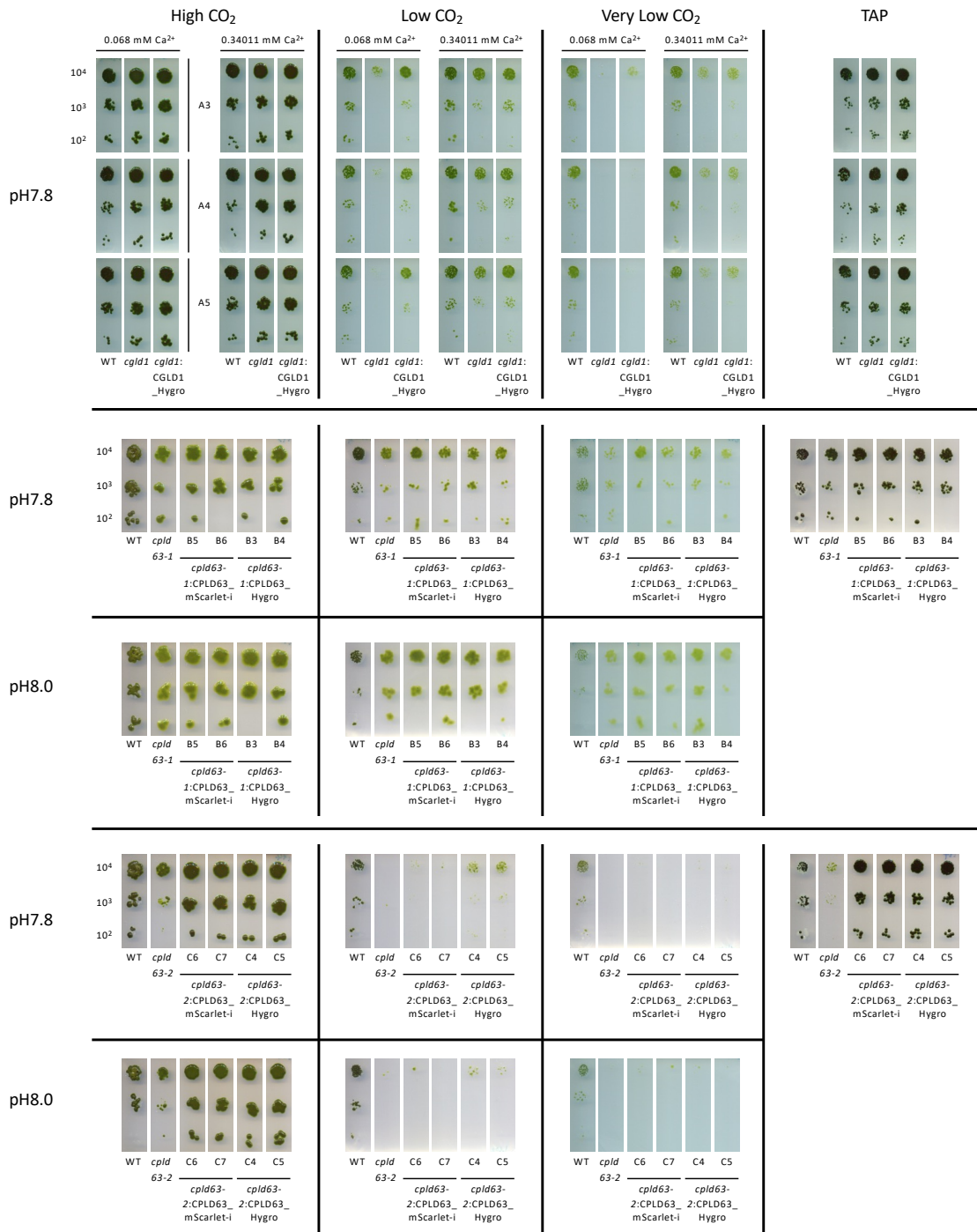
Figure 3.5 Spot test results of WT, mutants of CGLD1 and CPLD63, and their respective tagged and untagged complemented lines in different media conditions.

The complemented lines were grown in groups on individual plates and their growth was compared to the WT and mutant strains on the same plate as them. For mutant *cgld1*, three complemented lines (*cgld1*:CGLD1_Hygro) showing the most rescued phenotypes were shown here. The three lines were named A3, A4 and A5 and were each tested on an individual plate (separated by the rows of spots in the top big row). Therefore, the WT and *cgld1* strains on each of their plate was also shown here (separated from the complemented lines by the columns of spots in the top big row). For mutant *cpld63-1*, the tagged complemented lines (*cpld63-1*:CPLD63_mScarlet-i) were labelled B5 and B6 while the untagged complemented lines (*cpld63-1*:CPLD63_Hygro) were labelled B3 and B4. They were tested together on the same plate. For mutant *cpld63-2*, the tagged complemented lines (*cpld63-2*:CPLD63_mScarlet-i) were labelled C6 and C7 while the untagged complemented lines (*cpld63-2*:CPLD63_Hygro) were labelled C4 and C5. They were also tested together on the same plate. Each sample was grown with a series of dilution: 10^4 (top), 10^3 (middle), and 10^2 (bottom) cells in total. They were also spotted on a TAP plate that was incubated under 50 µmol photons m^{-2} s^{-1} light as a control. It is noted that the WT strain showed contamination in the tests with the two *cpld63* mutants.

To check whether the complemented lines of *cpld63-1* had rescued its paler green colour under autotrophic condition, their chlorophyll content was measured and compared to

that of WT and *cpld63-1* after growing to as close as log phase cell density in liquid TP shaken in air CO_2 (equivalent to LCO_2 condition) under spot test light condition. Due to limited time left in the project and restricted space in the growth room, only one biological replicate was tested but three technical replicates were sampled from each strain for chlorophyll measurement. A box-and-whisker plot showed that *cpld63-1* had a lower chlorophyll a, b and total chlorophyll (a+b) contents compared to the other strains (Figure 3.6). However, a calculation done with independent t-test showed that there was no significant difference between all three chlorophyll contents of WT and *cpld63-1*, as well as between those of *cpld63-1*:CPLD63_Hygro line B3 and *cpld63-1* ($p > 0.05$). It was also found that all the complemented lines showed no significant different compared to the WT ($p > 0.05$) in all three chlorophyll calculations. For *cpld63-1*:CPLD63_mScarlet-i lines B5 and B6, their total chlorophyll and chlorophyll b contents showed no significant difference compared to that of *cpld63-1* ($p > 0.05$), but their chlorophyll a contents were both significantly higher than that of the mutant ($p < 0.05$). The only complemented line that contained significantly higher contents in all three chlorophyll calculations compared to *cpld63-1* was the *cpld63-1*:CPLD63_Hygro line B4. These all suggested that lines B5 and B6 had partially complemented the lower chlorophyll content phenotype (the paler green colour) in *cpld63-1* (chlorophyll b) while B4 had complemented it completely. However, this conclusion was questionable as the statistical test showed no significant difference between *cpld63-1* and WT, suggesting that there was no lower chlorophyll content phenotype to begin with. These results might have been caused by lack of biological replicates, as well as the large variation between one of the technical replicates (chlorophyll a: 2.084 µg ml^{-1}; b: 1.622 µg ml^{-1}; a+b: 3.706 µg ml^{-1}) and the other two (chlorophyll a: 3.443 and 3.513 µg ml^{-1}; b: 4.839 and 4.806 µg ml^{-1}; a+b: 8.282 and 8.318 µg ml^{-1}) in WT. In fact, such great variations between the replicates could be seen in the other lines as well (each replicate was represented by the upper and lower error bars and the inner circular point). As a result, the results obtained here might not be accurate in presenting the true biology phenotypes. Biological replicates should be included in the future to improve the accuracy of the test.
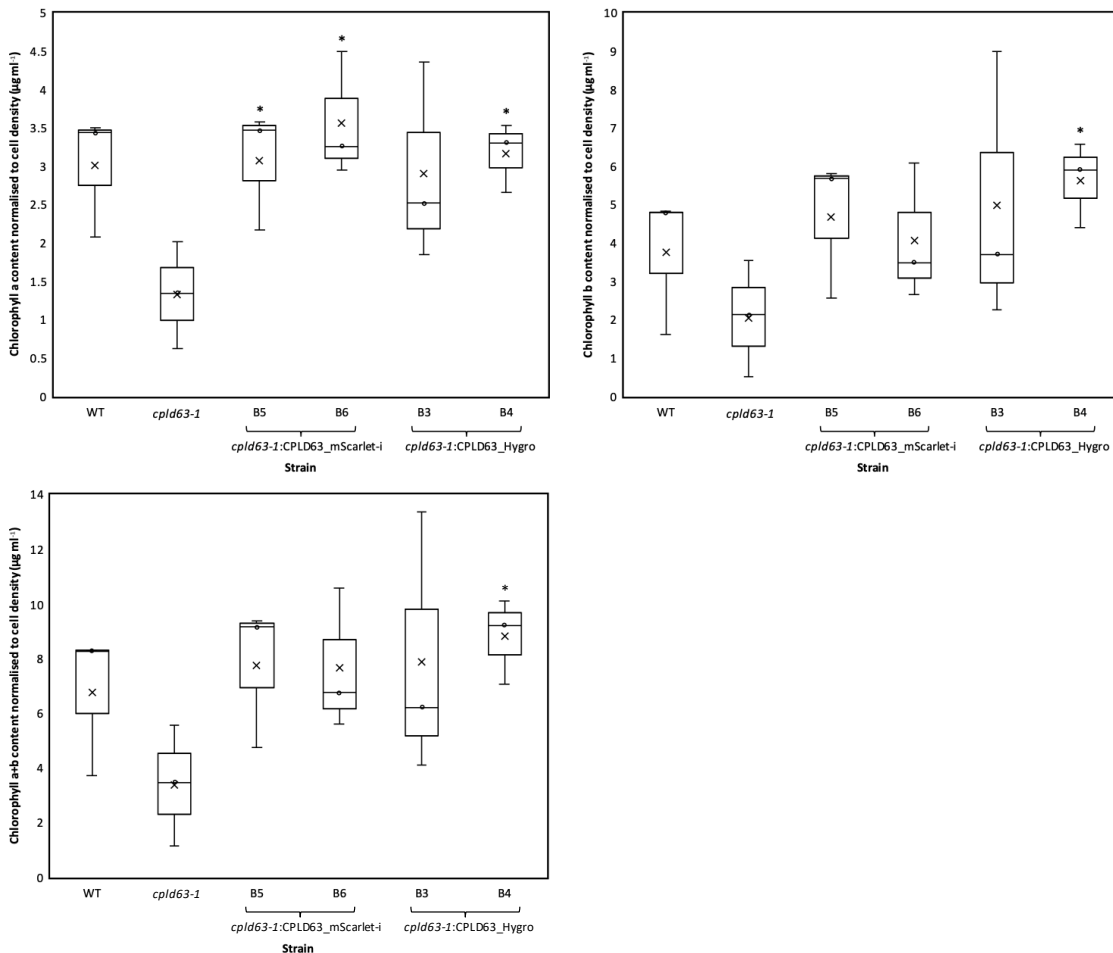
Figure 3.6 Chlorophyll content of WT, *cpld63-1* and its complemented lines grown in TP medium under spot test light conditions and in air CO_2 conditions.

The median calculated form the three technical replicates for each sample is represented as a line in the box with error bars showing the interquartile range. The mean was represented by an x while inner point was represented as a circle in the box. The significance of the difference between each sample and WT or *cpld63-1* was assessed statistically using an independent t-test (* = $P < 0.05$ compared to *cpld63-1*).

To check whether the target genes were expressed in the complemented lines RT-PCR was performed on the cDNA. As the CIB1 cassette is inserted in the intron between Exon 3 and 4 of *CGLD1* in *cgld1*, a primer pair with the forward primer crossing the junction between Exon 3 and 4 (Figure 3.7a) was designed to amplify this region of *CGLD1* transcript in the cDNA of WT, *cgld1* and its complemented lines. The primers should amplify a 100 bp fragment in WT. For the two mutants of CPLD63, the CIB1 cassette is inserted in slightly different positions in Exon 5 of *CPLD63*. A primer pair was then designed to amplify from the 3' end of Exon 4 across the two CIB1 insertion sites to near the 3' end of Exon 5 of *CPLD63* transcript the cDNA of WT, the *cpld63* mutants and their complemented lines (Figure 3.7c). The primers should amplify a 233 bp fragment in WT. If the two target genes were not expressed in their respective mutants and complemented lines, there should be no products amplified using the two primer pairs. As seen from the gel photo (Figure 3.7b), the *CGLD1* primers amplified a fragment of

about 100 bp (labelled as C1) in WT and the *cgld1*:CGLD1_Hygro lines A3, A4 and A5, suggesting that *CGLD1* was expressed in them. A very small amount of this fragment could be seen in *cgld1* as well. This implied that there was a small amount of *CGLD1* transcript expressed in this mutant. This is likely because the CIB1 cassette is inserted in an intron in *cgld1* and is spliced away with the intron during some instances of transcription, therefore generating WT transcripts of *CGLD1* in this mutant. On the other hand, the *CPLD63* primers amplified a fragment just above 200 bp (Figure 3.7d) in WT and all the complemented lines (B3-6 and C4-7), suggesting that *CPLD63* was expressed in them. Once again, it appeared that this fragment could be seen faintly in the two *cgld63* mutants. The reason behind this is unclear as there should not be any amplification in the two mutants in which CIB1 is inserted in the coding region of *CPLD63*. If the CIB1 cassette was also transcribed in the mutant, the size of the fragment amplified by the same pair of primers would be much larger as CIB1 is 2223 bp long. The most likely explanation would be contamination from neighbouring lanes or cross-contamination between the cDNA of WT or complemented lines and the two mutants. Nevertheless, it is certain that *CPLD63* was expressed in the complemented lines.

a *CGLD1* transcript

b

c *CPLD63* transcript

d
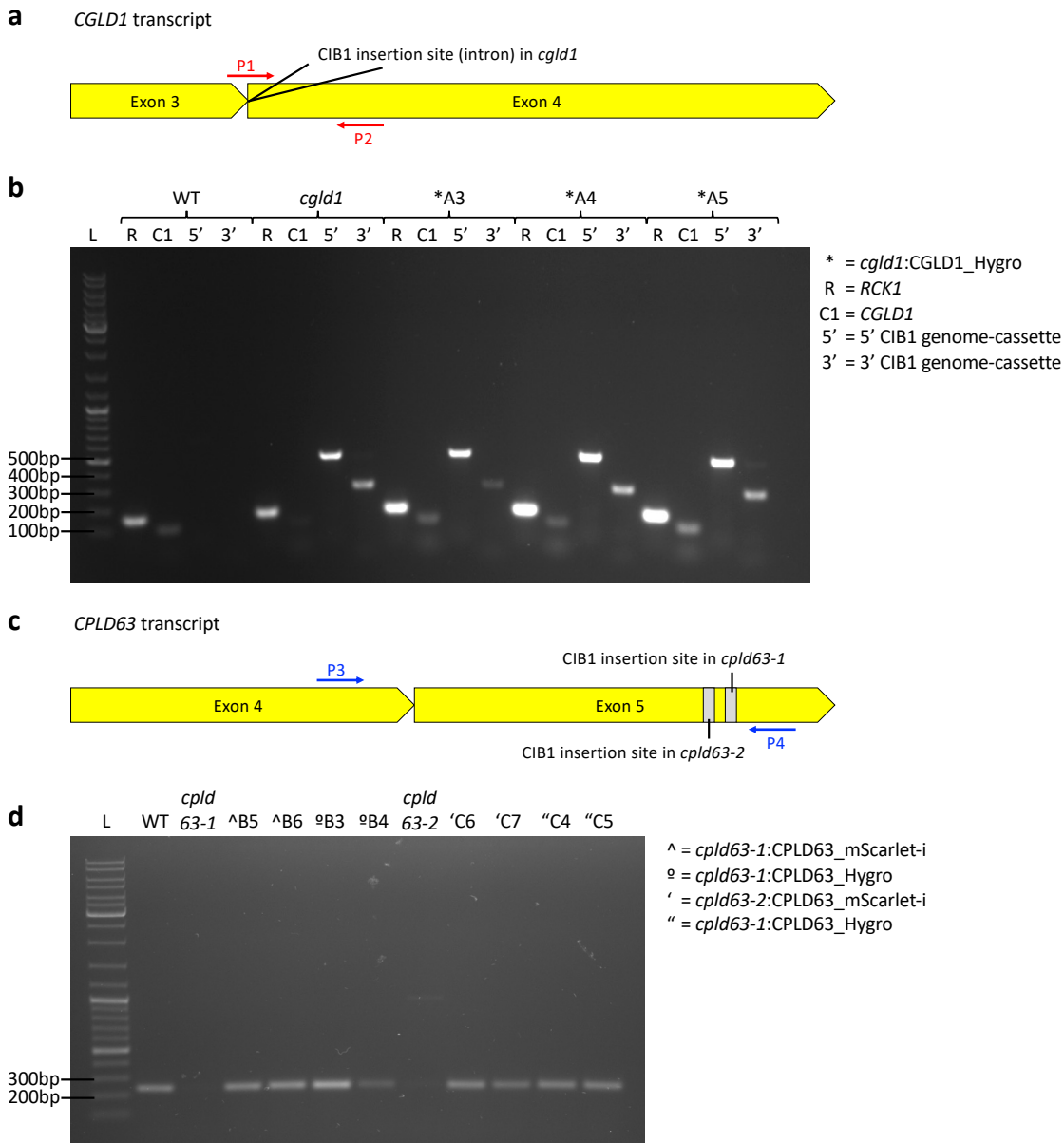
Figure 3.7 Schematic and agarose gel photos of RT-PCR check of *CGLD1* and *CPLD63* expression in *cgld1*, *cpld63-1*, *cpld63-2* and their complemented lines.

(a) A schematic representation of the region of *CGLD1* transcript that was amplified with primer P1 and P2 in PCR check of the cDNA of *cgld1* and its complemented lines, and the region where the CIB1 cassette was inserted in *cgld1*. The CIB1 cassette was inserted in the intron between Exon 3 and 4 of *CGLD1* transcript in *cgld1*. (b) 1% agarose gel photos showing the PCR products amplified from the cDNA of WT, *cgld1* and its complemented lines. * = *cgld1*:CGLD1_Hygro, R = amplified product of the referencing gene *RCK1*, C1 = amplified *CGLD1* using primer pair P1/2, 5' = amplified CIB1 genome-cassette junction on the 5' of *CGLD1*, 3' = amplified CIB1 genome-cassette junction on the 3' of *CGLD1*. (c) A schematic representation of the region of *CPLD63* transcript that was amplified with primer P3 and P4 in PCR check of the cDNA of the *cpld63* mutants and their complemented lines, and the region where the CIB1 cassette was inserted in the mutants. The CIB1 cassette was inserted in Exon 5 of *CPLD63* transcript for both *cpld63* mutants. (d) 1% agarose gel photos showing the PCR products amplified from the cDNA of WT, the *cpld63* mutants and its complemented lines using primer pair P3/4. ^ = *cpld63-1*:CPLD63_mScarlet-i, º = *cpld63-1*:CPLD63_Hygro, ' = *cpld63-2*:CPLD63_mScarlet-i, " = *cpld63-1*:CPLD63_Hygro

3.4.4   Localisation of CGLD1 and CPLD63 in WT and complemented mutant cells

Signals of mScarlet-i from CGLD1 and CPLD63 were detected in WT strains transformed with CGLD1_mScarlet-i and CPLD63_mScarlet-i respectively (Figure 3.8a, top two rows). The two lines will be referred to as WT:CGLD1_mScarlet-i and WT:CPLD63_mScarlet-i. CGLD1 was predicted to localise in the secretory pathway by PredAlgo and in

compartments not including the mitochondrion, chloroplast or thylakoid lumen by Target2.0. However, its homologue in *Arabidopsis*, BICAT1, is found to localise to the thylakoid membrane so it is possible that CGLD1 is also expressed in the thylakoid membrane (Frank et al., 2019). As shown in Figure 3.8a, CGLD1 signals were seen weakly dispersed throughout the chloroplast but also enriched around the pyrenoid and inside the pyrenoid. A small amount of them could also be seen as small blobs and a hollow circular structure in the cytosol, resembling the secretory pathway. In *Chlamydomonas*, the thylakoid traverses the pyrenoid and forms thylakoid-pyrenoid tubules inside. This enrichment around and in the pyrenoid showed that CGLD1 is likely localised in the thylakoid membrane. On the other hand, CPLD63 was predicted to localise in the chloroplast by both PredAlgo and Target2.0. This is highly possible as its *Arabidopsis* homologue, BICAT2, is located to the chloroplast envelope (Frank et al., 2019). Figure 3.8a showed that the mScarlet-i signals of CPLD63 were dispersed across the chloroplast and the pyrenoid. Again, its signals were also distributed as patches and a bright blob in the cytosol, possibly representing the secretory pathway or the vacuole/lysosome. In addition, there was significant signal at the edge of the chloroplast and around the pyrenoid. Collectively, these suggest that CPLD63 could be located to both the chloroplast envelope and the thylakoid membrane.

Plasmids CGLD1_mScarlet-i and CPLD63_mScarlet-i were also transformed into *cgld1* and the two *cpld63* mutants respectively to complement the mutations of CGLD1 and CPLD63 and check if they localise similarly as they do in WT. After verification of the mScarlet-i signals inside the transformants, it was found that the transformation of CGLD1_mScarlet-i into *cgld1* was unsuccessful while the two *cpld63* mutants were successfully transformed with CPLD63_mScarlet-i. The lines would be referred to as *cpld63-1*:CPLD63_mScarlet-i and *cpld63-1*:CPLD63_mScarlet-i respectively and two transformants from each lines were imaged (Figure 3.8a, bottom four rows). The images showed that CPLD63 was expressed in the two mutants and they localised similarly to the tagged CPLD63 seen in WT:CPLD63_mScarlet-i. The signals were seen in the chlorophyll, pyrenoid and the cytosol with enrichment at the periphery of the chloroplast and that of the pyrenoid. These suggested that to an extent the expressed CPLD63 proteins in the two complemented lines should function as the WT CPLD63 do because they are all localised similarly in the cells.

To further confirm whether CGLD1 and CPLD63 are indeed localised to the thylakoid membrane and chloroplast envelope respectively, two dual-tagged WT lines were constructed with one expressing both mScarlet-i-tagged CGLD1 and Venus-tagged PSAF, hence named WT:CGLD1:PSAF, while the other one expressing both mScarlet-i-tagged CPLD63 and Venus-tagged TIC20, hereafter named WT:CPLD63:TIC20 . PSAF is a subunit of the photosystem I (PSI) that localised to the thylakoid membrane on the lumen side (Franzén et al., 1989; Farah et al., 1995; Emrich-Mills et al., 2021), while TIC20 is part of the TIC-TOC complex involved in protein import across the chloroplast envelope and is located at the chloroplast inner envelope membrane (Kouranov et al., 1998; Machettira et al., 2011; Töpel and Jarvis, 2011; Ramundo et al., 2020). The images showed that CGLD1 and PSAF localised similarly in WT *Chlamydomonas* (Figure 3.8b, top two rows). Their signals could be seen enriched around the pyrenoid, where the thylakoid starts to form tubules that traverse into the pyrenoid, as well as inside the pyrenoid where the thylakoid tubules are located. There was a difference between the localisation patterns of the two proteins: CGLD1 was more dispersed in the pyrenoid while PSAF was more concentrated to the tubule structure in it. As for CPLD63 and TIC20, the images showed that both of them were enriched at the chloroplast envelope and their signals overlapped each other when merged together (Figure 3.8b, top two rows). Interestingly, there was also signals of TIC20 in the pyrenoid, similar to CPLD63 signals, suggesting that either those were result from autofluorescence or that there was also TIC20 at the thylakoid membrane. One noticeable difference between the two was that CPLD63 had stronger signals dispersed throughout the chloroplast stroma and in the pyrenoid compared to the TIC20 signals located at the same place.
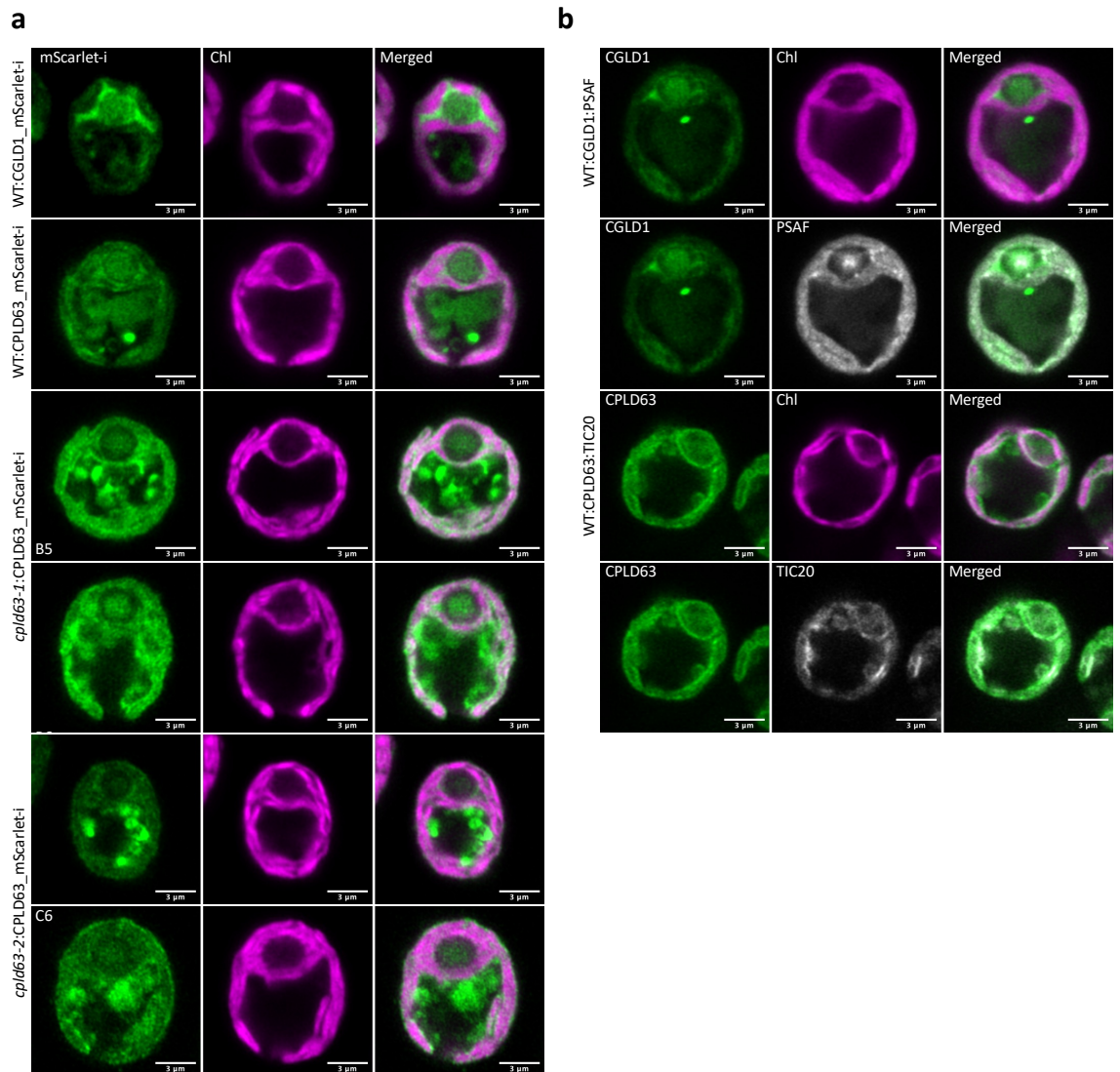
Figure 3.8 Localisation of CGLD1 and CPLD63 in WT and complemented *cpld63* lines and co-localisation with PSAF and TIC20 in WT.

The cells were imaged with a 63x oil objective lens. The scale bar shows the distance of 3 µm. (a) Airyscan images of WT transformed with fluorescently-tagged CGLD1 or CPLD63 and tagged complemented lines of *cpld63-1* and *cpld63-2*. Each row represents an individual transformant. (b) Airyscan images of WT dual tagged fluorescently with CGLD1 and PSAF or with CPLD63 and TIC20. A merge of signals were shown between CGLD1 and chlorophyll, and between CGLD1 and PSAF in the WT:CGLD1:PSAF line, while a merge of signals were shown between CPLD63 and chlorophyll, and between CPLD63 and TIC20 in WT:CPLD63:TIC20 line.

3.4.5 Ca^{2+} staining in *Chlamydomonas* cells

In order to investigate whether CGLD1 and CPLD63 play a role in transporting Ca^{2+} needed for elevation of Ca^{2+} ions in the *Chlamydomonas* involved in the CCM, an experimental plan was drawn up to visualise the Ca^{2+} dynamics in the WT and mutants of the two target genes when transition from HCO$_2$ to LCO$_2$ conditions using a fluorescent Ca^{2+} indicator and confocal microscope imaging. This has been done using the indicator CalciumGreen-1, AM in *Chlamydomonas* cells by Wang et al., 2016c. Using their protocol, WT cells acclimated to air CO$_2$ were incubated with 15 µM CalciumGreen-1, AM for 30 min in Ca^{2+} free TP and then imaged with a confocal microscope. However, as seen in Figure 3.9a (first row), the signals of the indicator could only be seen in the cytosol and

chloroplast but none was seen in the pyrenoid. As a result, several additional incubations were carried out with different conditions in hope of optimising the protocol further to allow visualisation of Ca^{2+} concentration in the pyrenoid in LCO$_2$. The varied conditions tested include: changing TP to HSM (Figure 3.9b), using either 15, 30 or 75 µM CalciumGreen-1, AM, and incubating the cells with the indicator for either 30 min or more than 2.5 hours. The results showed that there were still no Ca^{2+} stained in the pyrenoid in all conditions tested (Figure 3.9). The higher concentration of the Ca^{2+} and longer incubation time did not produce any noticeable change either. The staining of Ca^{2+} in the WT pyrenoid failed and due to time limit the experiment plan was never carried out.
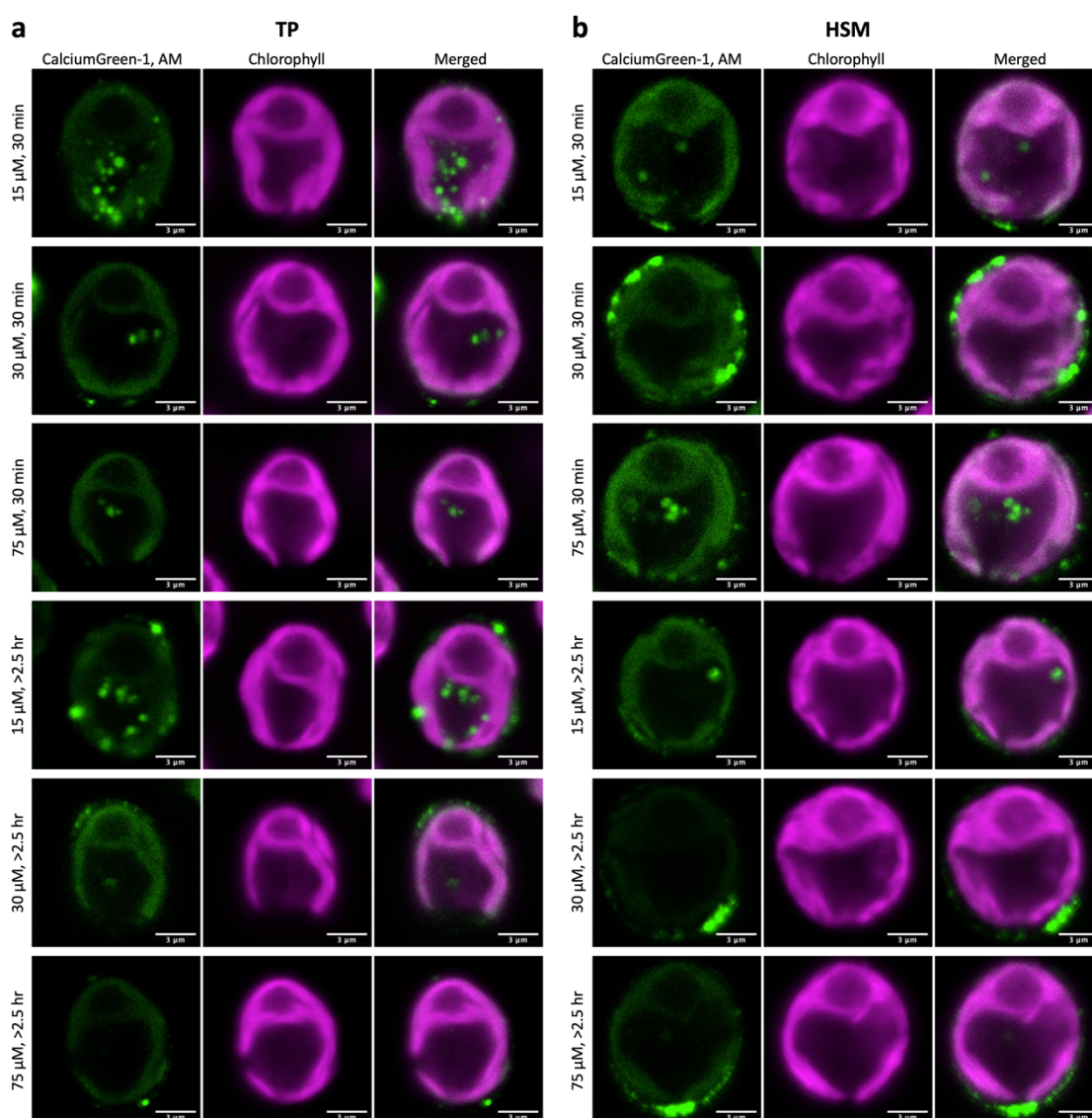
Figure 3.9 Ca^{2+} staining in *Chlamydomonas* WT cells by CalciumGreen-1, AM.
The cells were first acclimated in air (0.04% CO$_2$) in TP medium under ~150 µmol photons m^{-2} s^{-1} light first before incubation with either 15, 30, or 75 µM CalciumGreen-1, AM. Either (a) TP medium or (b) HSM was used for the incubation step and the duration time of the incubation with CalciumGreen-1, AM was either 30 min or >2.5 hours.

3.4.6 Expression of CGLD1 and CPLD63 in *E. coli* cells

Another experiment was also planned to link Ca^{2+} transport activity to CGLD1 and CPLD63. It involved the expression of the two proteins in *E. coli* cells and measurement of the Ca^{2+} influx into these cells using another fluorescent dye Fura-2, AM using the protocol for the Ca^{2+} assays in BL21 pLysS cells expressing BICAT1 proteins as described by Frank et al., 2019. Transcripts of CGLD1 and CPLD63 were cloned into the pET expression plasmid without codon optimisation due to limiting time using the LIC method but only pET-1B-CGLD1 was successfully constructed. It was later transformed into Rosetta 2(DE3)pLysS cells and expression was induced according to the protocol Frank et al., 2019 except that 0.5 mM IPTG was used to induce expression instead of 1% L-arabinose. The pBAD-BICAT1 plasmid used in the paper was also obtained from the corresponding lab and transformed into the same cell strain in order to provide a positive control for the Ca^{2+} influx assay. BICAT1 expression was then induced just as stated in the paper. However, both inductions did not yield any CGLD1 or BICAT1 expression. It is possible that the induction conditions for pET-1B-CGLD1 needs to be optimised to successfully express CGLD1, but it was unsure why the induction of BICAT1 failed. The induction experiment was carried out again with varying conditions to optimise the procedure for BICAT1 expression, meanwhile induction of BST1 in Rosetta 2(DE3)pLysS lines were also carried out to check if the negative results were due to technical errors when processing the cells for the SDS-PAGE gel and Western Blot. As seen in Figure 3.10a, the varied conditions used during induction did not yield any BICAT1. The changed conditions include: induction was carried out either when OD600 reached 0.6-0.8 or 0.9-1.0 (labelled as 1 or 2), either 1%, 0.1% or 0.01% L-arabinose was used to induce expression (stated in the labels), and that the expression was carried out in either Rosetta 2(DE3)pLysS or BL21 pLysS cells. The molecular weight of the expressed His-tagged BICAT1 is 43.1 kDa but no bands of this size could be seen in the samples taken 16 hours after induction on the SDS-PAGE gel or the Western blot. Only a few strong bands from the previously purified His-tagged Cas9 protein could be seen. This is the same case for the repeated CGLD1 induction in Rosetta 2(DE3)pLysS cells (Figure 3.10b), where no band representing the 28.28 kDa His-tagged CGLD1 was present in the sample after 16 hours of induction. However, a band corresponding the 50.2 kDa His-tagged BST1 could be seen in the sample after 4 hours of induction on the Western blot. The bands from His-tagged Cas9 could also be seen, suggesting that the absence of CGLD1

and BICAT1 were not caused by any technical errors in the procedures after taking the samples out of the cultures.

a BICAT1 expression in Rosetta 2(DE3)pLysS   BICAT1 expression in BL21 pLysS

b CGLD1 and BST1 expression in Rosetta 2(DE3)pLysS
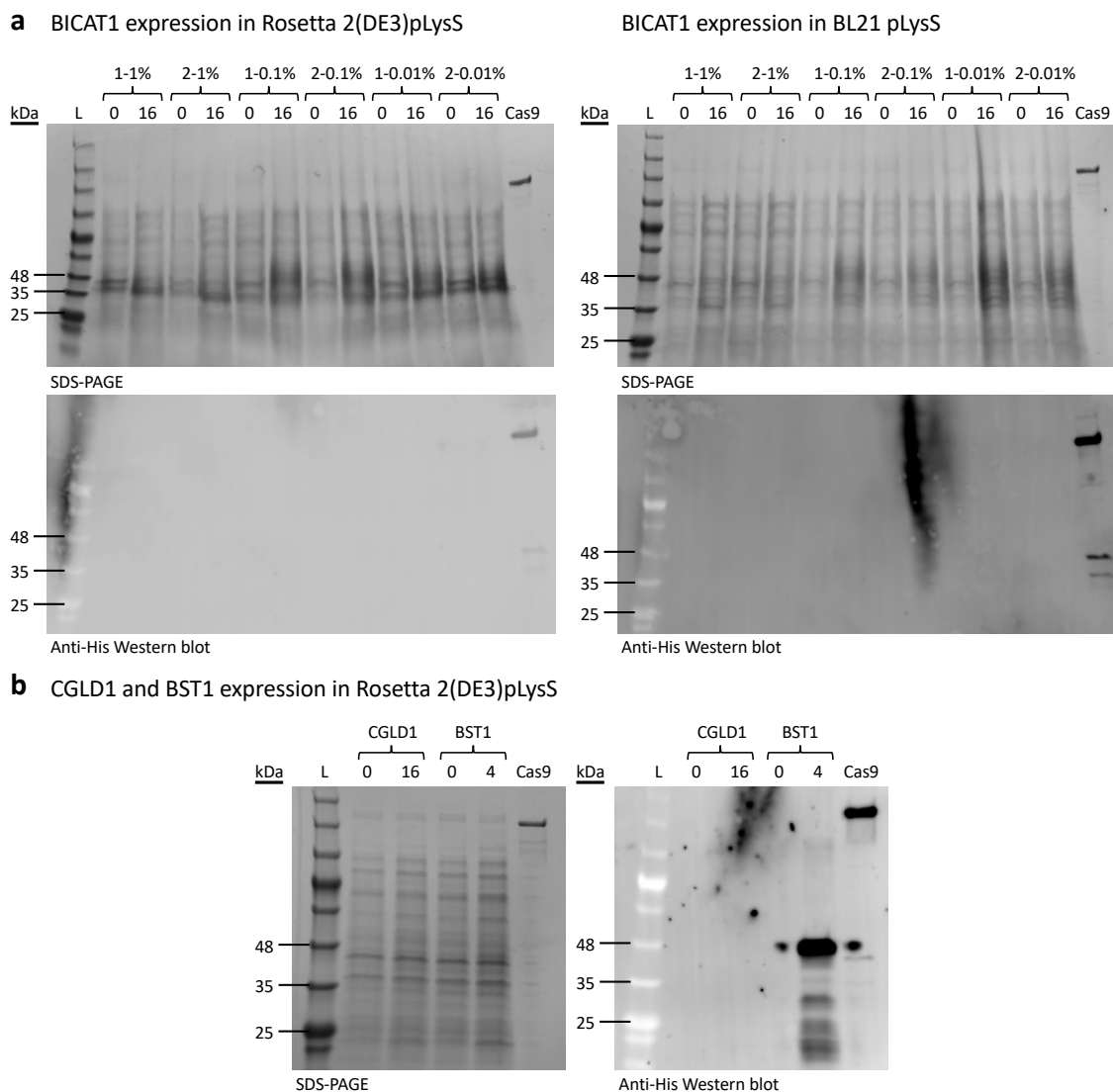
Figure 3.10 Expression of BICAT1 and CGLD1 in different *E. coli* expression lines.
(a) SDS-Page gel and anti-His tag Western blot check of BICAT1 expression in Rosetta 2(DE)pLysS and BL21 pLysS lines in different induction conditions. For each condition tested, sample was taken before induction (0 hours) and 16 hours after induction and they are indicated by the number of hours relative to the induction time in the images. The label of the name indicates the different condition used: 1 = OD600 of 0.6-0.8 when induced, 2 = OD600 of 0.9-1.0 when induced, % = amount of L-arabinose used for induction. The positions of the samples were the same on the SDS-PAGE gel and Western blot. (b) SDS-Page gel and anti-His tag Western blot check of CGLD1 and BST1 expression in Rosetta 2(DE)pLysS. The number just above the gel and blot once again indicate the number of hours relative to the induction time. Expression of BST1 was included as a technical control for the procedure involved in processing the cells for running the SDS-PAGE gel and Western blot. His-tagged Cas9 was included as the positive technical control for the Western blot procedure. The molecular weights of the tagged proteins BICAT1, CGLD1 and BST1 are 43.1, 28.28 and 50.2 kDa respectively.

3.5 Discussion

This part of the study aimed to characterise the functional roles of CGLD1 and CPLD63 and identify any evidence that they play a part in Ca^{2+} transport and CCM regulation. The data gathered provides some insights into their functions in *Chlamydomonas*, however evidence for direct Ca^{2+} transport is still lacking.

The protein sequence and 3D structure alignments between the two *Chlamydomonas* proteins and their homologues in *Arabidopsis* and yeast confirmed that CGLD1 and CPLD63 had the essential features needed for Ca^{2+} transport activity. As seen in the sequence alignments (Figure 3.2), the important acidic and uncharged polar residues in the consensus UPF0016 motifs align perfectly amid CGLD1, BICAT1 and Gdt1p as well as amongst CPLD63, BICAT2 and Gdt1p. When these amino acids were visualised on the aligned predicted 3D structures (Figure 3.3), their positions match well on the innermost helices (presumably the pore-lining helices) between CGLD1 and BICAT1 or Gdt1p, and among CPLD63 and BICAT2 or Gdt1p. This architectural similarity suggests that CGLD1 and CPLD63 are likely to contain a functional Ca^{2+}-binding pocket for transporting Ca^{2+} similar to that proposed for Gdt1p from a previous study (Colinet et al., 2017).

On another note, the 3D structure models predicted for BICAT1, BICAT2 and CPLD63 showed that they have the topology of the UPF0016 subfamily VII: an extra helix is present before the first transmembrane region with the consensus motif (Demaegd et al., 2014). With the extra transmembrane helix, the N-terminal extension of these three would be facing the cytosol instead of the lumen. Meanwhile, CGLD1 does not contain this extra helix, adopting the typical topology shared among the other eukaryotic subfamilies with both terminuses situating at the lumen side (Figure 3.1). This difference is suggested to reflect the different regulatory mechanisms adopted for the proteins depending on the position (cytosol or lumen) of their N-terminal regulatory subunits (Demaegd et al., 2014). However, the predicted 3D structure of Gdt1p also presents an extra helix before the first transmembrane region, contrasting the predicted topology from previous literatures in which this helix is absent (Figure 3.1) (Demaegd et al., 2014; Colinet et al., 2017). This discrepancy might have been caused by the different prediction algorithm used between this study (ColabFold that combines MMseqs2 and AlphaFold2) and previous studies (TMHMM and Memsat-SVM). Nevertheless, the two consensus motifs are located to the innermost helices and facing each other directly on the 3D

models, corresponding to the pore-lining helices with the same motifs in the predicted topology from the literatures (Figure 3.1), implying that the 3D models are still relatively accurate in representing the architectural arrangement of the Ca^{2+}-binding site in Gdt1p and therefore the other proteins as well.

With structure similar to the members in the eukaryotic UPF0016 subfamily, the BICATs and CGLD1 and CPLD63 likely work as monomers in *Arabidopsis* and *Chlamydomonas*. BICAT1 was first discovered as a putative Ca^{2+}/H^+ antiporter and later confirmed to be needed for Ca^{2+} transport in the thylakoid (Wang et al., 2016a; Frank et al., 2019). Gdt1p is also proposed to be a Ca^{2+}/H^+ antiporter as an increase of extracellular pH enhances Gdt1p-mediated Ca^{2+} influx into *Lactococcus lactis* cells expressing the transporter (Colinet et al., 2016). Another homologue of CGLD1 and CPLD63, the human protein TMEM165, is also found to be important for pH homeostasis in both fibroblast from patients with mutated TMEM165 and HeLa cells with TMEM165 knocked down (Demaegd et al., 2013), suggesting that it could be a Ca^{2+}/H^+ antiporter. These all indicate that CGLD1 and CPLD63 might also be Ca^{2+}/H^+ antiporters in *Chlamydomonas*. Further studies on how pH affect their functions would be needed to investigate this.

The spot test with different Mn^{2+} and Ca^{2+} concentrations showed that CGLD1 could be involved in the homeostasis of both ions in *Chlamydomonas*, while it is unclear in the case of CPLD63. Members of the UPF0016 family have been shown to be important for regulating Mn^{2+} homeostasis such as Gdt1p, the BICAT proteins, and MneA in *Vibrio cholerae* (Fisher et al., 2016; Schneider et al., 2016; Wang et al., 2016a; Dulary et al., 2018; Thines et al., 2018; Zhang et al., 2018; Frank et al., 2019). Mn^{2+} homeostasis is important for the function of PSII as the cation is a cofactor crucial for the oxygen-evolving complex (OEC) to catalyse the water-splitting reaction. In fact, the supplement of Mn^{2+} has been shown to rescue the defected PSII activity in two different mutants of *CGLD1* by Schneider *et al.*, 2016 and Xing *et al.*, 2017. It could be that with a higher concentration of Mn^{2+} (60 μM) the PSII activity in *cgld1* was improved further, allowing a better growth in LCO_2 condition compare to the lower Mn^{2+} concentrations (Figure 3.4). However, it did not fully rescue the CCM phenotype of the mutant as seen in the reduced growth in $VLCO_2$ even at a high Mn^{2+} concentration. Meanwhile, this CCM phenotype was more severe when the Ca^{2+} concentration was reduced but not rescued when it was in excess (Figure 3.4). These suggest that *CGLD1* might still play a role in Ca^{2+} transport

that is important for CCM induction. Meanwhile, the different Ca^{2+} and Mn^{2+} concentrations did not show any effect on the two *cpld63* mutants (Figure 3.4). This suggests that either CPLD63 does not play a role in the homeostasis of both cations, or that increasing the concentration of both ions was not enough to restore the disruption of their homeostasis caused by the mutation of *CPLD63*.

The spot test of complemented lines provided more insights into the possible function of CGLD1 and CPLD63 in the green algae. The partially rescued CCM phenotype in the *cgld1*:CGLD1_Hygro lines suggested that CGLD1 is essential for the functioning of the algal CCM. Meanwhile, the low expression of *CGLD1* in the *cgld1* mutant shown by RT-PCR could explain why it showed only a subtle CCM phenotype in the spot tests. The generation of mutants with complete disruption of CGLD1 in the future, or further study of the CGLD1 mutants made by Schneider et al., 2016; Xing et al., 2017 would be most helpful in confirming whether CGLD1 is important for the algal CCM or not.

Meanwhile, the spot test of the two *cpld63* mutants and their complemented lines presented a more complicated situation. Firstly, there was the difference in the phenotypes between *cpld63-1* and *cpld63-2* where the former only showed subtle light-sensitive phenotype while the latter could not grow well at all in both photosynthetic and non-photosynthetic conditions under light. As the mutant PCR check and the RT-PCR check here showed that *CPLD63* is mutated and the WT transcript of this gene is not present in both mutants, the only explanation for this would be that there is off-target mutation(s) in *cpld63-2* not detected by Li et al., 2019a when sequencing the CLiP mutants they created. Seeing that both the tagged and untagged complemented lines of *cpld63-2* rescued the mutant phenotype completely on TAP and in HCO_2 but not in LCO_2, it is possible that the off-target mutated gene(s) play a role in the CCM while CPLD63 is important for the function of other photosynthetic processes or photoprotection. It would be ideal to redo the chlorophyll measurement with biological replicates and to avoid technical errors in order to ensure that statistical relevance can be established better for the chlorophyll content difference between the WT, mutant and complemented lines. This could help confirm whether the mutation of CPLD63 is the causation of the paler green in *cpld63-1*. As for *cpld63-2*, precautions must be taken when interpreting its phenotype in future experiments to distinguish between the mutation of *CPLD63* and the unknown CCM gene(s).

The confocal microscope imaging of fluorescently-tagged CGLD1 and CPLD63 in the WT cells confirmed that they are localised to the chloroplast. CGLD1 is shown to locate in the thylakoid membrane across the chloroplast as well as inside the pyrenoid. Its enrichment around the pyrenoid and inside the pyrenoid suggested that it could have a more specific function at the pyrenoid, the site of CO_2 concentration during the CCM. A localisation assay between HCO_2 to LCO_2 transition would be helpful in seeing whether CGLD1 would actually translocate from all over the thylakoid network in the chloroplast to focus in the tubules traversing the pyrenoid like CAS1 does. On the other hand, while CGLD1 and PSAF share similar localisation pattern, CGLD1 does not localise into a knot-like pattern resembling the thylakoid pyrenoid tubules inside the pyrenoid like PSAF does. It is likely due to the different localisation patterns between the two proteins in the thylakoid membrane. Cylindrical pyrenoid tubules have been shown by *in situ* cryo-electron tomography to extend from thylakoid stacks in the chloroplast stroma into the pyrenoid matrix through fenestrations on the starch sheath (Engel et al., 2015). Then they lose their cylindrical shape and join together to form an interconnected network at the centre, resembling a knot. PSAF could be more concentrated to the interconnected network while CGLD1 could be more evenly distributed throughout the tubules that just traversed into the pyrenoid, thus forming a slightly different localisation pattern with each other. As for CPLD63, although it is enriched at the chloroplast envelope to some extent similar to TIC20, it is also seen all across the chloroplast and inside the pyrenoid. This could be because CPLD63 dual-localises to the chloroplast envelope and the thylakoid membrane, or that the C-terminal tag has caused the protein to mislocalise (Tanz et al., 2013). However, an expression of C-terminal fluorescent tag on BICAT2 did not cause it to localise to the thylakoid membrane in *Arabidopsis* (Frank et al., 2019), suggesting that it is highly unlikely that the tag has caused mislocalisation of CPLD63. Further test should be conducted to investigate the real localisation of CPLD63 such as subcellular fractionation of chloroplast envelope and thylakoid membrane (Schottkowski et al., 2012) and raising an antibody to immunoblot CPLD63 in the fractions, or expressing fluorescent tag on the N-terminus side (with the transit peptide still attached) or more internal regions (Velay et al., 2022).

Despite the uncertainty about whether CPLD63 is also localised to the thylakoid membrane or not, its enrichment at the chloroplast envelope still suggested that it could be located there. The localisation data indicated that if CGLD1 and CPLD63 were indeed

Ca^{2+} transporter, they could transport Ca^{2+} across the thylakoid membrane and the chloroplast envelope respectively. This would help explain why *cgld1* had a disturbed CCM but *cpld63-1* and *2* had a light sensitive or disturbed photosynthesis phenotype instead. CGLD1 might be more important for the elevation of Ca^{2+} in the pyrenoid needed for activating a retrograde signal sent from CAS1 to the nucleus to up-regulate and maintain the expression of HLA3 and LCIA in the CCM, while CPLD63 acts as a Ca^{2+} transporter across the chloroplast envelope and is more essential for maintaining the Ca^{2+} homeostasis in the chloroplast and therefore affecting photosynthesis in general (Wang et al., 2019). It is possible that CPLD63 could act upstream of CGLD1 to facilitate the active transport of Ca^{2+} into the pyrenoid for the induction of the CCM. Future studies such as the measurement of Ci affinity and photosynthetic activity in the mutants of CGLD1 and CPLD63 in different CO_2 conditions and also phenotype assays of double mutants of *CGLD1* and *CPLD63* would help in learning more on their roles in the CCM and photosynthesis.

However, the study failed to establish the direct link between Ca^{2+} transport activity and the two target proteins due to the failures of staining Ca^{2+} in the chloroplast and pyrenoid and the expression of the two proteins and the positive control of BICAT1 in *E. coli* strains for Ca^{2+} uptake assays. It is unsure why after following the exact detailed protocol provided by Wang et al., (2016c) staining of the chloroplast or pyrenoid was not achieved using CalciumGreen-1, AM-stain. It was still not successful even after testing several different experimental procedures as shown in section 3.4.5. This could be due to the problems of compartmentalisation and uneven loading seen before with acetoxymethyl ester derivatives of Ca^{2+} fluorescent dyes (Braun and Hegemann, 1999; Pivato and Ballottari, 2021). Without further optimisation, the efficiency of staining the *Chlamydomonas* chloroplast Ca^{2+} would remain low. Alternatively, biolistic delivered cell impermeable dextran conjugates of Ca^{2+} fluorescent dyes (Bothwell et al., 2006; Wheeler, Joint and Brownlee, 2008; Bickerton et al., 2016), or genetically encoded Ca^{2+} indicators (GECIs) like aequorin-based sensors (Ottolini, Calì and Brini, 2014; Aiyar et al., 2017; Costa, Navazio and Szabo, 2018; Fort et al., 2021) could be used in the future to ensure robust and specific Ca^{2+} concentration determination in the chloroplast of *Chlamydomonas*. Similarly, although the protocol described by Frank et al., 2019 in inducing the expression of BICAT1 in Rosetta 2(DE3)pLysS or BL21 pLysS cells transformed with the pBAD-BICAT1 plasmid used by them was followed through with

several other optimisation attempts made as seen in section 3.4.6, there was still no expression of BICAT1 in either cell lines. The possible caused could be technical errors made when handling the cells during induction and incubation as the successful detection of expressed BST4 in Rosetta 2(DE3)pLysS cell and purified His-tagged Cas9 proteins proved that the downstream process was not the cause of absence of BICAT1 expression. Meticulous measures should be applied when repeating the expression experiment of healthy Rosetta 2(DE3)pLysS or BL21 pLysS cells transformed with pBAD-BICAT1 again to avoid any technical errors in the future. On the other hand, CGLD1 also failed to express from the experiment. This could be due to non-optimal induction conditions or that the CGLD1 insert on the construct pBAD-CGLD1 is using *Chlamydomonas* codons. Optimisation of the induction protocol like testing varied IPTG amount used for induction and different incubation temperature or time after induction, or use of expression plasmids with codon-optimised CGLD1 inserts could be carried out in the future to express CGLD1 in *E. coli*. Additionally, LIC procedure for cloning CPLD63 into the expression plasmid would also need further optimisation to successfully construct a CPLD63 plasmid for the expression of CPLD63 in *E. coli*. Once all of the above procedures are optimised and successful, the actual experiments for investigating whether CGLD1 and CPLD63 have Ca^{2+} transporting activity can be performed.

To sum up, the function of CGLD1 and CPLD63 in *Chlamydomonas* remain unclear but there is evidence that they are important in regulating the CCM and photosynthesis respectively, possibly by acting as Ca^{2+} transporters at the thylakoid membrane and the chloroplast envelope. More characterisation experiments would be needed in the future to fully understand their roles and localisation as well as to determine whether they have Ca^{2+} transport activity in *Chlamydomonas*.

4 Analysis of core CCM genes in *cgld1* and *cpld63* mutants

4.1 Abstract

When the CCM is induced in *Chlamydomonas*, both transcriptional and cellular localisation changes can be seen for its core CCM genes. As CGLD1 and CPLD63 have been found in previous chapters to play a role in the CCM and photosynthesis in the green alga, they might regulate some of these changes directly. This study aims to investigate the relationship between some of the core CCM genes and the two potential Ca^{2+} transporters. The results showed that both CGLD1 and CPLD63 are needed for the timely upregulation of some core CCM genes as well as relocalisation of LCIB and CAS1 when transferring from HCO_2 to LCO_2. The stronger delay of these changes in *cgld1* compared to *cpld63-1*, especially in the accumulation of *LCIA*, showed that CGLD1 plays a larger role in the induction of the CCM while CPLD63 might have a more indirect role. It is still unknown the exact relationship between the two Ca^{2+} transporters and their exact functions in *Chlamydomonas*, which will hopefully be revealed with more characterisation work in the future.

4.2 Introduction

When the concentration of CO_2 in the environment becomes limiting, *Chlamydomonas reinhardtii* induces its CCM to ensure active concentration of CO_2 around Rubisco for maintaining efficient carbon fixation needed for photosynthesis. This initiates a series of downstream transcriptomic and cellular structural changes to facilitate the concentration process that can be used as indicators of a functional CCM. Studying them in mutants of *CGLD1* and *CPLD63* and comparing them to that in WT could help us understand more the exact roles these genes might play in the *Chlamydomonas* CCM.

Transcriptomic studies carried out previously have helped reveal important transcriptional regulators of important CCM genes such as those covered in Chapter 1 (Brueggeman et al., 2012; Fang et al., 2012; Mitchell, Meyer and Griffiths, 2014; Wang et al., 2014). Most of these genes, such as the Ci transporters HLA3, LCI1 and LCIA as well as the CA LCIB, are induced within 1 h of incubation in LCO_2 or $VLCO_2$ in WT cells. Through the study of the transcriptomes in mutants of candidate CCM regulator genes, CIA5, LCR1 and CAS1 were discovered to be important transcription regulators of the CCM. CIA5 was found as a master regulator of many LCO_2-inducible genes which include the four core CCM genes HLA3, LCI1, LCIA and LCIB, as its deletion inhibited the LCO_2-induced upregulation of these genes (Xiang, Zhang and Weeks, 2001; Fang et al., 2012). LCR1 was also identified as downstream of CIA5 and is the upstream regulator of the expression of CCM genes *CAH1*, *LCI1* and *LCI6* in limiting CO_2 (Yoshioka et al., 2004). Meanwhile, mutation of CAS1 was shown to inhibit the accumulation of HLA3 and LCIA needed in LCO_2 conditions and is proposed to regulate *HLA3* and *LCIA* expression during CCM induction through Ca^{2+}-activated retrograde signalling to the nucleus (Wang et al., 2014, 2016c). As *CGLD1* and *CPLD63* potentially encode putative Ca^{2+} transporters, they could be regulatory components involved in the Ca^{2+}-mediated CCM response like CAS1 signalling. Comparing the gene expression pattern of core CCM genes between WT and mutants of *CGLD1* and *CPLD63* could help investigate whether this is the case or not.

The transfer from HCO_2 to LCO_2 or $VLCO_2$ in light also prompts cellular structural alterations in *Chlamydomonas* and the redistribution of CCM proteins in the chloroplast (Figure 4.1). Three important CCM components were found to undergo this change: LCIB, CAS1 and CAH3. LCIB interacts and forms a complex with LCIC (Yamano et al., 2010; Jin et al., 2016; Yamano et al., 2022). When in HCO_2, the LCIB/LCIC complexes are dispersed

evenly throughout the chloroplast stroma; after transferring to LCO_2, they relocalise to aggregate around the pyrenoid within 6 h (Yamano et al., 2010; Wang and Spalding, 2014; Yamano et al., 2014; Toyokawa, Yamano and Fukuzawa, 2020; Yamano et al., 2022). CAS1 proteins are located to the thylakoid membrane and distributed throughout the thylakoid in HCO_2; when incubated in LCO_2, they relocate into the thylakoid tubules traversing the pyrenoid within 2 h, forming a wheel spoke-like pattern in it, and further concentrating to the centre of the pyrenoid after 12 h, forming a central knot-like core (Wang et al., 2016c; Yamano, Toyokawa and Fukuzawa, 2018). Finally, CAH3 proteins are found to be evenly distributed across the thylakoid lumen in both the chloroplast stroma and pyrenoid areas in HCO_2; in LCO_2, more CAH3 becomes concentrated to the lumen of the thylakoid-pyrenoid tubules within 3 h (Blanco-Rivero et al., 2012). Comparing the relocalisation of these proteins in LCO_2 between WT and the mutants of *CGLD1* and *CPLD63* could also help investigate the roles these two target genes play in the CCM.
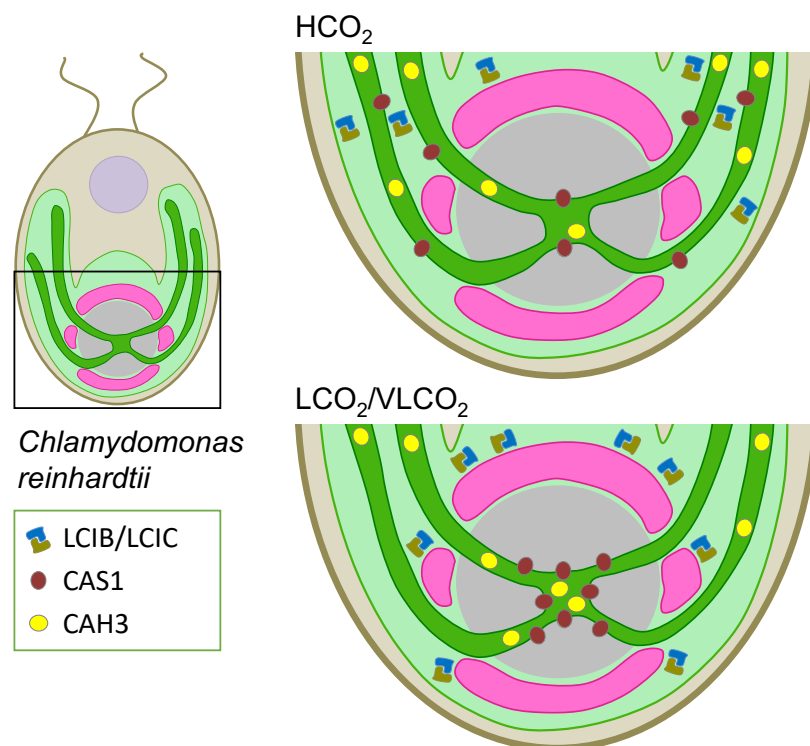
Figure 4.1 Cellular localisation of LCIB/LCIC complex, CAS1 and CAH3 in HCO_2 and limiting CO_2 conditions.

Several core CCM genes were selected for the gene expression study in *cgld1*, *cpld63-1* and *cpld63-2* mutants. They included *HLA3* and *LCIA* as they are linked to the Ca^{2+}-mediated CCM response through CAS1. *LCIB* was also included as it is an essential CCM gene and as mentioned relocalises in limiting CO_2 conditions. *CIA5* and *CAS1* were also targeted to investigate the regulatory relationship between them and the two potential Ca^{2+} transporters. And finally, the genes of the two transporters were also included to

check whether they have regulatory effect on each other and whether they are expressed in their respective mutants. As for the study of relocalisation of CCM proteins in the mutants, LCIB and CAS1 were chosen to be the targets because of their clear distinctive localisation patterns between HCO_2 and LCO_2.

This study aims to analyse the expression patterns of chosen CCM genes in LCO_2 as well as the relocalisation of LCIB and CAS1 in WT, *cgld1*, *cpld63-1* and *cpld63-2*. The gene expression study was carried out using qRT-PCR while confocal microscope imaging and quantification of fluorescence signals from tagged LCIB and CAS1 were performed for the localisation study. Together, they shed some lights on the possible roles of CGLD1 and CPLD63 in the *Chlamydomonas* CCM.

4.3 Materials and Methods

4.3.1 Algal strains and culture conditions

All strains were maintained on plate and in liquid growth as described in Chapter 3.

4.3.2 Sampling of WT and mutant strains at HCO$_2$ and LCO$_2$ for gene expression assay

Three biological replicates of each *Chlamydomonas* strain (WT and mutants) were first grown in TAP media until cell density reached ~2-6 x 10^6 cells ml^{-1}. They were then diluted and transferred to TP medium at pH 7.8 under light intensity of ~150 μmol photons m^{-2} s^{-1} and aerated with HCO$_2$ (3%) for three days until cell density reached ~2-6 x 10^6 cells ml^{-1} again. After that, they were transferred to LCO$_2$ (0.04%) aeration. Samples were taken from each strain at different time points for RNA extraction: at HCO$_2$ (0 min), then at 30 min, 1 h and 5 h after transferring to LCO$_2$. 2 ml of sample was taken for each biological replicate at each time point and centrifuged at 4000 x g for 4 min at 4°C. The supernatant was discarded and each cell pellet was resuspended with 750 μl TRIzol^{TM} Reagent (Invitrogen, #15596018). They were then stored at -20°C for later processing.

4.3.3 RNA extraction and cDNA generation from samples

After completion of sampling, the stored samples were thawed on ice and RNA was extracted from them following the TRIzol^{TM} Reagent RNA isolation protocol provided by the manufacturer. The extracted RNA was then treated with DNase-I, RNase-free (Thermo Fisher Scientific, #EN0521) according to the manufacturer's protocol (1 unit of enzyme per 2.5 μg RNA). After that, cDNA was generated from 500 ng of the DNAse-treated RNA for each sample in a 20 μl reaction mix following the manufacturer's protocol for SuperScript^{TM} IV Reverse Transcriptase (Invitrogen, #18090050). Reagents used for the reverse transcription not included in the transcriptase kit included: Oligo(dT)$_{18}$ Primer (Thermo Fisher Scientific, #SO132), dNTP mix (Thermo Fisher Scientific, #R0192), and RNaseOUT™ Recombinant Ribonuclease Inhibitor (Invitrogen, #10777019). The cDNA was stored at -20°C for later use.

4.3.4 Quantitative real-time Reverse Transcription PCR (qRT-PCR)

Primers for amplifying each target gene- *HLA3*, *LCIA*, *LCIB*, *CIA5*, *CAS1*, *CGLD1*, *CPLD63*- in the qRT-PCR experiment were designed using the Primer3 plugin in the software Geneious (https://www.geneious.com) (Appendix C, Table C.1). The constitutively expressed gene *RCK1* (Receptor of activated protein kinase C1; also known as *CBLP* or

GBLP) was used as an internal control to normalise the expression across the samples since it has been used in previous studies for the same purpose (Ma et al., 2011; Fang et al., 2012; Mitchell, Meyer and Griffiths, 2014; Colina et al., 2019; Tokutsu et al., 2019). The qPCR experiments were performed using the FAST SYBR™ Green Comparative CT program on a Thermo Fisher Scientific QuantStudio™ 3 system. Each 20 µl qPCR reaction mix consisted of FAST SYBR™ Green Master Mix (Thermo Fisher Scientific), 350 nM forward and reverse primers (175 nM for primer pair of *CGLD1*), molecular biology grade water and 4 µl of the 1:5 dilution of the cDNA made from the reverse transcription described previously. Three technical replicates were tested for each cDNA sample and the average of their Cq (quantification cycle) values were used to calculate the relative expression. The raw Cq values obtained for every testing sample is summarised in Appendix C, Table C.2-Table C.8. Molecular biology grade water was used as negative control and a mixture of cDNA of the three WT biological replicates obtained at the last time point was used as positive control for each qPCR experiment. The relative expression was calculated using one of the efficiency corrected calculation models (Pfaffl, 2006).

$$\text{ratio} = \frac{(E_{target})^{\Delta C_q \ target^{(control - sample)}}}{(E_{Ref})^{\Delta C_q \ Ref^{(control - sample)}}}$$

Here, E_{target} represents the primer efficiency of the target gene while E_{Ref} represents that of the reference gene. $\Delta C_q \ target^{(control - sample)}$ represents the difference between the average Cq value of the biological replicates at the first time point and the Cq value of the individual sample (replicate) in the amplification of the target gene. $\Delta C_q \ Ref^{(control - sample)}$ represents the same Cq value difference but in the amplification of the reference gene.

4.3.5 Plasmids construction and transformation of *Chlamydomonas* strains

The same recombineering and *Chlamydomonas* strains transformation methods described in Chapter 3 were used to construct a plasmid with LCIB tagged with Venus (LCIB-Venus) and another with CAS1 tagged with Venus (CAS1-Venus) using the backbone from tagging plasmid Hygro_Venus (with hygromycin resistant and CrVenus tag) and create WT and mutant lines with either of the plasmids.

4.3.6 Quantification of the localisation patterns of Venus-tagged LCIB and CAS1

For assay looking at LCIB and CAS1 localisation in HCO_2 and LCO_2 condition, WT and mutant strains tagged with LCIB-Venus or CAS1-Venus were first grown in TAP medium until cell density reached 2-6 x 10^6 cells ml^{-1}. They were then diluted and transferred to TP medium at pH 7.8 under light intensity of ~150 μmol photons m^{-2} s^{-1} and bubbled with HCO_2 (3%) until the cell density reached about 2-6 x 10^6 cells ml^{-1} again. After that, they were transferred to LCO_2 (0.04%) bubbling. Samples were taken for each strain before transferring to LCO_2 and at 2, 6, 12 and 24 h after transfer to LCO_2 and imaged using a Zeiss LSM 880 with Airyscan on a fully motorised invert microscope within 30 min (514nm Ex, 525-550nm Em for Venus, 633nm Ex, >660nm Em for Chlorophyll). Fiji was used to defined the regions of interest in each cell on the images using the chlorophyll channel: region x was defined by selecting the whole cell area just outside the chloroplast, and region y was defined by either circling the pyrenoid area and enlarging it by 0.5 μm for LCIB-tagged lines or just circling the pyrenoid area for CAS1-tagged lines. Background signals were then subtracted from the Venus channel of all images in the software using the rolling ball radius plugin with a radius of 15 pixels before quantification (Shihan et al., 2021). The integrated density of each region was than measured using the same channel. The percentage of LCIB or CAS1 signals at the pyrenoid regions was then calculated by dividing the integrated density of region y by that of region x.

4.3.7 Statistical analysis

All statistical tests used for the expression and localisation tests, and the corresponding assumption tests were carried out using SPSS (IMB Corp, 2020).

4.4 Results

4.4.1 Comparison of expression pattern of core CCM genes in WT and mutants in HCO₂ and LCO₂

The qRT-PCR showed that there were differences in expression patterns of some core CCM genes between WT and the mutants of CGLD1 and CPLD63 after induction of the CCM (Figure 4.2). All the statistics are summarised in Table 4.1.

Table 4.1 Statistics of relative gene expression of core CCM genes in WT and mutants in HCO_2 and LCO_2

Gene	Mixed ANOVA time points by strains statistics	Sphericity assumed or Greenhouse-Geisser correction?	Strain	ANOVA with repeated measures time points statistics	Mean Log2 fold change			
					0 min	30 min	1 h	5 h
HLA3	$F_{(9, 24)} = 2.4$, $p < 0.05$	Sphericity assumed	WT	$F_{(3, 6)} = 9.7$, $p < 0.05$	0.0	3.0	6.4	9.6
			cgld1	$F_{(3, 6)} = 8.5$, $p < 0.05$	0.0	2.2	3.3	5.5
			cpld63-1	$F_{(3, 6)} = 43.1$, $p < 0.05$	0.0	-0.8	3.2	10.8
			cpld63-2	$F_{(3, 6)} = 43.1$, $p < 0.05$	0.0	1.4	5.5	8.3
LCIA	$F_{(4.3, 11.4)} = 3.3$, $p < 0.05$	Greenhouse-Geisser	WT	$F_{(3, 6)} = 32.0$, $p < 0.05$	0.0	10.8	13.8	13.7
			cgld1	$F_{(3, 6)} = 14.6$, $p < 0.05$	0.0	1.0	1.8	6.8
			cpld63-1	$F_{(3, 6)} = 15.2$, $p < 0.05$	0.0	5.6	10.3	13.8
			cpld63-2	$F_{(3, 6)} = 8.9$, $p < 0.05$	0.0	7.8	10.2	10.6
LCIB	$F_{(4.8, 12.8)} = 3.1$, $p < 0.05$	Greenhouse-Geisser correction	WT	$F_{(3, 6)} = 59.3$, $p < 0.05$	0.0	6.0	6.7	4.8
			cgld1	$F_{(3, 6)} = 20.8$, $p < 0.05$	0.0	3.1	4.6	6.1
			cpld63-1	$F_{(3, 6)} = 21.6$, $p < 0.05$	0.0	3.6	5.5	4.7

					0.0	6.0	7.4	7.1
			cpld63-2	F(3, 6) = 33.2, p < 0.05	0.0	6.0	7.4	7.1
CIA5	F(9, 24) = 2.7, p < 0.05	Sphericity assumed	WT	F(3, 6) = 8.3, p < 0.05	0.0	0.5	1.0	1.3
			cgld1	LCO$_2$, F(3, 6) = 9.9, p < 0.05	0.0	0.7	0.9	1.6
			cpld63-1	F(3, 6) = 1.2, p > 0.05	0.0	0.2	0.4	0.7
			cpld63-2	LCO$_2$ F(3, 6) = 134.4, p < 0.05	0.0	1.6	2.0	2.4
CAS1	F(3.6, 9.7) = 5.3, p < 0.05	Greenhouse-Geisser	WT	F(3, 6) = 7.4, p < 0.05	0.0	0.1	-0.4	-1.5
			cgld1	F(3, 6) = 8.4, p < 0.05	0.0	1.2	1.0	1.9
			cpld63-1	F(3, 6) = 4.6, p > 0.05 for *cpld63-1*	0.0	0.1	-0.5	-0.8
			cpld63-2	F(3, 6) = 1.5, p > 0.05	0.0	0.8	0.6	0.1
CGLD1	F(9, 24) = 2.8, p < 0.05	Sphericity assumed	WT	F(3, 6) = 29.1, p < 0.05	0.0	2.8	2.9	3.4
			cgld1	F(3, 6) = 2.4, p > 0.05	0.0	1.5	2.9	0.6
			cpld63-1	F(3, 6) = 10.7, p < 0.05	0.0	0.4	1.2	1.8
			cpld63-2	F(3, 6) = 41.0, p < 0.05	0.0	3.2	3.7	2.8
CPLD63	F(6, 18) = 4.2, p < 0.05	Sphericity assumed	WT	F(3, 6) = 1.1, p > 0.05	0.0	0.2	-0.2	0.1
			cgld1	F(3, 6) = 3.9, p > 0.05	0.0	1.3	0.4	2.1
			cpld63-1	N/A	N/A	N/A	N/A	N/A
			cpld63-2	F(3, 6) = 24.1, p < 0.05	0.0	2.5	2.1	2.1
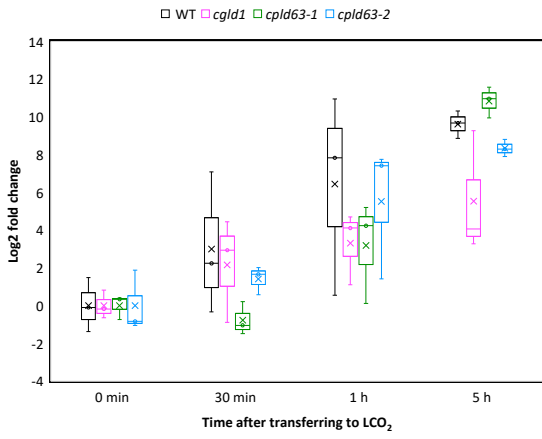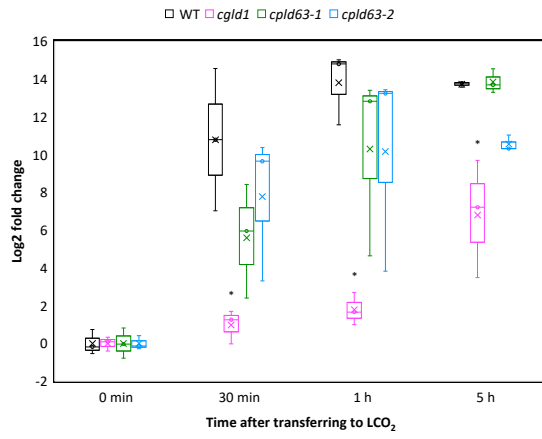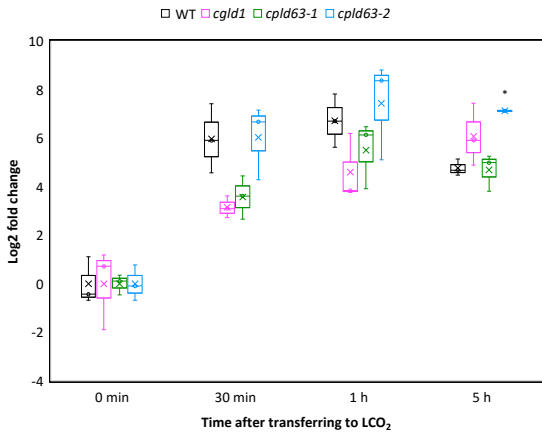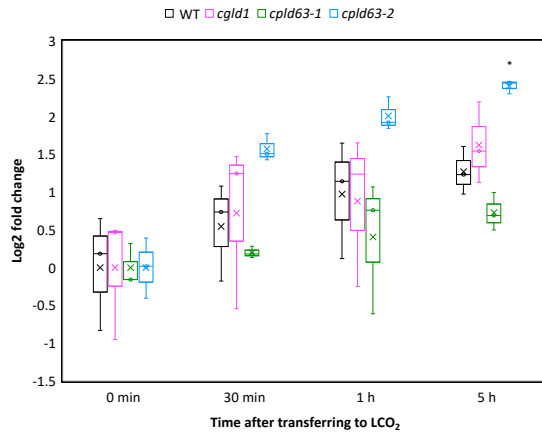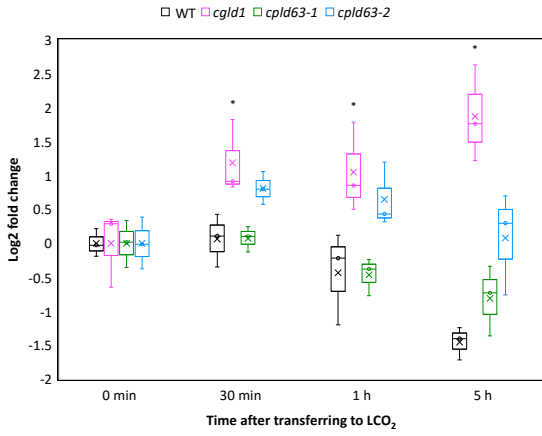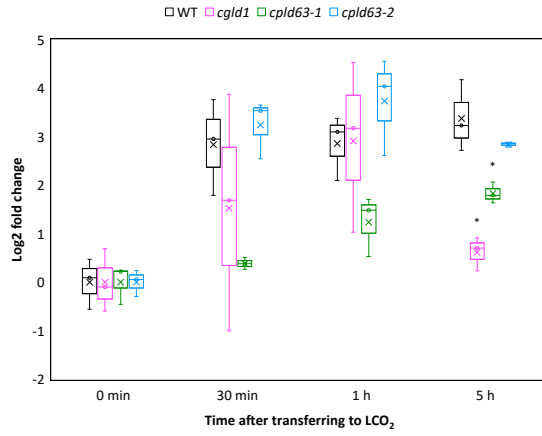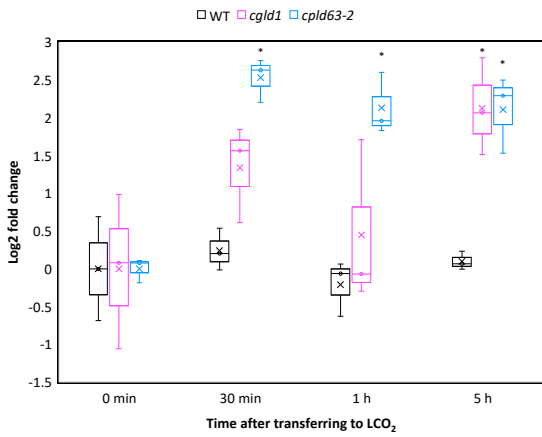
Figure 4.2 Relative gene expression of core CCM genes in WT and mutants in HCO_2 and LCO_2.
Samples were taken for each strain at HCO_2 (0 min) before transferring to LCO_2, and then at 30 mins, 1 h and 5 h in LCO_2. *RCK1* was used as a referencing gene. Data for the expression of *CPLD63* in *cpld63-1* was not shown as its Cq values were mostly over 33.5 or undetermined. On each box, X marks the mean of the three biological replicates fold change, circle marks the inner point, and the line marks the median. The box depicts the interquartile range. *p < 0.05 compared to WT, one-way ANOVA with Tukey's test.

For *HLA3*, its relative expression increased steadily over time after transferring from HCO_2 to LCO_2 in WT but only the Log2 fold change at 5 h was significantly higher when compared to 0 min (p < 0.5) using Bonferroni corrected pairwise comparison. This was similar to the expression trend of *HLA3* found in the literature: *HLA3* is highly induced within 1 h of transferring from HCO_2 (5%) to LCO_2 (0.04%) or $VLCO_2$ (0.01%) and stayed upregulated after 3-5 h (Brueggeman et al., 2012; Mitchell, Meyer and Griffiths, 2014). The study by Fang et al., 2012 also showed this upregulation when comparing the expression between WT populations acclimated in HCO_2 or LCO_2/$VLCO_2$ for 4 h. In *cgld1*, the relative expression of *HLA3* also increased steadily over time when in LCO_2. It appeared to increase to a similar level to WT from 0 min to 30 min, but at 1 h and 5 h the Log2 fold change was slightly lower than that in WT. One-way ANOVA with post hoc Tukey test calculated no significant difference between the Log2 fold change of *HLA3* in WT and *cgld1* at any of the time points (p > 0.05). This suggests that *HLA3* expression was upregulated similarly in *cgld1* and WT in the first 30 min, but then the upregulation became slightly slower in the mutant from 1 h to 5 h. In the two *cpld63* mutants, *HLA3* expression also increased steadily over 5 h in LCO_2 like that in WT. However, the Log2 fold change was slightly lower at 30 min in both mutants compared to the WT, and at 1 h in *cpld63-1* compared to WT. Again, one-way ANOVA with Tukey test did not find any significant difference between the Log2 fold change of *HLA3* in WT and the two mutants at any of the time points. This suggested that there was a very small but not significant delay in the upregulation of *HLA3* in the two *cpld63* mutants compared to that in WT.

Meanwhile, the relative expression of *LCIA* in WT increased significantly from 0 min to 5 h (p < 0.05) in LCO_2. Again, this matches the data found in the literature where the expression *LCIA* in WT was found to be highly induced within 1 h in limiting CO_2 conditions (Brueggeman et al., 2012; Mitchell, Meyer and Griffiths, 2014). This pattern was also seen in the two *cpld63* mutants, in which the Log2 fold change was significantly higher at 5 h compared to 0 h (p < 0.05). As one-way ANOVA with Tukey's test showed no significant difference between the Log2 fold change of WT and the *cpld63* mutants at any of the time points (p > 0.05 all), it could be concluded that *LCIA* expression was

upregulated in both mutants similarly to that in WT. On the other hand, *cgld1* had a different *LCIA* expression pattern compared to WT. ANOVA statistics showed that there was a significance in the Log2 fold change of *LCIA* expression over time in LCO_2, however the pairwise comparison test did not calculate any significant differences among the time points. This suggested that there was a subtle upregulation of *LCIA* expression in *cgld1* after transferring from HCO_2 to LCO_2 for 5 h that was not significant when comparing the timepoints in a pairwise fashion. One-way ANOVA with Tukey's test showed that except from the first time point in HCO_2 ($p > 0.05$), the Log2 fold change of *LCIA* expression in *cgld1* was significantly lower than that in WT at the time points in LCO_2 incubation ($p < 0.05$ for all). All these indicated that the upregulation of *LCIA* induced by LCO_2 condition was inhibited in the *cgld1* mutant.

For the relative expression of *LCIB*, it exhibited a significant increase from within 30 min ($p < 0.05$) in LCO_2 and stayed relatively stable across 1 and 5 h in WT. This matches the expression data of LCIB in the literature: *LCIB* is induced greatly within 1 h of incubation in LCO_2 and stayed upregulated for 3-5 h in WT (Brueggeman et al., 2012; Fang et al., 2012; Mitchell, Meyer and Griffiths, 2014). In *cgld1* and *cpld63-1*, *LCIB* was upregulated similarly to WT after 5 h in LCO_2. However, the Log2 fold change in both mutants at 30 min appeared slightly lower than that in WT. There was not a significant difference found between the two mutants and WT at any of the time points as calculated by one-way ANOVA. Therefore, it can be concluded that *LCIB* was upregulated to similar levels after transferring from HCO_2 to LCO_2 among the three strains, but the upregulation was slightly slower in the mutants. In *cpld63-2*, *LCIB* was upregulated in LCO_2 similarly to the WT but to a higher level at 5 h as the Log2 fold change was significantly higher in the mutant at this time point ($p < 0.05$).

Interestingly, *CIA5* expression showed significant increase in WT after 1 h ($p < 0.05$) in LCO_2 and remained stable to 5 h, although this increase was only about 2-fold. This suggested that there was a slight upregulation of *CIA5* in WT that was distinctive after transferring from HCO_2 to LCO_2 for 1 h and it levelled off afterwards. This is different from the data in literature where *CIA5* did not show any fluctuations in expression between HCO_2 and limiting CO_2 (Fang et al., 2012). In *cgld1* and *cpld63-1*, the expression of *CIA5* did not show significant difference in any of the time points in LCO_2 compared to 0 h in HCO_2 ($p > 0.05$ in pairwise comparisons). One-way ANOVA also showed no

significant difference in the Log2 fold change of *CIA5* between the two mutants and WT ($p > 0.05$ all). This suggested that the upregulation of *CIA5* in WT was very subtle. On the other hand, the expression of *CIA5* in *cpld63-2* showed a significant increase after 30 min ($p < 0.05$) in LCO_2, and continued to increase significantly at 5 h (< 0.05). This indicated that there was an upregulation of *CIA5* within 30 min of incubation in LCO_2 after transferring from HCO_2 in the mutant, and this upregulation continued steadily to 5 h. One-way ANOVA showed that the Log2 fold change was significantly higher in *cpld63-2* compared to in WT at 5 h ($p < 0.05$). This suggested that there was continuous upregulation of *CIA5* in the mutant that was to a significantly higher degree compared to that in WT.

The relative expression of *CAS1* experienced a subtle downregulation that was not significant when the time points were compared in a pairwise fashion in WT when transferred from HCO_2 to LCO_2 (ANOVA with repeated measures shows $p < 0.05$ but pairwise comparisons showed no significant difference among the time points). This appeared to be similar to the data shown by Wang et al., 2014 where the expression of *CAS1* was slightly lower in LCO_2 compared to in HCO_2. In *cgld1*, *CAS1* was upregulated across the 5 h in LCO_2. One-way ANOVA with a Bonferroni correction calculated that *cgld1* had a significantly higher Log2 fold change of *CAS1* ($p < 0.05$) compared to WT at the time points in LCO_2. This indicated that *CAS1* expression was regulated in opposite directions in the two strains within 5 h of CCM induction. Meanwhile, *CAS1* expression in the two *cpld63* mutants showed no significant difference ($p > 0.05$) over time in LCO_2. One-way ANOVA showed that there was no significance difference between WT and both mutants at any of the time points ($p > 0.05$ all). This suggested that the LCO_2-induced downregulation of *CAS1* in WT was too subtle for the Log2 fold change to be significantly different from the *cpld63* mutants over 5 h in LCO_2.

The relative expression of *CGLD1* was upregulated significantly within 1 h ($p < 0.05$) in LCO_2 in WT. Strangely, there was no significant difference between 0 min and 5 h even though the Log2 fold change of the latter was not significantly different from 1 h. This implied that the fold change might have dropped down slightly from 1 h to 5 h that it was no longer statistically different from the starting point in HCO_2. All these suggested that there was an upregulation of *CGLD1* after 1 h of transferring to LCO_2 and then it either stopped or levelled off from 1 to 5 h. This upregulation in LCO_2 is not seen in the

expression study by Fang et al., 2012 where *CGLD1* expression is not affected by difference in CO_2 concentration, but is reduced in *cia5* mutant. On the other hand, it was unexpected that there was expression of *CGLD1* in *cgld1*. However, the level was relatively low as the average Cq values among the *cgld1* biological replicates over time remained close to 27 while that among the WT lower to around 24 after the significant increase at 1 h (Appendix C, Table C.7). This coincided with the small amount of *CGLD1* transcript amplified in the cDNA of *cgld1* shown in the RT-PCR test in Chapter 3. The expression of *CGLD1* in *cgld1* showed no significant change among the 5 h after CCM induction. Interestingly, later ANOVA test showed that there was no significant difference between the Log2 fold change of *CGLD1* of *cgld1* and WT at the time points ($p > 0.05$) except at 5 h where it was significantly lower in the mutant ($p < 0.05$). This suggested that although there was a slight drop in the expression of *CGLD1* in WT at this time point, it was still relatively higher than before CCM induction at the starting point. In *cpld63-1*, the expression of *CGLD1* showed no significant increase until 5 h ($p < 0.05$ compared to 30 min) in LCO_2. This suggested that was an upregulation of *CGLD1* in *cpld63-1* that started from 30 min after transferring to LCO_2. Later statistical test showed that the Log2 fold change of *CGLD1* was not significantly different among *cpld63-1* and WT at the first three time points ($p > 0.05$ all) but was significantly lower in the mutant at 5 h ($p < 0.05$). These all showed that there was a delay in the LCO_2-induced upregulation of *CGLD1* in *cpld63-1* compared to WT and that this upregulation was to a lower magnitude in the mutant as well. In the meantime, the relative expression of *CGLD1* in *cpld63-2* showed a similar trend to that in WT in LCO_2, with no significant difference in the Log2 fold change between the two strains at all time points ($p > 0.05$ all).

For the relative expression of *CPLD63*, there was no significant change in LCO_2 in WT ($p > 0.05$ for all time points pairwise comparisons). So far, there was no published data on the expression of *CPLD63* in limiting CO_2 conditions to help confirm the validity of this expression trend in WT. There was also no significant change in *CPLD63* expression in *cgld1*. However, one-way ANOVA with Tukey's test calculated a significant difference in the Log2 fold change of *CPLD63* between WT and *cgld1* at 5 h ($p < 0.05$) but not at the other time points ($p > 0.05$ all). This suggested that there could be a slight upregulation of *CPLD63* in *cgld1* between 1 h and 5 h in LCO_2 that was not seen in WT. Meanwhile, the amplification data of *CPLD63* in *cpld63-1* was never processed as its Cq values were

mostly over 33.5 or undefined (Appendix C, Table C.8). This also indicated that it was likely not transcribed at all in this mutant, making *cpld63-1* a complete knock-out of *CPLD63*. However, in *cpld63-2*, there was expression of *CPLD63* in *cpld63-2* although again this expression was relatively low as the average Cq was around 32 while the average Cq in WT was around 27 (Appendix C, Table C.8). Nevertheless, this expression in *cpld63-2* showed significant increase from 0 min to 30 min ($p < 0.05$) and remained relatively stable to 5 h ($p > 0.05$). In addition, one-way ANOVA with Tukey's test found that the Log2 fold change was significantly higher in *cpld63-2* compared to that in WT at the three time points in LCO_2 ($p < 0.05$). These all implied that *CPLD63* was upregulated significantly as early as 30 min after transferring from HCO_2 to LCO_2 and continued at the same level across to 5 h in *cpld63-2*. However, as the mutant was discovered to have the CIB1 cassette inserted in the exon of *CPLD63*, the transcript detected in the qRT-PCR might not be a fully functional version of the gene.

4.4.2   Localisation of LCIB in WT and mutants in HCO_2 and LCO_2

To check whether CGLD1 and CPLD63 are important for the correct relocalisation of LCIB when the *Chlamydomonas* CCM is induced in LCO_2, confocal images of WT and the three mutants transformed with the LCIB-Venus plasmid were taken at different timepoints before and after transferring from HCO_2 to LCO_2 growth. Two transformants were imaged for each transformed line to validate the results. The localisation of LCIB was then quantified by calculating the percentage of LCIB-Venus signals around the pyrenoid at different time points. All the statistical data is summarised in Table 4.2. Data from first round transformants were analysed successfully for all four strains, but only data from the second round transformants of WT and *cgld1* were processable as the LCIB-Venus signals in the second set transformants of *cpld63-1* and *cpld63-2* were lost. The Airyscan processed images of the first transformants (Figure 4.3) showed that in both WT and *cgld1* the LCIB-Venus signals started to relocalise from being dispersed all over the chloroplast in HCO_2, to concentrating around the pyrenoid as small blobs after transferring into LCO_2 for 6 h, and then to forming a ring-like structure around the pyrenoid completely after 12 h in LCO_2. In *cpld63-1* and *cpld63-2*, on the other hand, this relocalisation appeared to be slower with a majority of LCIB-Venus still spread out in the chloroplast after 6 h in LCO_2. Nevertheless, LCIB-Venus still formed a ring-like structure after 12 h in LCO_2 in the two strains like in WT and *cgld1*.

However, the statistical analysis of the quantification of LCIB-Venus suggested slightly different LCIB-Venus relocalisation patterns in these transformants (Figure 4.5a). In WT, the amount of LCIB-Venus around the pyrenoid showed no statistically supported differences from 0 h to 12 h ($p > 0.05$) in LCO_2. However, the amount of LCIB-Venus localising to the pyrenoid periphery at 24 h was significantly larger than that at 0, 2 and 6 h ($p < 0.05$ all). These all showed that the relocalisation of LCIB-Venus to a ring-like structure in limiting CO_2 conditions happened steadily across the time points in WT. In *cgld1*, there was significant increase in the LCIB-Venus around the pyrenoid from 6 hours to 12 hours ($p < 0.05$). A Kruskal-Wallis test with post hoc Dunn's pairwise comparison revealed that the LCIB-Venus around the pyrenoid was significantly lower in *cgld1* compared to WT at 2 h and 6 h (Dunn's test, $p < 0.05$ both). These all suggested that there might be a delay of LCIB relocalisation in *cgld1* in LCO_2 compared to WT.

Table 4.2 Statistics of quantification of LCIB-Venus around the pyrenoid in tagged WT and mutants in HCO_2 and LCO_2

Transformants	Strain	Friedman test time points statistics	Median % of LCIB-Venus around the pyrenoid				
			0 h	2 h	6 h	12 h	24 h
1st	WT	$\chi2(4) = 28.2$, $p < 0.05$	20.3	23.3	31.5	43.0	81.9
	cgld1	$\chi2(4) = 53.7$, $p < 0.05$	16.8	18.0	19.9	63.4	73.4
	cpld63-1	$\chi2(4) = 49.7$, $p < 0.05$	20.6	14.0	60.5	91.6	78.9
	cpld63-2	$\chi2(4) = 34.2$, $p < 0.05$	21.6	19.8	28.5	47.9	91.0
2nd	WT	$\chi2(4) = 53.2$, $p < 0.05$	19.7	24.7	51.2	77.2	82.5
	cgld1	$\chi2(4) = 41.3$, $p < 0.05$	19.4	19.7	33.7	64.4	80.9

In *cpld63-1*, the relocalisation of LCIB in LCO_2 also experienced a delay compared to WT as the Kruskal-Wallis test with post hoc test showed that the LCIB-Venus around the pyrenoid in *cpld63-1* was significantly lower at 2 h compared to WT (Dunn's test, $p < 0.05$ both). However, this delay recovered faster than that in *cgld1* and reached a saturated point earlier than that in WT as the LCIB-Venus around the pyrenoid in *cpld63-1* was statistically similar to WT at 6 h (Dunn's test, $p > 0.05$) but significantly higher at 12 h

(Dunn's test, $p < 0.05$). It is noted that there were three outliers (two were very close together making it appeared as one in the graph) of 24.0%, 25.1% and 25.4% above the upper extreme (17.2%) of the data gathered at 2 h. Meanwhile in *cpld63-2*, the relocalisation of LCIB followed a trend similar to *cgld1*: with a delay that started to recover after 6 h in LCO_2. Further statistical tests showed that the amount of LCIB-Venus around the pyrenoid in *cpld63-2* had no significant difference compared to WT across the time points ($p > 0.05$) except at 24 h where it became significantly larger ($p < 0.05$). This suggests that the recovery of LCIB relocalisation was able to reach a point where significantly more LCIB is aggregated to around the pyrenoid compared to WT. Once again there were three outliers presented among the data- 12.3%, 19.1% and 45.3%- and this time below the lower extreme (60.2%) at 24 h.

The images obtained for the second round transformants of WT and *cgld1* showed similar LCIB-Venus relocalisation patterns as in the images of the first transformants (Figure 4.4), and this time the quantification data revealed similar patterns (Figure 4.5b). In WT, there was a significant change in the amount of LCIB-Venus around the pyrenoid after transferring from HCO_2 to LCO_2 for 6 h ($p < 0.05$ compared to 0 h), and continued to increase steadily across the remaining time points that it was significantly greater at 24 h compared to 6 h ($p < 0.05$). This showed that the relocalisation of LCIB-Venus in WT happened steadily across the 24 h in LCO_2. On another note, there was one outlier- 16.9%- below the lower extreme (23.8%) among the data at 12 h. In *cgld1*, the LCIB-Venus around the pyrenoid also increased steadily over that it become significantly greater at 6 h compared to 0 h ($p < 0.05$). A Kruskal-Wallis test showed that the amount of LCIB-Venus around the pyrenoid in *cgld1* was significantly lower than that in WT at 2 and 6 h ($p < 0.05$) but not at the other time points ($p > 0.05$). These implied that although LCIB relocalisation in *cgld1* also happened steadily in LCO_2, it was still slower than in WT. Again, there were outliers seen in the population: 38.9% above the upper extreme (26.2%) at 2 h, and 19.6%, 27.3%, 31.2% and 38.4% below the lower extreme (66.4%) at 24 h.

A Kruskal-Wallis test of the quantification data of the first and second transformants (Figure 4.5) showed that there were no significant differences in the amount of LCIB-Venus around the pyrenoid between them in WT at all time points ($p > 0.05$ all). This was the same for *cgld1* at most time points ($p \geq 0.05$ all) except at 6 h where it was

significantly lower in the first transformant compared to the second transformant (p < 0.05). Also, the relocalisation of LCIB-Venus in the first transformants of both WT and *cgld1* appeared to be slower than in the second transformants. Nevertheless, a delay could be seen in *cgld1* in both sets of transformants.

Figure 4.3 Representative images obtained from the first round transformants of LCIB-Venus-transformed WT and mutants.

Samples were taken for each strain at HCO_2 (0 min) before transferring to LCO_2, and then at 2 h, 6 h, 12 h and 24 h in LCO_2. The cells were imaged with a 63x oil objective lens. The scale bar shows the distance of 3 μm.

Figure 4.4 Representative images obtained from the second round transformants of LCIB-Venus-transformed WT and mutants.
Samples were taken for each strain at HCO_2 (0 min) before transferring to LCO_2, and then at 2 h, 6 h, 12 h and 24 h in LCO_2. The cells were imaged with a 63x oil objective lens. The scale bar shows the distance of 3 μm.

a

b

Figure 4.5 Quantification of LCIB-Venus around the pyrenoid in tagged WT and mutants in HCO_2 and LCO_2.
(a) First round transformants. (b) Second round transformants. Samples were taken for each strain at HCO_2 (0 min) before transferring to LCO_2, and then at 2 h, 6 h, 12 h and 24 h in LCO_2. On each box, X marks the mean of the three biological replicates fold change, circle marks the inner point, and the line marks the median. The box depicts the interquartile range. Circle outside the box marks the outlier. *$p < 0.05$ compared to WT, Kruskal-Wallis test with post hoc Dunn's pairwise comparison.

4.4.3   Localisation of CAS1 in WT and mutants at HCO_2 and LCO_2

The same localisation experiment was conducted on the WT and mutants transformed with the CAS1-Venus plasmid to investigate the importance of CGLD1 and CPLD63 in relocalisation of CAS1 when the algal CCM is induced. This time, all the data obtained

from both transformants of the four strains were processed successfully. The statistics involved in the quantification of CAS1-Venus in the pyrenoid is summarised in Table 4.3. The images obtained from the first set transformants showed that the relocalisation of CAS1 was not apparent in all strains in LCO_2 (Figure 4.6). CAS1-Venus was already concentrated as a node in the pyrenoid in HCO_2 and adopted a more defined star/wheel-like feature across time after transferring to LCO_2 in all strains. There were also weaker CAS1-Venus signals dispersed across the chloroplast at all time points in all of them. Only in *cpld63-1* that the relocalisation of CAS1-Venus to the pyrenoid appeared to be more apparent as the CAS1-Venus signals in the chloroplast were very weak after 12 h and 24 h in LCO_2.

Table 4.3 Statistics of quantification of CAS1-Venus around the pyrenoid in tagged WT and mutants in HCO_2 and LCO_2

Transformants	Strain	Friedman test time points statistics	Median % of CAS1-Venus in the pyrenoid				
			0 h	2 h	6 h	12 h	24 h
1st	WT	$\chi2(4) = 17.9$, $p < 0.05$	19.1	22.1	26.1	27.0	23.4
	cgld1	$\chi2(4) = 38.8$, $p < 0.05$	14.9	15.5	27.8	20.8	25.1
	cpld63-1	$\chi2(4) = 30.0$, $p < 0.05$	11.8	16.4	25.5	23.8	24.1
	cpld63-2	$\chi2(4) = 0.2$, $p > 0.05$	13.2	13.6	15.4	17.6	16.5
2nd	WT	$\chi2(4) = 38.7$, $p < 0.05$	12.9	17.8	20.9	23.4	17.3
	cgld1	$\chi2(4) = 23.9$, $p < 0.05$	9.6	16.0	16.4	17.9	15.2
	cpld63-1	$\chi2(4) = 30.1$, $p < 0.05$	21.2	18.5	22.0	23.1	27.3
	cpld63-2	$\chi2(4) = 22.0$, $p < 0.05$	10.6	11.9	15.6	15.8	16.9

The quantification of CAS1-Venus in the pyrenoid helped identify the subtle relocalisation or its absence in the strains over the different time points (Figure 4.8a). In the first set transformants of WT, the CAS1-Venus in the pyrenoid increased significantly after 6 h in LCO_2 ($p < 0.05$ compared to 0 h). This suggested that CAS1 relocalisation to the pyrenoid happened across 0 and 6 h in LCO_2 in WT. In *cgld1*, the amount of CAS1-Venus in the pyrenoid also increased significantly after 6 h in LCO_2 ($p < 0.05$ compared to 2 h). A Kruskal-Wallis test with Dunn's pairwise comparison showed that the amount of CAS1-Venus in the pyrenoid in *cgld1* was the same as in WT at most of the time points (p

> 0.05 all) except at 2 h when it was significantly lower (p < 0.05). This suggested that there was a delay in CAS1 relocalisation in *cgld1* compared to that in WT. One thing to note was the presence of an outlier- 31.8%- above the upper extreme (21.7%) of the data at 0 h.

In *cpld63-1*, CAS1-Venus in the pyrenoid also exhibited a significant increase at 6 h (p < 0.05) compared to 2 h. A Kruskal-Wallis test with Dunn's test calculated that *cpld63-1* had no significantly different CAS1-Venus in the pyrenoid compared to WT at most time points (p > 0.05 all) except that it was significant lower at 0 h (p < 0.05). This suggested that there might be less CAS1 localised to the pyrenoid in the mutant compared to WT at HCO_2. For *cpld63-2*, there was no considerable change in the CAS1-Venus in the pyrenoid, suggesting that there was no relocalisation of CAS1 after transferring from HCO_2 to LCO_2. This was also shown in the Kruskal-Wallis and Dunn's tests that the CAS1-Venus in the pyrenoid of *cpld63-2* was significantly lower than in WT at all time points (p < 0.05 all). There were two outliers found: 25.8% above the upper extreme (19.2%) at 0 h, and 28.3% above the upper extreme (23.9%) at 24 h.

The second round transformants of the strains showed slightly different CAS1-Venus localisation patterns in the images (Figure 4.7). Again, in all strains the concentrated CAS1-Venus signals in the pyrenoid was already present in HCO_2 and their star/wheel-like features became more defined across time after transferring to LCO_2. Weaker CAS1-Venus signals were also dispersed across the chloroplast in the strains at all time points. The relocalisation of CAS1 in LCO_2 was again not visually apparent in the images.

The actual quantification of the pyrenoid CAS1-Venus signals again showed the subtle change in the localisation pattern of CAS1-Venus in the second transformants (Figure 4.8b). In WT, the pyrenoid CAS1-Venus increased significantly at 6 h (p < 0.05 compared to 2 h) and experienced a significant drop at 24 h (p < 0.05 compared to 12 h). This implied that CAS1-Venus relocalisation to the pyrenoid started between 2 and 6 h but dispersed back to the chloroplast between 12 and 24 h in this transformant. Of note, there were three outliers seen: 27.7% above the upper extreme (20.9%) at 2 h, and 25.1% and 25.7% above the upper extreme 19.8%) at 24 h. In *cgld1*, there was a significant increase of CAS1-Venus in the pyrenoid from 0 h to 2 h (p < 0.05), and then it stayed similar across later time points (p > 0.05 all). The Kruskal-Wallis and Dunn's tests showed that there was no significant difference between the CAS1-Venus in the pyrenoid in *cgld1*

and WT at most time points (p > 0.05) except at 12 h where it was significantly lower in *cgld1* (p < 0.05). This indicated that CAS1-Venus in WT is still localising to the pyrenoid from 6 h to 12 h even though there was no significant difference between them. All these suggested that although CAS1-Venus relocalisation in *cgld1* occurred as early as between 0 to 2 h, it was to a lesser extent compared to WT. Again, single outliers were present at different time points: 19.1%, 26.6%, 31.5% and 28.9% above the upper extremes (15.1%, 19.0%, 24.3% and 21.3%) at 0, 2, 6 and 24 h respectively.

In *cpld63-1*, CAS1-Venus in the pyrenoid elevated significantly at 6 h (p < 0.05 compared to 2 h) and remained stable across later time points (p > 0.05). Later statistical tests showed that CAS1-Venus in the pyrenoid of *cpld63-1* was significantly higher than that of WT at 0 and 24 h (p < 0.05 both) but not at the other time points (p > 0.05 all). This suggested that there was more CAS1-Venus already localised to the pyrenoid of *cpld63-1* compared to WT in HCO_2 and more relocalised from the chloroplast to the pyrenoid after 24 h in LCO_2. It is noted that there were outliers above the upper extremes at 6 h (43.0% over 29.7%) and 24 h (39.6% and 41.2% over 37.7%). In *cpld63-2*, statistics calculation suggested that CAS-Venus had a relocalisation pattern similar to that in *cpld63-1* (significant at 6 h but remained stable afterwards). However, Kruskal-Wallis and Dunn's tests showed that the amount of CAS1-Venus in the pyrenoid of *cpld63-2* was significantly lower than that of *cpld63-1* at all time points (p < 0.05 all). In fact, apart from 0 h (no significant change, p > 0.05), the pyrenoid CAS1-Venus in *cpld63-2* was also significantly less than in WT (p < 0.05) over time in LCO_2. This implied that there was less CAS1-Venus relocalised to the pyrenoid in this mutant compared to *cpld63-1* and WT when transferred from HCO_2 to LCO_2. Again, there was one outlier- 28.0%- above the upper extreme (23.5%) at 12 h.
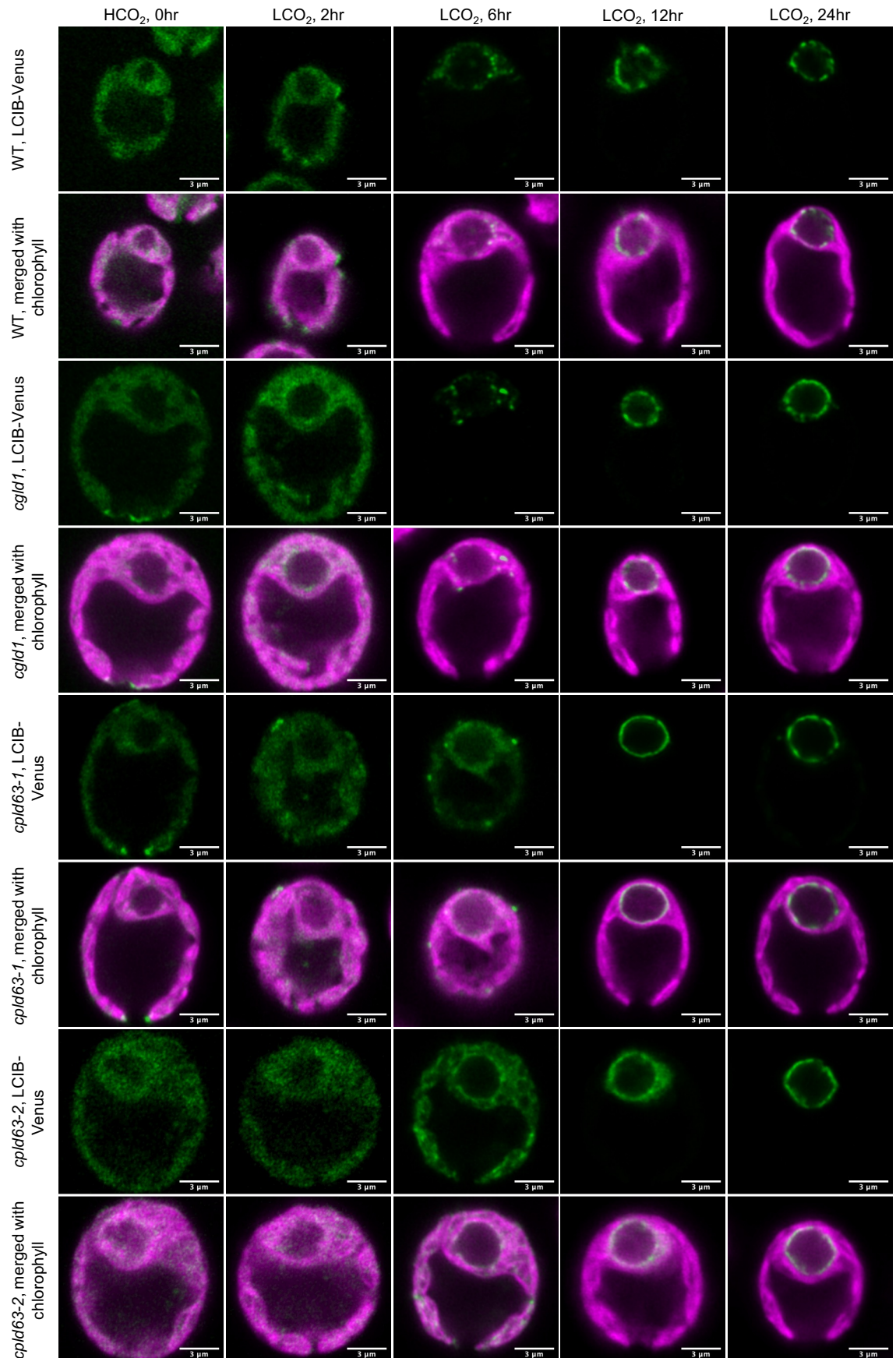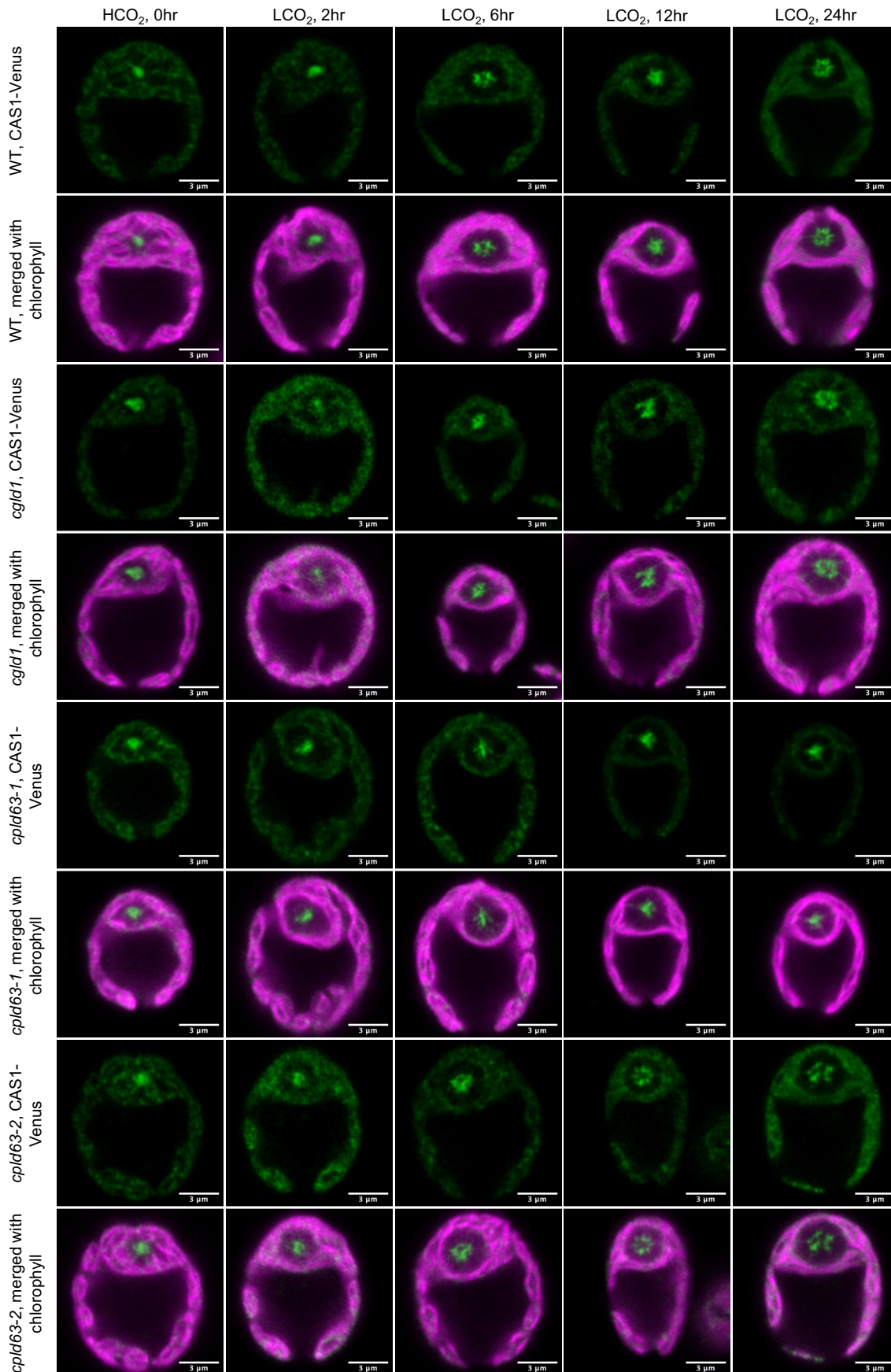
Figure 4.6 Representative images obtained from the first round transformants of CAS1-Venus-transformed WT and mutants.

Samples were taken for each strain at HCO$_2$ (0 min) before transferring to LCO$_2$, and then at 2 h, 6 h, 12 h and 24 h in LCO$_2$. The cells were imaged with a 63x oil objective lens. The scale bar shows the distance of 3 μm.
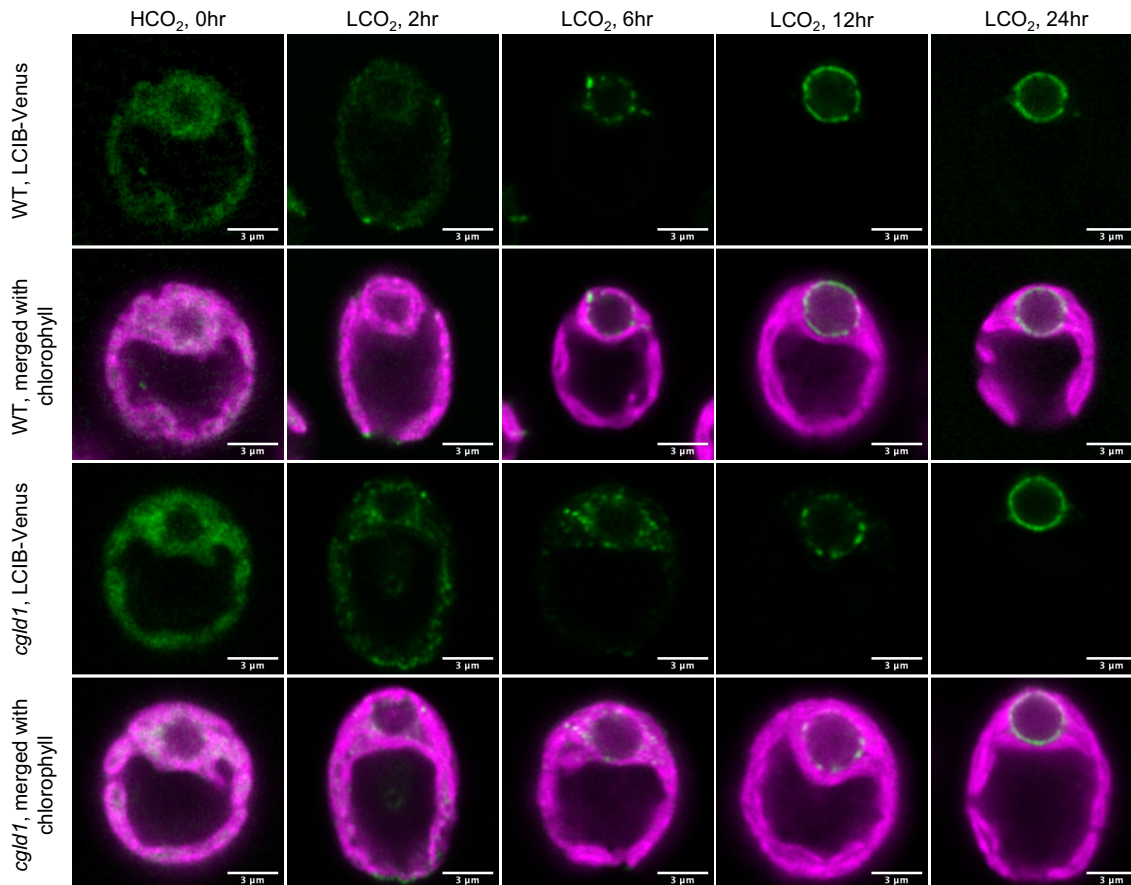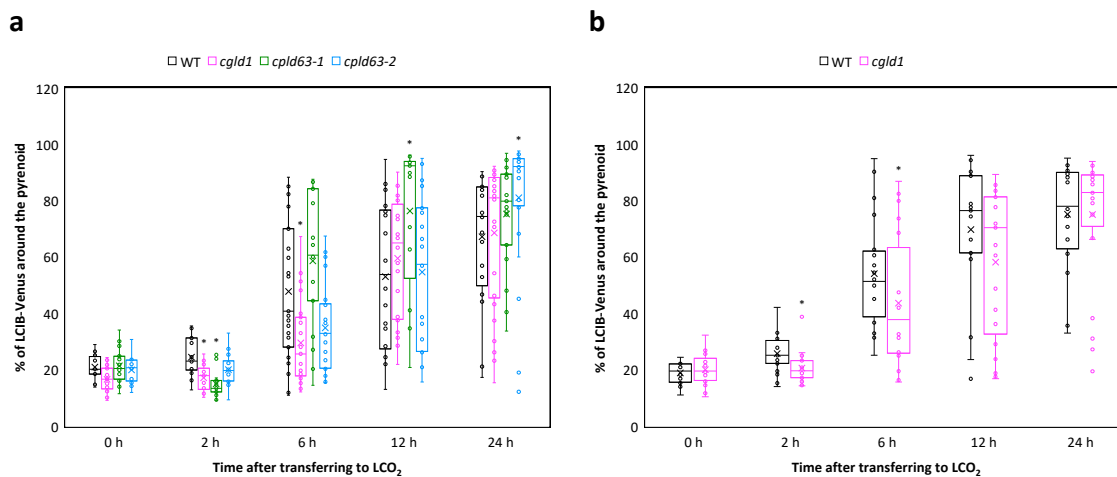
130
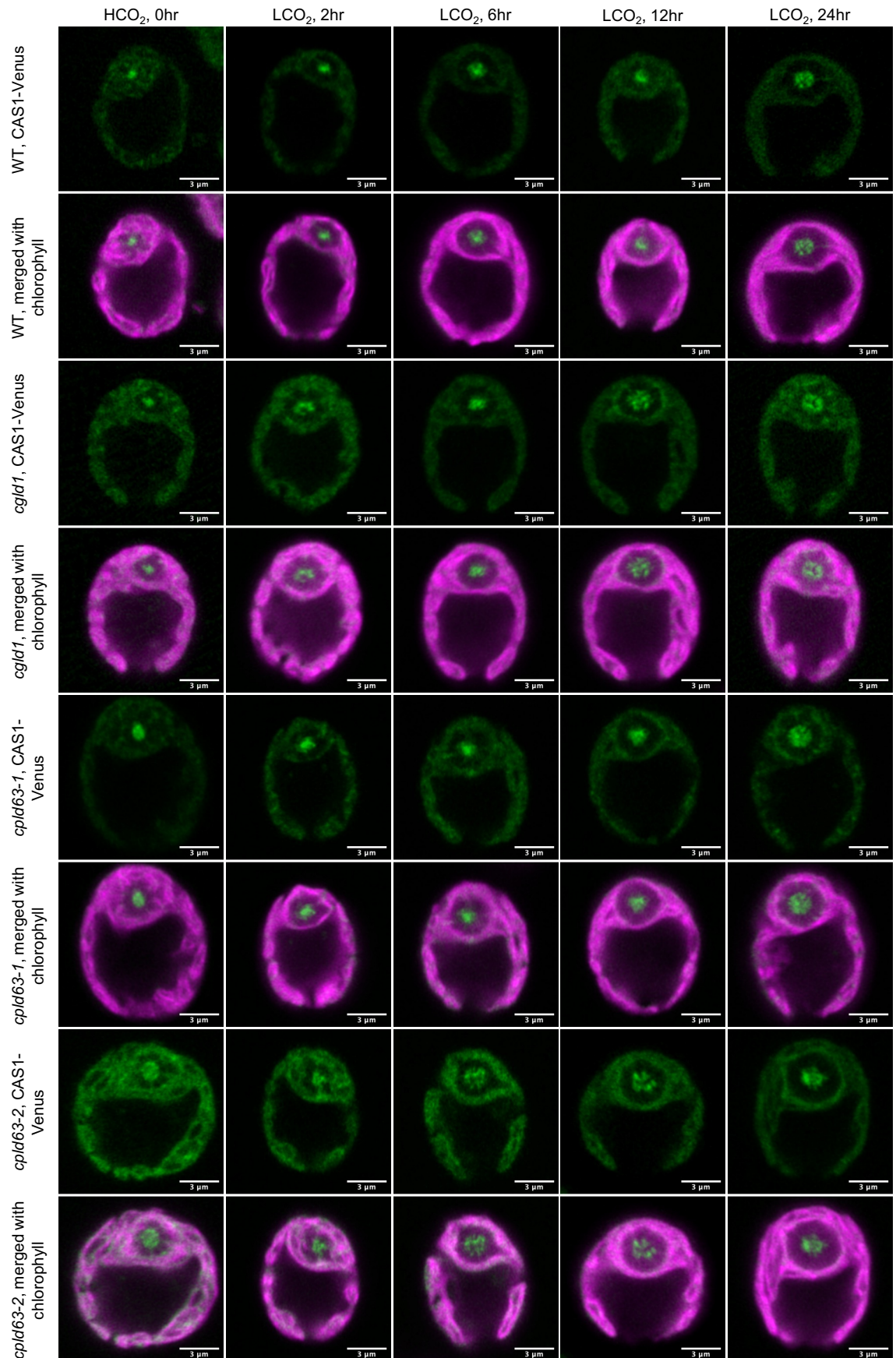
Figure 4.7 Representative images obtained from the second round transformants of CAS1-Venus-transformed WT and mutants.

Samples were taken for each strain at HCO_2 (0 min) before transferring to LCO_2, and then at 2 h, 6 h, 12 h and 24 h in LCO_2. The cells were imaged with a 63x oil objective lens. The scale bar shows the distance of 3 μm.

The first and second rounds transformants of the strains showed some disparities in the relocalisation of CAS1-Venus in LCO$_2$ (Figure 4.8). In WT, CAS1-Venus relocalisation to the pyrenoid happened much more abruptly between 2 and 6 h in the second transformant. Also, the pyrenoid CAS1-Venus never started dispersing back to the chloroplast at 24 h in the first transformant like they did in the second transformant. A Kruskal-Wallis test showed that the second transformant had significantly less CAS1-Venus in the pyrenoid compared to the first transformant in WT at all time points ($p < 0.05$ all) except showing no significant difference at 2 h ($p > 0.05$). In *cgld1*, the relocalisation of CAS1-Venus to the pyrenoid happened earlier in the second transformant at 2 h instead of 6 h in the first transformant. The Kruskal-Wallis test revealed once again that, except at 2 h (no significant change, $p > 0.05$), the CAS1-Venus in the pyrenoid of the second transformant was significantly lower than that of the first transformant ($p < 0.05$ all). In *cpld63-1*, the relocalisation of CAS1-Venus showed the same pattern in both transformants. However, the amount of CAS1-Venus in the pyrenoid at 0 and 24 h was significantly higher ($p < 0.05$) in the second transformant compared to the first transformant as shown by the Kruskal-Wallis test. The biggest difference in CAS1-Venus relocalisation pattern could be seen in *cpld63-2*, where it was absent in the first transformant but present in the second transformant and started between 2 and 6 h. After conducting a Kruskal-Wallis test, it was found that there was no significant difference between the CAS1-Venus in the pyrenoid between the two transformants ($p > 0.05$ all) except at 24 h when it was significantly lower in the second transformant ($p < 0.05$).
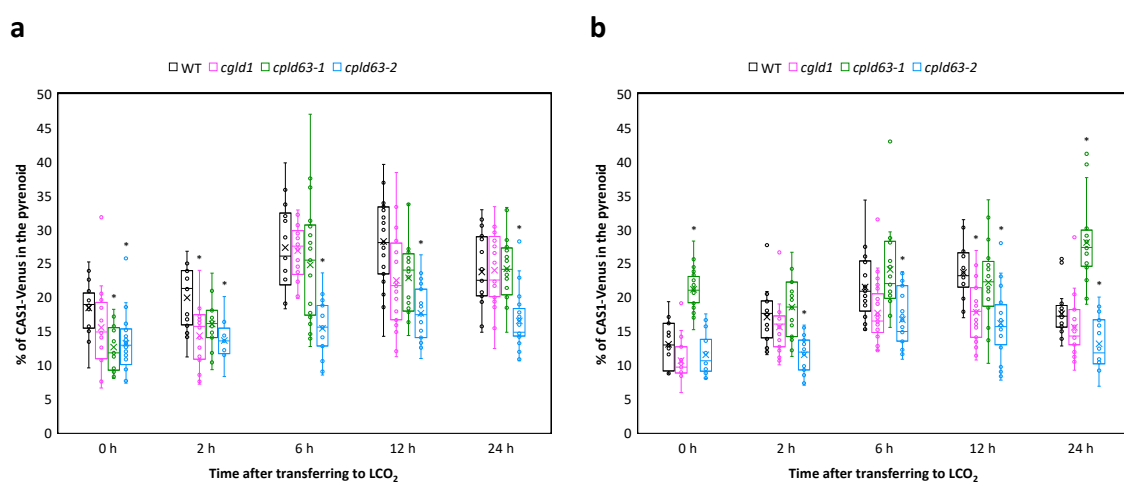
Figure 4.8 Quantification of CAS1-Venus around the pyrenoid in tagged WT and mutants in HCO$_2$ and LCO$_2$.
(a) First round transformants. (b) Second round transformants. Samples were taken for each strain at HCO$_2$ (0 min) before transferring to LCO$_2$, and then at 2 h, 6 h, 12 h and 24 h in LCO$_2$. On each box, X marks the mean of the three biological replicates fold change, circle marks the inner point, and the line marks the median. The box depicts the interquartile range. Circle outside the box marks the outlier. *$p < 0.05$ compared to WT, Kruskal-Wallis test with post hoc Dunn's pairwise comparison.

4.5   Discussion

In this study, the effect of mutating *CGLD1* and *CPLD63* on the transcripts of core CCM genes and the localisation of core CCM proteins was investigated. The data gathered suggested that the mutation of both genes caused a delay in CCM induction as seen in the slower LCO$_2$-induced upregulation of expression of some core CCM genes as well as relocalisation of LCIB. The difference seen between the mutants also implied that the mutation of CGLD1 had a bigger impact on the CCM compared to that of CPLD63.

When looking at the expression data of the core CCM genes, it was clear that there were differences between WT and the mutants, no matter how subtle they were. The LCO$_2$-induced upregulation of *HLA3* and *LCIB* could be seen to experience a slight delay in both *cgld1* and the two *cpld63* mutants. This is not as serious as the inhibition of *HLA3* in *cas1* and *cia5* mutants, or the inhibition of *LCIB* in *cia5* mutant shown in literature (Fang et al., 2012; Wang et al., 2014). This suggests that the subtle delay seen in the mutants are likely caused by the disturbed CCM and photosynthesis phenotype in the mutants as presented in the spot tests from Chapter 2 and 3. As the phenotypes were subtle in *cgld1* and *cpld63-1*, it is reasonable that there was only a slight delay in the upregulation of the two CCM genes. On the other hand, *cpld63-2* had a severe growth defect under light that was worse in autotrophic conditions. Yet again only a slight delay was observed in the upregulation of *HLA3* and *LCIB*. This data suggests that CGLD1 and CPLD63 only play a partial role in regulating the expression of *HLA3* and *LCIB* during the CCM. Interestingly, LCIB showed a significantly larger upregulation in *cpld63-2* at 5 h in LCO$_2$ compared to WT with about 2-fold higher increase in expression, which was not seen in *cpld63-1*. This suggested that this is likely caused by the off-target mutation in *cpld63-2*. The unknown mutated gene(s) might be involved in the LCO$_2$-induced regulation of *LCIB* expression.

Meanwhile, *LCIA* upregulation showed similar trends in the *cpld63* mutants compared to WT but was largely inhibited in *cgld1*. This inhibition was similar to that seen in the mutants of *CIA5* and *CAS1*, two important regulators of *LCIA* (Fang et al., 2012; Wang et al., 2016c). This suggested that CGLD1 has a larger role in regulating LCO$_2$-induced *LCIA* expression compared to *HLA3* and *LCIB*. As absence of LCIA has been shown to cause a diminished *HLA3* mRNA accumulation (Yamano et al., 2015), it is possible that the inhibited *LCIA* induction in *cgld1* led to the delay in *HLA3* accumulation. However, since there was still a small level of *LCIA* expressed, the delay in *HLA3* accumulation was not at

a high level. As for the *cpld63* mutants, although statistically the trends of *LCIA* expression were not significantly different from WT, the graph did present a lower Log2 fold change at 30 min in the mutants. There could still be a slight delay in the upregulation of *LCIA* in them. Just like *HLA3* and *LCIB*, CPLD63 is unlikely to directly regulate the expression of *LCIA* during the CCM.

The expression patterns of *CIA5* and *CAS1* in the strains in LCO_2 indicated that some of the mutated genes might be repressors of these genes. Firstly, it must be noted that there was significant upregulation of *CIA5* in the WT after transferring from HCO_2 to LCO_2 for an hour while Fang et al., 2012 did not find any differential expression of the gene between HCO_2 and $LCO_2/VLCO_2$. If anything, the statistically stable *CIA5* expression over time in *cgld1* and *cpld63-1* matched their data better. This could be a result of different expression analysis used as it has been found in the literature that a small proportion of analysed genes show different expression patterns between qPCR and RNAseq data (Everaert et al., 2017). These genes consisted of 15% of the genes analysed and most of them either had low fold change or were shorter and had fewer exons compared to genes showing matching expression patterns in the two analysis methods. The low fold change in *CIA5* expression (about 2-fold increase) in the WT of this study could be the cause behind the difference seen with Fang et al., 2012 data. Meanwhile, a much more significant increase (about 4-fold) in *CIA5* levels was seen in *cpld63-2* over time in LCO_2. Considering that this was not seen in *cpld63-1* and that *cpld63-2* contained off-target mutations that appeared to enhance the photosynthetic defect phenotype caused by the mutation of *CPLD63*, it is possible the off-target mutated gene might be a negative regulator of *CIA5*. It would be of interest to study *CPLD63* in a *cia5* mutant to investigate whether they share a regulatory relationship.

Meanwhile, this study showed that *CAS1* expression was upregulated slightly in *cgld1* and this was an opposite trend compared to that in WT and the *cpld63* mutants, implying that *CGLD1* might be a partial repressor of *CAS1*. However, this contradicts with the expression study of *CAS1* in the mutant of *trp2*, which has also been proposed to be a chloroplast Ca^{2+} channel needed for the induction of the CCM (Christensen et al., 2020). In this study, *CAS1* was shown to be knocked down in $VLCO_2$ (<0.02%) in the *trp2* mutant using RT-PCR, suggesting that *TRP2* is a positive regulator of *CAS1*. Since both CGLD1 and TRP2 are predicted to contain conserved structure found to be involved in Ca^{2+}

passage/transport, it is unlikely that this contradiction dis-proves the importance of either of them in the Ca^{2+} signalling pathway in the CCM. As Ca^{2+} signals regulate a vast diversity of biological processes and often rely on unique patterns of spatial and temporal spikes of Ca^{2+} concentration to convey specificity in different organisms (Li, Stefan and Le Novère, 2012; Wheeler, 2017; Pivato and Ballottari, 2021; Stoler et al., 2022), TRP2 and CGLD1 might work in different types of Ca^{2+} regulation of CAS1 and the CCM. Perhaps one is required for a prolonged Ca^{2+} activation of CAS1 while another is needed for a faster response in the CCM. Further study on the function of CGLD1 and TPR2 might help identify any diverse Ca^{2+} signalling pattern needed for the versatile regulation of the CCM.

In the meantime, the repression of *CAS1* by CGLD1 was very subtle and appeared to be not influenced by *CPLD63* as *CAS1* expression was not upregulated in both *cpld63* mutants. If CGLD1 indeed partially repressed *CAS1* expression during the CCM, this would explain the subtle decrease of *CAS1* in WT after 5 h in LCO_2 in this study and after 12 h in the paper by Wang et al., 2014. Looking into how *CGLD1* was expressed in *cas1* mutant could help establish the regulatory relationship between the genes. Furthermore, it would also be interesting to investigate whether *CAS1* was further inhibited over 12 h in LCO_2 under light.

The expression of *CGLD1* and *CPLD63* themselves in the mutants showed interesting trends. Again, *CGLD1* expression had a significant increase (about 8-fold) in WT after 1 h in LCO_2 in this study but the study by Fang et al., 2012 did not find any significant change in its expression between different CO_2 conditions. This time, the cause could be the smaller transcript size (741 bp) and number of exons (4 of them) in *CGLD1*. The qPCR result showed that *CGLD1* expression was upregulated in LCO_2 in WT like the expression of many other core CCM genes. However, the increase in its expression was only 8-fold and was far much lower than the ≥64-fold increase of *HLA3*, *LCIA* and *LCIB* expression. Together with the finding that *CGLD1* is regulated by *CIA5* by Fang et al., 2012, it could be concluded that *CGLD1* is likely a CCM gene under the same master regulator as others like *HLA3* and *LCIA*. In the meantime, the expression of *CGLD1* in *cgld1* confirmed the findings in the RT-PCR in Chapter 3 and was likely caused by a small amount of *CGLD1* transcript that was present because the intron with the CIB1 cassette had been spliced away. Again, this could explain why the CCM phenotype was rather subtle in this mutant

in the spot test. As for the *cpld63* mutants, the larger delay and lower level of *CGLD1* expression in *cpld63-1* implied that either CPLD63 has a partial regulatory effect on *CGLD1* or the disturbed photosynthesis caused this delay. On the other hand, the off-target mutations appeared to have rescued this phenotype in *cpld63-2*. However, this would imply that the off-target gene was a negative regulator of *CGLD1* and its mutation should not have led to a CCM phenotype as seen in the spot test of complemented *cpld63-2* lines. There might be a more complex regulatory pathway involved which would require identification of the off-target mutated gene and more phenotype studies of single mutants of this gene. To reduce the complexity of future study on the function of *CGLD1* and its relationship with *CPLD63*, it would be best to only use single mutants and double mutants of the two genes.

As for *CPLD63*, its expression had no significant fluctuations across time in LCO$_2$ in WT, suggesting that the gene was not transcriptionally regulated by CO$_2$ concentration. Since the data gathered so far suggested that it could play a larger role in photosynthesis, *CPLD63* is likely to be expressed in a stable level all the time in autotrophic conditions. In *cgld1*, there was a slight upregulation of *CPLD63* after 5 h in LCO$_2$. This suggested that *CGLD1* might be a partial repressor of *CPLD63*. Unexpectedly *CPLD63* was expressed in *cpld63-2* and upregulated significantly while it was not expressed in *cpld63-1* at all. Since the insertion site of CIB1 cassette in the two mutants were next to each other on Exon 5 of *CPLD63*, the *CPLD63* transcript in *cpld63-2* most likely contained the CIB1 cassette. This would either caused a shift in the open reading frame of the bases or translation of the cassette too, and both cases would most likely lead to a mis-folded or non-functional protein. A Western blot would provide insights into whether they were different from the WT proteins. On the other hand, the upregulation of *CPLD63* in this mutant might be caused by the off-target mutations. As those mutations were found to disrupt the CCM, the CCM itself might have a small repression effect on *CPLD63*.

The expression of different CCM genes showed that the mutation of *CGLD1* had a stronger and faster effect on the CCM compared to that of *CPLD63*. This matches previous data that showed it playing a larger role in the CCM and *CPLD63* having a role in photosynthesis. It would be interesting to study the expression of CCM genes in the mutants at longer time points in LCO$_2$ to see whether *CPLD63* might have a longer and slower regulatory effect on the genes.

There were also differences between the relocalisation trend of LCIB and CAS1 in WT and the mutants. For LCIB, its trend of relocalising to around the pyrenoid in LCO_2 in WT matches that in existing literatures (Yamano et al., 2010, 2014; Toyokawa, Yamano and Fukuzawa, 2020; Yamano et al., 2022). There was a delay of this relocalisation in the mutants. This delay was longer in *cgld1* and *cpld63-2* (at least 6 h) compared to that in *cpld63-1* (at least 2 h). This suggests that CGLD1 plays a larger role in the regulation of LCIB localisation compared to CPLD63. LCIB relocalisation has been shown to be aberrant in mutants with a disturbed CCM as well as abnormal pyrenoid or pyrenoid starch sheath (Yamano et al., 2014; Toyokawa, Yamano and Fukuzawa, 2020; Yamano et al., 2022). As the pyrenoid in the mutants did not show irregular features while the starch sheath was not inspected (Figure 4.3 & Figure 4.4), the delay of LCIB relocalisation was likely caused by the slightly disturbed CCM in *cgld1* and photosynthesis in *cpld63-1*. The longer delay in *cpld63-2* was likely produced by the off-target mutations. In addition, these mutations possibly led to the significantly higher % of LCIB around the pyrenoid in this mutant compared to WT at the final time point. This was either the result from the significantly higher level of upregulation of *LCIB* expression in this mutant compared to WT as seen in the qRT-PCR results, or that the off-target gene(s) were involved in the mechanism behind in the actual relocalisaion of LCIB.

As a similar delay of the LCIB relocalisation could be seen among the first and second transformants of WT and *cgld1*, this delay is likely an accurate biological representation rather than a technical/transformant specific artefact. Meanwhile, the accuracy of the LCIB localisation trends in the *cpld63* mutants would require future experiment on new sets of transformants to be confirmed. It is noted that among some of the measured population, the individual replicates showed quite a wide range of variation, especially in populations measured at 6 h and later time points (see the long boxes and whiskers of these time points in Figure 4.5). As each replicate represented a single cell, perhaps this variation was caused by asynchronisation. On the other hand, there were outliers either at the lower limit or the upper limit in some lines. Those below the lower limit could be unhealthy cells picked up randomly when the images were taken, or just like those above the upper limit represented the very extremes in the population. As all cells within a population were sampled from the same liquid culture, technical errors were unlikely the cause if these outliers. It would be good to quantify LCIB localisation in synchronised

cells or cells that have been synchronised first to see whether there would be such a great variation between the replicates.

For CAS1, its relocalisation in LCO_2 in WT in this study was not apparent compared to the literature and there was already concentration of CAS1 as a knot-like form in the pyrenoid in HCO_2 while the literature images showed CAS1 being evenly distributed over the chloroplast and no knot-like structure was seen in the pyrenoid in HCO_2-acclimated cells under light (Wang et al., 2016c; Yamano, Toyokawa and Fukuzawa, 2018). Possible reasons behind this could be the different tagging techniques used. Wang et al., 2016 used indirect immunofluorescence assay with formaldehyde fixation to tag and image the localisation of CAS1 in WT and mutant *Chlamydomonas* cells while localisation of Venus-tagged CAS1 expressed in live cells were imaged in this study. Chemical fixation might affect the dynamics of protein localisation on the thylakoid membrane as it crosslinks or aggregate proteins and sometimes can disrupts interactions between proteins leading to different localisation (Li et al., 2015; Ichikawa et al., 2022). Meanwhile, Yamano, Toyokawa and Fukuzawa, 2018 imaged the localisation of Clover-tagged CAS1 expressed in WT cells but the expression plasmid used contain a chimeric HSP70A/RBCS2 promoter which enable strong constitutive expression of transgenes (Heitzer and Zschoernig, 2007; Lauersen, Kruse and Mussgnug, 2015). The CAS1-Venus plasmid used here included the native promoter of CAS1 instead of a constitutive promoter. There might be a stronger expression of fluorescently-tagged CAS1 in the WT cells in the paper by Yamano, Toyokawa and Fukuzawa, 2018, thus enhancing the signals of the CAS1 in the chloroplast area outside of pyrenoid in HCO_2. Repeating the localisation experiments with *Chlamydomonas* strains transformed with the plasmid used in the paper could help investigate the cause of the differences seen.

Nevertheless, there was relocalisation of CAS1 after transferring from HCO_2 to LCO_2 shown by the quantification data. There were some differences between the relocalisation trends of the first and second transformants in the strains. As a result, it is not fully clear exactly how the relocalisation of CAS1 occurs across each time point in the strains. However, it was certain that there was relocalisation of CAS1 to the pyrenoid in WT, *cgld1* and *cpld63-1*, and that a small delay was seen in the mutants at one of the time points. This delay showed that CGLD1 and CPLD63 likely play a role in regulating CAS1 localisation in LCO_2, possibly indirectly through maintaining the functioning of the

CCM and photosynthesis. However, in the Wang et al., (2016c) paper, mutation of CIA5 did not affect the visual relocalisation of CAS1 after transferring from HCO_2 to LCO_2 for 2 and 12 h. This makes the delay of it seen in *cgld1* rather confusing as CIA5 is a positive transcription regulator of CGLD1 (Fang et al., 2012). A possible explanation is that the delay might have occurred in the *cia5* mutant but was so small that it could not be recognised through naked eye. As for *cpld63-2*, although there was no relocalisation of CAS1 in the first transformant it was present in the second transformant, the amount of CAS1 in the pyrenoid remained significantly lower compared to WT for the majority of the time points. This could either be caused by the greatly disrupted photosynthesis in *cpld63-2* or the off-target mutations.

Similar to the LCIB localisation experiment, there were big ranges of variation in the % of CAS1 in the pyrenoid seen between the biological replicates as well as many outliers above or below the upper and lower extremes among some populations. The reasons behind these are likely similar to those for the LCIB localisation assay. Again, repeated tests with synchronised cells might be useful in avoiding the big extremes within the population. In addition, untagged cells should be included as controls in the experiment to help normalise the differences seen between transformants for each strain.

In conclusion, CGLD1 appeared to play a larger role in the transcriptional regulation of core CCM genes, especially LCIA, than CPLD63 does. Both genes also have a role in regulating the relocalisation of LCIB and CAS1 from HCO_2 to LCO_2, though probably indirectly through their potential roles in the CCM and photosynthesis. The suggestions for future work mentioned previously, as well as more characterisation experiments such as O_2 evolution to check photosynthetic Ci affinities, PSII quantum yield measurement to check its efficiency, or quantification of CCM proteins translated in WT and mutants, could provide more insights into the two proteins' roles in the regulation of the CCM and photosynthesis.

5 General Discussion and Conclusion

5.1 Main Findings

This thesis originally aimed to identify components important in CO_2 sensing needed for the *Chlamydomonas* CCM. Although it did not identify a clear candidate CO_2 sensor due to the inconsistency between replicated mutant growth assays, it did generate a list of possible candidate genes (see Chapter 2) as guidance for future studies on CO_2 sensing in the alga. Nonetheless, it still identified two important components - CGLD1 and CPLD63 - that could potentially transport Ca^{2+} to the pyrenoid to regulate CAS1-mediated accumulation of LCIA and partially HLA3. The findings in Chapter 2 showed that CGLD1 is needed for the functioning of the CCM when there is higher $HCO_3^-:CO_2$ ratio at higher pH, while CPLD63 has a more general role in photosynthesis. Chapter 3 concluded that CGLD1 could potentially transport Ca^{2+} across the thylakoid membrane while CPLD63 could potentially transport Ca^{2+} across the chloroplast membrane. The results in Chapter 4 showed that *CGLD1* is induced in LCO_2 and has a major role in regulating *LCIA* expression in LCO_2 while CPLD63 has a more indirect role in the regulation of the CCM. These findings help lay a foundation to dissecting the Ca^{2+}-signalling pathway and upstream CO_2 sensor needed in regulating the algal CCM.

5.2 Roles of CGLD1 and CPLD63 in the CCM
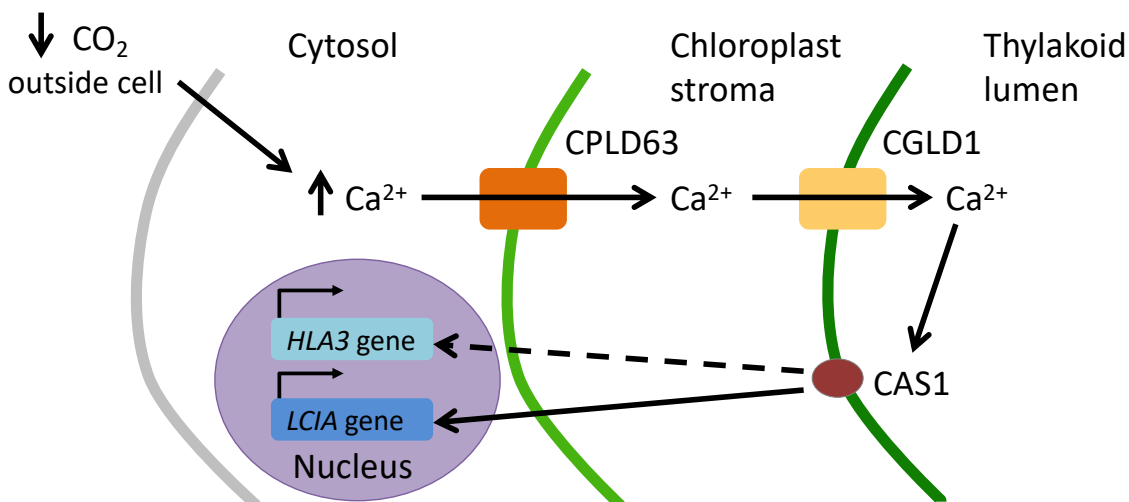
Figure 5.1 Hypothesised roles of CPLD63 and CGLD1 in regulation of the *Chlamydomonas* CCM.
CPLD63 and CGLD1 could play a role in transporting Ca^{2+} into the thylakoid lumen to activate the retrograde signalling pathway from CAS1 to induce *LCIA* expression for the CCM. They might only partially regulate *HLA3* induction during the CCM, implying other upstream regulator(s) are needed for this regulation.

The results of the various spot tests first confirmed that CGLD1 and CPLD63 had a role in the CCM and photosynthesis respectively. The various bioinformatics analysis on them

and their homologues suggested that they could transport Ca^{2+} in *Chlamydomonas*. As localisation data showed CGLD1 and CPLD63 localised to the thylakoid membrane and the chloroplast envelope, they might mediate the Ca^{2+} transport across the two organelle membranes respectively, similar to the roles of their homologues BICAT1 and BICAT2 in *Arabidopsis* (Frank et al., 2019). In fact, the spot test with different Ca^{2+} concentrations showed that CGLD1 is important in Ca^{2+} homeostasis needed for the CCM when extracellular Ca^{2+} is limiting. The gene expression study of CCM genes showed that *CGLD1* expression is upregulated by LCO_2 and is important for the upregulation of *LCIA* in LCO_2, while the mutation of CPLD63 appeared to not affect the expression of the investigated CCM genes. This suggests that CGLD1 has a role in regulating the CCM but CPLD63 might not do so. Nevertheless, the localisation experiment of LCIB and CAS1 suggested that CPLD63 still has an indirect role in the CCM as its mutation caused a slight delay in the relocalisation of the two CCM proteins in LCO_2. With these findings and the study by Wang et al., 2016c that shows the important role of Ca^{2+} and the Ca^{2+}-binding CAS1 in maintaining the upregulation of HLA3 and LCIA in the CCM, hypothesis on the role of CGLD1 and CPLD63 in the CCM can be established (Figure 5.1): as the CO_2 concentration outside the cell becomes limited, an unknown upstream regulator activates the increase of Ca^{2+} in the cytosol from internal organellar Ca^{2+} storage such as contractile vacuoles (Pivato and Ballottari, 2021), which leads to a transporting cascade of Ca^{2+} into the chloroplast stroma through CPLD63 and then into the thylakoid lumen through CGLD1, increasing the concentration of Ca^{2+} in the thylakoid tubules in the pyrenoid. The increased Ca^{2+} ions then bind to CAS1 with high capacity, activating the protein to send a retrograde signal to the nucleus to induce transcription of the Ci transporter *LCIA*, thus inducing/maintaining the CCM. However, as *HLA3* expression was not affected in *cgld1* or the *cpld63* mutants, this process might only activate the transcription of *HLA3* partially, suggesting there could be another upstream regulator of CAS1 and HLA3.

Since their homologues BICAT1, Gdt1p and TMEM165 are shown to potentially be Ca^{2+}/H^+ antiporter (Demaegd et al., 2013; Colinet et al., 2016; Wang et al., 2016a), CGLD1 and CPLD63 might also function as this type of transporter and rely on a pH gradient to transport Ca^{2+}. However, as this study failed to set up the experiments for visualising Ca^{2+} in *Chlamydomonas* cells and expression of CGLD1 and CPLD63 in *E. coli* for Ca^{2+} influx to investigate whether the two proteins have Ca^{2+} transporting activity, it is still unknown if they actually transport Ca^{2+} or what type of Ca^{2+} transporter they are. The successful

visualisation of Ca^{2+} influx in *Chlamydomonas* WT and mutants of *CGLD1* and *CPLD63*, as well as expression of the two proteins in *E. coli* for Ca^{2+} influx assays would help confirm their Ca^{2+} transporting roles.

The role of CGLD1 in regulating *LCIA* expression helps explain the apparent dependency on HCO_3^- of CGLD1 shown in the spot tests, where its mutant only had a CCM phenotype in the higher pH 7.8 and 8.0 but grew similarly to WT at the lower pH 7.4. This dependency is likely due to the importance of LCIA in the active transport of HCO_3^- into the chloroplast stroma in the CCM (Miura et al., 2004; Wang and Spalding, 2014; Yamano et al., 2015). However, we cannot dismiss the possibility that the affinity for HCO_3^- could also be because CGLD1 is regulated by an upstream HCO_3^- sensor in limiting CO_2. Identifying the upstream regulatory components of CGLD1 (and CPLD63 as well) would be helpful in dissecting the Ci sensing pathway needed for regulating the algal CCM.

5.3   Other roles of CGLD1 and CPLD63 in *Chlamydomonas*

The data from this thesis as well as literatures suggest that CGLD1 and CPLD63 have other roles in *Chlamydomonas* apart from transporting Ca^{2+} in the CCM. For one, they could also transport Mn^{2+} needed for the functioning of PSII. It has been shown that their homologues - the BICATs, Gdt1p and TMEM165 - are also needed for Mn^{2+} homeostasis (Potelle et al., 2016; Schneider et al., 2016; Wang et al., 2016a; Dulary et al., 2018; Eisenhut et al., 2018; Thines et al., 2018; Hoecker et al., 2021). In fact, CGLD1 has been shown to be important for Mn^{2+} homeostasis as well as efficient PSII activity in *Chlamydomonas* (Schneider et al., 2016; Xing et al., 2017). This is also shown by the slightly rescued growth of *cgld1* in higher Mn^{2+} concentration in the spot tests. On the other hand, although the same spot test showed that the phenotype of the *cpld63* mutants was not affected by the different Mn^{2+} levels, CPLD63 might still play a role in transporting Mn^{2+} into the chloroplast because there might be redundant gene(s) that play(s) a similar role. This would explain why its mutation only created a very subtle growth defect in *cpld63-1* under autotrophic growth in the spot test. Other Ca^{2+} transporters (e.g. CAX5, Cation Exchanger 5) have also been found to transport Mn^{2+} in *Arabidopsis* (He et al., 2021), implying that it is feasible for CGLD1 and CPLD63 to transport both ions.

In the meantime, CPLD63 appears to have a more general role in *Chlamydomonas* photosynthesis, as shown by the many spot tests conducted in this study. This is likely because of its possible role in transporting Ca^{2+}/Mn^{2+} into the chloroplast, which if disrupted would disturb the homeostasis of these two ions in the whole photosynthetic apparatus and hinder its function greatly (Wang et al., 2019; Alejandro et al., 2020). Future studies that investigate the photosynthetic efficiency of *cpld63* mutant would help in confirming the role of CPLD63 in photosynthesis.

5.4   Providing guidance on dissecting and engineering the algal CCM

The thesis identified two putative Ca^{2+} transporters that could potentially play a role in the *Chlamydomonas* CCM. Further characterisation of their functionality could potentially help us understand the actual molecular mechanism behind the LCO_2-induced Ca^{2+} elevation in the pyrenoid needed for the CCM. Furthermore, identifying the downstream targets of CGLD1 and CPLD63 using approaches such as RNAseq, would also help identify other components involved in the Ca^{2+}-signalling pathway in the CCM. These could all help in dissecting the pathways involved in the regulation of the algal CCM, thus providing a blueprint for implementing a tightly controlled mechanism (e.g. engineering a permanently active positive regulator of HLA3 and LCIA) into the algal CCM for both industrial use and engineering into C3 crop plants.

5.5   Concluding remarks

The world is facing a serious food security problem. It is imminent that we increase global crop production vastly or food shortage will become one of the challenges we face every day. As more research is carried out to clarify remaining unknowns of the *Chlamydomonas* CCM and engineering already identified essential CCM components into higher plant system, it is hopeful that the final goal of engineering a fully functional and controllable CCM into C3 crop plants will not be far away. This will require the collaboration of research institutes across the world and disciplines. Hopefully, this project has also contributed to this goal by providing guidance for future studies of the regulation of the *Chlamydomonas* CCM.

Appendix A

Table A.1 Primers used in PCR check of mutants of CDPK13, CGLD1 and CPLD63

Strain	Primer pair sequences
cdpk13-1	5' TTTGAGGAGCTCGACAAGGT 3'
	5' GGCCGTCCTATTGTCACCTA 3'
cdpk13-2	5' TGATGGTTTTGCAGTGGTGT 3'
	5' ATGATGGCGATTTCCTTGAG 3'
cgld1	5' GGTGCTGTCCCAACTGATTT 3'
	5' TCCGATCTCGATTTTGTTCC 3'
cpld63-1	5' GTGGGTGGGTAGGTGGTATG 3'
	5' AGTCAATCAGTCTTGCGGCT 3'
cpld63-2	5' GTGGGTGGGTAGGTGGTATG 3'
	5' AGTCAATCAGTCTTGCGGCT 3'
CIB1 cassette	5' GCACCAATCATGTCAAGCCT 3'
	5' GACGTTACAGCACACCCTTG 3'
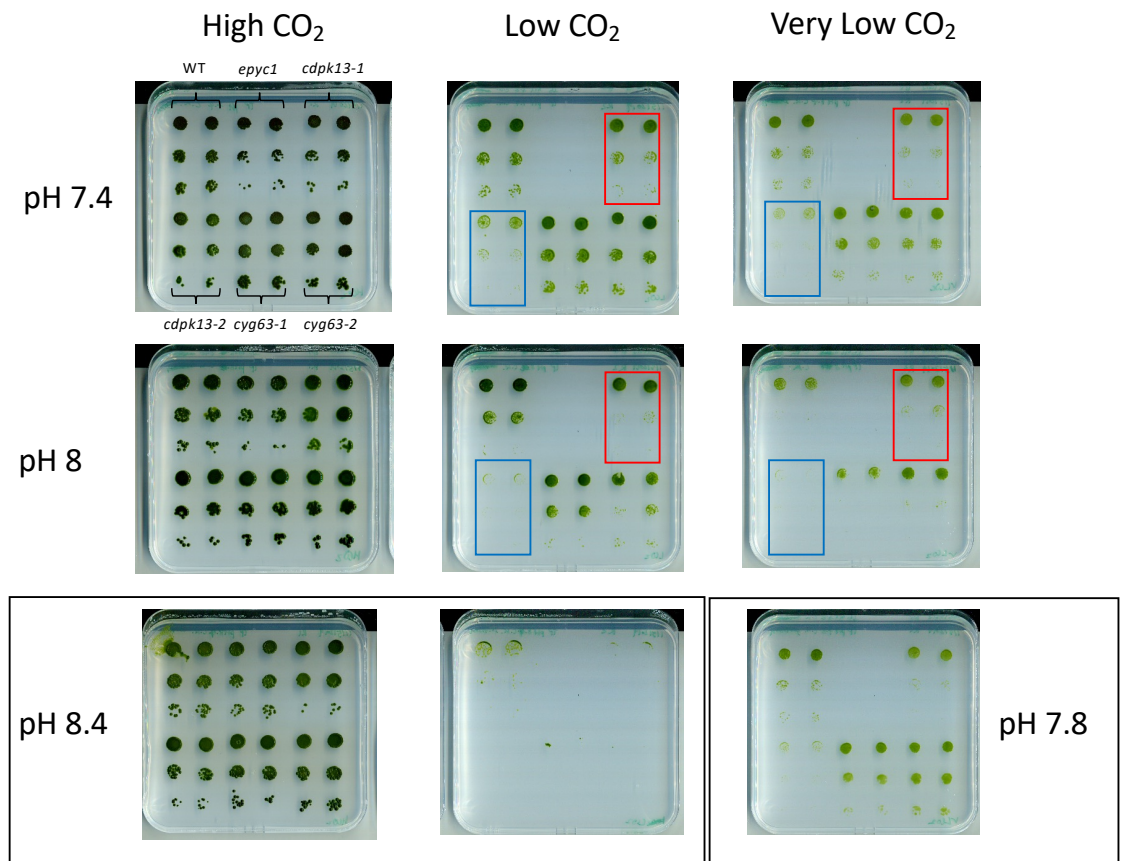
Figure A.1 Initial spot test of mutants of CDPK13 and CYG63 under continuous light.

Each sample was grown with a series of dilution: 10^4, 10^3, and 10^2 cells in total and spotted on the plate twice as technical replicates. The plates were scanned after the WT showed adequate growth in all conditions. The growth of the mutant strains was compared to the WT strain on the same plate. The red rectangle shows the technical replicates of mutant *cdpk13-1* while the blue rectangle shows the technical replicates of mutant *cdpk13-2* in limiting CO_2.
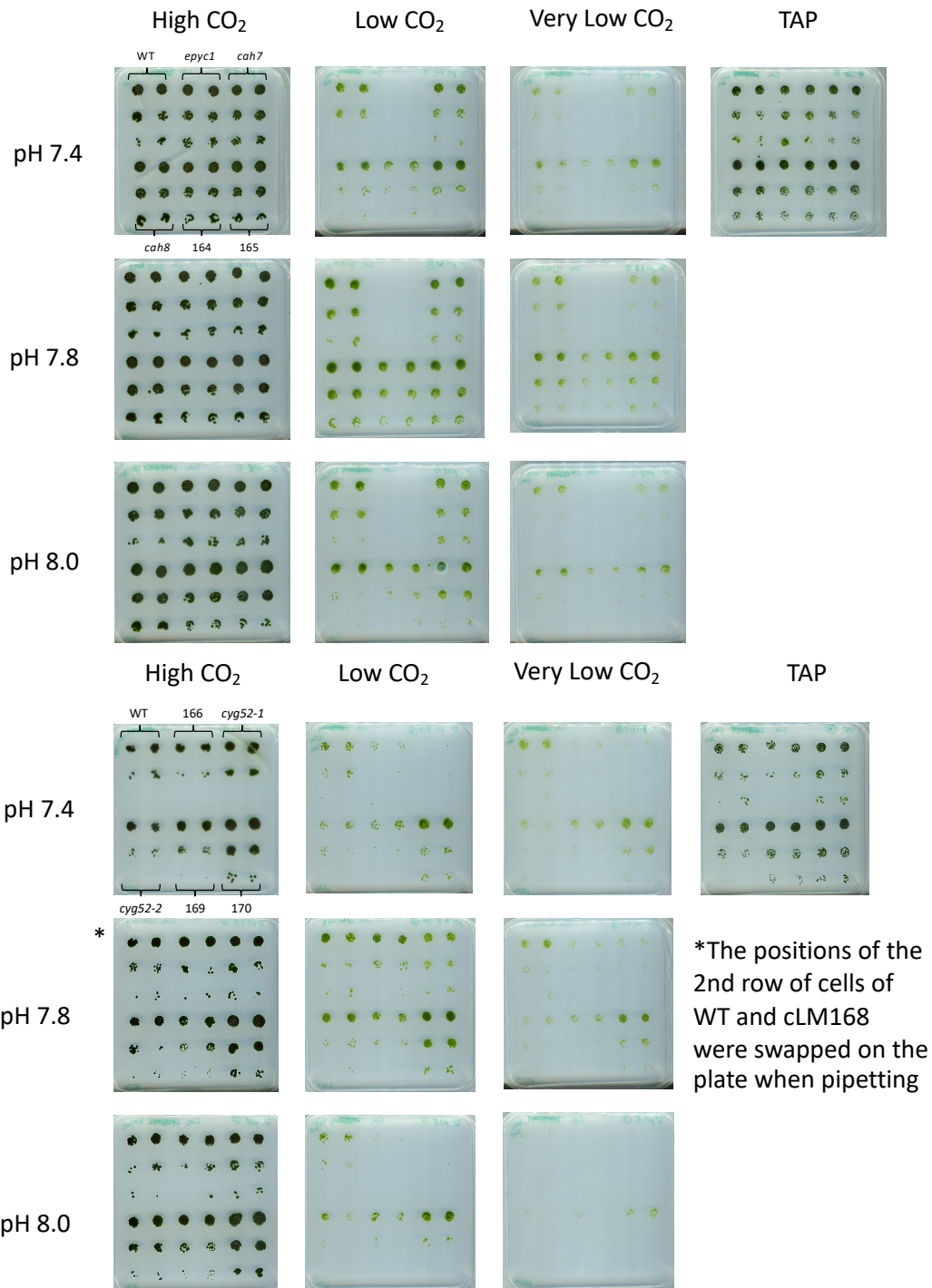
Figure A.2 Initial spot test of first batch of CLiP mutants under light:dark cycle.
All strains were first synchronised to the 12:12 light:dark cycle and then incubated in groups on individual plates also under the same light-dark cycle. Each sample was grown with a series of dilution: 10^4, 10^3, and 10^2 cells in total and spotted on the plat twice as technical replicates. The plates were scanned after the WT showed adequate growth in all conditions. The growth of the mutant strains was compared to the WT strain on the same plate. However, the WT on some plates did not grow well and therefore, the data of those plates were considered invalid. All mutant strains are labelled with the disrupted gene name (Italic) or with the cLM ID number used in the lab if there has not yet been a gene name assigned for the disrupted gene.

*The positions of the 2nd row of cells of WT and cLM168 were swapped on the plate when pipetting

Figure A.3 Initial spot test of second batch of CLiP mutants under light:dark cycle.
All strains were first synchronised to the 12:12 light:dark cycle and then incubated in groups on individual plates also under the same light-dark cycle. Each sample was grown with a series of dilution: 10^4, 10^3, and 10^2 cells in total and spotted on the plat twice as technical replicates. The plates were scanned after the WT showed adequate growth in all conditions. The growth of the mutant strains was compared to the WT strain on the same plate. However, the WT on some plates did not grow well and therefore, the data of those plates were considered invalid. All mutant strains are labelled with the disrupted gene name (Italic) or with the cLM ID number used in the lab if there has not yet been a gene name assigned for the disrupted gene.

Figure A.4 Initial spot test of third batch of CLiP mutants under light:dark cycle.
All strains were first synchronised to the 12:12 light:dark cycle and then incubated in groups on individual plates also under the same light-dark cycle. Each sample was grown with a series of dilution: 10^4, 10^3, and 10^2 cells in total and spotted on the plat twice as technical replicates. The plates were scanned after the WT showed adequate growth in all conditions. The growth of the mutant strains was compared to the WT strain on the same plate. However, the WT on some plates did not grow well and therefore, the data of those plates were considered invalid. All mutant strains are labelled with the disrupted gene name (Italic) or with the cLM ID number used in the lab if there has not yet been a gene name assigned for the disrupted gene.

Figure A.5 Initial spot test of final batch of CLiP mutants under light:dark cycle.

All strains were first synchronised to the 12:12 light:dark cycle and then incubated in groups on individual plates also under the same light-dark cycle. Each sample was grown with a series of dilution: 10^4, 10^3, and 10^2 cells in total and spotted on the plat twice as technical replicates. The plates were scanned after the WT showed adequate growth in all conditions. The growth of the mutant strains was compared to the WT strain on the same plate. However, the WT on some plates did not grow well and therefore, the data of those plates were considered invalid. All mutant strains are labelled with the disrupted gene name (Italic) or with the cLM ID number used in the lab if there has not yet been a gene name assigned for the disrupted gene.

Appendix B

Table B.1 Primers used in amplifying the backbone from tagging plasmid Hygro-Scarlet-i for recombineering

Final plasmid	Primer pair sequences
CGLD1_Scarlet-i	5'GCTCTCTCTTCCTTGTGTTCGCGGGGGCGACCATCGTGGACCTGTTCGTGGGAGATCTGGGTGGCTCCG3'
	5'ATGAGAACTGCGCAGTGGAGTAAGATGGGAATGGAAAACGTTTGTTCATAGAAGATCCTTTGATCTTTTCTACGGG3'
CGLD1_Hygro (no tag)	5'GCTCTCTCTTCCTTGTGTTCGCGGGGGCGACCATCGTGGACCTGTTCGTGTGATGGCAGCAGCTGGACC3'
	5'ATGAGAACTGCGCAGTGGAGTAAGATGGGAATGGAAAACGTTTGTTCATAGAAGATCCTTTGATCTTTTCTACGGG3'
CPLD63_Scarlet-i	5'GCGGCATCCTGTTCCTAGTGTTCGCGGCCGCTACCGCTTTCAGCATGCTGGGAGATCTGGGTGGCTCCG3'
	5'TATAAGATGCAAGCGCGCATATCGCGGTTGTTGCGCATATCGCAGTTGTTGAAGATCCTTTGATCTTTTCTACGGG3'
CPLD63_Hygro (no tag)	5'GCGGCATCCTGTTCCTAGTGTTCGCGGCCGCTACCGCTTTCAGCATGCTGTGATGGCAGCAGCTGGACC3'
	5'TATAAGATGCAAGCGCGCATATCGCGGTTGTTGCGCATATCGCAGTTGTTGAAGATCCTTTGATCTTTTCTACGGG3'

Table B.2 Primers designed for LIC cloning of *CGLD1* and *CPLD63* into the expression plasmid pET His6 TEV LIC cloning vector (1B

Gene	Primer pair sequences
CGLD1	5' TACTTCCAATCCAATGCAATGGCGCTGGCGGCATCG 3'
	5' TTATCCACTTCCAATGTTATTATTACACGAACAGGTCCACGATGGTCG 3'
CPLD63	5' TACTTCCAATCCAATGCAATGCTCAGGGCTGGGCAG 3'
	5' TTATCCACTTCCAATGTTATTATCACAGCATGCTGAAAGCGG 3'

Table B.3 Primers used for screening *cgld1* and *cpld63* untagged complemented lines

Lines	Primer pair sequences
cgld1:CGLD1_Hygro	5' GTTCTTCATCGCGCTACTGC 3'
	5' AACCAAGTCGACGTGCCTAC 3'
cpld63-1/cpld63-2:CPLD63_Hygro	5' ACTGTCAACCTCATCAGCGG 3'
	5' AACCAAGTCGACGTGCCTAC 3'

Table B.4 Primers used in the RT-PCR check of complemented *cgld1* and *cpld63* lines in Chapter 3.

Gene locus amplified	Primer pair sequences
RCK1	5' CTGGGCGAGTGCAAGTACAC 3'
	5' CTTGCAGTTGGTCAGGTTCCAG 3'
CGLD1	5' TTCAAGACGCTGAAGGACGC 3'
	5' CCTCACTGCTGCTCTTGAGG 3'
5' CIB1 genome-cassette junction	5' TCTTCTTCAGCGAGATCGGC 3'
	5' GACGTTACAGCACACCCTTG 3'
3' CIB1 genome-cassette junction	5' GCACCAATCATGTCAAGCCT 3'
	5' CGAGGAAGGACTTGTCACCC 3'
CPLD63	5' TTATCTTCCTGGCGGAGTGG 3'
	5' CCTCCCCTACAAACCCACAC 3'

Appendix C

Table C.1 Primer pair sequences used for the target genes and reference gene in the qRT-PCR in Chapter 4

Gene	Primer pair sequences
HLA3	5' AGAAGCTTAAGGACCAGGATGGC 3'
	5' AGTTGACGTGGGACAGCAGA 3'
LCIA	5' ACTTCGGCAACTTCGTGGG 3'
	5' AGTTGCACAGGATGGAGCG 3'
LCIB	5' TCACTGGTGACAACACCATCGC 3'
	5' TGTTGAACGAGGAGCCGAAGATG 3'
CIA5/CCM1	5' CTATTCGTGTGTCCGTGGCG 3'
	5' GCAGCCGGCAATTCAGTGTC 3'
CAS1	5' CAAACTGACTGTACGCGCAC 3'
	5' TACACTGCAGGCCACTTGAG 3'
CGLD1	5' CGCGGTAGATTGGTGGGATC 3'
	5' CTCGATTTTGTTCCGGCCTC 3'
CPLD63	5' CGGGTGTCTACTGACGAGTG 3'
	5' TGCACATGCGCACGATAATG 3'
RCK1 (*CBLP*)	5' CTGGGCGAGTGCAAGTACAC 3'
	5' CTTGCAGTTGGTCAGGTTCCAG 3'

Table C.2 *HLA3* and *RCK1* qRT-PCR Cq values in Chapter 4

Biological Replicate-Time point	Gene	WT Cq	*cgld1* Cq	*cpld63-1* Cq	*cpld63-2* Cq
R1-0 min	HLA3	32.7	36.4	32.9	35.3
R2-0 min	HLA3	33.7	36.8	32.1	33.7
R3-0 min	HLA3	31.5	33.5	34.6	32.2
R1-30 min	HLA3	31.3	35.6	32.9	31.7
R2-30 min	HLA3	33.6	33.9	33.7	34.0
R3-30 min	HLA3	26.7	32.3	34.4	32.2
R1-1 h	HLA3	26.3	35.6	28.8	27.1
R2-1 h	HLA3	31.3	32.3	32.6	32.1
R3-1 h	HLA3	23.7	31.6	30.0	25.7
R1-5 h	HLA3	24.6	32.2	24.1	25.7
R2-5 h	HLA3	26.1	31.7	23.5	24.3
R3-5 h	HLA3	24.3	27.4	25.4	25.2
R1-0 min	HLA3	31.4	34.9	32.9	33.1
R2-0 min	HLA3	32.1	33.8	32.2	33.3
R3-0 min	HLA3	29.8	34.4	33.8	30.8
R1-30 min	HLA3	30.0	36.1	32.9	31.5
R2-30 min	HLA3	32.5	33.2	34.4	32.7
R3-30 min	HLA3	25.2	31.5	34.5	31.0
R1-1 h	HLA3	25.1	34.3	28.5	26.9
R2-1 h	HLA3	30.2	32.1	33.7	31.2
R3-1 h	HLA3	22.8	31.6	29.3	25.7
R1-5 h	HLA3	24.5	32.0	23.4	25.8
R2-5 h	HLA3	25.8	31.8	23.1	24.3
R3-5 h	HLA3	24.2	27.2	24.9	25.7
R1-0 min	HLA3	30.3	35.5	32.0	33.3
R2-0 min	HLA3	32.0	35.1	31.6	33.2
R3-0 min	HLA3	29.2	34.6	33.2	30.6
R1-30 min	HLA3	29.5	35.2	32.6	31.8
R2-30 min	HLA3	31.5	33.4	34.2	32.6
R3-30 min	HLA3	25.2	31.4	34.0	31.3
R1-1 h	HLA3	25.3	33.7	28.1	26.2
R2-1 h	HLA3	30.4	32.3	33.2	30.8
R3-1 h	HLA3	23.1	30.8	29.4	25.5
R1-5 h	HLA3	24.7	31.4	23.1	25.6
R2-5 h	HLA3	25.8	31.3	22.8	24.1
R3-5 h	HLA3	24.1	26.9	24.6	25.3
R1-0 min	RCK1	19.8	21.1	21.6	22.1
R2-0 min	RCK1	19.8	21.0	20.8	21.6
R3-0 min	RCK1	19.6	20.7	21.9	21.7
R1-30 min	RCK1	20.4	20.9	21.5	22.0
R2-30 min	RCK1	20.6	22.0	21.8	22.6
R3-30 min	RCK1	19.6	21.5	21.7	22.2
R1-1 h	RCK1	20.2	21.5	21.2	21.8

R2-1 h	*RCK1*	19.3	21.8	21.4	21.5
R3-1 h	*RCK1*	20.5	21.3	21.5	20.7
R1-5 h	*RCK1*	21.5	20.5	21.6	21.1
R2-5 h	*RCK1*	21.8	21.0	20.2	20.1
R3-5 h	*RCK1*	20.6	20.6	21.6	21.1
R1-0 min	*RCK1*	19.9	21.4	21.6	22.2
R2-0 min	*RCK1*	20.1	21.3	20.9	21.7
R3-0 min	*RCK1*	19.8	21.0	22.3	21.7
R1-30 min	*RCK1*	20.7	21.2	22.0	22.0
R2-30 min	*RCK1*	21.0	22.5	22.2	22.9
R3-30 min	*RCK1*	20.0	21.7	22.1	22.3
R1-1 h	*RCK1*	20.7	21.6	21.6	21.9
R2-1 h	*RCK1*	19.6	22.1	22.4	21.4
R3-1 h	*RCK1*	21.0	21.5	22.2	20.8
R1-5 h	*RCK1*	22.2	20.6	22.0	21.0
R2-5 h	*RCK1*	22.1	21.1	20.9	20.1
R3-5 h	*RCK1*	20.9	20.9	22.1	21.0
R1-0 min	*RCK1*	19.8	21.5	21.9	22.3
R2-0 min	*RCK1*	19.9	21.6	21.0	21.9
R3-0 min	*RCK1*	19.9	21.4	22.2	22.0
R1-30 min	*RCK1*	20.9	21.4	21.9	22.4
R2-30 min	*RCK1*	21.0	22.5	22.3	23.0
R3-30 min	*RCK1*	20.2	21.8	22.1	22.4
R1-1 h	*RCK1*	20.7	22.2	21.6	22.0
R2-1 h	*RCK1*	19.4	22.0	22.6	21.7
R3-1 h	*RCK1*	20.7	21.6	22.1	20.9
R1-5 h	*RCK1*	21.8	20.8	21.9	21.1
R2-5 h	*RCK1*	22.0	21.3	20.8	20.1
R3-5 h	*RCK1*	20.6	21.1	22.1	21.0

Table C.3 *LCIA* and *RCK1* qRT-PCR Cq values in Chapter 4

Biological Replicate-Time point	Gene	WT Cq	*cgld1* Cq	*cpld63-1* Cq	*cpld63-2* Cq
R1-0 min	LCIA	Undetermined	Undetermined	37.6	36.8
R2-0 min	LCIA	34.7	34.7	35.1	34.7
R3-0 min	LCIA	36.6	34.0	34.8	35.5
R1-30 min	LCIA	26.3	36.5	27.4	26.1
R2-30 min	LCIA	30.1	35.2	34.4	32.0
R3-30 min	LCIA	20.8	33.2	30.2	25.7
R1-1 h	LCIA	20.8	34.3	22.7	21.6
R2-1 h	LCIA	22.4	32.8	30.6	31.3
R3-1 h	LCIA	20.6	34.2	23.2	21.0
R1-5 h	LCIA	22.0	31.2	21.6	23.7
R2-5 h	LCIA	22.7	27.8	21.9	24.0
R3-5 h	LCIA	21.6	25.4	24.0	23.6
R1-0 min	LCIA	36.6	37.3	37.0	35.1
R2-0 min	LCIA	33.8	35.0	33.9	34.5
R3-0 min	LCIA	34.7	35.5	36.3	33.8
R1-30 min	LCIA	23.8	34.6	26.3	25.3
R2-30 min	LCIA	28.0	34.0	33.0	31.5
R3-30 min	LCIA	19.4	34.9	29.5	25.2
R1-1 h	LCIA	19.8	34.3	21.9	21.3
R2-1 h	LCIA	22.1	32.4	29.8	31.0
R3-1 h	LCIA	19.5	33.5	22.5	20.6
R1-5 h	LCIA	21.3	30.5	21.7	23.3
R2-5 h	LCIA	22.5	27.1	21.0	23.4
R3-5 h	LCIA	20.7	24.4	22.6	22.4
R1-0 min	LCIA	34.3	34.4	36.4	33.8
R2-0 min	LCIA	33.5	Undetermined	35.0	33.3
R3-0 min	LCIA	34.4	34.5	Undetermined	35.0
R1-30 min	LCIA	23.9	33.2	26.4	25.1
R2-30 min	LCIA	27.7	33.5	33.0	31.4
R3-30 min	LCIA	19.4	33.7	29.4	24.8
R1-1 h	LCIA	19.9	34.4	23.4	21.1
R2-1 h	LCIA	22.4	32.4	29.8	31.4
R3-1 h	LCIA	19.9	32.8	22.8	20.7
R1-5 h	LCIA	21.5	30.6	21.5	23.6
R2-5 h	LCIA	22.4	27.6	20.9	23.4
R3-5 h	LCIA	20.8	24.8	22.4	22.6
R1-0 min	RCK1	19.9	22.0	20.8	20.8
R2-0 min	RCK1	19.3	21.4	20.0	20.4
R3-0 min	RCK1	19.2	21.5	19.9	20.3
R1-30 min	RCK1	20.3	21.2	19.8	21.1
R2-30 min	RCK1	20.3	22.4	20.3	20.8
R3-30 min	RCK1	19.2	21.7	20.2	21.5
R1-1 h	RCK1	19.7	21.7	20.5	20.4

R2-1 h	*RCK1*	18.7	21.7	19.3	20.9
R3-1 h	*RCK1*	19.9	21.5	21.0	20.1
R1-5 h	*RCK1*	20.3	20.9	21.0	19.8
R2-5 h	*RCK1*	20.9	21.4	19.7	19.8
R3-5 h	*RCK1*	19.8	21.1	21.1	19.9
R1-0 min	*RCK1*	20.0	22.2	20.9	21.0
R2-0 min	*RCK1*	19.6	21.6	20.3	20.7
R3-0 min	*RCK1*	19.5	21.8	20.1	20.7
R1-30 min	*RCK1*	20.4	21.4	19.8	21.2
R2-30 min	*RCK1*	20.5	22.7	20.6	20.9
R3-30 min	*RCK1*	19.5	21.9	20.3	21.7
R1-1 h	*RCK1*	20.1	22.0	20.2	20.8
R2-1 h	*RCK1*	19.0	22.0	19.4	21.1
R3-1 h	*RCK1*	20.3	21.9	21.1	20.4
R1-5 h	*RCK1*	20.6	21.0	21.0	20.0
R2-5 h	*RCK1*	21.5	21.7	19.8	20.1
R3-5 h	*RCK1*	19.9	21.6	21.2	20.1
R1-0 min	*RCK1*	20.3	22.2	20.7	20.9
R2-0 min	*RCK1*	19.7	21.7	20.0	20.5
R3-0 min	*RCK1*	19.7	21.7	20.1	20.8
R1-30 min	*RCK1*	20.6	21.5	19.9	21.4
R2-30 min	*RCK1*	20.7	22.7	20.6	21.0
R3-30 min	*RCK1*	19.6	22.0	20.4	21.9
R1-1 h	*RCK1*	20.2	22.3	20.2	20.9
R2-1 h	*RCK1*	19.0	22.1	19.4	21.2
R3-1 h	*RCK1*	20.1	22.1	21.0	20.5
R1-5 h	*RCK1*	20.5	21.0	21.0	20.0
R2-5 h	*RCK1*	21.1	21.5	19.7	20.1
R3-5 h	*RCK1*	19.8	21.4	21.0	20.1

Table C.4 *LCIB* and *RCK1* qRT-PCR Cq values in Chapter 4

Biological Replicate-Time point	Gene	WT Cq	*cgld1* Cq	*cpld63-1* Cq	*cpld63-2* Cq
R1-0 min	LCIB	27.2	31.6	27.0	27.9
R2-0 min	LCIB	26.9	29.4	26.9	27.8
R3-0 min	LCIB	24.5	29.3	25.5	26.9
R1-30 min	LCIB	21.2	27.9	21.8	22.3
R2-30 min	LCIB	22.7	28.0	24.1	24.1
R3-30 min	LCIB	19.5	27.8	23.1	22.4
R1-1 h	LCIB	21.1	27.2	21.2	20.8
R2-1 h	LCIB	20.4	25.1	22.4	23.9
R3-1 h	LCIB	19.6	27.3	22.7	20.0
R1-5 h	LCIB	22.1	25.8	22.7	21.0
R2-5 h	LCIB	23.5	25.5	22.1	21.2
R3-5 h	LCIB	22.0	24.1	24.0	20.9
R1-0 min	LCIB	26.1	32.3	26.6	27.7
R2-0 min	LCIB	25.8	29.2	25.7	27.2
R3-0 min	LCIB	24.4	28.8	25.3	26.4
R1-30 min	LCIB	20.7	27.0	21.6	21.7
R2-30 min	LCIB	22.4	27.5	23.7	23.4
R3-30 min	LCIB	18.7	27.5	22.6	21.9
R1-1 h	LCIB	19.4	26.9	20.2	20.1
R2-1 h	LCIB	19.6	24.7	21.2	22.8
R3-1 h	LCIB	18.8	26.6	20.1	19.3
R1-5 h	LCIB	21.5	25.2	21.7	20.3
R2-5 h	LCIB	22.6	25.0	20.8	20.5
R3-5 h	LCIB	21.2	23.3	22.9	20.2
R1-0 min	LCIB	24.7	30.9	25.9	26.9
R2-0 min	LCIB	24.3	28.5	24.0	26.0
R3-0 min	LCIB	22.9	28.3	24.5	25.1
R1-30 min	LCIB	20.4	27.3	21.2	21.3
R2-30 min	LCIB	21.3	27.1	23.0	22.7
R3-30 min	LCIB	17.8	26.9	22.0	20.8
R1-1 h	LCIB	18.4	26.4	19.7	19.2
R2-1 h	LCIB	18.9	24.3	21.0	22.5
R3-1 h	LCIB	18.0	26.1	20.8	18.7
R1-5 h	LCIB	20.5	24.3	21.1	19.7
R2-5 h	LCIB	21.7	24.1	20.3	19.7
R3-5 h	LCIB	20.6	23.1	22.4	19.8
R1-0 min	RCK1	20.5	22.2	20.8	21.2
R2-0 min	RCK1	20.4	21.8	20.2	21.1
R3-0 min	RCK1	19.6	21.8	19.9	20.8
R1-30 min	RCK1	20.7	21.7	19.7	21.5
R2-30 min	RCK1	20.9	22.7	20.4	21.1
R3-30 min	RCK1	19.6	22.0	20.1	21.9
R1-1 h	RCK1	19.9	22.0	20.4	21.1

R2-1 h	*RCK1*	19.0	21.9	19.2	21.5
R3-1 h	*RCK1*	20.1	21.9	21.0	20.7
R1-5 h	*RCK1*	20.7	21.1	20.9	20.2
R2-5 h	*RCK1*	21.5	21.8	19.7	20.6
R3-5 h	*RCK1*	20.2	21.7	21.1	20.2
R1-0 min	*RCK1*	20.5	22.2	20.8	21.1
R2-0 min	*RCK1*	20.3	21.7	20.2	21.0
R3-0 min	*RCK1*	19.7	21.9	19.9	20.9
R1-30 min	*RCK1*	20.7	21.8	19.6	21.5
R2-30 min	*RCK1*	21.1	22.8	20.4	21.1
R3-30 min	*RCK1*	19.7	22.1	20.1	21.9
R1-1 h	*RCK1*	20.2	22.1	20.2	21.2
R2-1 h	*RCK1*	19.1	22.0	19.2	21.6
R3-1 h	*RCK1*	20.4	22.0	21.1	20.7
R1-5 h	*RCK1*	20.9	21.1	21.0	20.2
R2-5 h	*RCK1*	21.6	21.9	19.8	20.2
R3-5 h	*RCK1*	20.2	21.7	20.9	20.3
R1-0 min	*RCK1*	20.4	22.1	20.8	20.9
R2-0 min	*RCK1*	20.3	21.5	20.1	21.0
R3-0 min	*RCK1*	20.0	21.9	19.9	20.9
R1-30 min	*RCK1*	21.0	21.8	19.7	21.6
R2-30 min	*RCK1*	21.2	22.8	20.5	21.1
R3-30 min	*RCK1*	19.9	22.1	20.2	22.1
R1-1 h	*RCK1*	20.4	22.1	20.5	21.1
R2-1 h	*RCK1*	19.1	22.0	19.2	21.6
R3-1 h	*RCK1*	20.4	22.0	21.1	20.7
R1-5 h	*RCK1*	20.7	21.0	20.9	20.2
R2-5 h	*RCK1*	21.5	21.8	19.7	20.2
R3-5 h	*RCK1*	20.0	21.7	21.0	20.3

Table C.5 *CIA5* and *RCK1* qRT-PCR Cq values in Chapter 4

Biological Replicate-Time point	Gene	WT Cq	*cgld1* Cq	*cpld63-1* Cq	*cpld63-2* Cq
R1-0 min	CIA5	29.2	32.0	30.4	31.1
R2-0 min	CIA5	29.8	30.9	29.9	30.5
R3-0 min	CIA5	27.9	30.8	29.3	30.0
R1-30 min	CIA5	28.7	31.2	29.2	29.3
R2-30 min	CIA5	30.0	31.1	29.5	28.5
R3-30 min	CIA5	28.0	30.3	29.4	29.6
R1-1 h	CIA5	27.8	31.4	32.6	28.5
R2-1 h	CIA5	27.6	29.9	27.9	28.8
R3-1 h	CIA5	27.6	30.3	29.0	27.4
R1-5 h	CIA5	28.0	29.8	29.7	27.0
R2-5 h	CIA5	29.1	29.9	28.8	26.7
R3-5 h	CIA5	27.8	28.8	29.7	26.7
R1-0 min	CIA5	28.9	32.8	29.5	30.4
R2-0 min	CIA5	29.5	30.4	29.0	29.5
R3-0 min	CIA5	27.4	30.8	29.2	29.7
R1-30 min	CIA5	27.7	31.5	28.8	29.2
R2-30 min	CIA5	29.4	30.3	29.0	28.9
R3-30 min	CIA5	27.0	29.7	28.9	29.0
R1-1 h	CIA5	27.4	31.1	28.4	27.9
R2-1 h	CIA5	27.6	29.6	27.4	28.2
R3-1 h	CIA5	26.9	29.7	28.6	27.4
R1-5 h	CIA5	27.8	28.8	28.6	27.0
R2-5 h	CIA5	28.9	28.7	28.0	26.6
R3-5 h	CIA5	27.3	28.1	29.0	26.5
R1-0 min	CIA5	28.1	32.0	28.7	30.7
R2-0 min	CIA5	28.3	30.1	28.2	29.8
R3-0 min	CIA5	26.7	29.9	28.7	29.4
R1-30 min	CIA5	27.6	31.5	28.4	29.1
R2-30 min	CIA5	28.3	30.4	28.8	28.3
R3-30 min	CIA5	26.4	29.2	28.8	28.8
R1-1 h	CIA5	26.6	32.0	28.3	27.4
R2-1 h	CIA5	27.0	29.3	27.0	28.2
R3-1 h	CIA5	26.2	29.4	28.1	27.1
R1-5 h	CIA5	27.2	29.0	28.0	26.7
R2-5 h	CIA5	28.3	29.0	27.4	26.6
R3-5 h	CIA5	27.0	28.5	28.9	26.4
R1-0 min	RCK1	20.0	21.7	21.0	20.3
R2-0 min	RCK1	19.5	21.0	20.4	19.8
R3-0 min	RCK1	19.0	21.0	20.9	20.0
R1-30 min	RCK1	20.2	21.2	20.3	20.4
R2-30 min	RCK1	20.2	22.2	20.9	20.0
R3-30 min	RCK1	19.0	21.6	20.8	20.8
R1-1 h	RCK1	19.4	21.7	20.8	19.5

R2-1 h	*RCK1*	18.7	21.7	19.6	20.0
R3-1 h	*RCK1*	19.6	21.5	21.1	19.2
R1-5 h	*RCK1*	20.2	21.0	21.3	19.1
R2-5 h	*RCK1*	20.8	21.2	20.3	18.8
R3-5 h	*RCK1*	19.7	21.2	21.5	18.7
R1-0 min	*RCK1*	20.6	22.0	20.9	20.4
R2-0 min	*RCK1*	20.0	21.6	20.3	20.0
R3-0 min	*RCK1*	19.5	21.8	21.0	20.1
R1-30 min	*RCK1*	20.5	21.5	20.6	20.6
R2-30 min	*RCK1*	20.7	22.6	20.9	20.1
R3-30 min	*RCK1*	19.3	21.8	20.8	20.9
R1-1 h	*RCK1*	20.0	21.8	20.8	19.8
R2-1 h	*RCK1*	19.0	21.9	19.8	20.3
R3-1 h	*RCK1*	20.2	21.6	21.3	19.6
R1-5 h	*RCK1*	20.9	20.8	21.4	19.1
R2-5 h	*RCK1*	21.5	21.3	20.1	19.1
R3-5 h	*RCK1*	20.3	21.2	21.7	18.9
R1-0 min	*RCK1*	20.5	22.1	21.1	20.3
R2-0 min	*RCK1*	19.9	21.8	20.7	19.9
R3-0 min	*RCK1*	19.6	22.0	21.3	20.1
R1-30 min	*RCK1*	20.7	21.6	20.8	20.8
R2-30 min	*RCK1*	20.5	22.8	21.2	20.1
R3-30 min	*RCK1*	19.3	22.1	21.1	21.0
R1-1 h	*RCK1*	19.9	22.0	20.9	20.0
R2-1 h	*RCK1*	18.8	22.0	20.1	20.3
R3-1 h	*RCK1*	20.1	21.8	21.6	19.6
R1-5 h	*RCK1*	20.8	20.9	21.5	19.1
R2-5 h	*RCK1*	21.2	21.5	20.2	19.1
R3-5 h	*RCK1*	20.0	21.3	21.6	19.0

Table C.6 *CAS1* and *RCK1* qRT-PCR Cq values in Chapter 4

Biological Replicate-Time point	Gene	WT Cq	*cgld1* Cq	*cpld63-1* Cq	*cpld63-2* Cq
R1-0 min	CAS1	23.9	27.3	24.7	24.9
R2-0 min	CAS1	23.6	26.3	25.3	25.2
R3-0 min	CAS1	23.0	26.4	25.0	24.4
R1-30 min	CAS1	23.7	25.6	24.7	24.8
R2-30 min	CAS1	23.8	25.5	24.9	24.0
R3-30 min	CAS1	23.2	25.8	25.3	24.9
R1-1 h	CAS1	23.7	26.2	25.3	24.3
R2-1 h	CAS1	22.2	24.8	24.4	24.0
R3-1 h	CAS1	24.6	25.7	26.4	24.0
R1-5 h	CAS1	25.2	24.6	25.9	23.4
R2-5 h	CAS1	26.0	25.0	25.6	24.6
R3-5 h	CAS1	24.5	24.0	26.3	23.6
R1-0 min	CAS1	24.0	27.2	25.9	25.0
R2-0 min	CAS1	23.6	26.1	25.6	25.1
R3-0 min	CAS1	22.9	25.9	25.4	24.5
R1-30 min	CAS1	23.9	25.4	25.1	24.7
R2-30 min	CAS1	24.1	25.7	25.3	24.0
R3-30 min	CAS1	23.5	26.0	25.3	25.1
R1-1 h	CAS1	23.8	26.4	25.4	24.6
R2-1 h	CAS1	22.3	24.8	24.6	24.0
R3-1 h	CAS1	24.8	25.9	26.5	24.2
R1-5 h	CAS1	25.3	24.8	26.0	23.7
R2-5 h	CAS1	26.0	25.0	25.9	24.9
R3-5 h	CAS1	24.5	24.4	26.6	23.8
R1-0 min	CAS1	23.9	27.5	25.9	24.9
R2-0 min	CAS1	23.4	26.7	25.4	25.1
R3-0 min	CAS1	23.0	26.5	25.3	24.4
R1-30 min	CAS1	24.0	25.7	25.2	24.4
R2-30 min	CAS1	24.0	25.8	25.3	24.0
R3-30 min	CAS1	23.3	26.2	25.5	25.1
R1-1 h	CAS1	23.8	26.2	25.4	24.6
R2-1 h	CAS1	22.4	25.0	24.7	24.0
R3-1 h	CAS1	24.8	25.8	26.6	24.2
R1-5 h	CAS1	25.2	24.9	26.2	23.7
R2-5 h	CAS1	25.7	25.0	25.6	25.0
R3-5 h	CAS1	24.5	24.5	26.6	23.8
R1-0 min	RCK1	20.9	21.9	21.9	21.3
R2-0 min	RCK1	20.5	21.8	21.1	21.1
R3-0 min	RCK1	20.1	21.8	21.1	20.9
R1-30 min	RCK1	21.0	21.4	21.0	21.6
R2-30 min	RCK1	21.4	22.2	21.2	21.2
R3-30 min	RCK1	19.9	21.6	21.2	21.8
R1-1 h	RCK1	20.6	22.0	21.0	21.0

R2-1 h	*RCK1*	19.2	21.3	20.1	21.3
R3-1 h	*RCK1*	20.8	21.4	21.9	20.6
R1-5 h	*RCK1*	21.2	20.5	21.9	20.2
R2-5 h	*RCK1*	21.6	21.5	20.4	20.3
R3-5 h	*RCK1*	20.4	21.3	21.9	20.0
R1-0 min	*RCK1*	20.9	21.6	21.8	21.2
R2-0 min	*RCK1*	20.6	21.5	21.1	21.1
R3-0 min	*RCK1*	20.0	21.7	21.2	21.0
R1-30 min	*RCK1*	21.0	21.2	21.0	21.7
R2-30 min	*RCK1*	21.4	22.4	21.4	21.2
R3-30 min	*RCK1*	19.9	21.7	21.2	21.9
R1-1 h	*RCK1*	20.6	21.5	21.0	21.0
R2-1 h	*RCK1*	19.2	21.5	20.1	21.4
R3-1 h	*RCK1*	20.8	21.5	21.9	20.8
R1-5 h	*RCK1*	21.1	20.7	21.8	20.3
R2-5 h	*RCK1*	21.7	21.4	20.4	20.2
R3-5 h	*RCK1*	20.5	21.5	21.8	20.1
R1-0 min	*RCK1*	20.7	21.9	21.7	21.0
R2-0 min	*RCK1*	20.4	21.7	20.9	21.0
R3-0 min	*RCK1*	20.1	21.0	21.3	21.0
R1-30 min	*RCK1*	21.1	21.3	21.1	21.7
R2-30 min	*RCK1*	21.6	22.5	21.5	21.1
R3-30 min	*RCK1*	20.1	21.8	21.1	22.0
R1-1 h	*RCK1*	20.7	21.6	21.0	21.0
R2-1 h	*RCK1*	19.2	21.3	20.1	21.3
R3-1 h	*RCK1*	20.8	21.6	21.9	20.7
R1-5 h	*RCK1*	21.2	20.7	21.7	20.3
R2-5 h	*RCK1*	21.6	21.5	20.2	20.3
R3-5 h	*RCK1*	20.4	21.7	22.0	20.1

Table C.7 *CGLD1* and *RCK1* qRT-PCR Cq values in Chapter 4

Biological Replicate-Time point	Gene	WT Cq	*cgld1* Cq	*cpld63-1* Cq	*cpld63-2* Cq
R1-0 min	CGLD1	27.8	29.0	27.7	29.0
R2-0 min	CGLD1	28.1	28.1	26.5	28.9
R3-0 min	CGLD1	26.9	27.5	27.2	28.2
R1-30 min	CGLD1	25.3	28.9	27.0	25.6
R2-30 min	CGLD1	26.3	27.4	27.0	26.8
R3-30 min	CGLD1	23.4	24.8	27.3	25.9
R1-1 h	CGLD1	24.3	25.3	25.4	24.9
R2-1 h	CGLD1	24.3	27.5	26.6	25.9
R3-1 h	CGLD1	24.5	23.8	26.4	23.4
R1-5 h	CGLD1	25.9	27.0	25.6	25.1
R2-5 h	CGLD1	25.0	27.5	24.8	24.3
R3-5 h	CGLD1	23.0	27.7	26.0	25.2
R1-0 min	CGLD1	26.8	29.3	28.1	29.5
R2-0 min	CGLD1	27.2	28.4	26.4	29.1
R3-0 min	CGLD1	26.4	27.7	27.4	28.5
R1-30 min	CGLD1	24.7	29.0	26.9	25.7
R2-30 min	CGLD1	26.0	27.5	27.0	27.0
R3-30 min	CGLD1	23.0	24.7	27.1	26.0
R1-1 h	CGLD1	23.9	25.6	25.4	25.0
R2-1 h	CGLD1	24.2	27.5	26.2	26.1
R3-1 h	CGLD1	24.3	24.1	26.2	23.8
R1-5 h	CGLD1	26.0	27.1	25.7	25.2
R2-5 h	CGLD1	25.1	27.4	24.5	24.6
R3-5 h	CGLD1	23.6	27.8	25.9	25.2
R1-0 min	CGLD1	26.4	29.5	28.1	29.4
R2-0 min	CGLD1	26.9	28.3	26.5	29.2
R3-0 min	CGLD1	26.3	27.6	27.3	28.8
R1-30 min	CGLD1	24.6	29.6	26.8	26.0
R2-30 min	CGLD1	25.7	27.4	27.2	27.0
R3-30 min	CGLD1	23.0	24.7	27.1	26.2
R1-1 h	CGLD1	23.7	25.5	25.3	25.2
R2-1 h	CGLD1	24.1	27.6	26.5	26.4
R3-1 h	CGLD1	24.3	24.3	26.5	23.7
R1-5 h	CGLD1	25.9	27.0	25.4	25.6
R2-5 h	CGLD1	25.1	27.4	24.7	24.9
R3-5 h	CGLD1	23.4	28.1	26.0	25.2
R1-0 min	RCK1	20.1	22.5	21.8	22.0
R2-0 min	RCK1	20.0	21.6	20.9	21.5
R3-0 min	RCK1	20.1	21.9	21.9	21.5
R1-30 min	RCK1	20.8	22.0	21.5	21.9
R2-30 min	RCK1	20.8	22.7	21.9	22.1
R3-30 min	RCK1	19.7	22.1	21.8	22.3
R1-1 h	RCK1	20.4	22.2	21.1	21.7

R2-1 h	*RCK1*	19.3	22.0	21.2	21.5
R3-1 h	*RCK1*	20.4	22.0	22.1	21.0
R1-5 h	*RCK1*	21.9	21.2	22.0	20.9
R2-5 h	*RCK1*	21.4	21.7	20.7	20.2
R3-5 h	*RCK1*	20.6	21.6	21.8	20.8
R1-0 min	*RCK1*	20.3	21.9	21.9	22.2
R2-0 min	*RCK1*	19.9	21.5	21.1	21.7
R3-0 min	*RCK1*	20.0	21.4	22.0	21.5
R1-30 min	*RCK1*	21.0	21.3	21.7	22.4
R2-30 min	*RCK1*	21.0	22.4	21.8	22.2
R3-30 min	*RCK1*	20.3	22.0	21.9	22.5
R1-1 h	*RCK1*	20.5	21.9	21.5	22.0
R2-1 h	*RCK1*	19.3	21.9	21.2	21.5
R3-1 h	*RCK1*	20.5	22.0	22.3	21.0
R1-5 h	*RCK1*	21.8	21.0	22.0	20.8
R2-5 h	*RCK1*	21.5	21.6	20.9	20.1
R3-5 h	*RCK1*	20.8	21.2	22.0	20.8
R1-0 min	*RCK1*	20.3	21.7	22.0	22.5
R2-0 min	*RCK1*	20.0	21.3	21.1	21.7
R3-0 min	*RCK1*	20.1	21.6	22.0	21.9
R1-30 min	*RCK1*	21.0	21.3	21.9	22.6
R2-30 min	*RCK1*	20.9	22.4	22.2	22.7
R3-30 min	*RCK1*	20.0	21.8	21.8	22.6
R1-1 h	*RCK1*	20.6	21.9	21.6	22.3
R2-1 h	*RCK1*	19.6	21.8	21.5	21.9
R3-1 h	*RCK1*	20.8	21.9	22.3	21.0
R1-5 h	*RCK1*	21.8	21.0	22.2	21.1
R2-5 h	*RCK1*	21.4	21.7	21.0	20.5
R3-5 h	*RCK1*	20.6	21.4	22.3	21.1

Table C.8 *CPLD63* and *RCK1* qRT-PCR Cq values in Chapter 4

Biological Replicate-Time point	Gene	WT Cq	*cgld1* Cq	*cpld63-1* Cq	*cpld63-2* Cq
R1-0 min	CPLD63	26.1	31.3	Undetermined	32.7
R2-0 min	CPLD63	26.7	29.9	38	33.3
R3-0 min	CPLD63	25.8	29.0	Undetermined	33.3
R1-30 min	CPLD63	26.5	28.3	Undetermined	32.1
R2-30 min	CPLD63	27.1	29.1	Undetermined	31.8
R3-30 min	CPLD63	25.9	29.6	34.7	31.2
R1-1 h	CPLD63	26.3	30.8	Undetermined	31.7
R2-1 h	CPLD63	25.9	28.0	Undetermined	31.4
R3-1 h	CPLD63	26.6	30.2	Undetermined	30.9
R1-5 h	CPLD63	27.8	28.1	Undetermined	30.8
R2-5 h	CPLD63	27.4	28.3	33.7	31.3
R3-5 h	CPLD63	26.6	27.5	Undetermined	30.5
R1-0 min	CPLD63	26.5	31.4	34.6	34.1
R2-0 min	CPLD63	26.9	29.9	34.7	33.6
R3-0 min	CPLD63	25.9	29.2	35.3	32.7
R1-30 min	CPLD63	26.4	28.7	Undetermined	32.7
R2-30 min	CPLD63	27.0	29.1	Undetermined	32.0
R3-30 min	CPLD63	25.9	29.6	35.2	31.8
R1-1 h	CPLD63	26.7	30.0	Undetermined	31.5
R2-1 h	CPLD63	26.1	28.1	Undetermined	30.9
R3-1 h	CPLD63	26.7	30.8	Undetermined	30.8
R1-5 h	CPLD63	27.8	28.0	Undetermined	30.4
R2-5 h	CPLD63	27.5	28.0	33.7	30.5
R3-5 h	CPLD63	26.6	27.5	Undetermined	30.1
R1-0 min	CPLD63	26.8	31.5	34.5	33.2
R2-0 min	CPLD63	26.8	29.7	Undetermined	33.9
R3-0 min	CPLD63	25.7	29.3	Undetermined	34.3
R1-30 min	CPLD63	26.4	28.5	Undetermined	31.5
R2-30 min	CPLD63	27.0	29.2	34.6	30.6
R3-30 min	CPLD63	26.0	29.8	Undetermined	31.4
R1-1 h	CPLD63	26.3	30.3	Undetermined	31.6
R2-1 h	CPLD63	25.7	28.6	Undetermined	30.1
R3-1 h	CPLD63	26.7	30.3	Undetermined	30.8
R1-5 h	CPLD63	27.6	28.1	Undetermined	30.8
R2-5 h	CPLD63	27.4	28.0	33.9	30.6
R3-5 h	CPLD63	26.8	27.3	33.4	29.9
R1-0 min	RCK1	21.0	22.2	22.4	22.3
R2-0 min	RCK1	20.7	21.7	21.4	22.3
R3-0 min	RCK1	20.8	21.8	22.3	22.1
R1-30 min	RCK1	21.4	21.8	22.2	22.9
R2-30 min	RCK1	21.4	22.7	22.3	22.8
R3-30 min	RCK1	20.5	22.0	21.8	22.9
R1-1 h	RCK1	21.0	21.8	21.7	22.0

R2-1 h	*RCK1*	19.7	21.6	21.3	22.0
R3-1 h	*RCK1*	21.0	22.1	22.3	21.3
R1-5 h	*RCK1*	22.3	21.2	22.3	21.5
R2-5 h	*RCK1*	22.0	21.9	21.1	20.9
R3-5 h	*RCK1*	21.4	21.7	22.4	21.1
R1-0 min	*RCK1*	20.8	22.1	22.2	22.1
R2-0 min	*RCK1*	20.5	21.8	21.1	22.1
R3-0 min	*RCK1*	20.9	21.9	22.4	22.2
R1-30 min	*RCK1*	21.3	21.8	22.0	23.0
R2-30 min	*RCK1*	21.4	22.6	22.2	22.6
R3-30 min	*RCK1*	20.4	22.1	21.9	22.7
R1-1 h	*RCK1*	20.9	21.9	21.7	22.0
R2-1 h	*RCK1*	19.6	21.6	21.3	21.9
R3-1 h	*RCK1*	21.1	22.2	22.0	21.3
R1-5 h	*RCK1*	22.3	21.3	22.3	21.4
R2-5 h	*RCK1*	21.9	21.9	21.0	20.7
R3-5 h	*RCK1*	21.5	21.9	22.6	21.1
R1-0 min	*RCK1*	20.9	22.1	22.2	22.0
R2-0 min	*RCK1*	20.5	21.5	21.1	21.9
R3-0 min	*RCK1*	20.9	22.0	22.5	22.1
R1-30 min	*RCK1*	21.5	21.8	22.1	23.0
R2-30 min	*RCK1*	21.5	22.9	22.3	22.7
R3-30 min	*RCK1*	20.6	22.0	21.8	22.9
R1-1 h	*RCK1*	20.9	21.8	21.8	22.0
R2-1 h	*RCK1*	19.7	21.6	21.3	21.9
R3-1 h	*RCK1*	21.1	22.1	22.0	21.3
R1-5 h	*RCK1*	22.4	21.2	22.2	21.5
R2-5 h	*RCK1*	21.9	21.8	20.9	20.8
R3-5 h	*RCK1*	21.3	21.9	22.3	21.2

Abbreviations

3-PGA	3-phosphoglycerate
aa	Amino acid
ABA	Abscisic acid
AC	Adenylyl cyclase
AGC	Collection of PKA, PKG and PKC families
ANOVA	Analysis of variance
ATF6	Activating Transcription Factor6
ATP	Adenosine triphosphate
BAC	Bacterial artificial chromosome
BICAT	Bivalent Cation Transporter
bp	Base pair
bZIP	basic zipper
CA	Carbonic anhydrase
Ca^{2+}	Calcium ion
CAM	Crassulacean acid metabolism
CAMK	Calcium/calmodulin-dependent protein kinases
cAMP	Cyclic adenosine monophosphate
CAS	Calcium-sensing receptor
CAX5	Cation Exchanger 5
CBB	Calvin-Benson-Bassham
CCM	CO_2-concentrating mechanism
CCRE	CO_2-cAMP-Responsive Element
cDNA	Complementary DNA
CDPK13	Calcium-Dependent Protein Kinase 13
CDS	Coding sequence
CGLD1	Conserved in the Green Lineage and Diatoms 1
cGMP	Cyclic guanosine monophosphate
Ci	Inorganic carbon
CK1	Casein kinase 1
CLiP	Chlamydomonas Library Project
CMGC	Collection of CDK, MAPK, GSK3 and CLK families
CMGC	Collection of CDK, MAPK, GSK3 and CLK families
CMT1	Chloroplast manganese transporter 1
CO$_2$	Carbon dioxide
CPLD63	Conserved in Plantae and Diatoms 63
Cq	Quantification cycle
dTALE	designed TALE
EDTA	Ethylenediamine tetraacetic acid
Em	Emmision wavelength
EPYC1	Essential Pyrenoid Component 1
Ex	Excitation wavelength

G3P	Triose phosphate
GC	Guanylyl cyclase
gDNA	genomic DNA
GDP	Guanosine diphosphate
GDT1	Gcr1 Dependent Translation factor 1
GECI	Genetically encoded Ca^{2+} indicators
GTP	Guanosine triphosphate
GUS	β-glucuronidase
h	hour
H^+	Proton
HCO_2	High CO_2
HCO_3^-	Bicarbonate ions
His	Histadine
HLA3	High Light Activated 3
HSM	High salt medium
IPTG	Isopropyl β-d-1-thiogalactopyranoside
ISA1	Isoamylase1
kDa	Kilodalton
LCI1	Low CO_2 Inducible gene 1
LCIA	Low CO_2 Inducible protein A
LCIB	Low CO_2 Inducible protein B
LCIC	Low CO_2 Inducible protein C
LCO_2	Low CO_2
LCR1	Low-CO_2 stress Response 1
LIC	Ligation Independent Cloning
LSU	Rubisco large subunit
m	metre
MATE	Multidrug And Toxic compound Etrusion
min	minute
ml	millilitre
mM	Millimolar
Mn^{2+}	Manganese (II) ions
ng	Nanogram
NH_3	Ammonia
nm	nanometre
O_2	Oxygen
OD600	Optical density at 600 nm
OEC	Oxygen-evolving complex
P-glycolate	Phosphoglycolate
PAM71	Photosynthesis-Affected Mutant 71
PCR	Polymerase chain reaction
PSI	Photosystem I
PSII	Photosystem II
qRT-PCR	Quantitative reverse transcription PCR

RHC1	Resistant to High Carbon dioxide 1
RNAseq	RNA sequencing
RT-PCR	Reverse transcription PCR
Ru5P	Ribulose-5-phosphate
Rubisco	Ribulose-1,5-bisphosphate carboxylase/oxygenase
RuBP	Ribulose-1,5-bisphosphate
s	second
sAC	Soluble adenylyl cyclase
SAGA1	StArch Granules Abnormal 1
SDS-PAGE	Sodium dodecyl sulfate–polyacrylamide gel electrophoresis
SSU	Rubisco small subunit
STE	yeast Sterile 7, Sterile 11 and Sterile 20 kinases homologues
TALE	transcription activator-like element
TAP	Tris-acetate-phosphate
TBS	Tris-buffered saline
TCA	Tricarboxylic acid
TK	Tyrosine kinase
TKL	Tyrosine kinase-like
TM	Transmembrane
TMEM165	Transmembrane protein 165
TP	Tris-phosphate
Tris	2-Amino-2-hydroxymethyl-propane-1,3-diol
TRP2	Transient Receptor Potential 2
UPF0016	Uncharacterised Protein Family 0016
VLCO$_2$	Very low CO_2
WT	Wild-type
µg	microgram
µl	Microlitre
µm	micrometre
µM	Micromolar
µmol	Micromole

References

Abuaita, B. H. and Withey, J. H. (2009). Bicarbonate induces *Vibrio cholerae* virulence gene expression by enhancing ToxT activity. *Infection and Immunity*, 77 (9), pp.4111–4120. [Online]. Available at: doi:10.1128/IAI.00409-09.

Acin-Perez, R. et al. (2009a). Cyclic AMP Produced inside Mitochondria Regulates Oxidative Phosphorylation. *Cell Metabolism*, 9 (3), pp.265–276. [Online]. Available at: doi:10.1016/j.cmet.2009.01.012.

Acin-Perez, R. et al. (2009b). Modulation of mitochondrial protein phosphorylation by soluble adenylyl cyclase ameliorates cytochrome oxidase defects. *EMBO Molecular Medicine*, 1 (8–9), pp.392–406. [Online]. Available at: doi:10.1002/emmm.200900046.

Ahmar, S. et al. (2020). Conventional and molecular techniques from simple breeding to speed breeding in crop plants: Recent advances and future outlook. *International Journal of Molecular Sciences*, 21 (7), pp.1–24. [Online]. Available at: doi:10.3390/ijms21072590.

Aiyar, P. et al. (2017). Antagonistic bacteria disrupt calcium homeostasis and immobilize algal cells. *Nature Communications*, 8 (1), pp.1–12. [Online]. Available at: doi:10.1038/s41467-017-01547-8.

Alejandro, S. et al. (2020). Manganese in Plants: From Acquisition to Subcellular Allocation. *Frontiers in Plant Science*, 11, pp.1–23. [Online]. Available at: doi:10.3389/fpls.2020.00300.

Ambawat, S. et al. (2013). MYB transcription factor genes as regulators for plant responses: An overview. *Physiology and Molecular Biology of Plants*, 19 (3), pp.307–321. [Online]. Available at: doi:10.1007/s12298-013-0179-1.

Armenteros, J. J. A. et al. (2019). Detecting sequence signals in targeting peptides using deep learning. *Life Science Alliance*, 2 (5), pp.1–14. [Online]. Available at: doi:10.26508/lsa.201900429.

Aspatwar, A., Haapanen, S. and Parkkila, S. (2018). An Update on the Metabolic Roles of Carbonic Anhydrases in the Model Alga *Chlamydomonas reinhardtii*. *Metabolites*, 8 (1), p.22. [Online]. Available at: doi:10.3390/metabo8010022.

Atkinson, N. et al. (2017). Rubisco small subunits from the unicellular green alga *Chlamydomonas* complement Rubisco-deficient mutants of Arabidopsis. *New Phytologist*, 214 (2), pp.655–667. [Online]. Available at: doi:10.1111/nph.14414.

Atkinson, N. et al. (2019). The pyrenoidal linker protein EPYC1 phase separates with hybrid Arabidopsis-Chlamydomonas Rubisco through interactions with the algal Rubisco small subunit. *Journal of Experimental Botany*, 70 (19), pp.5271–5285. [Online]. Available at: doi:10.1093/jxb/erz275.

Atkinson, N. et al. (2020). Condensation of Rubisco into a proto-pyrenoid in higher plant chloroplasts. *Nature Communications*, 11, p.6303. [Online]. Available at: doi:10.1038/s41467-020-20132-0.

Badger, M. R. et al. (1998). The diversity and coevolution of Rubisco, plastids, pyrenoids, and chloroplast-based CO_2-concentrating mechanisms in algae. *Canadian Journal of Botany*, 76 (6), pp.1052–1071. [Online]. Available at: doi:10.1139/b98-074.

Badger, M. R., Kaplan, a and Berry, J. a. (1980). Internal Inorganic Carbon Pool of *Chlamydomonas reinhardtii*: EVIDENCE FOR A CARBON DIOXIDE-CONCENTRATING MECHANISM. *Plant physiology*, 66 (3), pp.407–413.

Bahn, Y. S. et al. (2005). Carbonic anhydrase and CO_2 sensing during *Cryptococcus neoformans* growth, differentiation, and virulence. *Current Biology*, 15 (22), pp.2013–2020. [Online]. Available at: doi:10.1016/j.cub.2005.09.047.

Baier, T. et al. (2020). Introns mediate post-Transcriptional enhancement of nuclear gene expression in the green microalga *Chlamydomonas reinhardtii*. *PLoS Genetics*, 16 (7), pp.1–21. [Online]. Available at: doi:10.1371/journal.pgen.1008944.

Bailey-Serres, J. et al. (2019). Genetic strategies for improving crop yields. *Nature*, 575 (7781), pp.109–118. [Online]. Available at: doi:10.1038/s41586-019-1679-0.

Benlloch, R. et al. (2015). Crystal Structure and Functional Characterization of Photosystem II-Associated Carbonic Anhydrase CAH3 in *Chlamydomonas reinhardtii*. *Plant Physiology*, 167 (3), pp.950–962. [Online]. Available at: doi:10.1104/pp.114.253591.

Benson, A. A. and Calvin, M. (1950). Carbon dioxide fixation by green plants. *Annual Review of Plant Physiology*, 1, pp.25–42. [Online]. Available at: doi:10.1021/cen-v074n046.p008.

Berman, S. A. et al. (2003). A Novel MAP Kinase Regulates Flagellar Length in *Chlamydomonas*. *Current Biology*, 13 (13), pp.1145–1149. [Online]. Available at: doi:10.1016/S0960-9822(03)00415-9.

Bickerton, P. et al. (2016). Spatial and temporal specificity of Ca^{2+} signalling in *Chlamydomonas reinhardtii* in response to osmotic stress. *New Phytologist*, 212 (4), pp.920–933. [Online]. Available at: doi:10.1111/nph.14128.

Blaby, I. K. et al. (2014). The Chlamydomonas genome project: A decade on. *Trends in Plant Science*, 19 (10), pp.672–680. [Online]. Available at: doi:10.1016/j.tplants.2014.05.008.

Blanco-Rivero, A. et al. (2012). Phosphorylation controls the localization and activation of the lumenal carbonic anhydrase in *Chlamydomonas reinhardtii*. *PloS one*, 7 (11), pp.1–10. [Online]. Available at: doi:10.1371/journal.pone.0049063.

Bongiorni, C. et al. (2008). Dual promoters control expression of the *Bacillus anthracis* virulence factor AtxA. *Journal of Bacteriology*, 190 (19), pp.6483–6492. [Online]. Available at: doi:10.1128/JB.00766-08.

Bothwell, J. H. F. et al. (2006). Biolistic delivery of Ca^{2+} dyes into plant and algal cells. *Plant Journal*, 46 (2), pp.327–335. [Online]. Available at: doi:10.1111/j.1365-313X.2006.02687.x.

Bourne, H. R., Sanders, D. A. and McCormick, F. (1990). The GTPase superfamily: A conserved switch for diverse cell functions. *Nature*, 348 (6297), pp.125–132. [Online]. Available at: doi:10.1038/348125a0.

Braun, F. J. and Hegemann, P. (1999). Direct measurement of cytosolic calcium and pH in living *Chlamydomonas reinhardtii* cells. *European Journal of Cell Biology*, 78 (3), pp.199–208. [Online]. Available at: doi:10.1016/S0171-9335(99)80099-5.

Brueggeman, A. J. et al. (2012). Activation of the Carbon Concentrating Mechanism by

CO_2 Deprivation Coincides with Massive Transcriptional Restructuring in *Chlamydomonas reinhardtii*. *The Plant Cell*, 24 (5), pp.1860–1875. [Online]. Available at: doi:10.1105/tpc.111.093435.

Buck, J. and Levin, L. R. (2011). Physiological sensing of carbon dioxide/bicarbonate/pH via cyclic nucleotide signaling. *Sensors*, 11 (2), pp.2112–2128. [Online]. Available at: doi:10.3390/s110202112.

Cann, M. J. et al. (2003). A defined subset of adenylyl cyclases is regulated by bicarbonate ion. *Journal of Biological Chemistry*, 278 (37), pp.35033–35038. [Online]. Available at: doi:10.1074/jbc.M303025200.

Caspari, O. D. et al. (2017). Pyrenoid loss in *Chlamydomonas reinhardtii* causes limitations in CO_2 supply, but not thylakoid operating efficiency. *Journal of Experimental Botany*, 68 (14), pp.3903–3913. [Online]. Available at: doi:10.1093/jxb/erx197.

De Castro, P. A. et al. (2014). The involvement of the Mid1/Cch1/Yvc1 calcium channels in *Aspergillus fumigatus* virulence. *PLoS ONE*, 9 (8). [Online]. Available at: doi:10.1371/journal.pone.0103957.

Chandrashekar, J. et al. (2009). The taste of carbonation. *Science (New York, N.Y.)*, 326 (5951), pp.443–445. [Online]. Available at: doi:10.1126/science.1174601.

Chen, B. et al. (2017). A novel activation domain is essential for CIA5-mediated gene regulation in response to CO_2 changes in *Chlamydomonas reinhardtii*. *Algal Research*, 24, pp.207–217. [Online]. Available at: doi:10.1016/j.algal.2017.03.006.

Chen, Y. et al. (2000). Soluble Adenylyl Cyclase as an Evolutionarily Conserved Bicarbonate Sensor. *Science*, 289 (5479), pp.625–628. [Online]. Available at: doi:10.1126/science.289.5479.625.

Choi, H. Il et al. (2016). Quantitative analysis of the chemotaxis of a green alga, *Chlamydomonas reinhardtii*, to bicarbonate using diffusion-based microfluidic device. *Biomicrofluidics*, 10 (1), p.014121. [Online]. Available at: doi:10.1063/1.4942756.

Christensen, R. et al. (2020). Identification and Characterization of a Transient Receptor Potential Ion Channel (TRP2) Involved in Acclimation to Low CO_2 Conditions in

Chlamydomonas reinhardtii. *Plant Molecular Biology Reporter*, 38 (3), pp.503–512. [Online]. Available at: doi:10.1007/s11105-020-01218-x.

Clapham, D. E. (2007). Calcium Signaling. *Cell*, 131 (6), pp.1047–1058. [Online]. Available at: doi:10.1016/j.cell.2007.11.028.

Colina, F. et al. (2019). Genome-wide identification and characterization of CKIN/SnRK gene family in *Chlamydomonas reinhardtii*. *Scientific Reports*, 9 (1), pp.1–16. [Online]. Available at: doi:10.1038/s41598-018-35625-8.

Colinet, A. S. et al. (2016). Yeast Gdt1 is a Golgi-localized calcium transporter required for stress-induced calcium signaling and protein glycosylation. *Scientific Reports*, 6, pp.1–11. [Online]. Available at: doi:10.1038/srep24282.

Colinet, A. S. et al. (2017). Acidic and uncharged polar residues in the consensus motifs of the yeast Ca^{2+} transporter Gdt1p are required for calcium transport. *Cellular Microbiology*, 19 (7), pp.1–12. [Online]. Available at: doi:10.1111/cmi.12729.

Costa, A., Navazio, L. and Szabo, I. (2018). The contribution of organelles to plant intracellular calcium signalling. *Journal of Experimental Botany*, 69 (17), pp.4175–4193. [Online]. Available at: doi:10.1093/jxb/ery185.

Cross, F. R. and Umen, J. G. (2015). The *Chlamydomonas* cell cycle. *Plant Journal*, 82 (3), pp.370–392. [Online]. Available at: doi:10.1111/tpj.12795.

Crozet, P. et al. (2018). Birth of a Photosynthetic Chassis: A MoClo Toolkit Enabling Synthetic Biology in the Microalga *Chlamydomonas reinhardtii*. *ACS Synthetic Biology*, 7 (9), pp.2074–2086. [Online]. Available at: doi:10.1021/acssynbio.8b00251.

Cummins, E. P. et al. (2014). Carbon dioxide-sensing in organisms and its impliactions for human disease. *Cellular and Molecular Life Sciences*, 71 (5), pp.831–845. [Online]. Available at: doi:10.1007/s00018-013-1470-6.Carbon.

Deka, R. and Tamuli, R. (2013). *Neurospora crassa ncs-1*, *mid-1* and *nca-2* double-mutant phenotypes suggest diverse interaction among three Ca^{2+}-regulating gene products. *Journal of Genetics*, 92 (3), pp.559–563. [Online]. Available at: doi:10.1007/s12041-013-0270-y.

Demaegd, D. et al. (2013). Newly characterized Golgi-localized family of proteins is involved in calcium and pH homeostasis in yeast and human cells. *Proceedings of the National Academy of Sciences of the United States of America*, 110 (17), pp.6859–6864. [Online]. Available at: doi:10.1073/pnas.1219871110.

Demaegd, D. et al. (2014). Molecular evolution of a novel family of putative calcium transporters. *PLoS ONE*, 9 (6). [Online]. Available at: doi:10.1371/journal.pone.0100851.

Demidchik, V. et al. (2018). Calcium transport across plant membranes: mechanisms and functions. *New Phytologist*, 220 (1), pp.49–69. [Online]. Available at: doi:10.1111/nph.15266.

Depège, N., Bellafiore, S. and Rochaix, J. D. (2003). Role of chloroplast protein kinase Stt7 in LHCII phosphorylation and state transition in *Chlamydomonas*. *Science*, 299 (5612), pp.1572–1575. [Online]. Available at: doi:10.1126/science.1081397.

Du, H. et al. (2012). The transcription factor Flo8 mediates CO_2 sensing in the human fungal pathogen *Candida albicans*. *Molecular Biology of the Cell*, 23 (14), pp.2692–2701. [Online]. Available at: doi:10.1091/mbc.E12-02-0094.

Duanmu, D., Wang, Y. and Spalding, M. H. (2009). Thylakoid Lumen Carbonic Anhydrase (*CAH3*) Mutation Suppresses Air-Dier Phenotype of *LCIB* Mutant in *Chlamydomonas reinhardtii*. *Plant Physiology*, 149 (2), pp.929–937. [Online]. Available at: doi:10.1104/pp.108.132456.

Duda, T. et al. (2015). Bicarbonate modulates photoreceptor guanylate cyclase (ROS-GC) catalytic activity. *Journal of Biological Chemistry*, 290 (17), pp.11052–11060. [Online]. Available at: doi:10.1074/jbc.M115.650408.

Duda, T., Pertzev, A. and Sharma, R. K. (2018). CO_2/bicarbonate modulates cone photoreceptor ROS-GC1 and restores its CORD6-linked catalytic activity. *Molecular and Cellular Biochemistry*, 448 (1–2), pp.91–105. [Online]. Available at: doi:10.1007/s11010-018-3317-9.

Dulary, E. et al. (2018). Investigating the function of Gdt1p in yeast Golgi glycosylation. *Biochimica et Biophysica Acta - General Subjects*, 1862 (3), pp.394–402. [Online]. Available at: doi:10.1016/j.bbagen.2017.11.006.

Eisenhut, M. et al. (2018). The Plastid Envelope CHLOROPLAST MANGANESE TRANSPORTER1 Is Essential for Manganese Homeostasis in *Arabidopsis*. *Molecular Plant*, 11 (7), pp.955–969. [Online]. Available at: doi:10.1016/j.molp.2018.04.008.

Emrich-Mills, T. Z. et al. (2021). A recombineering pipeline to clone large and complex genes in Chlamydomonas. *The Plant Cell*, 33 (4), pp.1161–1181. [Online]. Available at: doi:10.1093/plcell/koab024.

Engel, B. D. et al. (2015). Native architecture of the *Chlamydomonas* chloroplast revealed by in situ cryo-electron tomography. *eLife*, 2015 (4), pp.1–29. [Online]. Available at: doi:10.7554/eLife.04889.

Engineer, C. et al. (2016). CO_2 sensing and CO_2 regulation of stomatal conductance: advances and open questions. *Trends in Plant Science*, 21 (1), pp.16–30. [Online]. Available at: doi:10.1016/j.tplants.2015.08.014.CO.

Esposito, G. et al. (2004). Mice deficient for soluble adenylyl cyclase are infertile because of a severe sperm-motility defect. *Proceedings of the National Academy of Sciences*, 101 (9), pp.2993–2998. [Online]. Available at: doi:10.1073/pnas.0400050101.

Everaert, C. et al. (2017). Benchmarking of RNA-sequencing analysis workflows using whole-transcriptome RT-qPCR expression data. *Scientific Reports*, 7 (1), pp.1–11. [Online]. Available at: doi:10.1038/s41598-017-01617-3.

Fang, H. M. and Wang, Y. (2006). RA domain-mediated interaction of Cdc35 with Ras1 is essential for increasing cellular cAMP level for *Candida albicans* hyphal development. *Molecular Microbiology*, 61 (2), pp.484–496. [Online]. Available at: doi:10.1111/j.1365-2958.2006.05248.x.

Fang, W. et al. (2012). Transcriptome-Wide Changes in *Chlamydomonas reinhardtii* Gene Expression Regulated by Carbon Dioxide and the CO_2-Concentrating Mechanism Regulator *CIA5/CCM1*. *The Plant Cell*, 24 (5), pp.1876–1893. [Online]. Available at: doi:10.1105/tpc.112.097949.

Farah, J. et al. (1995). Isolation of a *psaF*-deficient mutant of *Chlamydomonas reinhardtii*: Efficient interaction of plastscyanin with the photosystem I reaction center is mediated by the PsaF subunit. *EMBO Journal*, 14 (20), pp.4976–4984. [Online]. Available at:

doi:10.1002/j.1460-2075.1995.tb00180.x.

Fauser, F. et al. (2022). Systematic characterization of gene function in the photosynthetic alga *Chlamydomonas reinhardtii*. *Nature Genetics*, 54 (5), pp.705–714. [Online]. Available at: doi:10.1038/s41588-022-01052-9.

Fei, C. et al. (2021). Diffusion barriers and adaptive carbon uptake strategies enhance the modeled performance of the algal CO_2-concentrating mechanism. *bioRxiv*, p.2021.03.04.433933. [Online]. Available at: https://www.biorxiv.org/content/10.1101/2021.03.04.433933v1%0Ahttps://www.biorxiv.org/content/10.1101/2021.03.04.433933v1.abstract.

Fischer, N. and Rochaix, J.-D. (2001). The flanking regions of *PsaD* drive efficient gene expression in the nucleus of the green alga *Chlamydomonas reinhardtii*. *Mol Genet Genomics*, 265 (5), pp.888–894. [Online]. Available at: doi:10.1007/s004380100485.

Fischer, T., Byerlee, D. and Edmeades, G. (2014). *Crop yields and global food security: will yield increase continue to feed the world?*

Fisher, C. R. et al. (2016). Identification and characterization of a putative manganese export protein in *Vibrio cholerae*. *Journal of Bacteriology*, 198 (20), pp.2810–2817. [Online]. Available at: doi:10.1128/JB.00215-16.

Fort, C. et al. (2021). Ca^{2+} elevations disrupt interactions between intraflagellar transport and the flagella membrane in *Chlamydomonas*. *Journal of Cell Science*, 134 (3), pp.1–15. [Online]. Available at: doi:10.1242/jcs.253492.

Frank, J. et al. (2019). Chloroplast-localized BICAT proteins shape stromal calcium signals and are required for efficient photosynthesis. *New Phytologist*, 221 (2), pp.866–880. [Online]. Available at: doi:10.1111/nph.15407.

Franzén, L. G. et al. (1989). Isolation and characterization of cDNA clones encoding the 17.9 and 8.1 kDa subunits of Photosystem I from *Chlamydomonas reinhardtii*. *Plant Molecular Biology*, 12 (4), pp.463–474. [Online]. Available at: doi:10.1007/BF00017585.

Freeman Rosenzweig, E. S. et al. (2017). The Eukaryotic CO_2-Concentrating Organelle Is Liquid-like and Exhibits Dynamic Reorganization. *Cell*, 171 (1), pp.148-162.e19. [Online].

Available at: doi:10.1016/j.cell.2017.08.008.

Fukuzawa, H. et al. (2001). *Ccm1*, a regulatory gene controlling the induction of a carbon-concentrating mechanism in *Chlamydomonas reinhardtii* by sensing CO_2 availability. *Proceedings of the National Academy of Sciences, USA*, 98 (9), pp.5347–5352. [Online]. Available at: doi:10.1073/pnas.081593498.

Funke, R. P., Kovar, J. L. and Weeks, D. P. (1997). Intracellular carbonic anhydrase is essential to photosynthesis in *Chlamydomonas reinhardtii* at atmospheric levels of CO_2: Demonstration via genomic complementation of the high-CO_2-Requiring mutant *ca-1*. *Plant Physiology*, 114 (1), pp.237–244. [Online]. Available at: doi:10.1104/pp.114.1.237.

Gao, H. et al. (2015). Expression activation and functional analysis of HLA3, a putative inorganic carbon transporter in *Chlamydomonas reinhardtii*. *Plant Journal*, 82 (1), pp.1–11. [Online]. Available at: doi:10.1111/tpj.12788.

Genkov, T. et al. (2010). Functional hybrid rubisco enzymes with plant small subunits and algal large subunits: engineered rbcS cDNA for expression in Chlamydomonas. *Journal of Biological Chemistry*, 285 (26), pp.19833–19841. [Online]. Available at: doi:10.1074/jbc.M110.124230.

Gokhale, A., Wirschell, M. and Sale, W. S. (2009). Regulation of dynein-driven microtubule sliding by the axonemal protein kinase CK1 in *Chlamydomonas* flagella. *Journal of Cell Biology*, 186 (6), pp.817–824. [Online]. Available at: doi:10.1083/jcb.200906168.

Gunning, B. E. S. and Schwartz, O. M. (1999). Confocal microscopy of thylakoid autofluorescence in relation to origin of grana and phylogeny in the green algae. *Functional Plant Biology*, 26 (7), p.695. [Online]. Available at: doi:10.1071/PP99076.

Gutz, I. G. R. (2012). *CurTiPot – pH and Acid–Base Titration Curves: Analysis and Simulation freeware, version 4.3.1*. [Online]. Available at: http://www.iq.usp.br/gutz/Curtipot_.html.

Hall, R. A. et al. (2010). CO_2 acts as a signalling molecule in populations of the fungal pathogen *Candida albicans*. *PLoS Pathogens*, 6 (11), p.e1001193. [Online]. Available at: doi:10.1371/journal.ppat.1001193.

Hallem, E. A. et al. (2011). Receptor-type guanylate cyclase is required for carbon dioxide sensation by *Caenorhabditis elegans*. *Proceedings of the National Academy of Sciences*, 108 (1), pp.254–259. [Online]. Available at: doi:10.1073/pnas.1017354108/-/DCSupplemental.www.pnas.org/cgi/doi/10.1073/pnas.1017354108.

Hamel, L.-P., Sheen, J. and Séguin, A. (2014). Ancient signals: comparative genomics of green plant CDPKs. *Trends in Plant Science*, 19 (2), pp.79–89. [Online]. Available at: doi:10.1016/j.tplants.2013.10.009.

Hammer, A., Hodgson, D. R. W. and Cann, M. J. (2006). Regulation of prokaryotic adenylyl cyclases by CO_2. *Biochemical Journal*, 396 (2), pp.215–218. [Online]. Available at: doi:10.1042/BJ20060372.

Harada, H. et al. (2006). CO_2 Sensing at Ocean Surface Mediated by cAMP in a Marine Diatom. *Plant Physiology*, 142 (3), pp.1318–1328. [Online]. Available at: doi:10.1104/pp.106.086561.

Harris, E. H. (2001). *Chlamydomonas* as a model organism. *Annu. Rev. Plant Physiol. Plant Mol. Biol*, 52 (1), pp.363–406. [Online]. Available at: doi:10.1146/annurev.arplant.52.1.363.

He, J. et al. (2021). Transport, functions, and interaction of calcium and manganese in plant organellar compartments. *Plant Physiology*, 187 (4), pp.1940–1972. [Online]. Available at: doi:10.1093/plphys/kiab122.

He, S. et al. (2020). The structural basis of Rubisco phase separation in the pyrenoid. *Nature Plants*, 6 (12), pp.1480–1490. [Online]. Available at: doi:10.1038/s41477-020-00811-y.

Heinnickel, M. L. and Grossman, A. R. (2013). The GreenCut: Re-evaluation of physiological role of previously studied proteins and potential novel protein functions. *Photosynthesis Research*, 116 (2–3), pp.427–436. [Online]. Available at: doi:10.1007/s11120-013-9882-6.

Heitzer, M. and Zschoernig, B. (2007). Construction of modular tandem expression vectors for the green alga *Chlamydomonas reinhardtii* using the Cre/lox-system. *BioTechniques*, 43 (3), pp.324–332. [Online]. Available at: doi:10.2144/000112556.

Herruzo, E. et al. (2021). Pch2 orchestrates the meiotic recombination checkpoint from the cytoplasm. Lichten, M. (Ed). *PLOS Genetics*, 17 (7), p.e1009560. [Online]. Available at: doi:10.1371/journal.pgen.1009560.

Hess, K. C. et al. (2005). The "Soluble" Adenylyl Cyclase in Sperm Mediates Multiple Signaling Events Required for Fertilization. *Developmental Cell*, 9 (2), pp.249–259. [Online]. Available at: doi:10.1016/j.devcel.2005.06.007.The.

Hoecker, N. et al. (2021). Gene Replacement in Arabidopsis Reveals Manganese Transport as an Ancient Feature of Human, Plant and Cyanobacterial UPF0016 Proteins. *Frontiers in Plant Science*, 12 (June), pp.1–15. [Online]. Available at: doi:10.3389/fpls.2021.697848.

Hörtenhuber, M. et al. (2017). Mapping genes for calcium signaling and their associated human genetic disorders. *Bioinformatics*, 33 (16), pp.2547–2554. [Online]. Available at: doi:10.1093/bioinformatics/btx225.

Hu, H. et al. (2010). Carbonic anhydrases are upstream regulators of CO_2-controlled stomatal movements in guard cells. *Nature Cell Biology*, 12 (1), pp.87–93. [Online]. Available at: doi:10.1038/ncb2009.

Hu, H. et al. (2015). Distinct Cellular Locations of Carbonic Anhydrases Mediate Carbon Dioxide Control of Stomatal Movements. *Plant Physiology*, 169 (2), pp.1168–1178. [Online]. Available at: doi:10.1104/pp.15.00646.

Hubbard, K. E. et al. (2012). Abscisic acid and CO_2 signalling via calcium sensitivity priming in guard cells, new CDPK mutant phenotypes and a method for improved resolution of stomatal stimulus-response analyses. *Annals of Botany*, 109 (1), pp.5–17. [Online]. Available at: doi:10.1093/aob/mcr252.

Ichikawa, T. et al. (2022). Chemical fixation creates nanoscale clusters on the cell surface by aggregating membrane proteins. *Communications Biology*, 5 (1), pp.1–9. [Online]. Available at: doi:10.1038/s42003-022-03437-2.

Itakura, A. K. et al. (2019). A Rubisco-binding protein is required for normal pyrenoid number and starch sheath morphology in *Chlamydomonas reinhardtii*. *Proceedings of the National Academy of Sciences of the United States of America*, 116 (37), pp.18445–

18454. [Online]. Available at: doi:10.1073/pnas.1904587116.

Jaiswal, B. S. and Conti, M. (2003). Calcium regulation of the soluble adenylyl cyclase expressed in mammalian spermatozoa. *Proceedings of the National Academy of Sciences*, 100 (19), pp.10676–10681. [Online]. Available at: doi:10.1073/pnas.1831008100.

Jiang, L. et al. (2018). The plasma membrane protein Rch1 and the Golgi/ER calcium pump Pmr1 have an additive effect on filamentation in *Candida albicans*. *Fungal Genetics and Biology*, 115, pp.1–8. [Online]. Available at: doi:10.1016/j.fgb.2018.04.001.

Jin, S. et al. (2016). Structural insights into the LCIB protein family reveals a new group of β-carbonic anhydrases. *Proceedings of the National Academy of Sciences*, 113 (51), pp.14716–14721. [Online]. Available at: doi:10.1073/pnas.1616294113.

Karlsson, J. et al. (1998). A novel α-type carbonic anhydrase associated with the thylakoid membrane in *Chlamydomonas reinhardtii* is required for growth at ambient CO_2. *EMBO Journal*, 17 (5), pp.1208–1216. [Online]. Available at: doi:10.1093/emboj/17.5.1208.

Kearse, M. et al. (2012). Geneious Basic: An integrated and extendable desktop software platform for the organization and analysis of sequence data. *Bioinformatics*, 28 (12), pp.1647–1649. [Online]. Available at: doi:10.1093/bioinformatics/bts199.

Kelley, L. A. et al. (2015). The Phyre2 web portal for protein modeling, prediction and analysis. *Nature Protocols*, 10 (6), pp.845–858. [Online]. Available at: doi:10.1038/nprot.2015.053.

Khan, M. I., Shin, J. H. and Kim, J. D. (2018). The promising future of microalgae: Current status, challenges, and optimization of a sustainable and renewable industry for biofuels, feed, and other products. *Microbial Cell Factories*, 17 (1), pp.1–21. [Online]. Available at: doi:10.1186/s12934-018-0879-x.

Kim, H. S. et al. (2015). Roles of three *Fusarium oxysporum* calcium ion (Ca^{2+}) channels in generating Ca^{2+} signatures and controlling growth. *Fungal Genetics and Biology*, 82, pp.145–157. [Online]. Available at: doi:10.1016/j.fgb.2015.07.003.

Klengel, T. et al. (2005). Fungal adenylyl cyclase integrates CO_2 sensing with cAMP signaling and virulence. *Current Biology*, 15 (22), pp.2021–2026. [Online]. Available at:

doi:10.1016/j.cub.2005.10.040.

Kono, A. et al. (2020). Structure and function of LCI1: a plasma membrane CO_2 channel in the *Chlamydomonas* CO_2 concentrating mechanism. *The Plant Journal*, 102 (6), pp.1107–1126. [Online]. Available at: doi:10.1111/tpj.14745.

Kouranov, A. et al. (1998). Tic20 and Tic22 are new components of the protein import apparatus at the chloroplast inner envelope membrane. *Journal of Cell Biology*, 143 (4), pp.991–1002. [Online]. Available at: doi:10.1083/jcb.143.4.991.

Kropat, J. et al. (2011). A revised mineral nutrient supplement increases biomass and growth rate in *Chlamydomonas reinhardtii*. *Plant Journal*, 66 (5), pp.770–780. [Online]. Available at: doi:10.1111/j.1365-313X.2011.04537.x.

Kuchitsu, K., Tsuzuki, M. and Miyachi, S. (1988). Changes of starch localization within the chloroplast induced by changes in CO_2 concentration during growth of *Chlamydomonas reinhardtii*: Independent regulation of pyrenoid starch and stroma starch. *Plant and Cell Physiology*, 29 (8), pp.1269–1278. [Online]. Available at: doi:10.1093/oxfordjournals.pcp.a077635.

Kudla, J. et al. (2018). Advances and current challenges in calcium signaling. *New Phytologist*, 218 (2), pp.414–431. [Online]. Available at: doi:10.1111/nph.14966.

Kumar, S. et al. (2018). MEGA X: Molecular evolutionary genetics analysis across computing platforms. *Molecular Biology and Evolution*, 35 (6), pp.1547–1549. [Online]. Available at: doi:10.1093/molbev/msy096.

Lange, M. and Peiter, E. (2020). Calcium Transport Proteins in Fungi: The Phylogenetic Diversity of Their Relevance for Growth, Virulence, and Stress Resistance. *Frontiers in Microbiology*, 10, p.3100. [Online]. Available at: doi:10.3389/fmicb.2019.03100.

Lauersen, K. J., Kruse, O. and Mussgnug, J. H. (2015). Targeted expression of nuclear transgenes in *Chlamydomonas reinhardtii* with a versatile, modular vector toolkit. *Applied Microbiology and Biotechnology*, 99 (8), pp.3491–3503. [Online]. Available at: doi:10.1007/s00253-014-6354-7.

Lehti-Shiu, M. D. and Shiu, S.-H. (2012). Diversity, classification and function of the plant

protein kinase superfamily. *Philosophical Transactions of the Royal Society B: Biological Sciences*, 367 (1602), pp.2619–2639. [Online]. Available at: doi:10.1098/rstb.2012.0003.

Lemeille, S. et al. (2010). Stt7-dependent phosphorylation during state transitions in the green alga *Chlamydomonas reinhardtii*. *Molecular and Cellular Proteomics*, 9 (6), pp.1281–1295. [Online]. Available at: doi:10.1074/mcp.M000020-MCP201.

Letunic, I. and Bork, P. (2019). Interactive Tree Of Life (iTOL) v4: recent updates and new developments. *Nucleic acids research*, 47 (W1), pp.W256–W259. [Online]. Available at: doi:10.1093/nar/gkz239.

Li, L., Stefan, M. I. and Le Novère, N. (2012). Calcium Input Frequency, Duration and Amplitude Differentially Modulate the Relative Activation of Calcineurin and CaMKII. Feng, Z.-P. (Ed). *PLoS ONE*, 7 (9), p.e43810. [Online]. Available at: doi:10.1371/journal.pone.0043810.

Li, M. W. et al. (2015). Paraformaldehyde fixation may lead to misinterpretation of the subcellular localization of plant high mobility group box proteins. *PLoS ONE*, 10 (8). [Online]. Available at: doi:10.1371/journal.pone.0135033.

Li, X. et al. (2016). An Indexed, Mapped Mutant Library Enables Reverse Genetics Studies of Biological Processes in *Chlamydomonas reinhardtii*. *The Plant Cell*, 28 (2), pp.367–387. [Online]. Available at: doi:10.1105/tpc.15.00465.

Li, X. et al. (2018). A genome-wide algal mutant library reveals a global view of genes required for eukaryotic photosynthesis. *bioRxiv*, pp.1–64. [Online]. Available at: doi:10.1101/464859.

Li, X. et al. (2019a). A genome-wide algal mutant library and functional screen identifies genes required for eukaryotic photosynthesis. *Nature Genetics*, 51 (4), pp.627–635. [Online]. Available at: doi:10.1038/s41588-019-0370-6.

Li, Y. et al. (2019b). Genome-Wide Identification of Calcium-Dependent Protein Kinases in *Chlamydomonas reinhardtii* and Functional Analyses in Nitrogen Deficiency-Induced Oil Accumulation. *Frontiers in Plant Science*, 10, p.1147. [Online]. Available at: doi:10.3389/fpls.2019.01147.

Liu, D. et al. (2018). Perspectives on the basic and applied aspects of crassulacean acid metabolism (CAM) research. *Plant Science*, 274 (June), pp.394–401. [Online]. Available at: doi:10.1016/j.plantsci.2018.06.012.

Long, B. M. et al. (2016). Cyanobacterial CO_2-concentrating mechanism components: Function and prospects for plant metabolic engineering. *Current Opinion in Plant Biology*, 31, pp.1–8. [Online]. Available at: doi:10.1016/j.pbi.2016.03.002.

Long, S. P. et al. (2006). Can improvement in photosynthesis increase crop yields? *Plant, Cell and Environment*, 29 (3), pp.315–330. [Online]. Available at: doi:10.1111/j.1365-3040.2005.01493.x.

Long, S. P., Marshall-Colon, A. and Zhu, X. G. (2015). Meeting the global food demand of the future by engineering crop photosynthesis and yield potential. *Cell*, 161 (1), pp.56–66. [Online]. Available at: doi:10.1016/j.cell.2015.03.019.

Lotlikar, S. R. et al. (2013). Three functional β-carbonic anhydrases in *Pseudomonas aeruginosa* PAO1: Role in survival in ambient air. *Microbiology (United Kingdom)*, 159 (8), pp.1748–1759. [Online]. Available at: doi:10.1099/mic.0.066357-0.

Ma, Y. et al. (2011). Identification of a Novel Gene, *CIA6*, Required for Normal Pyrenoid Formation in *Chlamydomonas reinhardtii*. *Plant Physiology*, 156 (2), pp.884–896. [Online]. Available at: doi:10.1104/pp.111.173922.

Machettira, A. B. et al. (2011). The localization of Tic20 proteins in *Arabidopsis thaliana* is not restricted to the inner envelope membrane of chloroplasts. *Plant Molecular Biology*, 77 (4–5), pp.381–390. [Online]. Available at: doi:10.1007/s11103-011-9818-5.

Mackinder, L. C. M. et al. (2016). A repeat protein links Rubisco to form the eukaryotic carbon-concentrating organelle. *Proceedings of the National Academy of Sciences*, 113 (21), pp.5958–5963. [Online]. Available at: doi:10.1073/pnas.1522866113.

Mackinder, L. C. M. et al. (2017). A Spatial Interactome Reveals the Protein Organization of the Algal CO_2-Concentrating Mechanism. *Cell*, 171 (1), pp.133-147.e14. [Online]. Available at: doi:10.1016/j.cell.2017.08.044.

Mackinder, L. C. M. (2018). The *Chlamydomonas* CO_2-concentrating mechanism and its

potential for engineering photosynthesis in plants. *New Phytologist*, 217 (1), pp.54–61. [Online]. Available at: doi:10.1111/nph.14749.

Manning, G. et al. (2002). The protein kinase complement of the human genome. *Science*, 298 (5600), pp.1912–1934. [Online]. Available at: doi:10.1126/science.1075762.

Marcus, Y. et al. (1986). Adaptation to CO_2 Level and Changes in the Phosphorylation of Thylakoid Proteins during the Cell Cycle of *Chlamydomonas reinhardtii*. *Plant physiology*, 80 (2), pp.604–607. [Online]. Available at: doi:Doi 10.1104/Pp.80.2.604.

Markelova, A. G. et al. (2009). Distribution and functional role of carbonic anhydrase Cah3 associated with thylakoid membranes in the chloroplast and pyrenoid of *Chlamydomonas reinhardtii*. *Russian Journal of Plant Physiology*, 56 (6), pp.761–768. [Online]. Available at: doi:10.1134/S1021443709060053.

McGrath, J. M. and Long, S. P. (2014). Can the Cyanobacterial Carbon-Concentrating Mechanism Increase Photosynthesis in Crop Species? A Theoretical Analysis. *Plant Physiology*, 164 (4), pp.2247–2261. [Online]. Available at: doi:10.1104/pp.113.232611.

Merchant, S. S. et al. (2007). The *Chlamydomonas* genome reveals the evolution of key animal and plant functions. *Science*, 318 (5848), pp.245–251. [Online]. Available at: doi:10.1126/science.1143609.

Meyer, M. T. et al. (2012). Rubisco small-subunit α-helices control pyrenoid formation in *Chlamydomonas*. *Proc Natl Acad Sci U S A*, 109 (47), pp.19474–19479. [Online]. Available at: doi:10.1073/pnas.1210993109/-/DCSupplemental.www.pnas.org/cgi/doi/10.1073/pnas.1210993109.

Mirdita, M. et al. (2022). ColabFold: making protein folding accessible to all. *Nature Methods*, 19 (June). [Online]. Available at: doi:10.1038/s41592-022-01488-1.

Mitchell, M. C. et al. (2017). Pyrenoid loss impairs carbon-concentrating mechanism induction and alters primary metabolism in *Chlamydomonas reinhardtii*. *Journal of Experimental Botany*, 68 (14), pp.3891–3902. [Online]. Available at: doi:10.1093/jxb/erx121.

Mitchell, M. C., Meyer, M. T. and Griffiths, H. (2014). Dynamics of Carbon-Concentrating

Mechanism Induction and Protein Relocalization during the Dark-to-Light Transition in Synchronized *Chlamydomonas reinhardtii*. *Plant Physiology*, 166 (2), pp.1073–1082. [Online]. Available at: doi:10.1104/pp.114.246918.

Mitra, M. et al. (2004). Identification of a New Chloroplast Carbonic Anhydrase in *Chlamydomonas reinhardtii*. *Plant Physiology*, 135 (1), pp.173–182. [Online]. Available at: doi:10.1104/pp.103.037283.

Miura, K. et al. (2004). Expression Profiling-Based Identification of CO_2-Responsive Genes Regulated by CCM1 Controlling a Carbon-Concentrating Mechanism in *Chlamydomonas reinhardtii*. *Plant Physiology*, 135 (3), pp.1595–1607. [Online]. Available at: doi:10.1104/pp.104.041400.

Mogensen, E. G. et al. (2006). *Cryptococcus neoformans* senses CO_2 through the carbonic anhydrase Can2 and the adenylyl cyclase Cac1. *Eukaryotic Cell*, 5 (1), pp.103–111. [Online]. Available at: doi:10.1128/EC.5.1.103-111.2006.

Mori, I. C. et al. (2006). CDPKs CPK6 and CPK3 function in ABA regulation of guard cell S-type anion- and Ca^{2+}- permeable channels and stomatal closure. *PLoS Biology*, 4 (10), pp.1749–1762. [Online]. Available at: doi:10.1371/journal.pbio.0040327.

Moroney, J. V. et al. (1989). Isolation and Characterization of a Mutant of *Chlamydomonas reinhardtii* Deficient in the CO_2 Concentrating Mechanism. *Plant Physiology*, 89 (3), pp.897–903. [Online]. Available at: doi:10.1104/pp.89.3.897.

Moroney, J. V. et al. (2011). The carbonic anhydrase isoforms of *Chlamydomonas reinhardtii*: Intracellular location, expression, and physiological roles. *Photosynthesis Research*, 109 (1–3), pp.133–149. [Online]. Available at: doi:10.1007/s11120-011-9635-3.

Moroney, J. V., Tolbert, N. E. and Sears, B. B. (1986). Complementation analysis of the inorganic carbon concentrating mechanism of *Chlamydomonas reinhardtii*. *MGG Molecular & General Genetics*, 204 (2), pp.199–203. [Online]. Available at: doi:10.1007/BF00425498.

Mukherjee, A. et al. (2019). Thylakoid localized bestrophin-like proteins are essential for the CO_2 concentrating mechanism of *Chlamydomonas reinhardtii*. *Proceedings of the*

National Academy of Sciences, 116 (34), pp.16915–16920. [Online]. Available at: doi:10.1073/pnas.1909706116.

Navazio, L. et al. (2020). Chloroplast Calcium Signaling in the Spotlight. *Frontiers in Plant Science*, 11, p.186. [Online]. Available at: doi:10.3389/fpls.2020.00186.

NCBI Resource Coordinators. (2016). Database resources of the National Center for Biotechnology Information. *Nucleic Acids Research*, 44 (D1), pp.D7–D19. [Online]. Available at: doi:10.1093/nar/gkx1095.

Ohnishi, N. et al. (2010). Expression of a low CO_2-inducible protein, LCI1, increases inorganic carbon uptake in the green alga *Chlamydomonas reinhardtii*. *The Plant Cell*, 22 (9), pp.3105–3117. [Online]. Available at: doi:10.1105/tpc.109.071811.

Ohno, N. et al. (2012). CO_2-cAMP-Responsive cis-Elements Targeted by a Transcription Factor with CREB/ATF-Like Basic Zipper Domain in the Marine Diatom *Phaeodactylum tricornutum*. *Plant Physiology*, 158 (1), pp.499–513. [Online]. Available at: doi:10.1104/pp.111.190249.

Ottolini, D., Calì, T. and Brini, M. (2014). Methods to measure intracellular Ca^{2+} fluxes with organelle-targeted aequorin-based probes. *Methods in Enzymology*, 543, pp.21–45. [Online]. Available at: doi:10.1016/B978-0-12-801329-8.00002-7.

Park, J. J. et al. (2015). The response of *Chlamydomonas reinhardtii* to nitrogen deprivation: A systems biology analysis. *Plant Journal*, 81 (4), pp.611–624. [Online]. Available at: doi:10.1111/tpj.12747.

Passalacqua, K. D. et al. (2009). Comparative transcriptional profiling of *Bacillus cereus* sensu lato strains during growth in CO_2-bicarbonate and aerobic atmospheres. *PLoS ONE*, 4 (3), p.e4904. [Online]. Available at: doi:10.1371/journal.pone.0004904.

Pchitskaya, E., Popugaeva, E. and Bezprozvanny, I. (2018). Calcium signaling and molecular mechanisms underlying neurodegenerative diseases. *Cell Calcium*, 70 (1), pp.87–94. [Online]. Available at: doi:10.1016/j.ceca.2017.06.008.

Pedersen, O., Colmer, T. D. and Sand-Jensen, K. (2013). Underwater Photosynthesis of Submerged Plants – Recent Advances and Methods. *Frontiers in Plant Science*, 4, p.140.

[Online]. Available at: doi:10.3389/fpls.2013.00140.

Pesaresi, P. et al. (2009). *Arabidopsis* STN7 Kinase Provides a Link between Short- and Long-Term Photosynthetic Acclimation. *The Plant Cell*, 21 (8), pp.2402–2423. [Online]. Available at: doi:10.1105/tpc.108.064964.

Petroutsos, D. et al. (2011). The chloroplast calcium sensor CAS is required for photoacclimation in *Chlamydomonas reinhardtii*. *Plant Cell*, 23 (8), pp.2950–2963. [Online]. Available at: doi:10.1105/tpc.111.087973.

Pfaffl, M. W. (2006). Relative quantification. In: Dorak, M. T. (Ed). *Real-time PCR*. pp.63–82.

Pirayesh, N. et al. (2021). Organellar calcium signaling in plants: An update. *Biochimica et Biophysica Acta (BBA) - Molecular Cell Research*, 1868 (4), p.118948. [Online]. Available at: doi:10.1016/j.bbamcr.2021.118948.

Pittman, J. K. et al. (2009). A cation-regulated and proton gradient-dependent cation transporter from *Chlamydomonas reinhardtii* has a role in calcium and sodium homeostasis. *Journal of Biological Chemistry*, 284 (1), pp.525–533. [Online]. Available at: doi:10.1074/jbc.M807173200.

Pivato, M. and Ballottari, M. (2021). *Chlamydomonas reinhardtii* cellular compartments and their contribution to intracellular calcium signalling. *Journal of Experimental Botany*, 72 (15), pp.5312–5335. [Online]. Available at: doi:10.1093/jxb/erab212.

Pohlers, S. et al. (2017). Lipid Signaling via Pkh1/2 Regulates Fungal CO_2 Sensing through the Kinase Sch9. *mBio*, 8 (1), pp.e02211-16.

Pollock, S. V. et al. (2005). Insights into the acclimation of *Chlamydomonas reinhardtii* to sulfur deprivation. *Photosynthesis Research*, 86 (3), pp.475–489. [Online]. Available at: doi:10.1007/s11120-005-4048-9.

Porra, R. J., Thompson, W. A. and Kriedemann, P. E. (1989). Determination of accurate extinction coefficients and simultaneous equations for assaying chlorophylls a and b extracted with four different solvents: verification of the concentration of chlorophyll standards by atomic absorption spectroscopy. *Biochimica et Biophysica Acta (BBA) -*

Bioenergetics, 975 (3), pp.384–394. [Online]. Available at: doi:10.1016/S0005-2728(89)80347-0.

Potelle, S. et al. (2016). Glycosylation abnormalities in Gdt1p/TMEM165 deficient cells result from a defect in Golgi manganese homeostasis. *Human Molecular Genetics*, 25 (8), pp.1489–1500. [Online]. Available at: doi:10.1093/hmg/ddw026.

Rae, B. D. et al. (2017). Progress and challenges of engineering a biophysical CO_2-concentrating mechanism into higher plants. *Journal of experimental botany*, 68 (14), pp.3717–3737. [Online]. Available at: doi:10.1093/jxb/erx133.

Ramazanov, Z. et al. (1994). The induction of the CO_2-concentrating mechanism is correlated with the formation of the starch sheath around the pyrenoid of *Chlamydomonas reinhardtii*. *Planta*, 195 (2), pp.210–216. [Online]. Available at: doi:10.1007/BF00199681.

Ramundo, S. et al. (2020). Coexpressed subunits of dual genetic origin define a conserved supercomplex mediating essential protein import into chloroplasts. *Proceedings of the National Academy of Sciences of the United States of America*, 117 (51), pp.32739–32749. [Online]. Available at: doi:10.1073/pnas.2014294117.

Rawat, M. et al. (1996). *Chlamydomonas reinhardtii* mutants without ribulose-1,5-bisphosphate carboxylase-oxygenase lack a detectable pyrenoid. *Planta*, 198 (2), pp.263–270. [Online]. Available at: doi:10.1007/BF00206252.

Ray, D. K. et al. (2013). Yield Trends Are Insufficient to Double Global Crop Production by 2050. *PLoS ONE*, 8 (6). [Online]. Available at: doi:10.1371/journal.pone.0066428.

Reinhardt, T. A., Lippolis, J. D. and Sacco, R. E. (2014). The Ca^{2+}/H^+ antiporter TMEM165 expression, localization in the developing, lactating and involuting mammary gland parallels the secretory pathway Ca^{2+} ATPase (SPCA1). *Biochemical and Biophysical Research Communications*, 445 (2), pp.417–421. [Online]. Available at: doi:10.1016/j.bbrc.2014.02.020.

Rochaix, J.-D. (2011). Assembly of the Photosynthetic Apparatus. *Plant Physiology*, 155 (4), pp.1493–1500. [Online]. Available at: doi:10.1097/00008469-199906000-00005.

La Rovere, R. M. L. et al. (2016). Intracellular Ca^{2+} signaling and Ca^{2+} microdomains in the control of cell survival, apoptosis and autophagy. *Cell Calcium*, 60 (2), pp.74–87. [Online]. Available at: doi:10.1016/j.ceca.2016.04.005.

Roy, S. (2016). Function of MYB domain transcription factors in abiotic stress and epigenetic control of stress response in plant genome. *Plant Signaling and Behavior*, 11 (1), pp.1–7. [Online]. Available at: doi:10.1080/15592324.2015.1117723.

Sager, R. and Palade, G. E. (1957). Structure and development of the chloroplast in Chlamydomonas. I. The normal green cell. *The Journal of biophysical and biochemical cytology*, 3 (3), pp.463–488.

San-Segundo, P. A. and Shirleen Roeder, G. (1999). Pch2 links chromatin silencing to meiotic checkpoint control. *Cell*, 97 (3), pp.313–324. [Online]. Available at: doi:10.1016/S0092-8674(00)80741-2.

Sasso, S. et al. (2018). From molecular manipulation of domesticated *Chlamydomonas reinhardtii* to survival in nature. *eLife*, 7, p.e39233. [Online]. Available at: doi:10.7554/eLife.39233.

Saunders, N. F. W. and Kobe, B. (2008). The Predikin webserver: improved prediction of protein kinase peptide specificity using structural information. *Nucleic Acids Research*, 36 (Web Server), pp.W286–W290. [Online]. Available at: doi:10.1093/nar/gkn279.

Schneider, A. et al. (2016). The evolutionarily conserved protein PHOTOSYNTHESIS AFFECTED MUTANT71 is required for efficient manganese uptake at the thylakoid membrane in Arabidopsis. *Plant Cell*, 28 (4), pp.892–910. [Online]. Available at: doi:10.1105/tpc.15.00812.

Schottkowski, M. et al. (2012). Biogenic membranes of the chloroplast in *Chlamydomonas reinhardtii*. *Proceedings of the National Academy of Sciences of the United States of America*, 109 (47), pp.19286–19291. [Online]. Available at: doi:10.1073/pnas.1209860109.

Schuler, M. L., Mantegazza, O. and Weber, A. P. M. (2016). Engineering C4 photosynthesis into C3 chassis in the synthetic biology age. *The Plant journal : for cell and molecular biology*, 87 (1), pp.51–65. [Online]. Available at: doi:10.1111/tpj.13155.

Schwarzenbach, G. and Meier, J. (1958). Formation and investigation of unstable protonation and deprotonation products of complexes in aqueous solution. *Journal of Inorganic and Nuclear Chemistry*, 8, pp.302–312. [Online]. Available at: doi:10.1016/0022-1902(58)80195-5.

Shihan, M. H. et al. (2021). A simple method for quantitating confocal fluorescent images. *Biochemistry and Biophysics Reports*, 25, p.100916. [Online]. Available at: doi:10.1016/j.bbrep.2021.100916.

Shiu, S. H. and Bleecker, A. B. (2001). Receptor-like kinases from *Arabidopsis* form a monophyletic gene family related to animal receptor kinases. *Proceedings of the National Academy of Sciences of the United States of America*, 98 (19), pp.10763–10768. [Online]. Available at: doi:10.1073/pnas.181141598.

Shutova, T. et al. (2008). The photosystem II-associated Cah3 in *Chlamydomonas* enhances the O_2 evolution rate by proton removal. *EMBO Journal*, 27 (5), pp.782–791. [Online]. Available at: doi:10.1038/emboj.2008.12.

Silflow, C. D. and Lefebvre, P. A. (2001). Assembly and Motility of Eukaryotic Cilia and Flagella. Lessons from *Chlamydomonas reinhardtii*. *Plant Physiology*, 127 (4), pp.1500–1507. [Online]. Available at: doi:10.1104/pp.010807.

Simanshu, D. K., Nissley, D. V. and McCormick, F. (2017). RAS Proteins and Their Regulators in Human Disease. *Cell*, 170 (1), pp.17–33. [Online]. Available at: doi:10.1016/j.cell.2017.06.009.

Sinetova, M. A. et al. (2012). Identification and functional role of the carbonic anhydrase Cah3 in thylakoid membranes of pyrenoid of *Chlamydomonas reinhardtii*. *Biochimica et Biophysica Acta - Bioenergetics*, 1817 (8), pp.1248–1255. [Online]. Available at: doi:10.1016/j.bbabio.2012.02.014.

Spalding, M. H. (1989). Photosynthesis and photorespiration in freshwater green algae. *Aquatic Botany*, 34 (1–3), pp.181–209. [Online]. Available at: doi:10.1016/0304-3770(89)90056-9.

Spalding, M. H., Spreitzer, R. J. and Ogren, W. L. (1983). Carbonic Anhydrase-Deficient Mutant of *Chlamydomonas reinhardii* Requires Elevated Carbon Dioxide Concentration

for Photoautotrophic Growth. *Plant Physiology*, 73 (2), pp.268–272. [Online]. Available at: doi:10.1104/pp.73.2.268.

Stoler, O. et al. (2022). Frequency- and spike-timing-dependent mitochondrial Ca^{2+} signaling regulates the metabolic rate and synaptic efficacy in cortical neurons. *eLife*, 11, pp.1–14. [Online]. Available at: doi:10.7554/eLife.74606.

Stothard, P. (2000). The Sequence Manipulation Suite: JavaScript Programs for Analyzing and Formatting Protein and DNA Sequences. *BioTechniques*, 28 (6), pp.1102–1104. [Online]. Available at: doi:10.2144/00286ir01.

Strenkert, D. et al. (2019). Multiomics resolution of molecular events during a day in the life of Chlamydomonas. *Proceedings of the National Academy of Sciences of the United States of America*, 116 (6), pp.2374–2383. [Online]. Available at: doi:10.1073/pnas.1815238116.

Su, Z. et al. (2009). Mechanical force and cytoplasmic Ca^{2+} activate yeast TRPY1 in parallel. *Journal of Membrane Biology*, 227 (3), pp.141–150. [Online]. Available at: doi:10.1007/s00232-009-9153-9.

Sun, L. et al. (2009). Guanylyl cyclase-D in the olfactory CO_2 neurons is activated by bicarbonate. *Proceedings of the National Academy of Sciences*, 106 (6), pp.2041–2046. [Online]. Available at: doi:10.1073/pnas.0812220106.

Tamura, K., Stecher, G. and Kumar, S. (2021). MEGA11: Molecular Evolutionary Genetics Analysis Version 11. *Molecular Biology and Evolution*, 38 (7), pp.3022–3027. [Online]. Available at: doi:10.1093/molbev/msab120.

Tanz, S. K. et al. (2013). Fluorescent protein tagging as a tool to define the subcellular distribution of proteins in plants. *Frontiers in Plant Science*, 4, pp.1–9. [Online]. Available at: doi:10.3389/fpls.2013.00214.

Tao, L. et al. (2017). Integration of the tricarboxylic acid (TCA) cycle with cAMP signaling and Sfl2 pathways in the regulation of CO_2 sensing and hyphal development in *Candida albicans*. [Online]. Available at: doi:10.1371/journal.pgen.1006949.

Tardif, M. et al. (2012). Predalgo: A new subcellular localization prediction tool dedicated

to green algae. *Molecular Biology and Evolution*, 29 (12), pp.3625–3639. [Online]. Available at: doi:10.1093/molbev/mss178.

Terashima, M. et al. (2012). Calcium-dependent regulation of cyclic photosynthetic electron transfer by a CAS, ANR1, and PGRL1 complex. *Proceedings of the National Academy of Sciences of the United States of America*, 109 (43), pp.17717–17722. [Online]. Available at: doi:10.1073/pnas.1207118109.

Thines, L. et al. (2018). The yeast protein Gdt1p transports Mn^{2+} ions and thereby regulates manganese homeostasis in the Golgi. *Journal of Biological Chemistry*, 293 (21), pp.8048–8055. [Online]. Available at: doi:10.1074/jbc.RA118.002324.

Thines, L., Stribny, J. and Morsomme, P. (2020). From the uncharacterized protein family 0016 to the GDT1 family: Molecular insights into a newly-characterized family of cation secondary transporters. *Microbial Cell*, 7 (8), pp.202–214. [Online]. Available at: doi:10.15698/MIC2020.08.725.

Tian, W. et al. (2015). A molecular pathway for CO_2 response in *Arabidopsis* guard cells. *Nature Communications*, 6, pp.1–10. [Online]. Available at: doi:10.1038/ncomms7057.

Tirumani, S. et al. (2014). Regulation of CCM genes in *Chlamydomonas reinhardtii* during conditions of light-dark cycles in synchronous cultures. *Plant Molecular Biology*, 85 (3), pp.277–286. [Online]. Available at: doi:10.1007/s11103-014-0183-z.

Tokutsu, R. et al. (2019). The CONSTANS flowering complex controls the protective response of photosynthesis in the green alga *Chlamydomonas*. *Nature Communications*, 10 (1), pp.2–5. [Online]. Available at: doi:10.1038/s41467-019-11989-x.

Töpel, M. and Jarvis, P. (2011). The Tic20 gene family: Phylogenetic analysis and evolutionary considerations. *Plant Signaling and Behavior*, 6 (7), pp.1046–1048. [Online]. Available at: doi:10.4161/psb.6.7.15631.

Toth, A. B., Shum, A. K. and Prakriya, M. (2016). Regulation of neurogenesis by calcium signaling. *Cell Calcium*, 59 (2–3), pp.124–134. [Online]. Available at: doi:10.1016/j.ceca.2016.02.011.

Townsend, P. D. et al. (2009). Stimulation of mammalian G-protein-responsive adenylyl

cyclases by carbon dioxide. *Journal of Biological Chemistry*, 284 (2), pp.784–791. [Online]. Available at: doi:10.1074/jbc.M807239200.

Toyokawa, C., Yamano, T. and Fukuzawa, H. (2020). Pyrenoid Starch Sheath Is Required for LCIB Localization and the CO_2-Concentrating Mechanism in Green Algae. *Plant Physiology*, 182 (4), pp.1883–1893. [Online]. Available at: doi:10.1104/pp.19.01587.

Tresguerres, M. et al. (2014). Established and potential physiological roles of bicarbonate-sensing soluble adenylyl cyclase (sAC) in aquatic animals. *Journal of Experimental Biology*, 217 (5), pp.663–672. [Online]. Available at: doi:10.1242/jeb.086157.

Tresguerres, M., Buck, J. and Levin, L. R. (2010). Physiological carbon dioxide, bicarbonate, and pH sensing. *Pflugers Archiv European Journal of Physiology*, 460 (6), pp.953–964. [Online]. Available at: doi:10.1007/s00424-010-0865-6.

Trippens, J., Reißenweber, T. and Kreimer, G. (2017). The chloroplast calcium sensor protein CAS affects phototactic behaviour in *Chlamydomonas reinhardtii* (Chlorophyceae) at low light intensities. *Phycologia*, 56 (3), pp.261–270. [Online]. Available at: doi:10.2216/16-67.1.

Uhlén, P. and Fritz, N. (2010). Biochemistry of calcium oscillations. *Biochemical and Biophysical Research Communications*, 396 (1), pp.28–32. [Online]. Available at: doi:10.1016/j.bbrc.2010.02.117.

Vance, P. and Spalding, M. H. (2005). Growth, photosynthesis, and gene expression in *Chlamydomonas* over a range of CO_2 concentrations and CO_2/O_2 ratios: CO_2 regulates multiple acclimation states. *Canadian Journal of Botany*, 83 (7), pp.796–809. [Online]. Available at: doi:10.1139/b05-064.

Vannier, B. et al. (1999). Mouse trp2, the homologue of the human trpc2 pseudogene, encodes mTrp2, a store depletion-activated capacitative Ca^{2+} entry channel. *Proceedings of the National Academy of Sciences of the United States of America*, 96 (5), pp.2060–2064. [Online]. Available at: doi:10.1073/pnas.96.5.2060.

Velay, F. et al. (2022). MoBiFC: development of a modular bimolecular fluorescence complementation toolkit for the analysis of chloroplast protein–protein interactions.

Plant Methods, 18 (1), pp.1–13. [Online]. Available at: doi:10.1186/s13007-022-00902-1.

Villarejo, A. et al. (2002). A photosystem II-associated carbonic anhydrase regulates the efficiency of photosynthetic oxygen evolution. *EMBO Journal*, 21 (8), pp.1930–1938. [Online]. Available at: doi:10.1093/emboj/21.8.1930.

Wakao, S. et al. (2021). Discovery of photosynthesis genes through whole-genome sequencing of acetate-requiring mutants of *Chlamydomonas reinhardtii*. Schroda, M. (Ed). *PLOS Genetics*, 17 (9), p.e1009725. [Online]. Available at: doi:10.1371/journal.pgen.1009725.

Wang, C. et al. (2016a). A Putative Chloroplast-Localized Ca^{2+}/H^+ Antiporter CCHA1 Is Involved in Calcium and pH Homeostasis and Required for PSII Function in *Arabidopsis*. *Molecular Plant*, 9 (8), pp.1183–1196. [Online]. Available at: doi:10.1016/j.molp.2016.05.015.

Wang, C. et al. (2016b). Reconstitution of CO_2 Regulation of SLAC1 Anion Channel and Function of CO_2 -Permeable PIP2;1 Aquaporin as CARBONIC ANHYDRASE4 Interactor. *The Plant Cell*, 28 (2), pp.568–582. [Online]. Available at: doi:10.1105/tpc.15.00637.

Wang, L. et al. (2014). Isolation and characterization of novel high-CO_2-requiring mutants of *Chlamydomonas reinhardtii*. *Photosynthesis Research*, 121 (2–3), pp.175–184. [Online]. Available at: doi:10.1007/s11120-014-9983-x.

Wang, L. et al. (2016c). Chloroplast-mediated regulation of CO_2-concentrating mechanism by Ca^{2+}-binding protein CAS in the green alga *Chlamydomonas reinhardtii*. *Proceedings of the National Academy of Sciences*, 113 (44), pp.12586–12591. [Online]. Available at: doi:10.1073/pnas.1606519113.

Wang, Q. et al. (2019). The significance of calcium in photosynthesis. *International Journal of Molecular Sciences*, 20 (6), pp.1–14. [Online]. Available at: doi:10.3390/ijms20061353.

Wang, X. et al. (2016d). Ocean acidification stimulates alkali signal pathway: A bicarbonate sensing soluble adenylyl cyclase from oyster *Crassostrea gigas* mediates physiological changes induced by CO_2 exposure. *Aquatic Toxicology*, 181, pp.124–135. [Online]. Available at: doi:10.1016/j.aquatox.2016.11.002.

Wang, X., Niu, Y. and Zheng, Y. (2021). Multiple functions of MYB transcription factors in abiotic stress responses. *International Journal of Molecular Sciences*, 22 (11). [Online]. Available at: doi:10.3390/ijms22116125.

Wang, Y. et al. (2005). Analyses of CIA5, the master regulator of the carbon-concentrating mechanism in *Chlamydomonas reinhardtii*, and its control of gene expression. *Canadian Journal of Botany*, 83 (7), pp.765–779. [Online]. Available at: doi:10.1139/b05-062.

Wang, Y. and Spalding, M. H. (2006). An inorganic carbon transport system responsible for acclimation specific to air levels of CO_2 in *Chlamydomonas reinhardtii*. *Proc Natl Acad Sci USA*, 103 (26), pp.10110–10115. [Online]. Available at: doi:10.1073/pnas.0603402103.

Wang, Y. and Spalding, M. H. (2014). Acclimation to Very Low CO_2: Contribution of Limiting CO_2 Inducible Proteins, LCIB and LCIA, to Inorganic Carbon Uptake in *Chlamydomonas reinhardtii*. *Plant Physiology*, 166 (4), pp.2040–2050. [Online]. Available at: doi:10.1104/pp.114.248294.

Wang, Y., Stessman, D. J. and Spalding, M. H. (2015). The CO_2 concentrating mechanism and photosynthetic carbon assimilation in limiting CO_2: How Chlamydomonas works against the gradient. *Plant Journal*, 82 (3), pp.429–448. [Online]. Available at: doi:10.1111/tpj.12829.

Wheeler, G. L. (2017). Calcium-Dependent Signalling Processes in Chlamydomonas. In: *Chlamydomonas: Molecular Genetics and Physiology*. Springer, Cham. pp.233–255. [Online]. Available at: doi:10.1007/978-3-319-66365-4_8.

Wheeler, G. L., Joint, I. and Brownlee, C. (2008). Rapid spatiotemporal patterning of cytosolic Ca^{2+} underlies flagellar excision in *Chlamydomonas reinhardtii*. *Plant Journal*, 53 (3), pp.401–413. [Online]. Available at: doi:10.1111/j.1365-313X.2007.03349.x.

Wilson, N. F. and Lefebvre, P. A. (2004). Regulation of flagellar assembly by glycogen synthase kinase 3 in *Chlamydomonas reinhardtii*. *Eukaryotic Cell*, 3 (5), pp.1307–1319. [Online]. Available at: doi:10.1128/EC.3.5.1307-1319.2004.

Xiang, Y., Zhang, J. and Weeks, D. P. (2001). The *Cia5* gene controls formation of the

carbon concentrating mechanism in *Chlamydomonas reinhardtii*. *Proceedings of the National Academy of Sciences*, 98 (9), pp.5341–5346. [Online]. Available at: doi:10.1073/pnas.101534498.

Xie, F. et al. (2006). Soluble adenylyl cyclase (sAC) is indispensable for sperm function and fertilization. *Developmental Biology*, 296 (2), pp.353–362. [Online]. Available at: doi:10.1016/j.ydbio.2006.05.038.

Xing, J. et al. (2017). Deletion of CGLD1 Impairs PSII and Increases Singlet Oxygen Tolerance of Green Alga *Chlamydomonas reinhardtii*. *Frontiers in Plant Science*, 8, p.2154. [Online]. Available at: doi:10.3389/fpls.2017.02154.

Yamano, T. et al. (2010). Light and low-CO_2-dependent LCIB–LCIC complex localization in the chloroplast supports the carbon-concentrating mechanism in *Chlamydomonas reinhardtii*. *Plant and Cell Physiology*, 51 (9), pp.1453–1468. [Online]. Available at: doi:10.1093/pcp/pcq105.

Yamano, T. et al. (2014). Isolation and characterization of mutants defective in the localization of LCIB, an essential factor for the carbon-concentrating mechanism in *Chlamydomonas reinhardtii*. *Photosynthesis Research*, 121 (2–3), pp.193–200. [Online]. Available at: doi:10.1007/s11120-013-9963-6.

Yamano, T. et al. (2015). Characterization of cooperative bicarbonate uptake into chloroplast stroma in the green alga *Chlamydomonas reinhardtii*. *Proceedings of the National Academy of Sciences*, 112 (23), pp.7315–7320. [Online]. Available at: doi:10.1073/pnas.1501659112.

Yamano, T. et al. (2022). CO_2-dependent migration and relocation of LCIB, a pyrenoid-peripheral protein in *Chlamydomonas reinhardtii*. *Plant Physiology*, 188 (2), pp.1081–1094. [Online]. Available at: doi:10.1093/plphys/kiab528.

Yamano, T., Toyokawa, C. and Fukuzawa, H. (2018). High-resolution suborganellar localization of Ca^{2+}-binding protein CAS, a novel regulator of CO_2-concentrating mechanism. *Protoplasma*, 255 (4), pp.1015–1022. [Online]. Available at: doi:10.1007/s00709-018-1208-2.

Yang, W. et al. (2014). Alternative acetate production pathways in *Chlamydomonas*

reinhardtii during dark anoxia and the dominant role of chloroplasts in fermentative acetate production. *Plant Cell*, 26 (11), pp.4499–4518. [Online]. Available at: doi:10.1105/tpc.114.129965.

Yang, X. et al. (2015). A roadmap for research on crassulacean acid metabolism (CAM) to enhance sustainable food and bioenergy production in a hotter, drier world. *New Phytologist*, 207 (3), pp.491–504. [Online]. Available at: doi:10.1111/nph.13393.

Ynalvez, R. A. et al. (2008). Identification and characterization of two closely related β-carbonic anhydrases from *Chlamydomonas reinhardtii*. *Physiologia Plantarum*, 133 (1), pp.15–26. [Online]. Available at: doi:10.1111/j.1399-3054.2007.01043.x.

Yoshioka, S. et al. (2004). The novel Myb transcription factor LCR1 regulates the CO_2-responsive gene *Cah1*, encoding a periplasmic carbonic anhydrase in *Chlamydomonas reinhardtii*. *Plant Cell*, 16 (6), pp.1466–1477. [Online]. Available at: doi:10.1105/tpc.021162.CO.

Zhang, B. et al. (2018). Inner Envelope CHLOROPLAST MANGANESE TRANSPORTER 1 Supports Manganese Homeostasis and Phototrophic Growth in *Arabidopsis*. *Molecular Plant*, 11 (7), pp.943–954. [Online]. Available at: doi:10.1016/j.molp.2018.04.007.

Zhang, W. et al. (2019). Role of Low-Affinity Calcium System Member *Fig1* Homologous Proteins in Conidiation and Trap-Formation of Nematode-trapping Fungus *Arthrobotrys oligospora*. *Scientific Reports*, 9 (1), pp.1–9. [Online]. Available at: doi:10.1038/s41598-019-40493-x.

Zones, J. M. et al. (2015). High-resolution profiling of a synchronized diurnal transcriptome from *Chlamydomonas reinhardtii* reveals continuous cell and metabolic differentiation. *Plant Cell*, 27 (10), pp.2743–2769. [Online]. Available at: doi:10.1105/tpc.15.00498.